

**Mechanical and Chemical Properties of High Density  
Polyethylene: Effects of Microstructure on Creep  
Characteristics**

by

Joy J. Cheng

A thesis

presented to the University of Waterloo

in fulfillment of the

thesis requirement for the degree of

Doctor of Philosophy

in

Chemical Engineering

Waterloo, Ontario, Canada, 2008

© Joy J. Cheng 2008

I hereby declare that I am the sole author of this thesis. This is a true copy of the thesis, including any required final revisions, as accepted by my examiners.

I understand that my thesis may be made electronically available to the public.

## **ABSTRACT**

Environmental stress cracking (ESC) can result in catastrophic failure of polyethylene (PE) structures without any visible warning. The use of PE in more demanding applications, such as trenchless piping, can accelerate ESC failure of the material. Besides public safety issues, the replacement and remediation of these failed polyethylene structures also cost both in money and labour. This thesis is part of a collaborative project between the disciplines of chemical and civil engineering to study environmental stress cracking resistance (ESCR) of polyethylene. By combining structural mechanics and (micro)molecular science, new insights into the ESCR behaviour of polyethylene could be achieved.

The test commonly used for determining ESCR of polyethylene can be time consuming and rather imprecise. In our study a new testing method has been developed which compares ESCR of resins based on the more direct measure of “hardening stiffness” rather than strain-hardening modulus. Our new method is much simpler than those proposed previously because it is conducted under ambient conditions and does not require specialized equipment for true stress-strain measurements. Comparisons between the conventional ESCR test method and the strain hardening test show that strain hardening can be used to rank ESCR of polyethylene in a reliable fashion. The strain hardening test developed in this thesis has the potential to replace the standard ESCR test that has been in use in industry for the past twenty five years.

Most ESCR research has so far focused on bridging-tie-molecules as the main source of inter-lamellar connections. We take a fresh approach and demonstrate in this thesis that physical chain entanglements also contribute to the formation of inter-lamellar linkages. Chain entanglements in the melt state are known to be preserved in the polymer upon solidification, therefore, rheological determination of the molecular weight between entanglements ( $M_e$ ) is used as a measure of chain entanglements for PE. A lower  $M_e$  value means a higher number of entanglements in the system. The inversely proportional relationship between  $M_e$  and ESCR indicates that low network mobility due to increasing number of chain entanglements increases ESCR of PE. With the understanding that

strain hardening is related to ESCR of polyethylene, the relationship between chain entanglements and tensile strain hardening has also been investigated. By combining experimental observations and parallel micromechanical modeling results, the presence of physical chain entanglements in the amorphous phase was demonstrated to be the factor controlling the strain hardening behaviour of polyethylene.

Studies of the effect of inter-lamellar linkages on ESCR of polyethylene have traditionally focused on changes in the amorphous phase. In this thesis, percentage crystallinity and lamella thickness of polyethylene resins were studied to determine their effects on ESCR. The study of the effect of the crystalline phase on ESCR was extended to investigate the lateral surface characteristics of the lamella. An increase in ESCR was observed with increases in lateral lamella area of resins. It was postulated that a larger lateral lamella area results in a higher probability of formation of inter-lamellar linkages. This increase in phase interconnectivity directly results in an increasing ESCR for the resins.

Finally, in order to facilitate practical applications of polyethylene (especially in pipes), attempts were made to develop a predictive tool for the quantitative estimation of the long-term ESCR of polyethylene based on the short-term notched constant load test (NCLT). Although previous work on slow crack growth models showed little sensitivity to crack activation energy, the ESC model pursued herein was found to be exponentially dependent on this parameter. Further refinement of the ESC model is needed but the modeling investigation proved fruitful in highlighting several other relationships amongst chemical, physical and mechanical properties of PE resins, such as, that between ESC crack activation energy and the  $\alpha$ -relaxation energy of polyethylene.

## **ACKNOWLEDGEMENTS**

I want to offer my deepest thanks to my supervisor, Prof. Alex Penlidis. Without his guidance and support this thesis would not be possible. Besides all the knowledge on polymers, I am grateful for the many life lessons I have learned from him. I consider myself to be very fortunate to have met and studied under such a distinguished mentor.

I would like to thank Dr. Maria A. Polak, Department of Civil and Environmental Engineering, University of Waterloo, for clarifying questions on structural mechanics. I would also like to acknowledge Dr. Shuihan Zhu, Department of Chemical Engineering, University of Waterloo, for considerable help with the rheology experiments. Many thanks go to ExxonMobil Chemical Canada (Imperial Oil Canada), Nova Chemicals (Canada) Ltd., and Repsol YPF, Spain, for kindly supplying resins and for interactions on the project.

I want to thank my parents for their understanding and support through my studies. Last, but not least, my sincere gratitude to all my friends. Thanks for all the Wednesday afternoon therapy sessions! The graduate school journey would have being infinitely less interesting without you all.

To my family

To ITHAKA

# TABLE OF CONTENTS

LIST OF TABLES .....	x
LIST OF FIGURES .....	xiii
CHAPTER 1 INTRODUCTION AND OBJECTIVES .....	1
1.1 Preamble for Setting the Scene .....	1
1.2 Thesis Outline .....	4
1.3 References.....	8
CHAPTER 2 GENERAL LITERATURE BACKGROUND .....	9
2.1 Molecular Properties of Polyethylene.....	9
2.1.1 Microstructure.....	9
2.1.2 Types of Polyethylene.....	11
2.1.3 Branch Structures.....	13
2.1.4 Chain Movement and Viscoelasticity .....	14
2.2 Mechanical Behaviour of Polyethylene.....	17
2.2.1 Ductile Failure .....	17
2.2.2 Brittle Failure .....	19
2.2.3 Strain Hardening.....	20
2.2.4 Environmental Stress Cracking.....	20
2.2.5 Factors Affecting ESCR of HDPE.....	22
2.3 Pipe Applications and Trenchless Technology.....	28
2.4 References.....	33
CHAPTER 3 EXPERIMENTAL METHODS.....	37
3.1 Tests for (Micro)Molecular Properties .....	37
3.1.1 Differential Scanning Calorimetry (DSC) .....	37
3.1.2 Crystallization Analysis Fractionation (CRYSTAF) .....	41
3.1.3 Size Exclusion Chromatography – SEC/GPC .....	43
3.1.4 <sup>13</sup> C - NMR.....	45
3.1.5 X-Ray Diffraction .....	47
3.2 Rheological Characterization.....	52
3.2.1 Oscillatory Shear Analysis.....	52
3.2.2 Dynamic Mechanical Analysis .....	56
3.3 Tests for (Macro)Mechanical Properties .....	57
3.3.1 Tensile Test.....	57
3.3.2 Notched Constant Load Test (NCLT).....	60
3.4 Resin Selection and Material Properties as Received.....	63
3.5 References.....	66
CHAPTER 4 MECHANICAL PROPERTY RELATIONS WITH ENVIRONMENTAL STRESS CRACKING RESISTANCE.....	69
4.1 Introduction.....	69
4.2 Experimental Methods .....	74

4.2.1	Polymer Characterization and Mechanical Testing .....	74
4.2.2	Experimental Design for NCLT.....	75
4.3	Results and Discussion .....	76
4.3.1	ESCR Results from NCLT Test.....	76
4.3.2	Strain Hardening and ESCR of Resins .....	86
4.3.3	Tensile Yield Point and ESCR.....	91
4.3.4	Natural Draw Ratio (NDR) and ESCR.....	92
4.3.5	Effect of Strain Rate.....	94
4.3.6	Reproducibility of Strain Hardening Test.....	97
4.3.7	Other Material Indicators for ESCR .....	100
4.3.8	Modeling Creep Behaviour of Polyethylene for Structural Applications.....	100
4.4	Concluding Remarks.....	100
4.5	References.....	103
CHAPTER 5 AMORPHOUS PHASE STRUCTURE AND MECHANICAL BEHAVIOUR OF POLYETHYLENE.....		106
5.1	Introduction.....	106
5.2	Experimental Methods.....	109
5.3	Network Mobility and ESCR.....	110
5.3.1	Rheological Characteristics .....	110
5.3.2	Long Chain Branching Effect .....	117
5.3.3	Chain Entanglements and Tensile Elongation .....	121
5.3.4	ESCR and Chain Entanglements .....	126
5.4	Micromechanical Modeling.....	130
5.4.1	Chain Entanglements and Strain Hardening – Justification via Micromechanical Modeling.....	132
5.5	Concluding Remarks.....	141
5.6	References.....	143
CHAPTER 6 PHASE INTERCONNECTIVITY AND ESCR.....		149
6.1	Introduction.....	149
6.2	Experimental Methods.....	152
6.3	Material Characteristics .....	153
6.3.1	Crystallinity and Lamella Thickness .....	153
6.3.2	Resin Crystallinity Measurements .....	154
6.3.3	Lamella Thickness Measurements.....	157
6.4	Crystalline Phase Characteristics and ESCR.....	160
6.4.1	Crystallinity and ESCR.....	160
6.4.2	Lamella Thickness and ESCR .....	163
6.4.3	Lamellar Lateral Surface and ESCR.....	164
6.5	Concluding Remarks.....	171
6.6	References.....	173
CHAPTER 7 LIFETIME PREDICTION BASED ON SHORT-TERM ESCR TEST FOR POLYETHYLENE.....		177
7.1	Introduction.....	177

7.2	Experimental Methods.....	181
7.3	Environmental Stress Cracking Model.....	181
7.4	ESC Model Analysis.....	183
7.4.1	Resin Characteristics.....	183
7.4.2	Geometry Correction Factor - Y.....	184
7.4.3	Determination of n.....	185
7.4.4	Crack Activation Energy.....	186
7.5	Relationship Between the $\alpha$ -Relaxation Energy and ESC Crack Activation Energy of Polyethylene.....	189
7.5.1	The $\alpha$ -Relaxation Energy of Polyethylene.....	190
7.5.2	Comparison of Activation Energies.....	195
7.6	Material Resistance to ESC.....	201
7.7	Concluding Remarks.....	208
7.8	References.....	210
CHAPTER 8	PRACTICAL TIPS AND PRESCRIPTIONS FOR ESCR OF POLYETHYLENE.....	214
8.1	Introduction.....	214
8.2	ESCR Heuristics.....	214
8.3	Prescriptions for ESCR of Polyethylene.....	216
8.4	Concluding Remarks.....	222
8.5	References.....	223
CHAPTER 9	CONCLUDING REMARKS, MAIN CONTRIBUTIONS AND RECOMMENDATIONS.....	224
9.1	Concluding Remarks.....	224
9.2	Main Contributions of the Thesis.....	225
9.3	Resin Property Summary.....	230
9.4	Recommendations for Future Steps.....	233
9.5	References.....	236
APPENDICES	.....	238
APPENDIX A:	SHORT CHAIN BRANCH DISTRIBUTION.....	239
APPENDIX B:	CRYSTALLIZATION ANALYSIS FRACTIONATION (CRYSTAF) AND ESCR.....	249
APPENDIX C:	MODELING CREEP BEHAVIOUR OF POLYETHYLENE FOR STRUCTURAL APPLICATIONS.....	260
APPENDIX D:	MICROMECHANICAL MODEL FOR POLYETHYLENE.....	276
APPENDIX E:	$\alpha$ -RELAXATION ENERGY AND ESC MODEL.....	280

## **LIST OF TABLES**

Table 2.1: Classification of polyethylene by density.....	12
Table 3.1: Resin properties as received from manufacturers.....	65
Table 4.1: List of experimental methods for Chapter 4.....	74
Table 4.2: Experimental design <sup>1</sup> for NCLT of PE 1.....	75
Table 4.3: Characteristics of resins.....	76
Table 4.4: NCLT results.....	77
Table 4.5: ANOVA of independent replicated test results for PE1.....	83
Table 4.6: NCLT results for PE1 at different levels of notch depth and yield stress.....	84
Table 4.7: ANOVA of effect of yield strength and notch depth on NCLT results (hours) .....	86
Table 4.8: Hardening stiffness (HS) and NDR of polyethylene.....	89
Table 4.9: ANOVA of PE8 at 7 mm/min strain rate.....	98
Table 4.10: ANOVA of hardening stiffness values at 0.5 mm/min strain rate.....	99
Table 4.11: ANOVA of hardening stiffness values at 7 mm/min strain rate.....	99
Table 4.12: Resins tested with NCLT and strain hardening test (summary).....	102
Table 5.1: List of experimental methods for Chapter 5.....	109
Table 5.2: Characteristics of resins.....	110
Table 5.3: Rheological characteristics of resins at 190°C.....	111
Table 5.4: Hardening stiffness (HS) and NDR of polyethylene.....	124
Table 6.1: List of experimental methods for Chapter 6.....	152
Table 6.2: Material characteristics of resins.....	153
Table 6.3: Crystallinity and lamella thickness of resins.....	154

Table 6.4: ANOVA of WAXS measurements for PE9.....	157
Table 6.5: ANOVA of SAXS measurements for PE9 .....	160
Table 6.6: Lamella area estimates of resins .....	168
Table 7.1: List of experimental methods for Chapter 7 .....	181
Table 7.2: Resin characteristics .....	184
Table 7.3: NCLT stress level, ESCR time, and n constant of PE1-4 and PE8 .....	186
Table 7.4: NCLT results at different temperatures and Q value of PE1-4 and PE8 .....	189
Table 7.5: $\alpha$ -relaxation energy values for PE1-4 and PE8 .....	193
Table 7.6: Crack activation energy (Q) and $\alpha$ -relaxation energy ( $\Delta H$ ) of PE1-4 and PE8 .....	196
Table 7.7: Material resistance (C) to environmental stress cracking for PE1-4 and PE8203	
Table 8.1: Molecular properties and ESCR relations of HDPE.....	215
Table 9.1: Molecular properties of polyethylene resins determined in the course of the thesis .....	231
Table 9.2: Mechanical properties of polyethylene resins determined in the course of the thesis .....	232
Table B.1: Weight percentage of crystallizable chains at different temperature ranges in CRYSTAF and other material properties .....	252
Table C.1: Relaxation time of each Kelvin element.....	262
Table C.2: Modulus estimated for PE1, PE2, PE4 and PE8 .....	264
Table C.3: Modulus estimated for PE1 and PE2. From refs. (5, 6).....	264
Table C.4: ANOVA of creep model for PE1 at 5.15 MPa .....	265
Table C.5: ANOVA of creep model for PE1 at 10.58 MPa .....	265
Table C.6: Model parameters estimated including $E_0$ .....	269
Table C.7: ANOVA of creep model with estimated $E_0$ for PE1 at 5.15 MPa .....	270

Table D.1: Material parameters for model simulations under uniaxial tension, ref. (1).	276
Table D.2: Micromechanical model with damage for semicrystalline polyethylene, ref. (1).....	277
Table E.1: $\alpha$ -relaxation energy of polyethylene .....	280
Table E.2: Material resistance (C) to ESC based on $Q = 90$ kJ/mol (2) and $Q = \Delta H$ for PE7-10.....	282

## LIST OF FIGURES

Figure 2.1: Schematic illustration of spherulite, lamella, and amorphous phase structures. Adapted from refs. (10, 11) .....	10
Figure 2.2: Structures of lamella; (a) the regularly folded chain model for semi-crystalline polymer; (b) non-regularly folded chain model for semi-crystalline polymer. From ref. (9) .....	10
Figure 2.3: Crystal structures of polyethylene. From ref. (15) .....	13
Figure 2.4: Branch structures of polyethylene. From ref. (16) .....	14
Figure 2.5: Thermal transition stages of polyethylene. From ref. (17).....	15
Figure 2.6: (a) reptation of a polymer chain, (b) primitive-path fluctuations (21) .....	16
Figure 2.7: Tensile deformation of polymer. From ref. (26) .....	18
Figure 2.8: Stages of Brittle Fracture; (a) lamellae start to pull away, (b) the tie-molecules are stretched tight, (c) clean break of lamellae. From ref. (11)....	19
Figure 2.9: Tie-molecule concentration as a function of short chain branching. From ref. (43) .....	26
Figure 2.10: Typical MWD with comonomer composition/SCB distribution for (a) polyethylene produced using Ziegler-Natta catalyst, (b) polyethylene produced using Ziegler-Natta catalyst in tandem process, (c) polyethylene produced using metallocene catalyst. From refs. (14, 46) .....	27
Figure 2.11: Drilling the pilot bore. From ref. (48) .....	30
Figure 2.12: Pulling in the pipe. From ref. (48).....	30
Figure 2.13: Microtunnelling system. From ref. (49) .....	31
Figure 3.1: Schematic representation of thermal events recorded by DSC. From ref. (1) .....	38
Figure 3.2: A typical DSC curve for a polyethylene sample .....	39
Figure 3.3: CRYSTAF results for a polyethylene sample .....	42
Figure 3.4: Schematic representation of separation of polymer molecules of different sizes in the GPC column. From ref. (14) .....	44

Figure 3.5: $^{13}\text{C}$ NMR spectrum of a polyethylene sample.....	46
Figure 3.6: Geometry for interference of an x-ray wave scattered from two planes separated by a spacing $d$ . From ref. (18) .....	47
Figure 3.7: X-ray spectra for different types of crystal structures. From ref. (18) .....	48
Figure 3.8: Schematic diagram of WAXS scattering pattern used in calculation of polymer crystallinity. From ref. (20) .....	49
Figure 3.9: Schematic diagram of a structure associated with the long period, $L$ - long period, $t$ – thickness of lamella. From ref. (20) .....	51
Figure 3.10: Schematic representation of stress and strain curves in an oscillatory shear experiment. From ref. (25) .....	53
Figure 3.11: Typical oscillatory shear responses of polyethylene. Taken from ref. (25). 55	
Figure 3.12: Tensile elongation behaviour of semicrystalline polymer .....	58
Figure 3.13: Dogbone dimensions for tensile test .....	59
Figure 3.14: Test arrangement for NCLT; (1) solution container, heated, (2) test medium, (3) lever, (4) compensating spindle, (5) timing contact, (6) upper holding device, (7) bottom holding device, (8) test piece holding device, (9) test sample, (10) holding device for weight, (11) weights, (12) collector. From ref. (32) .....	61
Figure 3.15: Schematic representation of NCLT test stress level in relation to the yield stress of polymers. Adapted from ref. (33).....	62
Figure 3.16: Dogbone dimensions for NCLT .....	63
Figure 4.1: MWD curves of PE 4-6.....	79
Figure 4.2: MWD curves of PE 1-3 .....	80
Figure 4.3: MWD curves of PE 7-10.....	80
Figure 4.4: Effect of % yield strength and % notch depth on NCLT results (hours) .....	85
Figure 4.5: Tensile elongation at constant strain rate of 0.5 mm/min .....	88
Figure 4.6: Shifted load-displacement curves of the strain hardening stage; 0.5 mm/min strain rate.....	90

Figure 4.7: Relation between ESCR and strain hardening stiffness of polyethylene at 0.5 mm/min strain rate .....	91
Figure 4.8: Tensile elongation curves at yield point, 0.5 mm/min strain rate .....	92
Figure 4.9: Relationship between ESCR and NDR of polyethylene at 0.5 mm/min strain rate.....	93
Figure 4.10: Shifted load-displacement curves of polyethylene; 7 mm/min strain rate ...	95
Figure 4.11: ESCR vs. hardening stiffness at different strain rates .....	96
Figure 4.12: ESCR vs. NDR at different strain rates .....	97
Figure 5.1: Zero shear viscosity ( $\eta_0$ ) vs. $M_w$ .....	115
Figure 5.2: Relationship between entanglement molecular weight ( $M_e$ ) and zero shear viscosity ( $\eta_0$ ).....	116
Figure 5.3: MWD curves of resin .....	118
Figure 5.4: Cole-Cole plot for PE7 and PE8 resins .....	120
Figure 5.5: Van Gurp-Palmen plot for PE7 and PE8 resins .....	120
Figure 5.6: Tensile elongation curves at 0.5 mm/min constant strain rate .....	123
Figure 5.7: Hardening stiffness vs. $M_e$ (the line is only a visual guide to the eye) .....	125
Figure 5.8: NDR vs. $M_e$ (the line is for the sole purpose of guiding the eye) .....	126
Figure 5.9: ESCR vs. $M_e$ for PE1-4 and PE7-10 .....	129
Figure 5.10: Simulation results of semicrystalline polyethylene (65): equivalent stress vs. equivalent strain behaviour under uniaxial tension .....	134
Figure 5.11: Schematic representation of polyethylene crystal and slip system, ref. (65) .....	135
Figure 5.12: Schematic illustration of the eight chain network model for the amorphous phase, ref. (65).....	135
Figure 5.13: Influence of the number of rigid links on the stress-strain response of the crystalline phase.....	137

Figure 5.14: Influence of the number of rigid links on the stress-strain response of the amorphous phase .....	138
Figure 5.15: Influence of the number of rigid links on stress-strain response for semicrystalline polyethylene .....	139
Figure 5.16: Shifted load-displacement curves of the strain hardening stage and corresponding $M_e$ of resins; deformation rate 0.5 mm/min.....	140
Figure 6.1: Percentage crystallinity of resins by DSC and WAXS .....	156
Figure 6.2: Ratio of DSC-lamella thickness value to SAXS-lamella thickness value....	158
Figure 6.3: Ratio of lamella thickness calculated using WAXS-crystallinity and DSC-crystallinity .....	159
Figure 6.4: ESCR vs. DSC-crystallinity for PE1-4 and PE7-10.....	162
Figure 6.5: ESCR vs. SAXS-lamella thickness for PE1-4 and PE7-10.....	164
Figure 6.6: Schematic illustration of spherulite and lamella, adapted from ref. (17, 38)	165
Figure 6.7: Rectangular prism representation of lamella.....	166
Figure 6.8: Lamella area estimates based on SAXS-lamella thickness and DSC-lamella thickness measurements .....	169
Figure 6.9: SCB influence on lamella thickness and lamella area for PE1-3 .....	170
Figure 6.10: ESCR vs. lamella area of resins based on SAXS-lamella thickness values	171
Figure 7.1: a) SEM view of craze, ref. (1), b) schematic illustration of crack and craze in polymer under tension.....	178
Figure 7.2: Arrhenius plot for determination of Q for PE1 and PE4.....	187
Figure 7.3: Curves for $\tan(\delta)$ vs. frequency for PE1.....	191
Figure 7.4: $\tan(\delta)$ vs. frequency curves for PE1 with independent replication .....	191
Figure 7.5: Shift factor vs. inverse temperature for PE1 .....	193
Figure 7.6: Schematic representation of polyethylene crystal and slip systems, ref. (28) .....	194
Figure 7.7: Ratio of $Q/\Delta H$ for PE1-4 and PE8.....	196

Figure 7.8: Q/ $\Delta$ H ratio and Mw for PE1-4 and PE8 .....	198
Figure 7.9: Q/ $\Delta$ H ratio vs. percentage crystallinity for PE1-4 and PE8 .....	199
Figure 7.10: Q/ $\Delta$ H ratio and SCB per 1000C for PE1-4 and PE8 .....	200
Figure 7.11: Material resistance to ESC based on average n value and individual n value .....	204
Figure 7.12: Log ESCR vs. material resistance to ESC for PE1-4 and PE8.....	205
Figure 7.13: Log ESCR vs. material resistance calculated based on Q = 90kJ/mol (9) for PE1-4 and PE8 .....	206
Figure 7.14: Relationship between Q, C and SCB content of polyethylene for PE1-4 and PE8 (the lines are only a visual guide to the eye).....	207
Figure 8.1: MW-SCB combination for high ESCR polyethylene .....	218
Figure 8.2: MW-SCB combination for low ESCR polyethylene .....	219
Figure 8.3: Flow chart for selecting resins with better ESCR .....	221
Figure 9.1: Flow chart for selecting resins with better ESCR in relation to thesis chapters .....	229
Figure A.1: PE1 MWD and “SCBD” .....	240
Figure A.2: PE2 MWD and “SCBD” .....	241
Figure A.3: PE3 MWD and “SCBD” .....	241
Figure A.4: PE4 MWD and “SCBD” .....	242
Figure A.5: PE5 MWD and “SCBD” .....	242
Figure A.6: PE6 MWD and “SCBD” .....	243
Figure A.7: PE7 MWD and “SCBD” .....	243
Figure A.8: PE8 MWD and “SCBD” .....	244
Figure A.9: PE9 MWD and “SCBD” .....	244
Figure A.10: PE10 MWD and “SCBD” .....	245

Figure A.11: Typical comonomer composition/SCB distribution for (a) polyethylene produced using Ziegler-Natta catalyst, (b) polyethylene produced using Ziegler-Natta catalyst in tandem process. From ref. (2).....	246
Figure A.12: FTIR nominal signal to noise ratio vs. polydispersity (PDI). From ref. (1) .....	247
Figure B.1: CRYSTAF result for PE10 .....	251
Figure B.2: CRYSTAF results with independent replication for PE10.....	251
Figure B.3: Weight percentage of chains crystallized in 75-85°C range and ESCR of resins .....	254
Figure B.4: ESCR vs. weight percentage of crystallized chains at different temperature ranges, PE1-4 (75-85°C), PE7-10 (85-90°C) .....	255
Figure C.1: Graphic presentation of Kelvin elements in series. From ref. (5) .....	261
Figure C.2: Creep compliance curves for PE1. From refs. (5, 6) .....	263
Figure C.3: Joint confidence plot for B1 and B2, PE1 7.14 MPa.....	267
Figure C.4: Joint confidence plot for B1 and B3, PE1 7.14 MPa.....	267
Figure C.5: Joint confidence plot for B2 and B3, PE1 7.14 MPa.....	268
Figure C.6: Joint confidence plot for B0 and B1, PE1 at 7.14 MPa (all-inclusive approach) .....	271
Figure C.7: Joint confidence plot for B0 and B2, PE1 at 7.14 MPa, (all-inclusive approach) .....	271
Figure C.8: Joint confidence plot for B0 and B3, PE1 at 7.14 MPa, (all-inclusive approach) .....	272
Figure C.9: Joint confidence plot for B1 and B2. PE1 at 7.14 MPa (all-inclusive approach).....	272
Figure C.10: Joint confidence plot for B1 and B3, PE1 at 7.14 MPa, (all-inclusive approach).....	273
Figure C.11: Joint confidence plot for B2 and B3, PE1 at 7.14 MPa (all-inclusive approach) .....	273

Figure E.1: Material resistance to ESC based on  $Q = 90 \text{ kJ/mol}$  (2) and  $Q = \Delta H$  for PE7-10 ..... 282

# **CHAPTER 1 INTRODUCTION AND OBJECTIVES**

## **1.1 Preamble for Setting the Scene**

Polyethylene (PE) is a consumer polymer which comes in a variety of forms, including polymer films, polymer containers, pipes, toys and others. Compared to traditional structural materials, polyethylene has the advantage of being lighter in weight, which reduces both transportation and installation costs; PE does not rust like metal and thus can be used in applications where rust would be a problem. Due to the aforementioned reasons, uses of polyethylene in pipe and other structural applications are widespread. However, creep rupture (slow crack growth) of polyethylene can result in brittle break of the material without any visible warning, thus posting a serious problem for PE in structural applications.

The slow crack growth (SCG) failure of polyethylene can be accelerated when the polymer is exposed to an aggressive environment, such as polar solvents and/or ultra violet (UV) rays. By convention, slow crack growth failure in the presence of an aggressive environment is commonly referred to as environmental stress cracking (ESC). Premature failure of PE structures due to ESC is related to both material and labor high costs, because of the need to replace failed structures before their expected lifespan (or conduct remediation in complex structural geometries). For example, PE pipes (underground pipe networks or gas pipelines) are expected to have a service life of fifty years or more, yet many of these PE pipes are known to fail in as little time as one year due to environmental stress cracking.

Environmental stress cracking of polymers has been studied by researchers worldwide. Huang and Brown (1) are probably the first who clarified and developed further the theory of tie-molecules, referring to the long polymer chains capable of crystallizing into two separate lamellae, thus helping to hold lamellae together and further reducing the rate of crazing that leads to slow crack growth. Huang and Brown (1) proposed a probabilistic method for estimating tie-molecule density in a polymer based on the molecular weight (MW) of the material. They found that polyethylene with higher tie-molecule density has higher slow crack growth resistance. Based on the idea of inter-lamellar links, polyethylene with higher comonomer content is found to have higher environmental stress cracking resistance (ESCR). Higher comonomer content in PE leads to the formation of higher levels of short chain branching (SCB). Short chain branches are believed to improve slow crack growth resistance of polyethylene by preventing chain slippage from the crystalline phase (1-3). Recent development of pipe resins with higher short chain branch content in the high molecular weight end of the molecular weight distribution has led to a significant increase in the ESCR of polyethylene pipes (4).

In the last twenty years or so, research on environmental stress cracking of polyethylene has focused nearly solely on the idea (theory) of tie-molecules. The possibility of any other sources of inter-lamellar links has generally been overlooked. The influences of molecular weight and short chain branch content were studied independently of one another with polyethylene samples (resins) over a relatively narrow property range. In

addition, ESCR values of polyethylene materials were compared on a relative basis, and no efforts were made to relate ESCR to a more reliable (and more fundamental) property of the resin. As a result, methods for predicting the overall ESCR lifetime of resins (something that the piping and construction industry, in general, would find very practical and interesting) are non-existent.

A collaborative effort between the disciplines of chemical and civil engineering was initiated with this thesis in order to study environmental stress cracking resistance of polyethylene. Civil engineering has expertise in structural mechanics, while chemical engineering has more experience with (micro)molecular properties of a polymer. The combination of skills from both disciplines has the potential to offer new insights into the environmental stress cracking resistance behaviour of polyethylene with a fresh perspective without prior biases and preferred theories. The current thesis (part of a long-term collaborative project) focuses more on (micro)molecular properties and their relationship to ESCR. The objectives for this thesis were set as follows:

1. Explore alternative methods for evaluating environmental stress cracking resistance (ESCR) of polyethylene materials in a timely and reliable manner.
2. Examine and revisit the relationships between (micro)molecular properties and mechanical behaviour of polyethylene over as wide a property range as possible (i.e. large range of molecular weight and molecular weight distributions).
3. Investigate sources of inter-lamellar links in addition to tie-molecules that enhance the ESCR of polyethylene.

4. Explore the possibility of developing a procedure for quantitative estimation of the environmental stress cracking lifetime of polyethylene material based on short term ESCR tests.
5. Finally, develop practical prescriptions for relating fundamental molecular properties to environmental stress cracking resistance of polyethylene.

## 1.2 Thesis Outline

This thesis is organized into nine chapters. The role of these chapters is as follows:

*Chapter 2* sets the theme by introducing general background information on physical-chemical material properties of polyethylene. In essence, what was the state of the art on ESCR of polyethylene at the beginning of this project?

*Chapter 3* describes experimental methods used in the thesis. This chapter is organized into three major categories. The first category contains tests for (micro)molecular properties of the polymer, the second category lists methods for rheological characterization, and the last category contains tests for mechanical properties. Methods and procedures for each experimental technique are briefly presented.

*Chapter 4* proposes a modification of a tensile test as an alternative way to evaluate the environmental stress cracking resistance of polyethylene. The tensile strain hardening test procedure developed is more practical compared to previously suggested tensile methods. The ESCR ranking of resins based on tensile strain hardening is compared to results obtained from the conventional ESCR test (the notched constant load

test (NCLT)). Our results show that strain hardening can be used to rank ESCR of high density polyethylene (HDPE) in a reliable fashion. In addition, the use of the natural draw ratio (NDR) as ESCR ranking indicator is examined. The reliability of any experimental test is always of importance, therefore, the reproducibility and precision of the proposed tensile method are investigated and established using statistical methods, probably for the first time in the history of such tests in the literature.

*Chapter 5* is divided into two major sections. In the first part, the connection between tensile strain hardening and ESCR of polyethylene is explained based on the concept of physical chain entanglements in the polymer. Inter-lamellar links are important structural properties affecting ESCR of polyethylene. Most ESCR research has previously focused on bridging-tie-molecules as the main source of inter-lamellar connections. In this chapter, we demonstrate that physical chain entanglements also contribute to the formation of inter-lamellar linkages. Since chain entanglements cannot be directly measured, effects of entanglements are studied through network mobility of high density polyethylene using rheological methods. In the second part of this chapter, tensile strain hardening experimental results are compared to independently obtained micro-mechanical modeling predictions for polyethylene in order to support further the observed relationship between physical chain entanglements and strain hardening behaviour of polyethylene. By combining experimental observations and modeling results, the presence of physical chain entanglements in the amorphous phase was demonstrated to be the controlling factor in the strain hardening behaviour of polyethylene.

*Chapter 6* concentrates on the influence of the crystalline phase on environmental stress cracking resistance of polyethylene. Studies of the effect of inter-lamellar linkages on ESCR of polyethylene have traditionally focused on changes in the amorphous phase. Since polyethylene is a semicrystalline polymer, the crystalline phase also plays an important role in the mechanical behaviour of the polymer. In this chapter, percentage crystallinity and lamella thickness of resins were studied to determine their effect on ESCR. Since polyethylene lamellae are three dimensional crystals, the study of the crystalline phase effect on ESCR was extended to investigating the lateral surface characteristics of the lamella. The investigation was carried out from the point of phase interconnectivity between the crystalline and amorphous phases.

*Chapter 7* presents an attempt to develop an ESCR lifetime model for polyethylene. The NCLT and other tests for determining ESCR of polyethylene can only give “good” or “bad” evaluations on a relative basis. In this chapter, a method is presented to give environmental stress cracking lifetime estimates of resins based on short-term ESCR tests, such as the NCLT test. The possible duality between environmental stress crack growth activation energy and the  $\alpha$ -relaxation energy of polyethylene is discussed.

*Chapter 8* offers a “bird’s eye view” of the relationships between molecular properties and environmental stress cracking resistance of polyethylene in the form of

heuristics based on experimental observations. Practical prescriptions are presented for production and selection of PE resins with “better” (higher) ESCR.

Finally, *Chapter 9* presents the main conclusions from the current work, based on ten PE resins covering a relatively wide range of property characteristics. In this chapter, significant research contributions from this thesis and recommendations for future research steps are also discussed.

Several appendices complement the material in the chapters of this thesis. These appendices represent “offsprings” of the research covered in the chapters and address peripheral but closely related issues (e.g., determination of short chain branch distribution, use of crystallization analysis fractionation as an alternative way to evaluate environmental stress cracking resistance of polyethylene, parameter estimation with creep data, etc.). A data CD containing relevant raw data files, such as modulus versus frequency plots from the rheology experiments, which are numerous and would add unnecessarily too many pages in this document, is available from Prof. Alexander Penlidis.

### 1.3 References

1. Huang, Y. & Brown, N. (1988), "The effect of molecular weight on slow crack growth in linear polyethylene homopolymers", *Journal of Materials Science*, vol. 23, pp. 3648-3655.
2. Janimak, J. J. & Stevens, G. C. (2001), "Inter-relationships between tie-molecule concentration, molecular characteristics and mechanical properties in metallocene catalysed medium density polyethylenes", *Journal of Materials Science*, vol. 36, no. 8, pp. 1879-1884.
3. Yeh, J. T., Chen, C. Y., & Hong, H. S. (1994), "Static fatigue behaviour of linear low-density polyethylene", *Journal of Materials Science*, vol. 29, pp. 4104-4112.
4. Scheirs, J., Böhm, L. L., Boot, J. C., & Leever, P. S. (1996), "PE100 resins for pipe applications: continuing the development into the 21st century", *Trends in Polymer Science*, vol. 4, no. 12, pp. 408-415.

## CHAPTER 2 GENERAL LITERATURE BACKGROUND

### 2.1 Molecular Properties of Polyethylene

#### 2.1.1 Microstructure

Polyethylene is a chemically simple polymer with the basic repeating unit ( $-\text{CH}_2-\text{CH}_2-$ ). It is a semicrystalline polymeric material with crystalline and amorphous phases. The crystalline lamellae provide polyethylene with structural integrity, while the amorphous parts provide polyethylene with its elastic properties (1). The semicrystalline nature of polyethylene allowed it to become one of the most widely used polymers worldwide.

In dilute solutions, it is possible to obtain polyethylene single crystals with nearly one hundred percent crystallinity (2). In practical applications polyethylene is usually crystallized from a melt. Melt-crystallized polyethylene has a spherulite morphology, where lamellae made up of spherulites are embedded in a matrix of amorphous material (3-5). The spherulites are made up of thin flat lamellae as shown in Figure 2.1. The structure of lamella generally consists of regular chain-folding arrangements with the molecular chains (or “stems”) perpendicularly aligned to the lateral lamellar surfaces (2, 6) (Figure 2.1 and Figure 2.2a). The regular chain-folding growth of a lamella results in crystals with lateral direction dimensions (1-50  $\mu\text{m}$ ) being much larger than their thickness (2-25 nm) (2, 6-8). In addition to the chain folding model, Flory and Yoon (9) proposed another type of lamella structure where a growing crystal feeds on whatever chains available and forms an arrangement as shown in Figure 2.2b. Work has shown

that both type of crystalline structures exist in melt-crystallized polyethylene (2, 8). For polyethylene studies, the regularly folded chain model is more widely used than the non-regularly folded chain model. At present, most of the work on polyethylene fracture mechanics is based on the regular chain folding model.

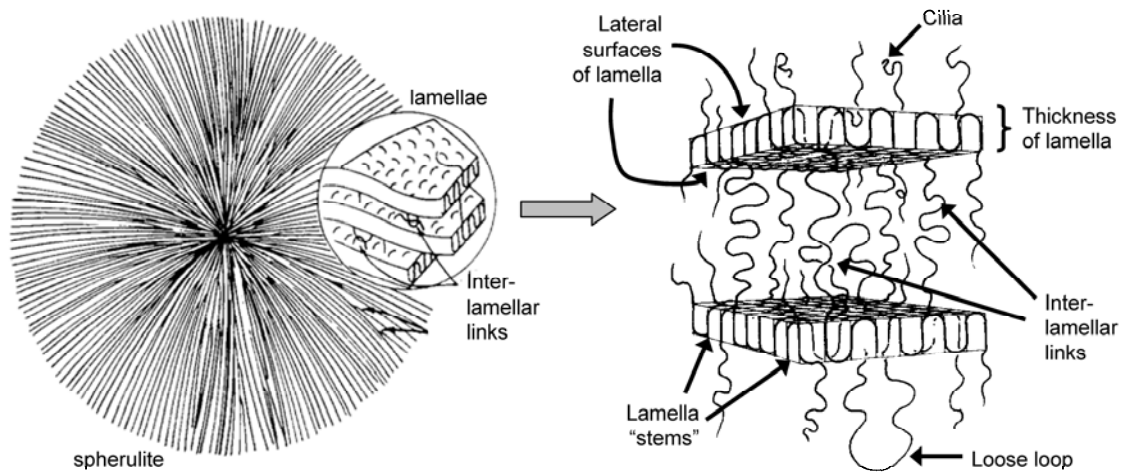


**Figure 2.1:** Schematic illustration of spherulite, lamella, and amorphous phase structures. Adapted from refs. (10, 11)

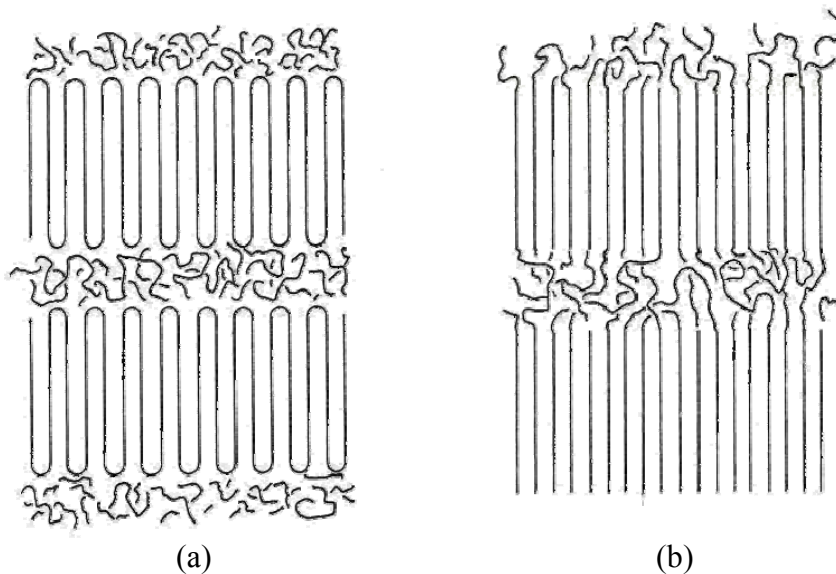


**Figure 2.2:** Structures of lamella; (a) the regularly folded chain model for semi-crystalline polymer; (b) non-regularly folded chain model for semi-crystalline polymer. From ref. (9)

For the amorphous phase of polyethylene, there are three types of inter-crystalline material, as illustrated in Figure 2.1. The first type, *cilia*, begins as a crystalline chain and ends as an amorphous chain. The second type begins and ends in a lamella with its mid-section in the amorphous phase, thus forming a *loose loop*. The third type consists of inter-lamellar links that connect two adjacent lamellae. There are two types of inter-lamellar links; the first are *tie-molecules* that are chains crystallized in two or more lamellae at the same time. The second type of inter-lamellar links consists of physical chain entanglements that can be made up by the entanglements of *cilia*, loose loops and even tie-molecules.

### **2.1.2 Types of Polyethylene**

As mentioned before, different types of polyethylene all have the same basic repeating unit (-CH<sub>2</sub> – CH<sub>2</sub> -). However, due to structure differences they have different properties and applications. Major properties that differentiate the various types of polyethylene are molecular weight (MW), molecular weight distribution (MWD), density, percentage crystallinity and degree of long chain and short chain branching.

Molecular weights and molecular weight distribution are main factors that affect processability and mechanical properties of polyethylene. Broad MWD material is easier to process due to the presence of shorter chains that act as “lubricant”. Polyethylene can have linear and branched chains. Short chain branching (SCB) can be introduced into polyethylene through the use of comonomer (like 1-hexene). Short chain branches

interfere with the formation of lamellae, and therefore affect crystallinity and density of semicrystalline polymer (12). Polyethylenes are classified into four density categories according to ASTM standards, as shown in Table 2.1. Figure 2.3 shows how changes in density are associated with changes in crystallinity and morphology of polyethylene. Linear low density polyethylene (LLDPE) and HDPE have a lamellar and spherulitic morphology, while plastomer and elastomer have bundle-like crystals embedded in amorphous material. An increase in crystallinity, hence an increase in density, of polyethylene increases the stiffness and tensile yield strength of the material (13). In pipe applications, high density polyethylene (HDPE) is the preferred choice (14) because of the high strength of the material. A further discussion about polyethylene for pipe applications will be presented in section 2.3.

**Table 2.1: Classification of polyethylene by density**

<b>PE Type</b>	<b>Density (g/cm<sup>3</sup>)</b>
Low	0.910 – 0.925
Medium	0.926 – 0.940
High	0.940 – 0.959
High density homopolymer	0.96 and above

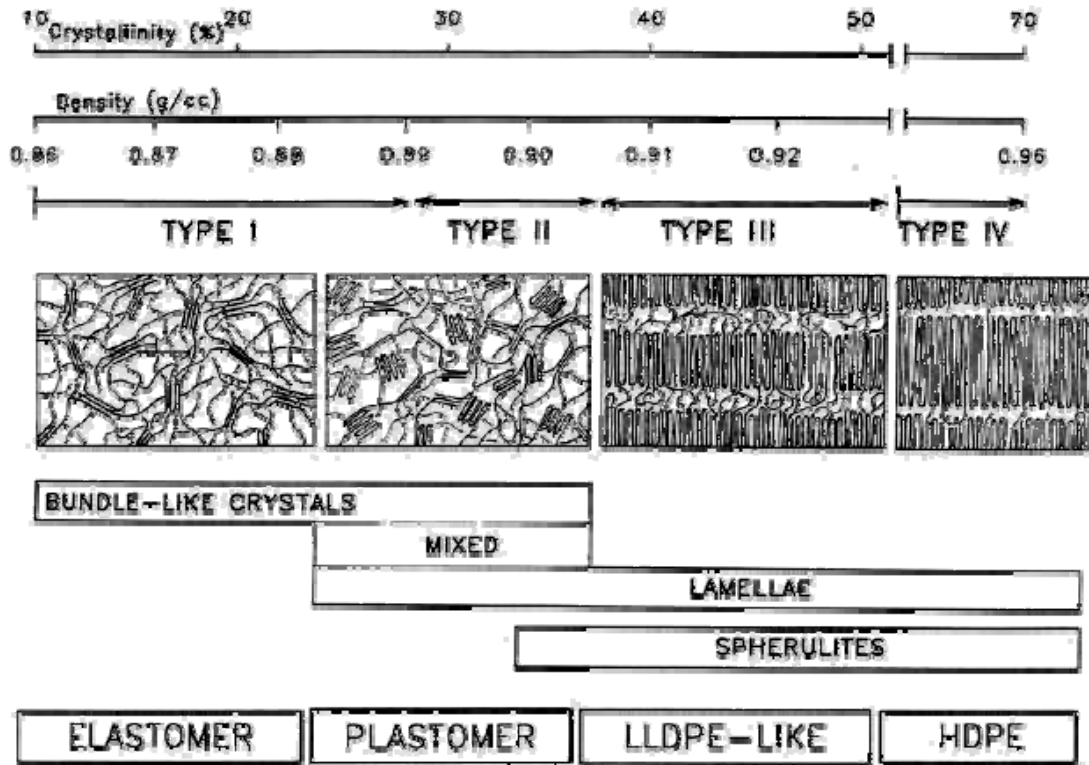


Figure 2.3: Crystal structures of polyethylene. From ref. (15)

### 2.1.3 Branch Structures

Branching in polyethylene chains affects material density and other properties (e.g. rheological properties). There are two types of branching, short chain branching (SCB), mostly due to introduction of comonomer, and long chain branching (LCB) formed from side reactions during polymerization. As illustrated in Figure 2.4, HDPE is generally linear with low SCB content. LLDPE has higher SCB content than HDPE with few or no long chain branches. Low density polyethylene (LDPE) on the other hand is known to have both high short chain branching and long chain branching contents. Presence of short chain branches interferes with formation of lamellae, hence LLDPE and LDPE with higher SCB content have lower density. Short chain branch distribution (SCBD) of

polyethylene is controlled by the type of catalyst used during the polymerization process. The influence of SCB content and SCBD on mechanical properties of polyethylene will be discussed later in section 2.2.5.2

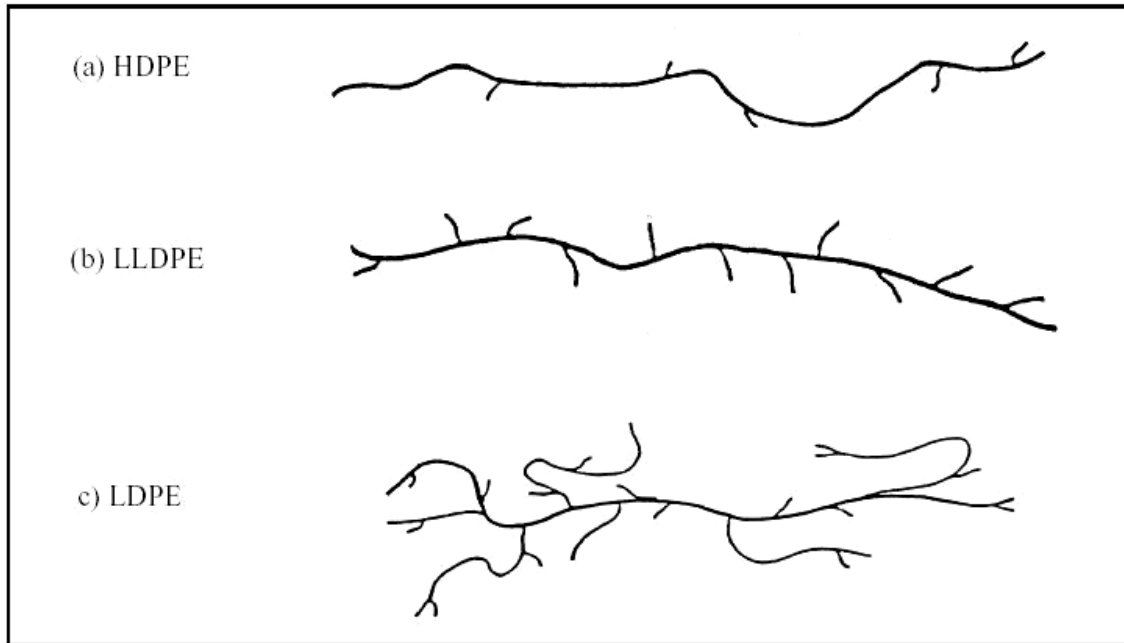


Figure 2.4: Branch structures of polyethylene. From ref. (16)

#### 2.1.4 Chain Movement and Viscoelasticity

Polyethylene is classified as a viscoelastic material, with both solid-like and liquid-like properties. With changes in temperature, mechanical behaviour of polyethylene changes due to movement of chains. In Figure 2.5, changes in the storage modulus ( $E'$ ) of polyethylene with changes in temperature are illustrated. At temperature lower than the glass transition temperature ( $T_g$ ), where only local movement of the polymer backbone and bending of side chains are possible, polyethylene behaves more like a rigid solid with high  $E'$  values. At temperature above  $T_g$ , larger scale chain movements in the amorphous

phase result in polyethylene taking on more liquid-like behaviour and the  $E'$  value decreases. At the melting temperature ( $T_m$ ), crystalline lamellae inside the polyethylene matrix start to melt, large scale chain slippage occurs and the  $E'$  value dramatically decreases (17). At temperature higher than the  $T_m$ , polyethylene loses its structural integrity and becomes a viscous melt.

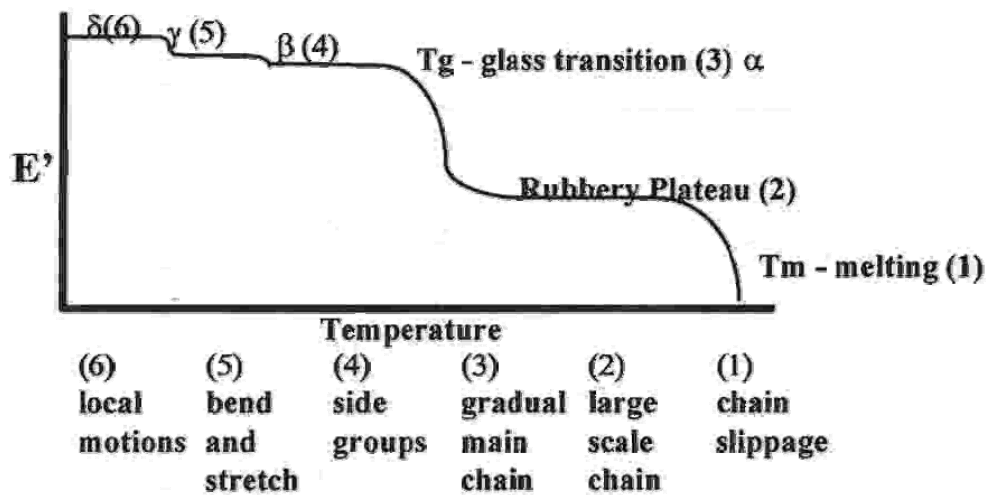
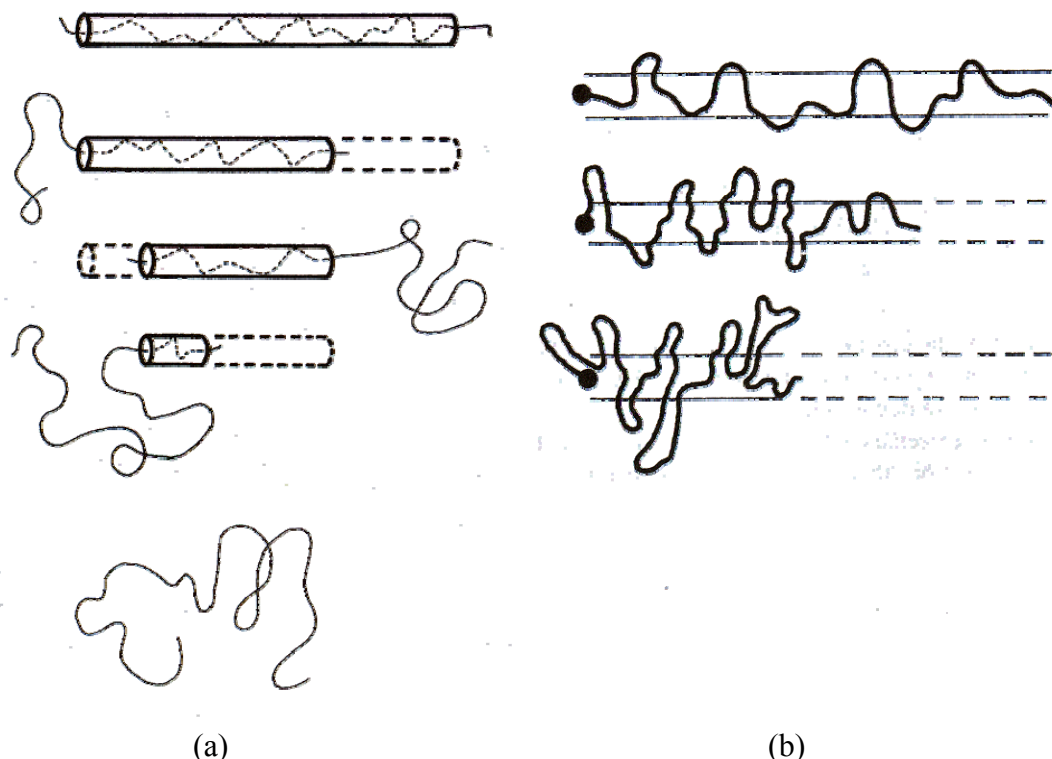


Figure 2.5: Thermal transition stages of polyethylene. From ref. (17)

In the solid state (above  $T_g$ ), creep of polymer chains influence many mechanical properties of polyethylene. Although chain movements in PE solid can take a long time due to restrictions from the crystalline phase and lower chain energy, the type of chain motion is essentially the same as that of chain motion in the melt. The movement (relaxation) of polymer chains in the melt is explained by the tube model (18). In this model, polymer chains move by reptation and primitive-path fluctuations. Reptation was first proposed by de Gennes (19) for the movement of a single long polymer chain. In reptation, the long chain moves in a snake-like motion along its own contour confined in

an imaginary tube (Figure 2.6a), and as the chain moves out of a section of the tube that section disappears. Since the chain is not anchored at either end the chain can move back and forth along the tube in both ways. Figure 2.6a illustrates the reptation movement in a straight imaginary tube; of course, in reality, the tube can bend and twist in a number of directions (20).



**Figure 2.6: (a) reptation of a polymer chain, (b) primitive-path fluctuations (21)**

For a polymer chain tethered at one end (e.g. a branch), movement by primitive-path fluctuations was proposed (22, 23). In primitive-path fluctuations the free end of the chain randomly pulls away from the end of the imaginary tube and re-relaxes into a new tube of lower energy (Figure 2.6b). When both reptation and primitive-path fluctuation occur in a polymer, the resulting chain movement is called double reptation. For a long

polymer chain, chain segments in the interior of the chain relax by reptation, while the chain ends relax by primitive-path fluctuation because it is faster than single reptation. As the MW of the polymer increases, the chain length increases as well, and the contribution to overall relaxation time by chain ends decreases (24). For high MW polymer chains, the contribution of primitive-path fluctuation becomes small enough that it may be ignored. The relaxation time of polymer is dominated by reptation of long chains, hence this explains why rheological properties of polymer are strongly influenced by the longest chains in the system (25).

## **2.2 Mechanical Behaviour of Polyethylene**

### **2.2.1 Ductile Failure**

Ductile failure is a type of failure that generally occurs over a short amount of time at high stress levels. At the macroscopic level, ductile tensile failure results in observation of visible deformation (necking) in the polymer sample. For polyethylene, tensile ductile behaviour is influenced by the semicrystalline nature of the material. In Figure 2.7, the stress-strain curve for tensile ductile deformation is accompanied by illustrations of what occurs within the polyethylene matrix (material) at the micro scale. At the beginning, before the yield point, no visible deformation of material is observed and the load is mainly carried by rigid crystalline lamellae. As strain increases, stress increases as well and yield occurs. During the time period between the point of yield and the onset of strain hardening, the load on the test sample remains at a relatively constant level. The deformation in this region is due to a combination of amorphous phase rearranging itself and crystal lamellae slipping past each other, but each individual crystal itself is still

intact. Between strain values of 0.5 and 1.0 in Figure 2.7, increasing orientation of the crystalline and the amorphous phases in the direction of drawing is seen with increasing stress-strain values. After the strain of 1.5, sharp increase in stress value with increasing in strain indicates the occurrence of strain hardening. During strain hardening, the amorphous phase has reached its full extension, and further deformation of the polymer in this stage is due to breaking and unfolding of lamellae as shown in Figure 2.7. The breaking of lamellae into smaller chunks results in the characteristic rough fibrous surface of ductile failure (11), as observed under the scanning electron microscope (SEM). As stress continues to increase with increasing strain, ultimate failure occurs and the material breaks (26).

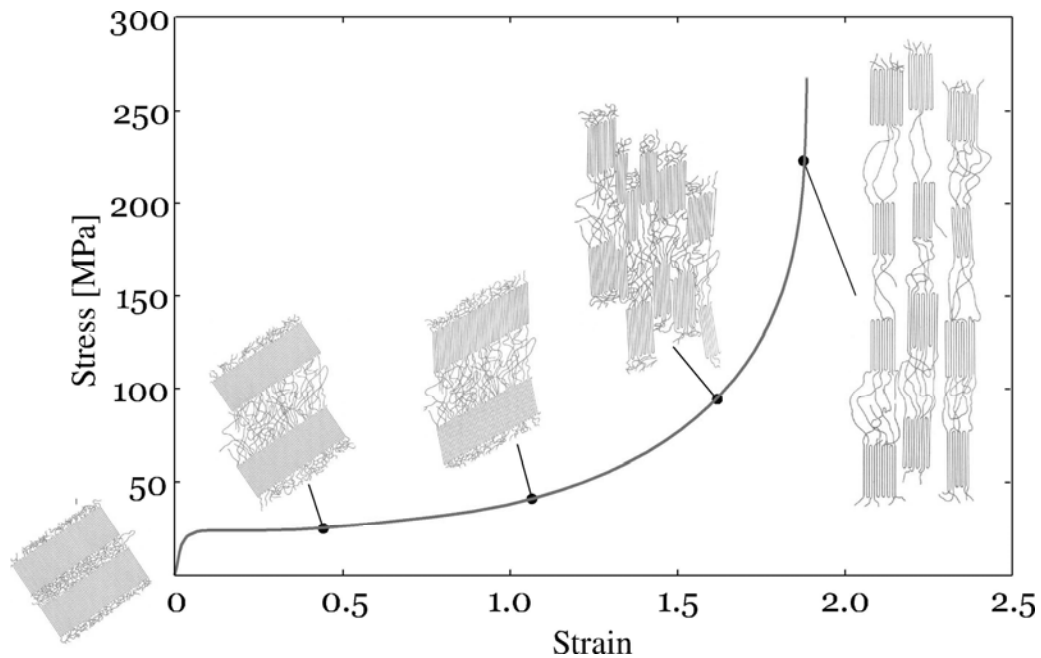
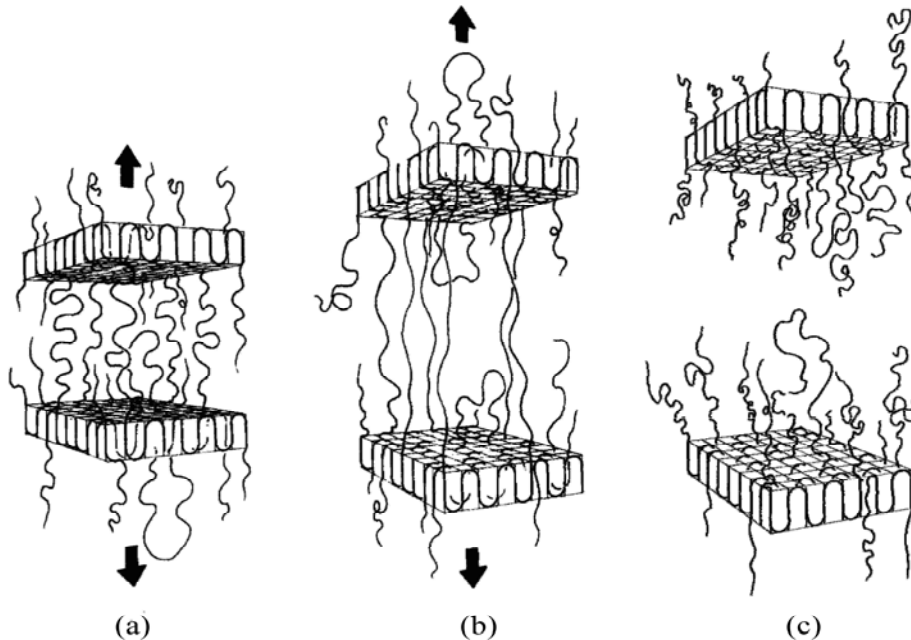


Figure 2.7: Tensile deformation of polymer. From ref. (26)

## 2.2.2 Brittle Failure

In comparison with ductile failure, a polymer that undergoes brittle failure has a clean break with little material deformation. To the naked eye, the fracture surface appears smooth. Under an SEM, it can be seen that the surface actually consists of short random pullouts (11). Brittle-type failure occurs when a low stress is applied over a long period of time. As shown in Figure 2.8 (a-b), in the initial steps of brittle fracture, the amorphous materials start to stretch under stress. Due to the longer time period, the inter-lamellar links under stress start to relax and untangle from each other until the number of remaining linkages becomes very low. When the few remaining inter-lamellar links are stretched to their limit, they are unable to pull apart lamellae, consequently, a brittle fracture of the polymer occurs, as illustrated in Figure 2.8 (c).



**Figure 2.8: Stages of Brittle Fracture; (a) lamellae start to pull away, (b) the tie-molecules are stretched tight, (c) clean break of lamellae. From ref. (11)**

### **2.2.3 Strain Hardening**

Strain hardening is a phenomenon observed in fully drawn (and cold-drawing of) polymers (1). The cause of increasing stress during strain hardening is reported to be due to molecular alignment of polymer chains that result in increasing strength of the material. This type of chain alignment can be seen as a form of strain-induced crystallization (1) and increasing crystallinity is known to increase tensile strength of polyethylene.

Onset of strain hardening occurs when the amorphous phase of polyethylene is stretched to its limiting extensibility (27), as shown in section 2.2.1. The extensibility of a polymer network is affected by the number of load-bearing junction points in the system. For crosslinked polymer, these junction points consist of crosslinks and chain entanglements. For semi-crystalline polymer, such as high density polyethylene, the network junction points are formed by physical entanglements and crystalline structures. However, the junction points formed from crystalline structures are temporary in cold-drawing cases where the drawing ratio is high. In high strain deformations like strain hardening, drastic morphology reorganization occurs for semi-crystalline polymers and the crystalline structure is destroyed (28-30). Hence, the role of a junction point falls on physical chain entanglements alone. Therefore, the number of chain entanglements affects strain hardening behaviour of polyethylene significantly.

### **2.2.4 Environmental Stress Cracking**

Environmental stress cracking (ESC) is the stress failure of a polymer when subjected to an aggressive environment, such as soapy water. It is a frequently observed problem in

pipe networks and other polymer structure applications (31). In most cases, the type of fracture associated with ESC is characterized by clean cracks, thus indicating a brittle fracture mechanism. Any cracking of polymer due to an aggressive environment can be called environmental stress cracking, such as degradation of polymer due to exposure to UV light, ultimately leading to mechanical failure of the material. However, most of the time ESC refers to stress cracking of polymer due to an active environment without any chemical alteration of the material; therefore, a purely physical process. This is the type of ESC studied in this project. Polar solvents such as alcohols, detergents, silicone oils and even emulsified water are examples of aggressive environments for polyethylene.

In normal conditions stress cracking of polyethylene can take a long time. Lagarón *et al.* (32, 33) conducted experiments on the effect of an active environment on the structure of polyethylene. They showed that surfactants, a commercial detergent in this case, reduce the free surface energy of the fibrils and prevent the fibrils from packing into a dense structure, thus leading to craze stabilization. Ultimately, this leads to the formation of cracks and the failure of the polymer. The exact mechanism of how Igepal (a common surfactant) facilitates slow crack growth (SCG) is not clear. Ward *et al.* (34) proposed that the long Igepal molecules align themselves with tie-molecules in the fibrils, thus reducing the frictional stress as tie-molecules disentangle from crystals. As tie-molecules become untangled more easily, the environmental stress cracking resistance (ESCR) of the polymer decreases. It is generally accepted that an active environment can act as ‘lubrication’ for chain disentanglement (34, 35), thus resulting in accelerated slow crack growth of polyethylene.

Research has shown (34) that the initial rate of ESC for polyethylene samples in Igepal solution is the same as for samples in air. It was only after a certain time period, after Igepal had time to diffuse into the crystalline region of the polymer that the cracking process was accelerated. The study in ref. (34) indicates that the initial rate of ESC is controlled by diffusional limitations of the active ingredient. The ESCR of polyethylene can be increased if diffusion of the aggressive agent is limited.

### **2.2.5 Factors Affecting ESCR of HDPE**

Environmental stress cracking occurs by a brittle fracture mechanism. It was explained previously that brittle fracture is believed to be caused by disentanglement of inter-lamellar links. The number and type of these tie-molecules play an important role on environmental stress cracking resistance of polyethylene.

There are two types of inter-lamellar linkages. The first kind is what is called bridging tie-molecules. The two ends of these molecules crystallize in two different lamellae, thus connecting them. Bridging tie-molecules have strength due to covalent bonds. The other type of inter-lamellar link is made of entanglements of loose loops and cilia and are believed to be held together by van der Waals forces (11). From this point on, only bridging tie-molecules will be referred to as tie-molecules. All other types of inter-lamellar linkages will be referred to as entanglements.

### 2.2.5.1 Tie-Molecules

The concept of tie-molecules was first proposed by Brown and Ward (36) in their study of brittle fracture of polyethylene. Brown and Ward (36) theorized that there are two types of load-bearing molecular bonds in the amorphous phase of polyethylene. The first type consists of the covalent bonds of bridging tie-molecules, whereas the second type involves van der Waals bonds between amorphous chains. The brittle fracture stress ( $\sigma_F$ ) (Equation 2.1) of a polymer is therefore a sum of the stresses carried by both type of bonds.

$$\sigma_F = \frac{1}{C} [f_T \cdot \sigma_T + (1 - f_T) \sigma_{vw}] \quad (2.1)$$

$\sigma_T$  is ideal stresses for the tie-molecules,  $\sigma_{vw}$  -ideal stresses for van der Waals bonds  
 $f_T$  is fraction of the inter-lamellar area covered by tie-molecules,  $C$  -stress concentration

Based on work by Brown and Ward (36), Huang and Brown (37) theorized that a polymer chain must have an end-to-end distance ( $r$ , radius of gyration) larger than the thickness of two crystalline lamella layers in order to crystallize in two lamellae and hence become a tie-molecule (see again Figures 2.1 and 2.2). The probability of a chain with end-to-end distance of length  $r$  is given by Equation 2.2, where  $a$  and  $b$  are parameters.

$$p(r) = ar^2 \exp(-b^2 r^2) \quad (2.2)$$

Therefore the probability of polymer chains becoming tie-molecules is given by Equation 2.3. The numerator of the equation is the probability of chains with end-to-end distance larger than twice the lamella thickness ( $L$  is the thickness of the lamella layer), and the denominator is the probability of chains with end-to-end distance of all lengths. The parameter  $a$  in Equation 2.2 is cancelled out and  $b$  is analytically found to be  $3/2 r^2$ . Huang and Brown (37) considered that there are only three types of amorphous phase material, namely, cilia, loose loop, and tie-molecule (see Figure 2.1), and any chain with end-to-end distance greater than  $2L$  has an equal chance of taking on any one of the three amorphous phase configurations, therefore, a chain only has  $1/3$  chance of becoming a tie-molecule.

$$P = \frac{\int_{2L}^{\infty} r^2 \exp(-b^2 r^2) dr}{3 \int_0^{\infty} r^2 \exp(-b^2 r^2) dr} \quad (2.3)$$

The radius of gyration of a molecule is a function of its molecular weight. Based on probability theory and (empirical) experimental observations, Huang and Brown (37) developed Equation 2.4 to account for the fraction of the area of the amorphous region occupied by bridging tie-molecules as a function of weight-average molecular weight ( $M_w$ ) of the polymer, as follows:

$$f_T = 4 \times 10^{-8} (M_w - 18000) \quad (2.4)$$

Equation 2.4 points out the importance of molecular weight in influencing environmental stress cracking resistance of a polymer. The value 18000 in Equation 2.4 is a critical molecular weight value Huang and Brown (37) observed for tie-molecule formation. Below a molecular weight of 18000 no tie-molecules can be found. Other research (37-39) also found that as weight-average molecular weight increases, the number of tie-molecules formed also increases. This means ESCR of polyethylene increases as weight-average molecular weight increases, since the tie-molecule concentration increases.

The Huang and Brown model (37) gave a good explanation for molecular weight effects on ESCR of polyethylene. In the last twenty years, most studies on environmental stress cracking resistance of polyethylene have thus focused solely on the effect of tie-molecules. However, Huang and Brown's theory (37) could not account for the higher ESCR of polyethylene with high comonomer content in the high molecular weight end of the molecular weight distribution. In addition, even though van der Waals bonds are much weaker than covalent bonds, Brown and Ward (36) felt they should not be ignored. Other research in the last ten to twenty years also speculated that in addition to tie-molecules, other inter-lamellar links (i.e. chain entanglements) could contribute to the overall environmental stress cracking resistance of polyethylene (39, 40).

#### 2.2.5.2 Short Chain Branching

Short chain branching (SCB) affects polymer properties by encouraging chain entanglements, at the same time reducing material density. Research (41, 42) has shown that when SCB content increases from 0 to 4.6 butyls/1000 carbon atoms, the observed

rate of slow crack growth decreases by a factor of  $10^4$ . Janimak and Stevens (43) demonstrated the relationship between short chain branching and tie-molecule density. They charted their results with data from Huang and Brown (37) on a plot of tie-molecule fraction versus branch density (Figure 2.9). Both sets of data showed an increase in tie-molecule fraction with an increase in SCB. In addition to the number of SCB, the length of the SCB also has an effect on ESCR of polyethylene. Work done by Yeh et al. (44) found that ESCR of polyethylene increased dramatically as SCB length increased from 2 to 6 carbon atoms. The reason for this is believed to be the increasing sliding resistance of the chain with longer SCB branches.

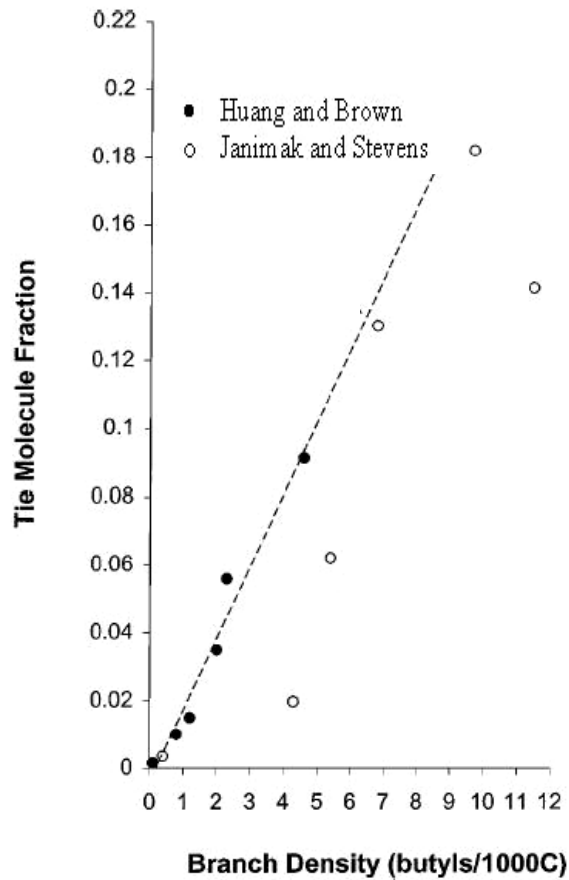
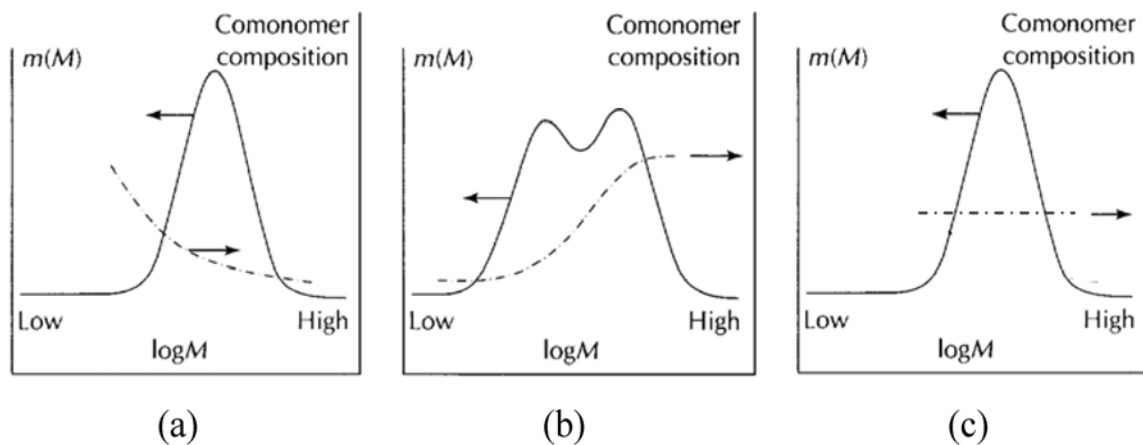


Figure 2.9: Tie-molecule concentration as a function of short chain branching. From ref. (43)

The type of catalyst used in polymerization affects short chain branch distribution (SCBD) in polyethylene. Polyethylene produced using Ziegler-Natta catalysts is known to have higher SCB content in the low molecular weight end of the MWD, as shown in Figure 2.10a. Use of Ziegler-Natta catalysts in tandem polymerization reactors on the other hand can produce PE with more short chain branches in the high molecular weight end of the MWD (Figure 2.10b) (14), while these polyethylenes also tend to have a bimodal MWD. Investigations on metallocene catalyst have shown that short chain branches are evenly distributed across the MWD as illustrated in Figure 2.10c (40, 45, 46). For metallocene catalyzed PE and tandem polymerized PE, presence of SCB in higher MW chains results in greater tie-molecule density and thus in a greater disruption of the regular chain folding mechanism for lamellae formation. Hence these two types of polyethylene would in general have higher ESCR than polyethylene produced using Ziegler-Natta catalysts in the standard process.



**Figure 2.10: Typical MWD with comonomer composition/SCB distribution for (a) polyethylene produced using Ziegler-Natta catalyst, (b) polyethylene produced using Ziegler-Natta catalyst in tandem process, (c) polyethylene produced using metallocene catalyst. From refs. (14, 46)**

SCB facilitates the formation of tie-molecules. However, SCB also disrupts the regularities of the crystallite and undermines the strength of the crystallite. Decrease in crystallinity means lower material density. Density is directly associated with the stiffness and tensile yield strength of polymer. By incorporating different amounts of model tie-molecules into linear polymers, it is found that an increase in tie-molecule density past a certain point results in loss in polymer crystallinity and tensile strength (47). For polyethylene used in structural applications, both high environmental stress cracking resistance and high mechanical strength are desirable qualities.

### **2.3 Pipe Applications and Trenchless Technology**

In the field, environmental stress cracking frequently originates from damages (or defects) on the surface of the polyethylene structure due to processing or installation. In the following section a brief introduction to trenchless piping technology is presented. This section illustrates the “harsh” conditions the polyethylene pipe is subjected to in today’s piping methods, the cause of many environmental stress cracking failures.

There are many types of trenchless piping installation and rehabilitation methods. The earliest methods were developed for installation of clay pipes where the pipes were pushed underground. With the advancement in polymeric materials, new methods were developed to utilize the flexible characteristics of polymers in pipe applications. When the existing pipe is in sound structural condition, polymer lining can be inserted into the existing structure to rehabilitate the pipe without replacement. There are three general methods of inserting linings into pipe lines, cured-in-place lining, slip-lining and close-fit

lining. Trenchless technology is also available for installing new pipe lines. Horizontal directional drilling and microtunnelling are two commonly used methods. Since this project is concerned with polyethylene pipes, which are commonly used in new installations, this serves as a brief introduction on such methods.

Horizontal directional drilling, also known as surface to surface directional drilling, can be used for construction of gravity sewer lines, water supply lines, drainage lines, etc. During drilling operation, the drilling rig is positioned at the launch pit and anchored in order to transfer the thrust and pull-back forces to the bore head. A pilot bore is first drilled by pressing the bore head through the ground following the planned pipe line route (Figure 2.11). Directional change is achieved by pressing forward the bore head without rotation until the desired change in drilling angle is achieved. After the pilot bore has been drilled, the bore head is removed from the reception pit and a reamer is fitted onto the drill string. After the pipe is mounted on the reamer, then the reamer and the pipe are drawn through the pilot bore from the reception pit to the launch pit (Figure 2.12). In addition to launch and reception pits, directional drilling also requires excavation of holding pits for drilling fluid and drilled-out materials. For long bores it is also necessary to drill relief holes to relieve the pressure from the drilling fluid. Without relief holes, high pressure can cause distortion to roads and surrounding terrain (48).

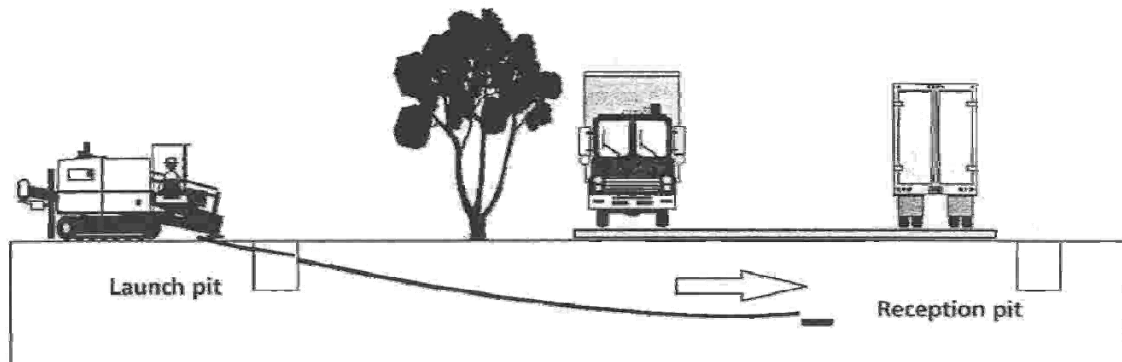


**Figure 2.11: Drilling the pilot bore. From ref. (48)**

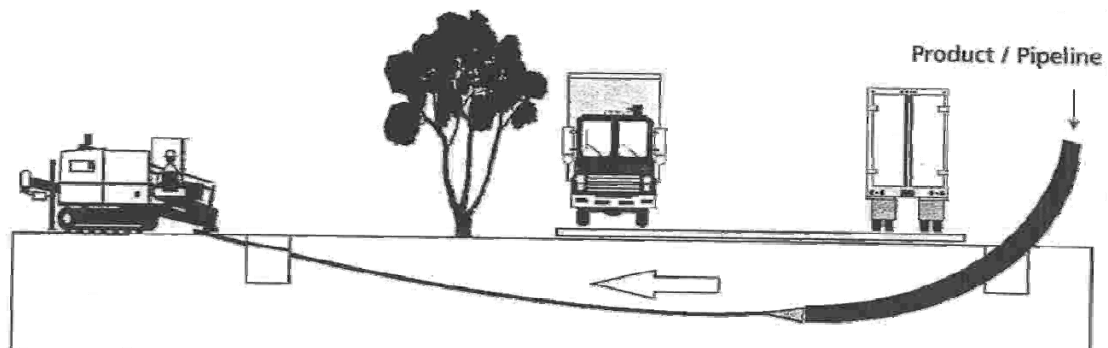


**Figure 2.12: Pulling in the pipe. From ref. (48)**

Microtunnelling (also known as pipe jacking) refers to installing pipes using hydraulic jacks from a launch pit (Figure 2.13). What distinguishes microtunnelling from conventional tunneling is the diameter of pipes installed. Microtunnelling is used for pipe where the diameters of the pipe are smaller than the permissible minimum for man entry. To jack the pipe string forward, the weight of the pipe and friction between the pipe and the tunnel need to be overcome. To reduce friction, a bentonite mixture (drilling mud) is injected into the bore tunnel. Unlike conventional pipes that are thicker at the joints, pipes used for pipe-jacking need to be uniform in diameter throughout to maintain

low friction during the installation process. The pipe face has to be completely perpendicular to the pipe axis during installation for even distribution of applied force. If force is applied asymmetrically on the pipe face, it will cause tension and possible fracture in the pipe line (48).

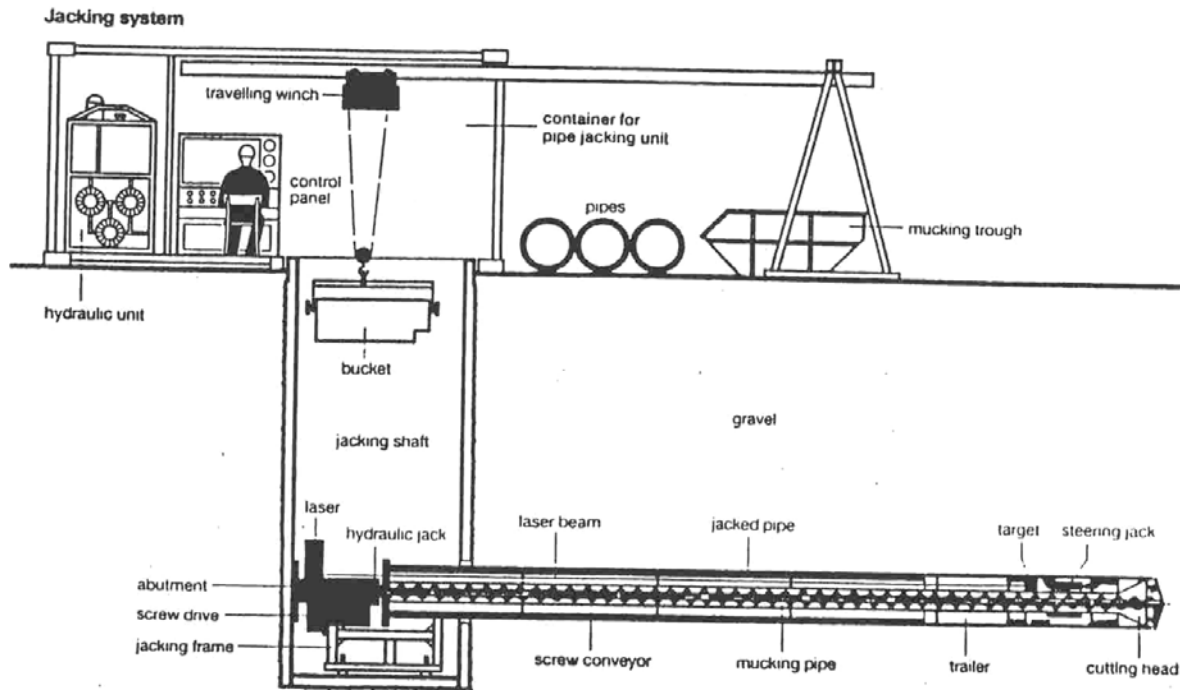


Figure 2.13: Microtunnelling system. From ref. (49)

In all the described methods for trenchless installation of polyethylene pipe, scratches and dents on the pipe are unavoidable. The exposure of these damages and defects to underground fluids, such as residue drilling fluids, can lead to environmental stress cracking failure of polyethylene pipe. Compared to other pipe installation techniques, the trenchless method subjects PE pipe to more severe conditions, thus serves as an example of an “extreme” case for industrial pipe in general. In addition, trenchless technology is

gaining increasing popularity in recent years because of the minimum disruption this method has on daily activities. With increasing use of the trenchless piping method, increasing cases of environmental stress cracking failure can be expected. To better understand the environmental stress cracking process, and hence, to offer insights for designing “better” PE pipe, is what gave the original motivation for our research.

## 2.4 References

1. Ward, I. M. (1971), *Mechanical Properties of Solid Polymers*, Wiley-Interscience, Toronto.
2. Keller, A. (1957), "A Note on Single Crystals in Polymers - Evidence for A Folded Chain Configuration", *Philosophical Magazine*, vol. 2, no. 21, pp. 1171-1175.
3. Keith, H. D. & Padden, F. J. (1959), "The Optical Behavior of Spherulites in Crystalline Polymers .1. Calculation of Theoretical Extinction Patterns in Spherulites with Twisting Crystalline Orientation", *Journal of Polymer Science*, vol. 39, no. 135, pp. 101-122.
4. Keith, H. D. & Padden, F. J. (1959), "The Optical Behavior of Spherulites in Crystalline Polymers .2. the Growth and Structure of the Spherulites", *Journal of Polymer Science*, vol. 39, no. 135, pp. 123-138.
5. Keller, A. (1959), "Investigations on banded spherulites", *Journal of Polymer Science*, vol. 39, pp. 151-173.
6. Fischer, E. W. (1957), "Step and spiral crystal growth of high polymers", *Zeitschrift fuer Naturforschung*, vol. 12a, pp. 753-754.
7. Till, P. H. (1957), "The Growth of Single Crystals of Linear Polyethylene", *Journal of Polymer Science*, vol. 24, no. 106, pp. 301-306.
8. Lin, L. & Argon, A. S. (1994), "Structure and plastic deformation of polyethylene", *Journal of Materials Science*, vol. 29, pp. 294-323.
9. Flory, P. J. & Yoon, D. Y. (1978), "Molecular morphology in semicrystalline polymers", *Nature*, vol. 272, no. 16, pp. 226-229.
10. Hoffman, J. D., Davis, G. T., & Lauritzen, J. I. Hannay, N. B.(1976), *Treatise on Solid State Chemistry*, Plenum, New York.
11. Lustiger, A. & Markham, R. L. (1983), "Importance of tie molecules in preventing polyethylene fracture under long-term loading conditions", *Polymer*, vol. 24, pp. 1647-1654.
12. Hosoda, S., Nomura, H., Gotoh, Y., & Kihara, H. (1990), "Degree of branch inclusion into the lamellar crystal for various ethylene/a-olefin copolymers", *Polymer*, vol. 31, pp. 1999-2005.
13. Lu, X., Qian, R., & Brown, N. (1995), "The Effect of Crystallinity on Fracture and Yielding of Polyethylenes", *Polymer*, vol. 36, no. 22, pp. 4239-4244.

14. Scheirs, J., Böhm, L. L., Boot, J. C., & Leever, P. S. (1996), "PE100 resins for pipe applications: continuing the development into the 21st century", *Trends in Polymer Science*, vol. 4, no. 12, pp. 408-415.
15. Bensason, S., Minick, J., Moet, A., Chum, S., Hiltner, A., & Baer, E. (1996), "Classification of homogeneous ethylene-octene copolymers based on comonomer content", *Journal of Polymer Science, Part B: Polymer Physics*, vol. 34, pp. 1301-1315.
16. Elvers, B., Hawkins, S., & Schulz, G. (1992), *Ullman's Encyclopedia of Industrial Chemistry*, 5 edn, VCH Publishers, New York.
17. Menard, K. P. (1999), *Dynamic Mechanical Analysis: A Practical Introduction*, CRC Press, New York.
18. Brochard, F. & de Gennes, P. G. (1986), "Polymer-polymer interdiffusion", *Europhysics Letters*, vol. 1, no. 5, pp. 221-224.
19. de Gennes, P. G. (1971), "Reptation of a polymer chain in the presence of fixed obstacles", *Journal of Chemical Physics*, vol. 55, no. 2, pp. 572-579.
20. Doi, M. & Edwards, S. F. (1986), *The Theory of Polymer Dynamics*, Clarendon Press, Oxford.
21. Graessley, W. W., Bhuiyan, A. L., Droscher, M., & Neuse, E. (1982), "Synthesis and degradation rheology and extrusion", *Advances in Polymer Science*, vol. 47, p. 145.
22. de Gennes, P. G. (1975), "Reptation of stars", *Journal de Physique*, vol. 36, pp. 1199-1203.
23. Doi, M. & Kuzuu, N. Y. (1980), "Nonlinear elasticity of rodlike macromolecules in condensed state", *Journal of Polymer Science, Polymer Physics Edition*, vol. 18, no. 3, pp. 409-419.
24. Larson, R. G. (1999), *The Structure and Rheology of Complex Fluids*, Oxford University Press, New York.
25. Ferry, J. D. (1980), *Viscoelastic Properties of Polymers*, 3 edn, Wiley, New York.
26. Alvarado-Contreras, J. A. (2007), *Micromechanical Modelling of Polyethylene*, PhD Thesis, Department of Civil Engineering, University of Waterloo, Waterloo, Ontario, Canada.
27. Allison, S. W., Pinnock, P. R., & Ward, I. M. (1966), "Cold drawing of poly(ethylene terephthalate)", *Polymer*, vol. 7, no. 1, pp. 66-69.

28. Hay, I. L. & Keller, A. (1965), "Polymer Deformation in Terms of Spherulites", *Kolloid-Zeitschrift and Zeitschrift fur Polymere*, vol. 204, no. 1-2, pp. 43-74.
29. Geil, P. H. (1964), "Polymer Deformation .3. Annealing of Drawn Polyethylene Single Crystals + Fibers", *Journal of Polymer Science Part A-General Papers*, vol. 2, no. 9, pp. 3835-3855.
30. Peterlin, A. (1965), "Crystalline Character in Polymers", *Journal of Polymer Science Part C-Polymer Symposium* no. 9, pp. 61-89.
31. Brostow, Witold and Corneliussen, Roger D.(1986), *Failure of plastics*, Hanser Publishers, New York.
32. Lagarón, J. M., Pastor, J. M., & Kip, B. J. (1999), "Role of an active environment of use in an environmental stress crack resistance (ESCR) test in stretched polyethylene: A vibrational spectroscopy and a SEM study", *Polymer*, vol. 40, pp. 1629-1636.
33. Lagaron, J. M., Dixon, N. M., Reed, W., Pastor, J. M., & Kip, B. J. (1999), "Morphological characterisation of the crystalline structure of cold-drawn HDPE used as a model material for the environmental stress cracking (ESC) phenomenon", *Polymer*, vol. 40, pp. 2569-2586.
34. Ward, A. L., Lu, X., Huang, Y., & Brown, N. (1991), "The mechanism of slow crack growth in polyethylene by an environmental stress cracking agent", *Polymer*, vol. 32, no. 12, pp. 2172-2178.
35. Scheirs, J. (2000), *Compositional and Failure Analysis of Polymers: A practical approach*, John Wiley & Sons, Ltd, Chichester, West Sussex, England.
36. Brown, N. & Ward, I. M. (1983), "The influence of morphology and molecular weight on ductile-brittle transitions in linear polyethylene", *Journal of Materials Science*, vol. 18, pp. 1405-1420.
37. Huang, Y. & Brown, N. (1988), "The effect of molecular weight on slow crack growth in linear polyethylene homopolymers", *Journal of Materials Science*, vol. 23, pp. 3648-3655.
38. Capaccio, G. & Ward, I. M. (1981), "Structural studies of ultrahigh-modulus linear polyethylene using nitric acid etching and gel permeation chromatography. I Determination of the crystal size distribution", *Journal of Polymer Science, Part B: Polymer Physics*, vol. 19, pp. 667-675.
39. Yeh, J. T. & Runt, J. (1991), "Fatigue crack propagation in high-density polyethylene", *Journal of Polymer Science, Part B: Polymer Physics*, vol. 29, pp. 371-388.

40. Hubert, L., David, L., Séguéla, R., Vigier, G., Corfias-Zuccalli, C., & Germain, Y. (2001), "Physical and mechanical properties of polyethylene for pipes in relation to molecular architecture. I. microstructure and crystallisation kinetics", *Journal of Applied Polymer Science*, vol. 42, pp. 8425-8434.
41. Brown, N., Lu, X., Huang, Y., Harrison, I. P., & Ishikawa, N. (1992), "The Fundamental Material Parameters That Govern Slow Crack-Growth in Linear Polyethylenes", *Plastics Rubber and Composites Processing and Applications*, vol. 17, no. 4, pp. 255-258.
42. Huang, Y. & Brown, N. (1990), "The dependence of butyl branch density on slow crack growth in polyethylene: kinetics", *Journal of Polymer Science, Part B: Polymer Physics*, vol. 28, pp. 2007-2021.
43. Janimak, J. J. & Stevens, G. C. (2001), "Inter-relationships between tie-molecule concentration, molecular characteristics and mechanical properties in metallocene catalysed medium density polyethylenes", *Journal of Materials Science*, vol. 36, no. 8, pp. 1879-1884.
44. Yeh, J. T., Chen, C. Y., & Hong, H. S. (1994), "Static fatigue behaviour of linear low-density polyethylene", *Journal of Materials Science*, vol. 29, pp. 4104-4112.
45. Gaucher-Miri, V., Elkoun, S., & Séguéla, R. (1997), "On the plastic behaviour of homogeneous ethylene copolymers compared with heterogeneous copolymers", *Polymer Engineering and Science*, vol. 37, no. 10, pp. 1672-1683.
46. DesLauriers, P. J. (2003), "Measuring compositional heterogeneity in polyolefins using size-exclusion chromatography/Fourier transform infrared spectroscopy", *American Chemical Society (ACS) Symposium Series*, vol. 893, pp. 210-229.
47. Miniely, S. (2001), *Environmental stress cracking resistance in semi-crystalline polyolefins*, M.A.Sc., Department of Chemical Engineering, University of Waterloo, Waterloo, Ontario, Canada.
48. *No-Dig Handbook*, (2002), International Society of Trenchless Technology.
49. Trenchless technologies. (1996), Centre for Advancement of Trenchless Technologies, Institute of Trenchless Technology Annual Report, University of Waterloo, Waterloo, Ontario, Canada.

## CHAPTER 3 EXPERIMENTAL METHODS

### 3.1 Tests for (Micro)Molecular Properties

#### 3.1.1 Differential Scanning Calorimetry (DSC)

Thermal properties of a material can give insights into its molecular structure. For example, a crystalline material will have greater latent heat of fusion than an amorphous material. Differential scanning calorimetry (DSC) is a thermoanalytical technique often used for studying phase transitions of polymers. DSC can also be used to study curing of thermoset polymers, as well as heat flow of polymerization processes (1).

In DSC experiments, a material sample is heated or cooled with a reference material of known heat capacity at the same heating or cooling rate. The heat flow to both the sample and the reference is the same until a thermal event occurs in the sample, such as melting. During the thermal event, in order to keep the temperature of the sample and the reference the same, more heat needs to be added to the sample (or removed from the sample depending on the process under study). The DSC records this heat flow as a function of temperature or time. The peaks on the DSC graph identify thermal transitions in the sample due to changes in enthalpy ( $\Delta H$ ) as temperature increases (2). Figure 3.1 gives an example of how the heat flow curve would look like for a few typical phase transition events for a polymer. Exothermic behaviour (crystallization) shows up as increase on the heat flow curve, thus resulting in a concave peak. On the other hand, an endothermic event (glass transition or melting) shows up as decrease in the heat flow

curve, thus as a drop or a convex peak. The enthalpy of crystallization and melting is proportional to the area of the corresponding peaks.

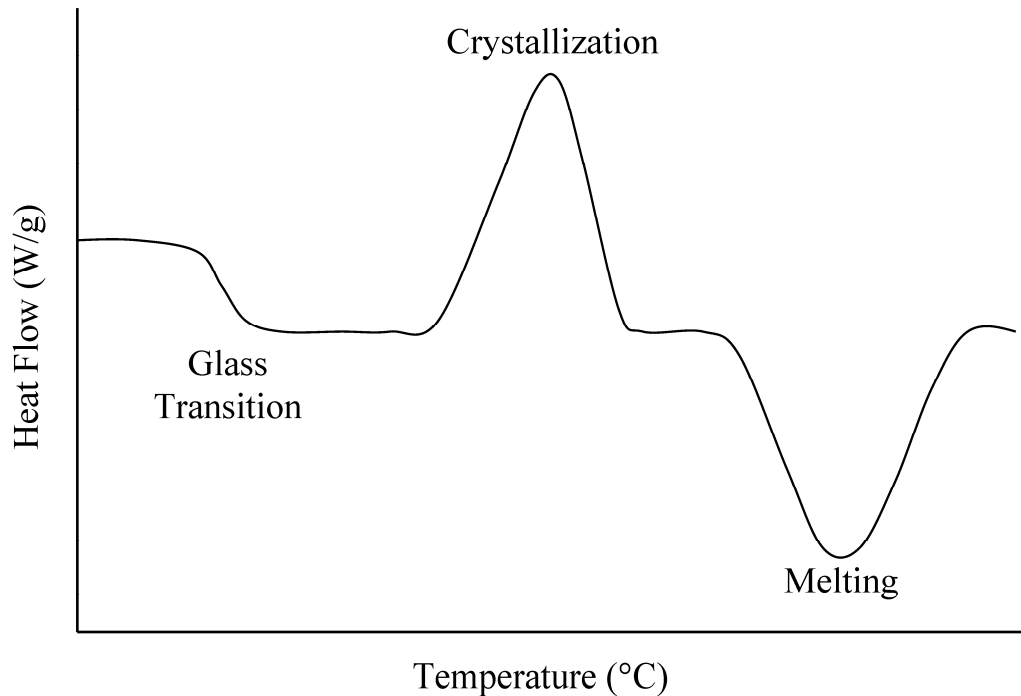


**Figure 3.1: Schematic representation of thermal events recorded by DSC. From ref. (1)**

Figure 3.2 is a heat flow (y-axis) versus temperature (x-axis) plot of a DSC experiment for a polyethylene (PE) sample. The convex peak indicates that melting of the sample has occurred. The melting temperature ( $T_m$ ) of the sample is indicated by the peak value at  $122^\circ\text{C}$ . The total amount of heat input for the melting event can be calculated by determining the total area of the peak. Based on the heat input and the mass of the sample, the enthalpy change due to fusion for the sample is determined to be  $113.9 \text{ J/g}$ .

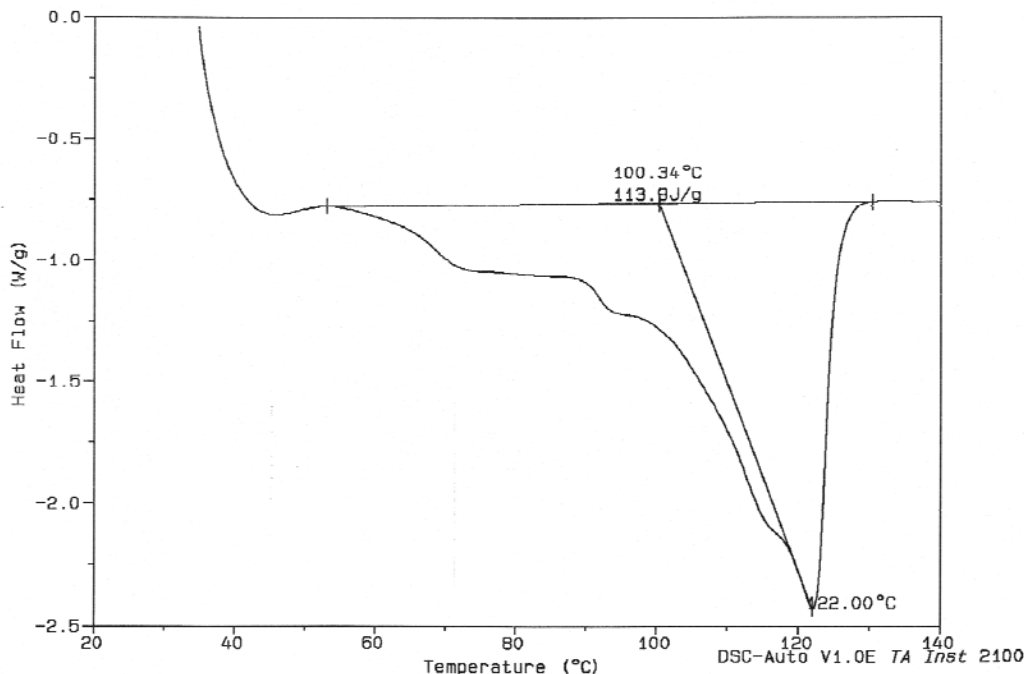


**Figure 3.2: A typical DSC curve for a polyethylene sample**

The crystallinity of a polymer can be calculated using the enthalpy of fusion ( $\Delta H$ ) and Equation 3.1 (2). Polyethylenes generally have high crystallinity, therefore the contribution by the amorphous material to the overall heat of melting is small and can be assumed to be zero, hence a more simplified equation (Equation 3.2) can be used to calculate the crystallinity of the polymer. The enthalpy of fusion for a 100% crystalline polyethylene is 293.6 J/g (3), thus, the percentage crystallinity for the sample shown in Figure 3.2 is estimated to be 38.8%.

$$\% \text{ crystallinity} = (\Delta H_a - \Delta H) / (\Delta H_a - \Delta H_c) \times 100 \quad (3.1)$$

$\Delta H$  –enthalpy of fusion for the sample

$\Delta H_a$  –enthalpy of fusion for a 100% amorphous standard

$\Delta H_c$  –enthalpy of fusion for a 100% crystalline standard

$$\% \text{ crystallinity} = \Delta H / \Delta H_c \times 100 \quad (3.2)$$

In addition to percentage crystallinity, the lamella thickness of a polyethylene sample can also be estimated using the melting temperature obtained from DSC and the well established Gibbs-Thomson equation (Equation 3.3) (4-6).

$$T_m = T_m^o \left( 1 - \frac{2\sigma_e}{\Delta h_m l} \right) \quad (3.3)$$

$T_m$  is the observed melting temperature of the resin at the peak of the DSC curve.  $l$  is the lamella thickness. The other parameter values used for polyethylene are based on the work by Wlochowicz and Eder (6).  $T_m^o = 415$  (K) is the equilibrium melting temperature of an infinite crystal;  $\sigma_e = 60.9 \times 10^{-3}$  (Jm<sup>-2</sup>) is the surface free energy of the basal plane; and  $\Delta h_m = 2.88 \times 10^8$  (Jm<sup>-3</sup>) is the enthalpy of fusion per unit volume. Using Equation 3.3, the lamella thickness estimated for the PE sample in Figure 3.2 is 8.78 nm ( $T_m = 122^\circ\text{C}$ ).

In this project, DSC analysis was carried out on a TA Instruments DSC 2920 module. The heating method used was a 10°C/min ramp from 40°C to 240°C. The theoretical value for a 100% crystalline polyethylene (PE) used in the calculation of percent crystallinity of samples was 293.6 J/g (3). Each DSC sample size used per run was about 5mg. Repeats and independent replicates were carried out, as discussed further in Chapter 6.

### 3.1.2 Crystallization Analysis Fractionation (CRYSTAF)

In a dilute polymer solution, polymer chains precipitate (dissolute) out of solution as the temperature of the solution decreases. Due to thermodynamic interactions between the solvent molecules and polymer chains, shorter polymer chains precipitate out of solution at a lower temperature than longer polymer chains (7, 8). In addition, polymer chains containing short chain branches “crystallize” at a lower temperature than linear chains of the same length (9). Crystallization analysis fractionation (CRYSTAF) analysis exploits this behaviour to study structural composition heterogeneity of a polymer (9, 10).

In CRYSTAF analysis, a polymer sample is initially dissolved in a compatible solvent at an elevated temperature. Polyethylene samples are usually dissolved in trichlorobenzene at temperatures of 140°C-160°C. After the sample is completely dissolved, the polymer solution is slowly cooled back to room temperature at a constant cooling rate. As the solution cools, polymer chains crystallize and precipitate and changes in the solution concentration are recorded as a function of temperature.

Figure 3.3 represents a typical plot from a CRYSTAF analysis of a polyethylene sample. The x-axis is temperature (T). The left y-axis is the cumulative distribution of polymer solution concentration (C). The right y-axis gives the first derivative of the cumulative distribution ( $dC/dT$ ). The total area under the  $dC/dT$  curve represents 100% weight percentage of polymer chains. The area under the 82°C peak of the  $dC/dT$  curve divided by the total area under the curve gives the weight percentage of linear chains in the sample, because linear chains crystallize at a higher temperature. On the other hand,

because PE molecules with short chain branches crystallize at a lower temperature, the area under the 63°C peak divided by the total area under the dC/dT curve gives the weight percentage of chains containing short chain branches. Thus the CRYSTAF analysis is able to provide structural composition information regarding the polymer sample.

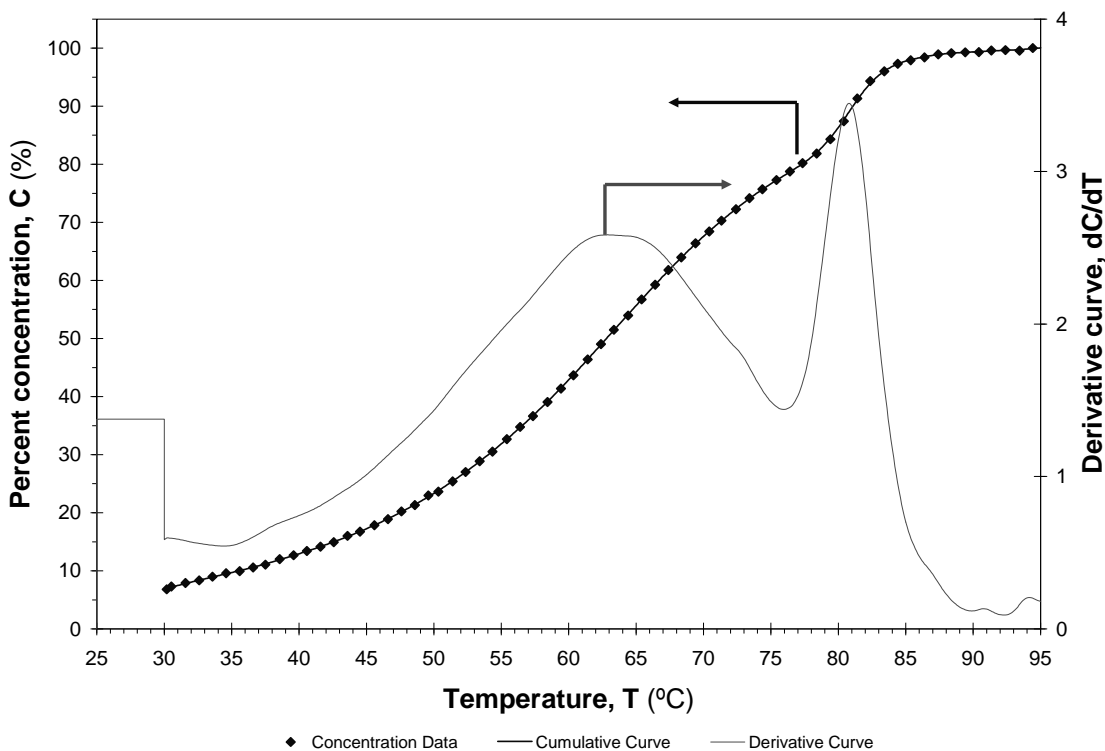


**Figure 3.3: CRYSTAF results for a polyethylene sample**

CRYSTAF analysis for polymers in this study was carried out on a CRYSTAF 200 instrument. The dissolution of polyethylene samples was carried out at 160°C in 1,2,4 trichlorobenzene. Each sample consisted of 20 mg of polyethylene in 40 ml of solvent. The polymer solution was held at equilibrium for 2 hours at 95°C and then cooled at a

constant cooling rate of 0.1°C/min. The change in solution concentration was measured from 95°C to 30°C.

### **3.1.3 Size Exclusion Chromatography – SEC/GPC**

Molecular weight (MW) and molecular weight distribution (MWD) of a polymer are usually characterized using gel permeation chromatography (GPC), a type of size-exclusion chromatography (SEC). In GPC, dissolved polymer molecules move through packed columns of porous particles, as shown in Figure 3.4. Large molecules cannot enter the pores of the porous particles, thus elute out of the column first. On the other hand, smaller molecules are trapped in the pores and come out of the column later. Due to difference in retention (elution) time of molecules, fractionation of a polymer sample according to different sizes is achieved and is related to the molecular weight distribution of the polymer sample. The eluted out polymer fractions are sent to a series of detectors down stream from the columns where the average molecular weights and other characteristics of the MWD of the sample are possibly determined (11). The exact method for calculation of MW and MWD depends on the detectors used. Some of the common detectors used in GPC are viscometer, differential refractometer (RI), UV detector, and low-angle or multi-angle (laser) light scattering (11, 12). Combining other more specialized detectors can give additional information regarding the sample. For example, combining GPC to an online Fourier transform infrared spectroscopy (FTIR) detector allows the determination of the comonomer distribution of a polymer (13).

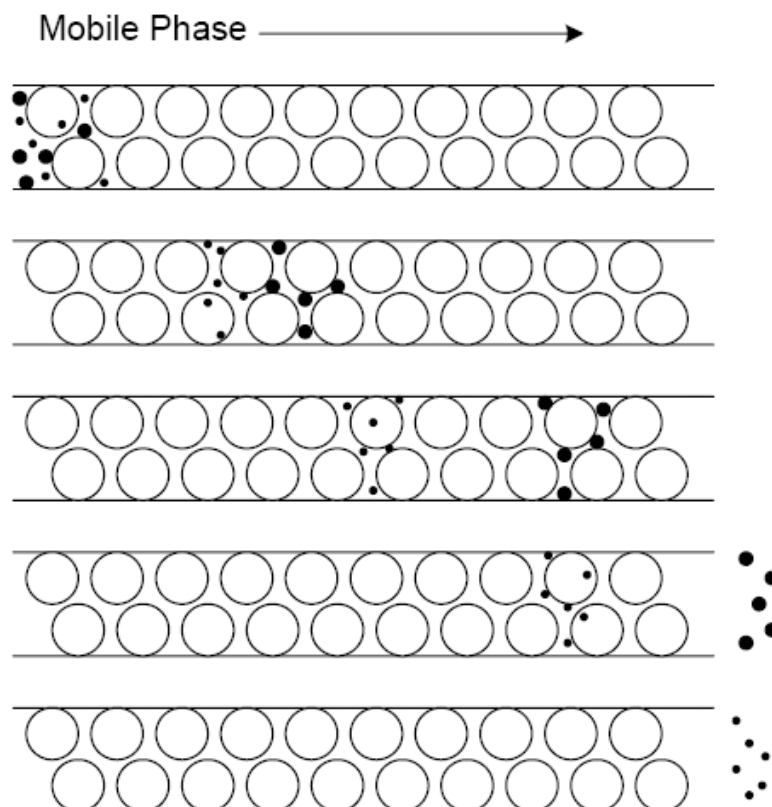


**Figure 3.4: Schematic representation of separation of polymer molecules of different sizes in the GPC column. From ref. (14)**

The average molecular weights and molecular weight distribution of resins in this study were determined using a high temperature GPC. For polyethylene, high temperature GPC is needed due to difficulties in dissolving the material. The equipment used was a Waters GPCV 150+ instrument equipped with a Viscotek 150R viscometer. Its operating temperature for testing polyethylene was 140°C. Each GPC sample consisted of 18 mg of PE in 9 ml of 1,2,4 trichlorobenzene (TCB). Average molecular weights were calculated using the universal calibration curve based on narrow polystyrene standards.

### 3.1.4 $^{13}\text{C}$ - NMR

Carbon-13 nuclear magnetic resonance spectroscopy ( $^{13}\text{C}$  NMR) is a type of NMR used for study of organic compounds. When a polymer sample is placed in a magnetic field and excited by electromagnetic radiation, carbon-13 and other NMR active nuclei ‘flip’ from one energy level to the next, thus generating the nuclear magnetic resonance spectrum. The energy absorbed by each type of nuclei is characteristic at a specific resonance frequency. Hence identification of different types of chemical compounds is possible by comparing sample NMR spectra to a reference spectrum. Different structures of the same type of nuclei also generate a slight difference in resonance frequency, called the chemical shift. In  $^{13}\text{C}$  NMR the chemical shift can be used to identify different types of branching structures in polyethylene (15).

Figure 3.5 is an example of an NMR spectrum for a polyethylene sample. The frequency of each peak is identified by numbers above the spectrum, at the top of the plot; the area under each peak is shown by values under the spectrum. The intensity of NMR spectrum peaks gives an indication of the amount of each type of nuclei present. The largest peak in Figure 3.5 is due to the carbon-carbon backbone of the PE. Quantitative estimation of each type of side chain branch is possible using the  $^{13}\text{C}$  NMR spectrum plot and Equation 3.4. Using Equation 3.4, by dividing the area under a spectrum peak, specific for one type of branch, by the area under the backbone peak, the number of branches per thousand carbon atoms can be estimated. For polyethylene copolymer, it is not possible to use the  $^{13}\text{C}$  NMR method for detection of long chain branches because the technique cannot distinguish side chains made up of six or more carbon atoms (16, 17).

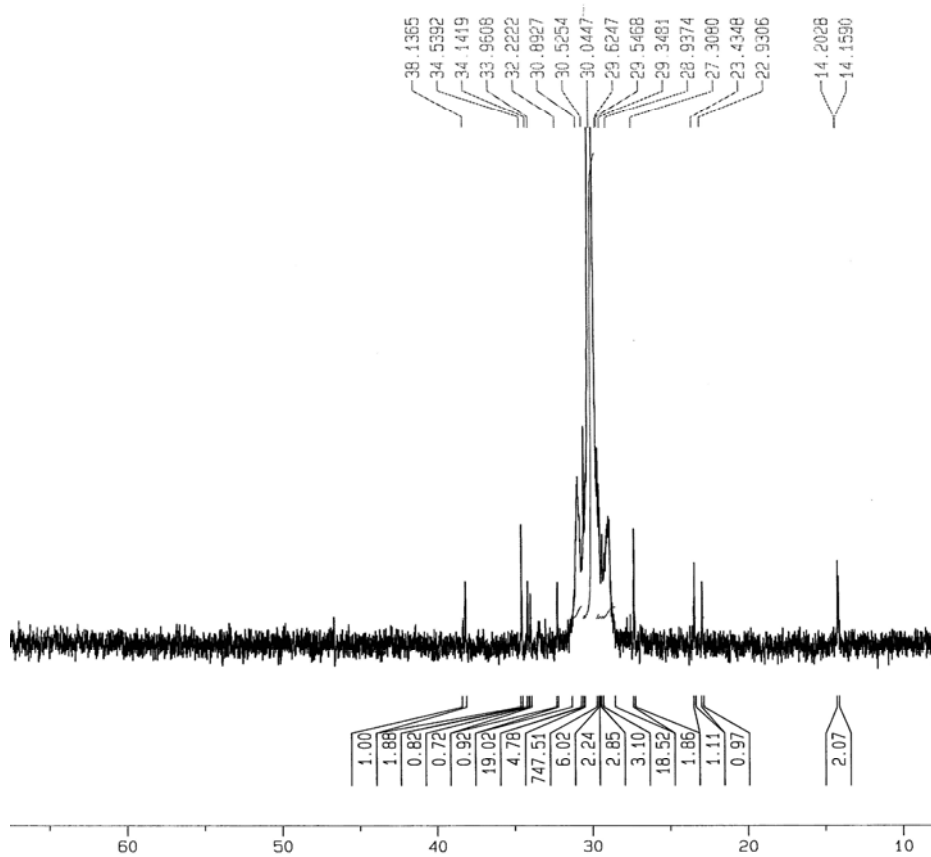


Figure 3.5:  $^{13}\text{C}$  NMR spectrum of a polyethylene sample

$$\text{branch type} / 1000 \text{ carbons} = \frac{\text{area under branch peak}}{\text{area under backbone peak}} \times 1000 \quad (3.4)$$

For short chain branch content of our resins,  $^{13}\text{C}$  NMR analysis was carried out using an AVANCE 500 Bruker NMR at  $120^\circ\text{C}$ . Each sample consisted of 5 mg of polymer dissolved in trichlorobenzene, with trichloroethylene (TCE) used as the tracer. Selective replications were carried out and showed good reproducibility.

### 3.1.5 X-Ray Diffraction

X-ray diffraction is a technique originally developed to study structures of crystals. In Figure 3.6 the general concept of x-ray scattering of a crystal is illustrated. When the incident ( $\vec{k}_i$ ) x-ray wave hits the crystal, the interplanar spacing ( $d$ ) difference gives rise to different path lengths for x-rays as they are scattered from different planes ( $\vec{k}_f$ ), and the path difference equals  $2d\sin\theta$ . Constructive wave interference occurs when the difference in x-ray path length is equal to one wavelength of the x-ray, thus constructive interferences produce x-ray spectra with peaks at specific  $\theta$  values. According to Bragg's law (18), the space between crystal lattices can be determined based on the wavelength of the x-ray and the diffraction angle (Equation 3.5).

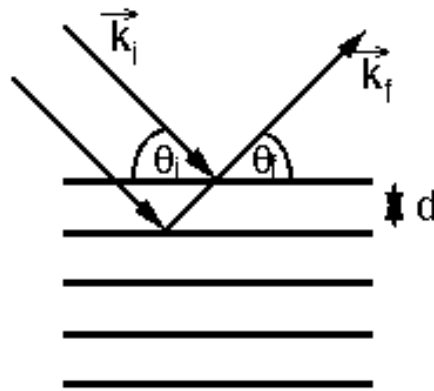


Figure 3.6: Geometry for interference of an x-ray wave scattered from two planes separated by a spacing  $d$ . From ref. (18)

$$2d \sin \theta = \lambda \quad (3.5)$$

$d$  - interplanar spacing,  $\theta$  - angle of incidence of two parallel rays

$\lambda$  - wavelength of the x-ray

A typical x-ray spectrum is usually shown as a plot of scattering intensity ( $I(q)$ ) versus diffraction angle (Figure 3.7). The shape of the peaks in an x-ray scattered spectrum gives information about the molecular structures of the crystal (18). For perfect crystals, the x-ray spectrum consists of perfectly sharp peaks (Figure 3.7). For imperfect crystals, the peaks are broadened, and for amorphous material no sharp peak is observed. Semicrystalline polymer shows broadened peaks due to the presence of the amorphous phase (19).

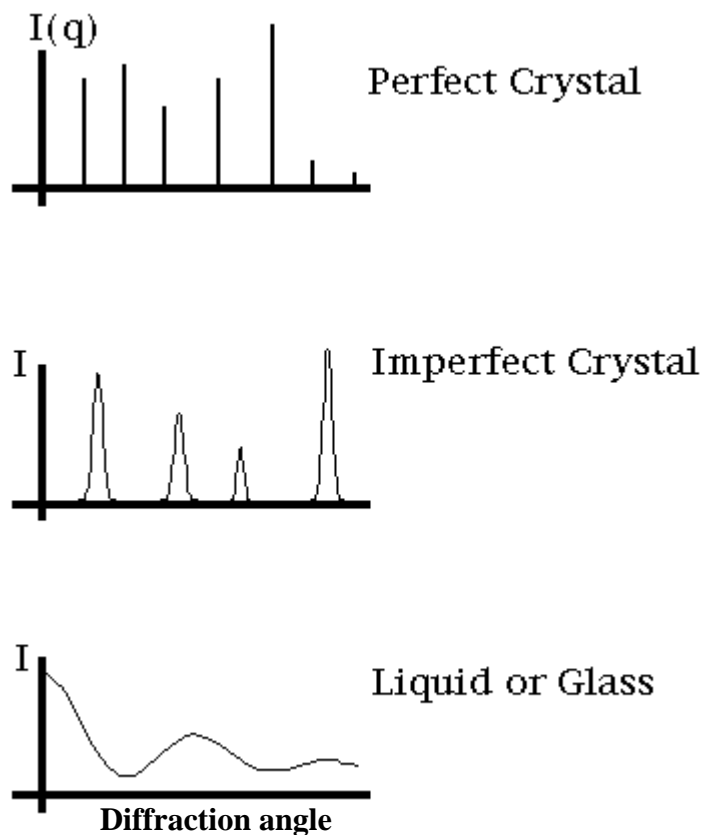
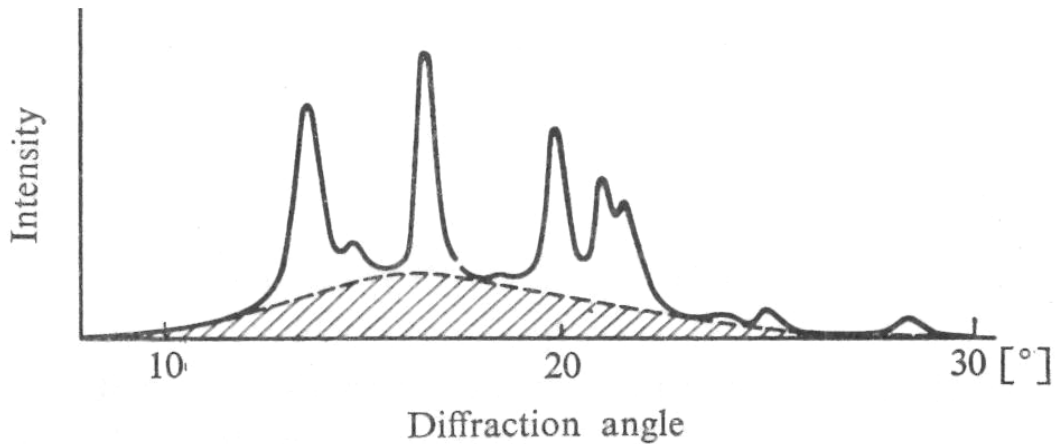


Figure 3.7: X-ray spectra for different types of crystal structures. From ref. (18)

Two types of x-ray scattering techniques were used in this study. The first is the standard x-ray diffraction, also known as wide angle x-ray scattering (WAXS). WAXS is generally used for an experiment with a scattering angle of  $6^\circ$  and greater. WAXS scattering spectrum gives information about the overall crystallinity of a semicrystalline polymer (20). Figure 3.8 is the diffraction pattern of an isotactic polypropylene. The shaded area is considered the scattering due to the amorphous phase, whereas un-shaded peaks represent scattering due to the crystalline phase. The shaded area has been shown to be proportional to the mass of the amorphous phase, and the area of the un-shaded peaks is proportional to the mass of the crystalline phase (20). Therefore, the overall crystallinity of a semicrystalline polymer can be calculated by integrating these peaks and using Equation 3.6.



**Figure 3.8: Schematic diagram of WAXS scattering pattern used in calculation of polymer crystallinity. From ref. (20)**

$$\%crystallinity = \frac{\int_0^{\infty} I_{cr}}{\int_0^{\infty} I_{cr} + \int_0^{\infty} I_{am}} \quad (3.6)$$

$I_{cr}$ ,  $I_{am}$  - scattering intensity of the crystalline and amorphous structure

In this thesis, a second type of x-ray scattering experiment was also conducted to give information about the lamella structure of polyethylene. Small angle x-ray scattering (SAXS) experiments have the same principle as WAXS experiments. The only difference is that a SAXS experiment starts from smaller diffraction angles, usually less than  $1^\circ$ , thus is able to give information regarding fine molecular structures that are not possible to detect with the WAXS technique.

With the SAXS information, the periodic structure within a material can be obtained (20). The thickness of the periodic structure is called the long period (L). In semicrystalline material, such as polyethylene, the long period is equal to the thickness of a crystalline lamella and an amorphous layer (Figure 3.9). To obtain the long period value, the Bragg equation (Equation 3.5) can be used with a slight modification. Due to the small diffraction angle of the experiment,  $\sin\theta = \theta = \varepsilon$ , thus the Bragg equation takes on the form of Equation 3.7. The long period consists of one crystalline layer and one amorphous layer, and the contribution of each layer to the long period is found to be proportional to the crystallinity of the polymer (20). Therefore, the lamella thickness of a polymer can be calculated using Equation 3.8.

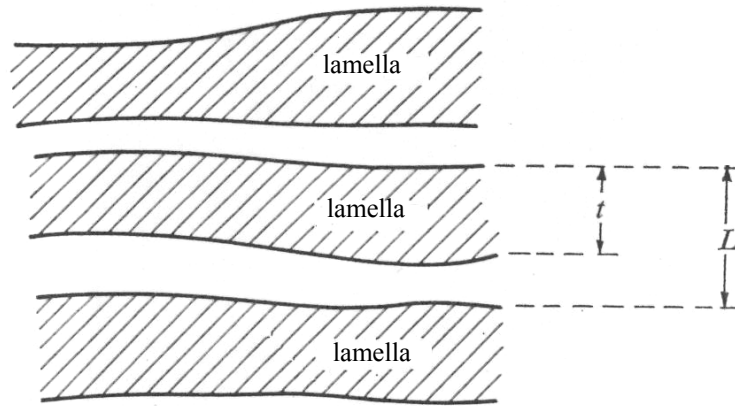


**Figure 3.9: Schematic diagram of a structure associated with the long period,  $L$  - long period,  $t$  - thickness of lamella. From ref. (20)**

$$L\epsilon = n\lambda \quad (3.7)$$

$L$  - long period,  $\epsilon$  - Bragg angle of the intensity maximum,  
 $n$  - level of scattering (usually has value of 1),  $\lambda$  - wavelength of the x-ray

$$\text{Lamella thickness} = \% \text{crystallinity} \times L \quad (3.8)$$

For x-ray scattering experiments, compression molded discs of 25mm diameter and 1mm thickness were used. Samples were molded at  $190^{\circ}\text{C} \pm 5^{\circ}$  and 10000 lbf, and then quench cooled. WAXS experiments were conducted using a Stoe two circle goniometer in a Bragg-Brentano geometry equipped with a Moxtek solid state detector and sourced by an Enraf Nonius 571 rotating anode generator. SAXS analysis was carried out on a Bruker AXS NaoStarU with a Hi-Star 2D detector.

## 3.2 Rheological Characterization

### 3.2.1 Oscillatory Shear Analysis

Rheological analysis is powerful and offers insights into the molecular architecture of a polymer (21). The standard practice for rheological experiments is to carry out experiments at 50°C or more above the melting temperature of the polymer. At elevated temperatures, movements of polymer chains can be more easily observed. In addition, high temperatures are needed in order to avoid any possible strain induced crystallization in the polymer melt (22, 23). Polyethylene generally has its melting point around 130~135°C, therefore we chose to conduct our experiments at 190°C. At elevated temperatures, the thermal stability of the polymer is a key requirement. In addition to carrying out experiments in a nitrogen atmosphere, resins in this study were compounded with 1 wt% IRGANOX B215 for thermal stability. Despite the addition of a considerable amount of stabilizer (the manufacturer recommended dose was 0.3 wt%), PE resins # 1, 2, 3, and 6 were not stable at 190°C for more than 90 minutes. Other resins were stable for about four hours. Due to this limitation in thermal stability of some of the materials, dynamic oscillatory shear experiments were chosen because of the relatively short test duration.

In dynamic oscillatory shear experiments, a stress or strain is applied to the sample at a specific frequency ( $\omega$ ) and the response of the material is recorded (24). Stress ( $\sigma$ ) in dynamic mechanical analysis is described by Equation 3.9, and the strain ( $\gamma$ ) is described by Equation 3.10. The stress and strain curves have the shape of a sine wave (Figure

3.10), with the amplitude of the curves being  $\sigma_0$  and  $\gamma_0$ . The stress and strain curves differ from each other by a phase angle difference  $\delta$ .

$$\sigma(t) = \sigma_0 \sin \omega t \quad (3.9)$$

$$\gamma(t) = \gamma_0 \sin(\omega t - \delta) \quad (3.10)$$

$\sigma$  -stress,  $\sigma_0$  -stress at  $t = 0$ ,  $\omega$  -frequency,  $t$  -time

$\gamma$  -strain,  $\gamma_0$  -strain at  $t = 0$ ,  $\delta$  -phase angle

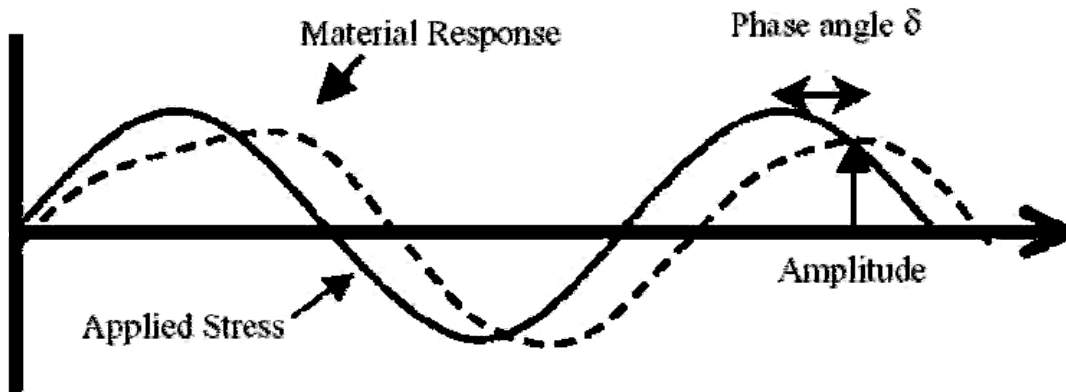


Figure 3.10: Schematic representation of stress and strain curves in an oscillatory shear experiment. From ref. (25)

Based on structural mechanics, stress and strain are related through the modulus (26). The shear modulus in oscillatory shear analysis is called the complex modulus ( $G^*$ ). As illustrated by Equation 3.11,  $G^*$  consists of a storage ( $G'$ ) and a loss modulus ( $G''$ ).  $G'$  is a measure of the ability of the material to store energy (for a perfectly viscous fluid  $G' = 0$ ). On the other hand,  $G''$  is a measure of its ability to dissipate energy (for a completely elastic material  $G'' = 0$ ). The ratio of the moduli is called damping, represented by  $\tan(\delta)$  (Equation 3.12). From the store and loss modulus, other material

properties such as compliance ( $J^*$ ) and viscosity ( $\eta^*$ ) can be calculated. Based on the Cox-Merz rule, the complex viscosity versus frequency plot can be viewed as giving the same information as a viscosity versus shear rate plot (24).

$$G^* = G' + iG'' \quad (3.11)$$

$$\tan(\delta) = \frac{G''}{G'} \quad (3.12)$$

Dynamic testing has the advantage of being able to measure material response over a range of temperatures (temperature sweep) and frequencies (frequency sweep) in one single experiment. In temperature sweep experiments, by varying the temperature at a specific rate, the modulus over a range of temperatures can be determined from the same experiment. On the other hand, by holding the temperature constant and varying the frequency, the modulus of a material over a frequency range can be obtained (24). Figure 3.11 shows a typical plot of frequency sweep results for an oscillatory shear experiment. The x-axis is the frequency of the experiment. The left y-axis is the complex viscosity, while the right y-axis gives the modulus.

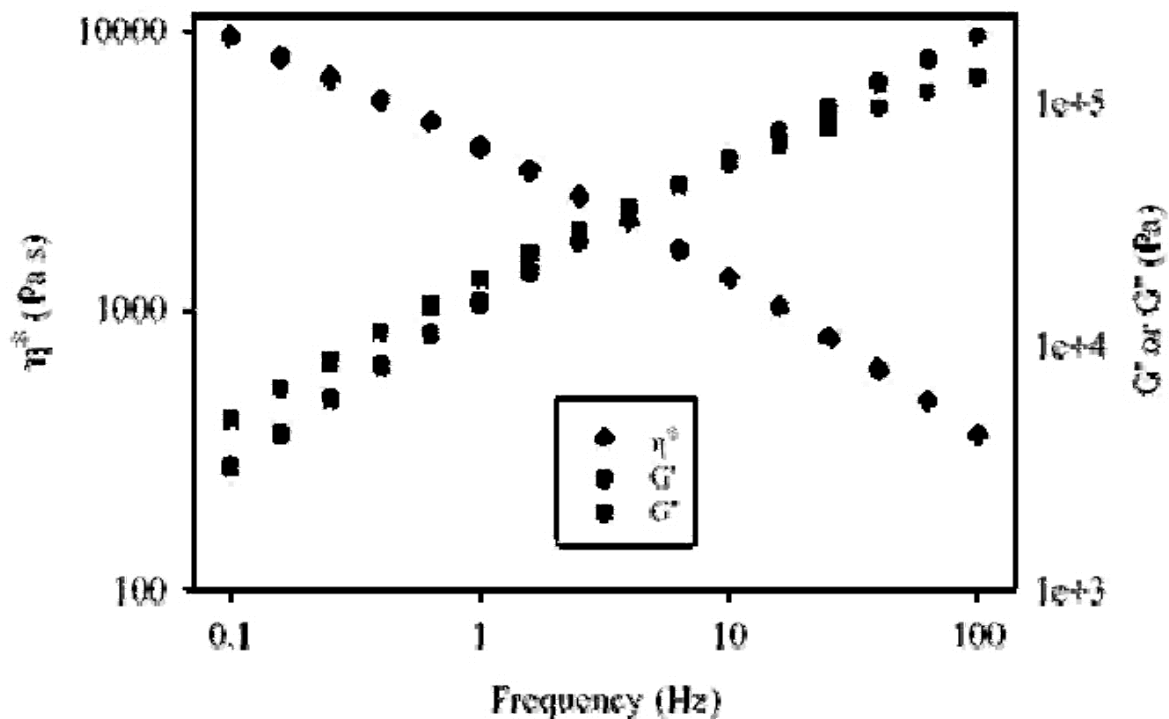


Figure 3.11: Typical oscillatory shear responses of polyethylene. Taken from ref. (25)

There are many test geometries available for dynamic oscillatory shear experiments, such as the cone and plate geometry and the parallel plate geometry (24). In the literature, the parallel plate geometry is the most frequently reported test setup used in oscillatory shear analysis of polyethylene. The parallel plate geometry has an uneven strain field across the plate, where the material at the center of the plate is strained very little, while the material at the edge of the plate is strained a lot. Therefore the obtained strain value from this geometry is an average value (24). Comparing to other geometries, the parallel plate geometry is more straightforward, and hence was selected for our experiments.

For rheological characterization of resins, a TA Instruments AR2000 rheometer was used. Experimental specimens were prepared by compression molding; resins were heated at  $190^{\circ}\text{C} \pm 5^{\circ}$  and then molded into 25mm discs with 10000 lb force, and then quench cooled

with water. All samples were tested using the 25mm steel plate parallel plate geometry with a gap of 1000 micro meters. Experiments were carried out at 190°C under a nitrogen atmosphere to prevent material degradation. Time sweep experiments were carried out to determine the length of time each resin is thermally stable. Strain sweeps were carried out to determine the linear response region of resins at different frequencies of 1Hz, 50Hz and 100Hz. Dynamic oscillatory shear experiments were carried out in the linear region of each resin, generally about 5% strain. The frequency used was 0.001-100 Hz. During the experiment shear storage ( $G'(\omega)$ ) and shear loss modulus ( $G''(\omega)$ ) of samples were obtained. A new disc was used for each experiment. Selected repeats were carried out and showed good reproducibility.

### **3.2.2 Dynamic Mechanical Analysis**

Dynamic mechanical analysis (DMA) experiments utilize the same dynamic test principles described for oscillatory shear experiments (section 3.2.1). The complex modulus ( $E^*$ ) measured in DMA can also be separated into the storage ( $E'$ ) and the loss modulus ( $E''$ ), as described in Equation 3.13. The main difference between DMA and oscillatory shear experiments described in section 3.2.1 is that the former is done on polymer in the solid state, whereas the latter on polymer in the melt state (24).

$$E^* = E' + iE'' \quad (3.13)$$

In order to study the  $\alpha$ -relaxation behaviour of polyethylene, DMA experiments in tensile mode were carried out on a DMTA V machine by Rheometric Scientific. Polyethylene

film samples were compression molded at  $190^{\circ}\text{C}\pm 5^{\circ}$  with 10000 lb force and then quench cooled. Test sample dimensions generally have length of  $5\pm 0.1$  mm, width of 9.5-1.05 mm and thickness of 0.2-0.4 mm. Strain sweep experiments were carried out and the observed material response was linear within the 0.009%-0.09% strain range. Step-temperature frequency sweep experiments were carried out at 0.05% strain. The experiment temperature range was  $80^{\circ}\text{C}$  to  $120^{\circ}\text{C}$ , with  $10^{\circ}\text{C}$  intervals. The soaking time (equilibrium time) for each test temperature was 10 minutes. The frequency sweep was over the frequency range of 0.1-10 rad/s. All experiments were carried out under a nitrogen blanket.

### **3.3 Tests for (Macro)Mechanical Properties**

#### **3.3.1 Tensile Test**

A uniaxial tension test is used to examine the elongation behaviour of a polymer. A dog-bone shape polymer sample is usually employed in this type of test. For semi-crystalline polymer such as polyethylene there are three distinct stages of deformation, as illustrated in Figure 3.12. Initially elastic behaviour before yield is represented by the first straight section of the load-displacement plot. The initial slope of the plot is a measure of the stiffness of the material (27). The load increases with increasing strain until yield occurs. After yield, the test sample undergoes ductile deformation or cold drawing. In the cold drawing phase, polymer chains and lamellae reorient in the direction of drawing (28) and the load level is relatively constant until strain hardening occurs when the polymer sample is fully drawn (27). In strain hardening, the load increases again with increasing

displacement/elongation until the material breaks. Crystalline polymers have higher stress at ultimate break than amorphous polymers due to reinforcement of crystalline regions (29).

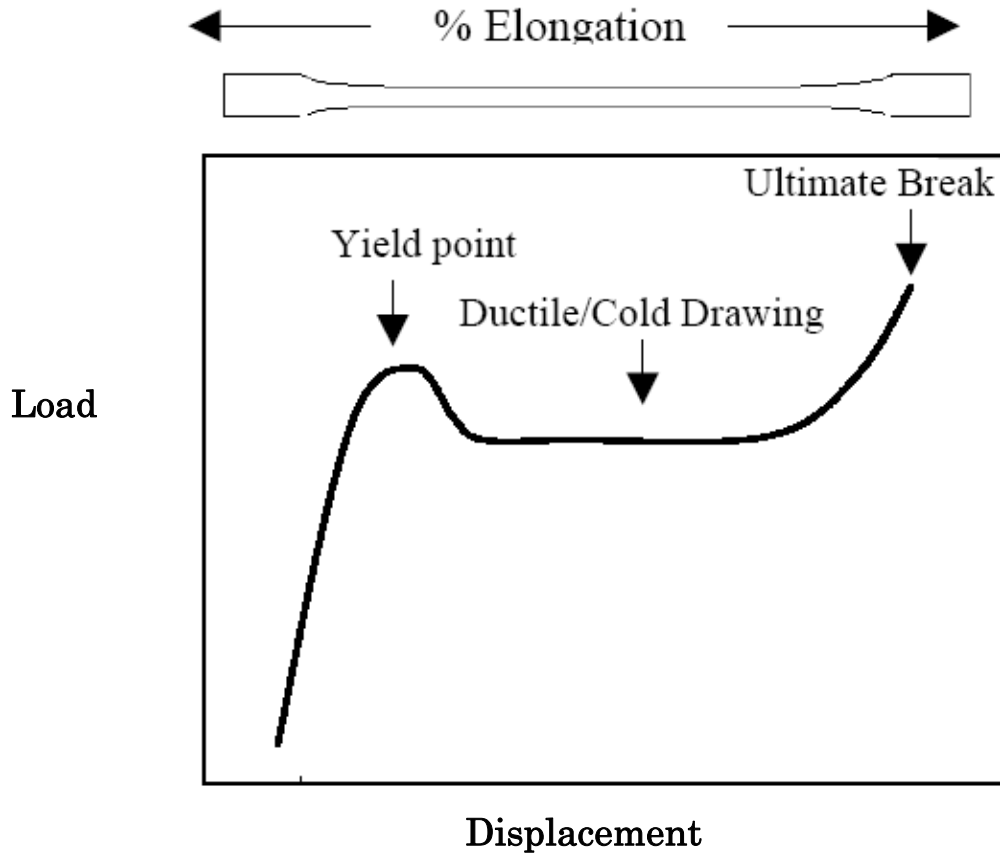


**Figure 3.12: Tensile elongation behaviour of semicrystalline polymer**

Tensile tests were carried out on an Instron 4465 machine at room temperature, using deformation rates of 0.5 mm/min and 7 mm/min. The dogbone sample was pulled at a constant deformation rate until ultimate break to study the strain hardening behaviour of HDPE. Load versus displacement was measured and the strain hardening stiffness calculated. In addition to strain hardening stiffness, the extensibility of the polymer

network in tensile deformation was studied. The natural draw ratio (NDR) (27, 30) is a measurement used to gauge the extensibility of a network. It is defined as the ratio of sample length at onset of strain hardening and its initial length (Equation 3.14).

$$NDR = \frac{\text{sample length at onset of strain hardening}}{\text{initial sample length}} \quad (3.14)$$

Dogbone samples for the tensile tests were punched from compression molded resin plates (Figure 3.13). Each resin plate was compression molded at  $190^{\circ}\text{C} \pm 5^{\circ}\text{C}$  and 10000 lbf; the plate was allowed to cool down in the mold at room temperature over a period of 24 hours before dogbones were cut out from it. The tensile test follows the guidelines of ASTM 638 standard. Independent replicates and repeats were carried out; further details are discussed in Chapter 4.

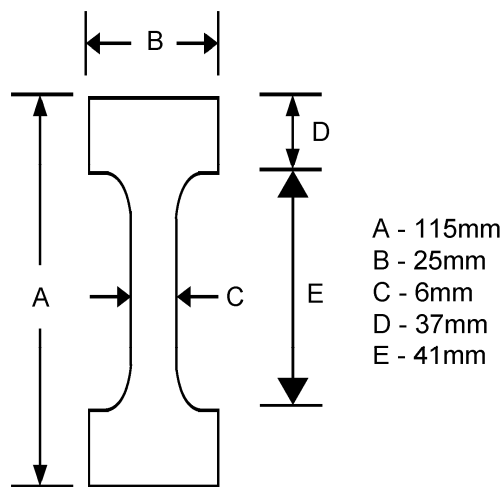


**Figure 3.13: Dogbone dimensions for tensile test**

### 3.3.2 Notched Constant Load Test (NCLT)

Creep of polymer occurs when the material is subjected to constant load over a longer period of time. During creep, polymer chains slowly reorganize themselves in order to minimize the applied stress, resulting in deformation of the original shape. When there is some initial damage in the form of a crack, the movement of polymer chains can lead to further growth of the crack, which results in creep rupture. Creep rupture is one of the mechanisms by which HDPE pipes can suddenly develop cracks under low stress over long periods of time (31). The notched constant load test (NCLT) is used to measure creep rupture response of polyethylene under an aggressive environment. Results of NCLT are used as an indication of the environmental stress cracking resistance (ESCR) of a polymer.

During an NCLT experiment, a notched dogbone is secured at the base of the apparatus illustrated in Figure 3.14. The top of the sample is attached to one end of a lever and a constant load attached to the other end of the lever. An automatic timing device is attached to the lever to record the time of failure when the dogbone breaks and the load is released. The failure time of the sample is taken as the ESCR value of the material. NCLT experiments are run at 50°C in a temperature bath containing 10% Igepal (nonyl phenyl ether glycol,  $C_{19}H_{19}-C_6H_4-O-(CH_2CH_2O)_8-CH_2CH_2OH$ ) solution (ASTM D5397). The Igepal (surfactant) solution is the aggressive environment used to simulate the aggressive environment in the field that causes environmental stress cracking.

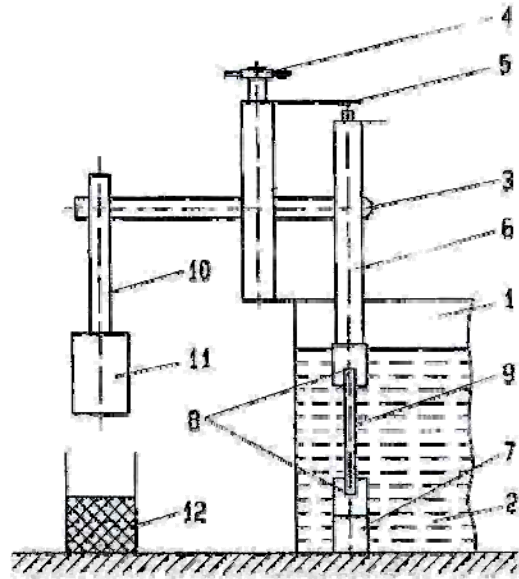


**Figure 3.14: Test arrangement for NCLT; (1) solution container, heated, (2) test medium, (3) lever, (4) compensating spindle, (5) timing contact, (6) upper holding device, (7) bottom holding device, (8) test piece holding device, (9) test sample, (10) holding device for weight, (11) weights, (12) collector. From ref. (32)**

In running the NCLT test, some researchers use the same level of stress, while others use the same percentage of yield stress for each PE material. The stratagem of running tests at a constant percentage of yield stress of each type of resin is preferred in order to ensure that the failure is well within the brittle fracture region of the material behaviour, even though this gives different test stress values for different resins (33). Figure 3.15 illustrates the possible pitfall of testing all materials at a constant stress level. The stress-strain curves of two polymers (1 and 2) with different yield stress are shown in Figure 3.15. At the chosen “NCLT test stress level” polymer-1 would experience ductile deformation while polymer-2 has brittle deformation, thus any NCLT test comparisons between polymers 1 and 2 would be incorrect. To ensure NCLT experiments were carried out within the brittle fracture behaviour region of our resins, experiments were

conducted using the constant percentage yield stress approach. For our experiments, the stress level used was 15% of the yield stress of each resin.

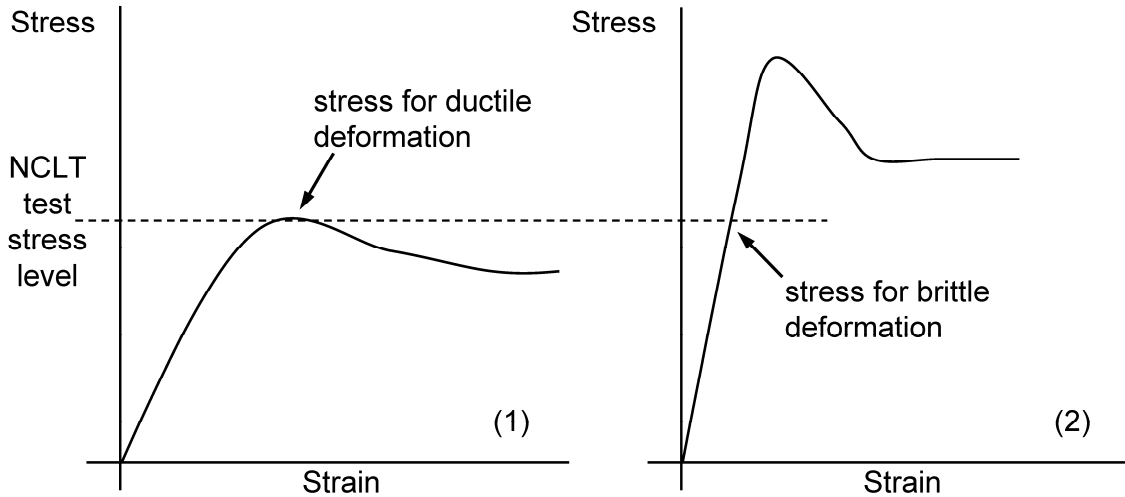


**Figure 3.15: Schematic representation of NCLT test stress level in relation to the yield stress of polymers. Adapted from ref. (33)**

Dogbone shaped samples for NCLT test were cut out from plates of polymer made from compression molding at  $190^{\circ}\text{C}\pm 5^{\circ}$ . Specimen dimensions are shown in Figure 3.16. The thickness of the sample was  $1.8\pm 0.1\text{mm}$ . A notch was introduced into the sample at the middle of the dogbone using a sharp razor blade, and a fresh blade was used after every five uses. For our test we used a notch that was 40% of the thickness of the sample instead of 20% (as indicated by ASTM D5397). The effect of this change is discussed in Chapter 4.

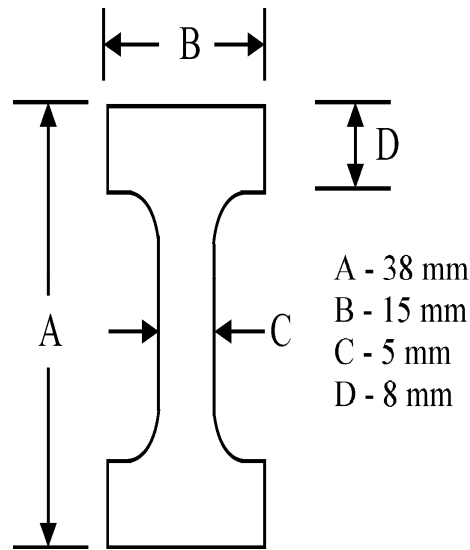


**Figure 3.16: Dogbone dimensions for NCLT**

### **3.4 Resin Selection and Material Properties as Received**

Ten industrial polyethylene resins were selected for this project. Six structural application high density polyethylene (HDPE) resins and four pipe application HDPE resins were acquired from several industrial sources. The six structural application resins consisted of three blow molding (PE1-3) and three injection molding resins (PE4-6). They were selected due to the diversity of their bent strip ESCR test values (Table 3.1) (the bent strip test, also known as Bell telephone test, is yet another test to evaluate ESCR of resins according to ASTM D1693). Finally, the four pipe resins (PE7-10) chosen were for large gas line applications.

Table 3.1 lists resin information obtained from the manufactures. The amount of information regarding fundamental properties of these resins is very limited. Table 3.1 serves as a kind of “bench mark” in order to show how little was known about the resins

at the beginning of the research project. Resin property updates to Table 3.1 will be presented later in section 9.3 to illustrate the progress in understanding of the molecular structure and properties of the materials that has been achieved during the course of this thesis.

**Table 3.1: HDPE resin properties as received from manufacturers**

	<b>PE1</b>	<b>PE2</b>	<b>PE3</b>	<b>PE4</b>	<b>PE5</b>	<b>PE6</b>	<b>PE7</b>	<b>PE8</b>	<b>PE9</b>	<b>PE10</b>
Density	0.95	0.963	0.963	0.948	0.95	0.951	0.945	0.958	0.958	0.955
Melt index (g/10min)	0.3	0.73	0.25	5	33	14	8.5 <sup>1</sup>			
Tensile Strength at Yield (MPa) <sup>2</sup>	27	32	31	23.3	21.8	23	23	30.2	29.9	29.9
Elongation at Break (%)	600	35	450	48	56	61	850			
Impact Brittleness Temperature (°C)	-76	-76	-76	-70	-70	-70	-100			
Environmental Stress Crack Resistance - bent strip test (hours)	65	10	15	18	2	3	>1000	>500	>1000	>1000
Resin type	Blow molding	Blow molding	Blow molding	Injection molding	Injection molding	Injection molding	Pipe	Pipe	Pipe	Pipe
Application(s)	Household, industrial containers	Liquid food containers	Containers	Carts, vehicle components	Containers, house wares, toys	Food containers, house wares	Pipe	Pipe	Pipe	Pipe

<sup>1</sup> measurement at 190°C and 21.9kg

<sup>2</sup> tensile strength at yield from resin suppliers

### 3.5 References

1. Mathot, V. B. F.(1993), *Calorimetry and thermal analysis of polymers*, Hanser Publishers, New York.
2. Stuart, B. (2002), *Polymer Analysis*, John Wiley & Sons, Ltd, Queensland.
3. van Krevelen, D. W. (1990), *Properties of Polymers*, 3 edn, Elsevier Scientific Publishing Company, New York.
4. Hannay, N. B.(1976), *Treaties on Solid State Chemistry: Volume 3 Crystalline and Noncrystalline Solids*, Plenum Press, New York.
5. Lippits, D. R., Rastogi, S., Höhne, G. W. H., Mezari, B., & Magusin, P. C. M. M. (2007), "Heterogeneous distribution of entanglements in the polymer melt and its influence on crystallization", *Macromolecules*, vol. 40, no. 4, pp. 1004-1010.
6. Wlochowicz, A. & Eder, M. (1984), "Distribution of Lamella Thicknesses in Isothermally Crystallized Polypropylene and Polyethylene by Differential Scanning Calorimetry", *Polymer*, vol. 25, no. 9, pp. 1268-1270.
7. Jackson, J. F., Mandelkern, L., & Long, O. C. (1968), "Solubility of crystalline polymers. I. Polyethylene fractions crystallized in bulk", *Macromolecules*, vol. 1, no. 3, pp. 218-223.
8. Jackson, J. F. & Mandelkern, L. (1968), "Solubility of crystalline polymers. II. Polyethylene fractions crystallized from dilute solutions", *Macromolecules*, vol. 1, no. 6, pp. 546-554.
9. Anantawaraskul, S., Soares, J. B. P., Wood-Adams, P. M., & Monrabal, B. (2003), "Effect of molecular weight and average comonomer content on the crystallization analysis fractionation (Crystaf) of ethylene  $\alpha$ -olefin copolymers", *Polymer*, vol. 44, pp. 2393-2401.
10. Pasch, H., Brüll, R., Wahner, U., & Monrabal, B. (2000), "Analysis of polyolefin blends by crystallization analysis fractionation", *Macromolecular Materials and Engineering*, vol. 279, no. 1, pp. 46-51.
11. Mori, S. & Barth, H. G. (1999), *Size exclusion chromatography*, Springer, New York.
12. Striegel, Andre M.(2003), *Multiple detection in size-exclusion chromatography*, American Chemical Society, Washington DC.
13. DesLauriers, P. J. (2003), "Measuring compositional heterogeneity in polyolefins using size-exclusion chromatography/Fourier transform infrared spectroscopy", *American Chemical Society (ACS) Symposium Series*, vol. 893, pp. 210-229.

14. Scolah, M. J. (2005), *Experimental and modelling investigation of a novel tetrafunctional initiator in free radical polymerization*, Doctor of Philosophy in Chemical Engineering, University of Waterloo.
15. Hore, P. J. (1995), *Nuclear Magnetic Resonance*, Oxford University Press Inc., New York.
16. Shroff, R. N. & Mavridis, H. (2001), "Assessment of NMR and Rheology for the characterization of LCB in essentially linear polyethylenes", *Macromolecules*, vol. 34, pp. 7362-7367.
17. Shroff, R. N. & Mavridis, H. (1999), "Long-chain-branching index for essentially linear polyethylenes", *Macromolecules*, vol. 32, pp. 8454-8464.
18. Heiney, P. A. High resolution x-ray diffraction. University of Pennsylvania . (12-30-1996).  
Ref Type: Electronic Citation
19. Fultz, B. & Howe, J. (2002), *Transmission electron microscopy and diffractometry of materials*, 2 edn, Springer, New York.
20. Kakudo, M. & Kasai, N. (1972), *X-ray diffraction by polymers*, Kodansha LTD. and Elsevier Publishing Company, Tokyo, Amsterdam, New York.
21. Ferry, J. D. (1980), *Viscoelastic Properties of Polymers*, 3 edn, Wiley, New York.
22. Seki, M., Thurman, D. W., Oberhauser, J. P., & Kornfield, J. A. (2002), "Shear-mediated crystallization of isotactic polypropylene: The role of long chain-long chain overlap", *Macromolecules*, vol. 35, no. 7, pp. 2583-2594.
23. Moffitt, M., Rharbi, Y., Chen, W., Tong, J. D., Winnik, M. A., Thurman, D. W., Oberhauser, J. P., Kornfield, J. A., & Ryntz, R. A. (2002), "Stratified morphology of a polypropylene/elastomer blend following channel flow", *Journal of Polymer Science Part B-Polymer Physics*, vol. 40, no. 24, pp. 2842-2859.
24. Menard, K. P. (1999), *Dynamic Mechanical Analysis: A Practical Introduction*, CRC Press, New York.
25. Li, P. S. C. (2002), *Approaches to tailoring the structure and properties of polyethylene*, Ph.D, Department of Chemical Engineering, University of Waterloo, Waterloo, Ontario, Canada.
26. McCrum, N. G., Buckley, C. P., & Bucknall, C. B. (1997), *Principles of Polymer Engineering*, 2 edn, Oxford University Press, Oxford, New York, Tokyo.
27. Ward, I. M. (1971), *Mechanical Properties of Solid Polymers*, Wiley-Interscience, Toronto.

28. Lin, L. & Argon, A. S. (1994), "Structure and plastic deformation of polyethylene", *Journal of Materials Science*, vol. 29, pp. 294-323.
29. Sperling, L. H. (2001), *Introduction to Physical Polymer Science*, 3 edn, Wiley-Interscience, Toronto.
30. Allison, S. W., Pinnock, P. R., & Ward, I. M. (1966), "Cold drawing of poly(ethylene terephthalate)", *Polymer*, vol. 7, no. 1, pp. 66-69.
31. Scheirs, J. (2000), *Compositional and Failure Analysis of Polymers: A practical approach*, John Wiley & Sons, Ltd, Chichester, West Sussex, England.
32. Schellenberg, J. & Fienhold, G. (1998), "Environmental stress cracking resistance of blends of high-density polyethylene with other polyethylenes", *Polymer Engineering and Science*, vol. 38, no. 9, pp. 1413-1419.
33. Brostow, Witold and Corneliussen, Roger D.(1986), *Failure of plastics*, Hanser Publishers, New York.

## **CHAPTER 4 MECHANICAL PROPERTY RELATIONS WITH ENVIRONMENTAL STRESS CRACKING RESISTANCE**

### **4.1 Introduction\***

Polyethylene materials do not show any signs of brittle fracture until the materials have failed completely. This poses a serious problem for polyethylene used in structural and pipe applications. Environmental stress cracking (ESC) is a type of brittle fracture failure often observed in polyethylene. Polyethylene pipe that should have a service life of fifty years or more is often known to crack within a year due to ESC (1). Therefore study and testing of environmental stress cracking resistance (ESCR) of polyethylene are of great interest. The notched constant load test (NCLT), ASTM D5397, is commonly used to measure ESCR of polymers. This is a time consuming test method, as high density polyethylene is known to have NCLT values in the range of thousands of hours (2).

Environmental stress cracking is the stress failure of a polymer when subjected to an aggressive environment, such as “soapy” water (water and emulsifier). In most cases, the type of fracture associated with ESC is characterized by clean cracks, which indicate a brittle fracture mechanism (3). Any cracking of polymer due to an aggressive environment can be referred to as environmental stress cracking (for example, the degradation of polymer due to exposure to UV light that may lead to mechanical failure

---

\* The contents of this chapter have appeared in "A tensile strain hardening test indicator of environmental stress cracking resistance", Journal of Macromolecular Science: Pure and Applied Chemistry, vol. 45, no. 8, pp. 599-611 (2008).

of the material). However, most of the time ESC refers to the stress cracking of polymer due to an active environmental effect without any chemical alteration of the material (therefore, a purely physical process). Polar solvents such as alcohols, detergents (soaps, emulsifiers) and silicone oils represent aggressive environments for polyethylene.

Stress cracking of polyethylene can take a long time. An active environment, such as a surfactant in water, is believed to reduce the surface free energy of the fibrils in a craze and prevent the fibrils from packing into a dense structure, thus leading to craze stabilization. Ultimately, this leads to the formation of cracks and the failure of the polymer (4). The exact mechanism of how commonly employed surfactants, such as Igepal, facilitate SCG (slow crack growth) is not clear. Ward *et al.* (5) proposed that the long Igepal molecules align themselves with tie-molecules (see below) in the fibrils, thus reducing the frictional stress as tie-molecules disentangle from crystals. As tie-molecules become untangled more easily, the ESCR of the polymer decreases. It is generally accepted that an active environment can act as 'lubrication' for chain disentanglement (6), thus resulting in accelerated SCG of polyethylene. Research has shown that the initial rate of SCG for polyethylene samples in Igepal solution is the same as for samples in air. It is only after a sufficient time period has elapsed, allowing Igepal to diffuse into the crystalline region of the polymer, that the cracking process is accelerated (5). This indicates that the initial rate of ESC is controlled by diffusional limitations of the active ingredient. The ESCR of polyethylene can thus be increased if diffusion of the aggressive agent is limited.

Environmental stress cracking occurs by a brittle fracture mechanism. Brittle fracture is believed to be caused by disentanglement of inter-lamellar links (3). The number and type of these inter-lamellar connections play an important role on ESCR of polyethylene. There are two types of these connections. The first kind is called bridging tie-molecules, or tie-molecules for short. The two ends of these molecules crystallize in two different lamellae, thus connecting them. Tie-molecules have strength due to covalent bonds. The other type of inter-lamellar links is made of entanglements of loose loops and cilia, which are believed to be held together by van der Waals forces (3) and chain coupling (7). From this point on, only bridging tie-molecules will be referred to as tie-molecules. All other types will be lumped together in what we refer to below as entanglements.

Physical chain entanglements in a polymer are the second type of inter-lamellar linkage that holds crystalline lamellae together. The importance of tie-molecules on environmental stress cracking of polyethylene has been studied extensively; however, physical chain entanglements have not. Since brittle fracture occurs through a mechanism of chain disentanglements (3), the time it takes for physical chain entanglements to separate from one another will also contribute to the ESCR of polyethylene. Research has certainly shown that physical chain entanglements influence tensile behaviour of polyethylene (8-10). Physical entanglements may not be as strong as tie-molecules (11), but probability calculations showed that the chance of occurrence of entanglements in the amorphous phase is much higher than the occurrence of tie-molecules (12). Therefore, both tie-molecules and chain entanglements are important for ESCR of polyethylene.

Environmental stress cracking resistance of a polymer is known to increase with increasing tie-molecules concentration (11, 13). Molecular weight (12, 14, 15) and short chain branching (SCB) play critical roles in tie-molecule formation (13, 16, 17). The higher the molecular weight of the material the more likely to have chains long enough to be embedded in two or more crystalline lamellae and hence form tie-molecules. On the other hand, SCB interrupts the chain folding process of lamella formation (18), therefore long polyethylene chains with SCB are more likely to have more tie-molecules and entanglements. Polyethylene resins for pipes developed over the years have incorporated many of the features that lead to better ESCR. The latest, PE100 resins (2), are made with both high molecular weight and high SCB content in mind. These resins are known to have desirable ESCR properties.

Strain hardening occurs when the amorphous phase of polyethylene is stretched to its maximum extension during tensile deformation. It is a phenomenon observed in fully drawn (and cold-drawing of) polymers. The cause of increase in stress at strain hardening is reported as due to molecular alignment resulting in increased drawing stress (19). As the material is drawn, strain-induced crystallization occurs and drawing stress increases. In semicrystalline polymers, such as polyethylene, both crystalline and amorphous phases play important roles in ductile deformation (20-22). In an uniaxial tension test, before yield, the stiffer crystalline phase of polyethylene undergoes little deformation whereas the amorphous phase deforms substantially to accommodate the overall deformation of the material sample. After the yield point but before strain

hardening, the slipping of lamellae occurs, and both crystalline and amorphous phases play a part in load bearing and straining. When the amorphous phase is fully stretched, the onset of strain hardening begins. In the strain hardening phase, the fully extended amorphous phase becomes the rigid load-bearing element, while crystalline lamellae break apart and unfold to accommodate the change in strain (23). The load-bearing elements in the amorphous phase of polyethylene are comprised of both tie-molecules and entanglements. Since these are very important elements for the ESCR of polyethylene, it follows that strain hardening and ESCR behaviour of polyethylene can be correlated.

Finally, the strain at onset of strain hardening is a function of the extensibility of the polymer network. The measurement used to characterize the extensibility of a polymer network is the natural draw ratio (NDR). In crosslinked polymers, extensibility of the material is controlled by the number of crosslinks. For polymer without crosslinks, chain entanglements control the extensibility of the material. Evidence supporting this relationship between network extensibility (and hence, NDR) and physical chain entanglements has been observed in the behaviour of melt-spun fibers (24).

In the strain hardening state, physical chain entanglements and tie-molecules are the molecular structural entities that hold the bulk of the material together. This is the basis of the recent suggestion by Kurelec *et al.* (25) and the practical extension proposed in the current chapter. In order to carry out their tests at a high strain rate (10 mm/min), Kurelec *et al.* (25) conducted their experiments at an elevated temperature of 80°C, with

the aid of an optical extensometer, an instrument not commonly found in most laboratories. In our work we propose a practical extension towards a much simpler tensile strain hardening test carried out at ambient conditions as a tool for screening ESCR values of high density polyethylene. Comparisons between the proposed strain hardening test method and the time consuming and rather imprecise, commonly used NCLT method suggest that strain hardening at ambient temperatures can successfully rank ESCR of HDPE, and hence has the potential of replacing the more tedious and noisy conventional test.

## 4.2 Experimental Methods

### 4.2.1 Polymer Characterization and Mechanical Testing

The experimental methods used for polymer characterization and mechanical testing were presented in Chapter 3. For the sake of brevity these methods will not be described again in this chapter. Table 4.1 contains the list of experimental methods used in this chapter, and corresponding material property determined. For a description of the principles of each method and other details, the reader is referred to the appropriate section in Chapter 3 of the thesis (Chapter 3 section #).

**Table 4.1: List of experimental methods for Chapter 4**

<b>Method</b>	<b>Property Determined</b>	<b>Chapter 3 section #</b>
DSC	Crystallinity	3.1.1
GPC	Molecular weight and molecular weight distribution	3.1.3
<sup>13</sup> C NMR	Short chain branch content	3.1.4
Tensile test	Strain hardening measurements and NDR	3.3.1
NCLT	ESCR values	3.3.2

## 4.2.2 Experimental Design for NCLT

A randomized central composite design (with blocking) was used to investigate the effects of different levels of tensile stress and notch depth on the outcome of NCLT tests. The resin used in this investigation was PE 1. (Table 4.3 summarizes the resins and some of their characteristics pertinent to this work). The test levels for the full design are listed in Table 4.2. A total of 15 tests were completed. For block-1 tests, the centre point of the design is shifted to 40% notch depth and 15% yield strength in order to compare to conditions of previous tests (see section 3.3.2), thus making the experimental design a “pseudo central” composite design. In block-2, a partial central composite design was used to clarify the behaviour at higher notch depth and percentage yield strength. Overall, the notch depth used ranged from 18.8%-74.1%, whereas the percentage yield strength (stress level) applied ranged from 4.4%-37.1%.

**Table 4.2: Experimental design<sup>1</sup> for NCLT of PE 1**

	Block	%Notch depth	%Yield Strength	%Notch depth	%Yield Strength
1	1	-1.33	-0.67	20.0%	10.0%
2	1	-1.33	1.33	20.0%	25.0%
3	1	0.67	-0.67	50.0%	10.0%
4	1	0.67	1.33	50.0%	25.0%
5	1	-1.41	0	18.8%	15.0%
6	1	1.41	0	61.2%	15.0%
7	1	0	-1.41	40.0%	4.4%
8	1	0	1.41	40.0%	25.6%
9 (C) <sup>1*</sup>	1	0	0	40.0%	15.0%
10 (C) <sup>1*</sup>	1	0	0	40.0%	15.0%
11	2	0	-1.41	60.0%	22.9%
12	2	0	1.41	60.0%	37.1%
13	2	-1.41	0	45.9%	30.0%
14	2	1.41	0	74.1%	30.0%
15 (C) <sup>*</sup>	2	0	0	60.0%	30.0%

<sup>1</sup>Conventional test settings: 15% yield strength, 40% notch depth

\*C: centre point

## 4.3 Results and Discussion

### 4.3.1 ESCR Results from NCLT Test

Ten industrial high density polyethylene resins were studied in this project (see Table 4.3). The resins included three blow molding resins (PE1-3), three injection molding resins (PE4-6), and four pipe resins (PE7-10). PE8 is a PE80 grade pipe resin, while PE7, PE9 and PE10 are PE100 grade pipe resins. In Table 4.3, Mn, Mw and Mz stand for number-, weight- and z- average molecular weights, respectively, whereas PDI denotes polydispersity.

**Table 4.3: Characteristics of resins**

Resin	Mn (kg/mol)	Mw (kg/mol)	Mz (kg/mol)	PDI Mw/Mn	Percent crystallinity	SCB (/1000C)
PE1	16.3	127.5	814.0	7.8	55%	2.8
PE2	15.7	118.5	837.1	7.6	59%	1.1
PE3	17.9	140.1	889.8	7.8	58%	0.9
PE4	19.7	79.4	239.3	4.0	55%	3.8
PE5	11.4	49.7	157.8	4.4	54%	7.0
PE6	14.0	62	195.0	4.4	57%	4.7
PE7	11.8	222.8	1593.5	18.9	53%	4.3
PE8	14.0	202.1	1398.4	14.4	56%	4.5
PE9	10.4	217.9	1244.2	20.9	62%	7.0
PE10	5.9	315.4	2129.3	53.3	51%	11.8

Results from NCLT on polyethylene resins in our study are listed in Table 4.4. Out of the ten resins in this study, PE5 and PE6 could not be tested using the NCLT method because the material was very brittle and could not survive the notching process. Pipe grade polyethylene resins (PE7-10) have dramatically longer time to failure than non-pipe grade resins (PE1-4). The ESCR time of pipe resins essentially follows the grading; PE100 resins are more resistant than PE80 resin. It is especially worth noting that the

PE10 samples did not fail even after 3000 hours. Blow molding resins (PE1-3) and injection molding resins (PE4-6) can not be compared to pipe resins in terms of the magnitude of NCLT failure time. Of the six non-pipe resins, PE1 and PE4 have the longest NCLT failure time.

**Table 4.4: NCLT results**

	NCLT	Standard deviation	Coefficient of variation
	(hours)	(hours)	
PE1	4.8	0.92	0.19
PE2	1.2	0.17	0.14
PE3	2.8	0.25	0.09
PE4	3.6	0.53	0.15
PE5	N/A	N/A	N/A
PE6	N/A	N/A	N/A
PE7	1395.8	338.74	0.24
PE8	198.3	44.74	0.23
PE9	843.4	338.90	0.39
PE10	>3000	-	-

Values in Table 4.4 are means (averages) over several independent replicates (usually, three dogbones from the same plate, and often two or three independent plates with two to five dogbones per plate). A detailed analysis of the variability of NCLT is presented later in section 4.3.1.1. The standard deviation of NCLT results is higher for higher molecular weight (MW) resins, as expected. Hence, the coefficient of variation (standard deviation over mean) for each resin is presented to clarify the masking effect of the differences in magnitude of ESCR values. The coefficient of variation values for all resins range from 0.09-0.39. The average coefficient of variation is 0.20. The lack of precision of test results is a known problem associated with NCLT. In industry, some NCLT results have been reported with coefficients of variation as high as 0.50 (26).

As mentioned earlier, ESCR of polyethylene is known to increase with increasing molecular weight. Pipe resins have much higher MW values (note the much higher weight- and z-average MW values) as compared to other types of resins, as can be seen in Table 4.3. Therefore, they exhibit larger (“better”) ESCR values. The importance of MW on ESCR can be further demonstrated by looking, for example, at resins PE4-6. PE4 has an average ESCR value of 3.6 hours, while PE5 and PE6 have negligible ESCR values. In Figure 4.1, the x-axis gives the logarithmic transformation of molecular weight values, and the y-axis gives the weight fraction of polymer chains with a specific molecular weight. The MWD curves of these three resins have a similar shape, with the only difference being that the curve for PE4 is shifted to higher MW values. The higher  $M_z$  average molecular weight is especially significant, since it is an indication of a longer and/or larger tail in the high molecular weight end of the molecular weight distribution. Large chains are more likely to form tie-molecules and entanglements that are critical to ESCR of HDPE.

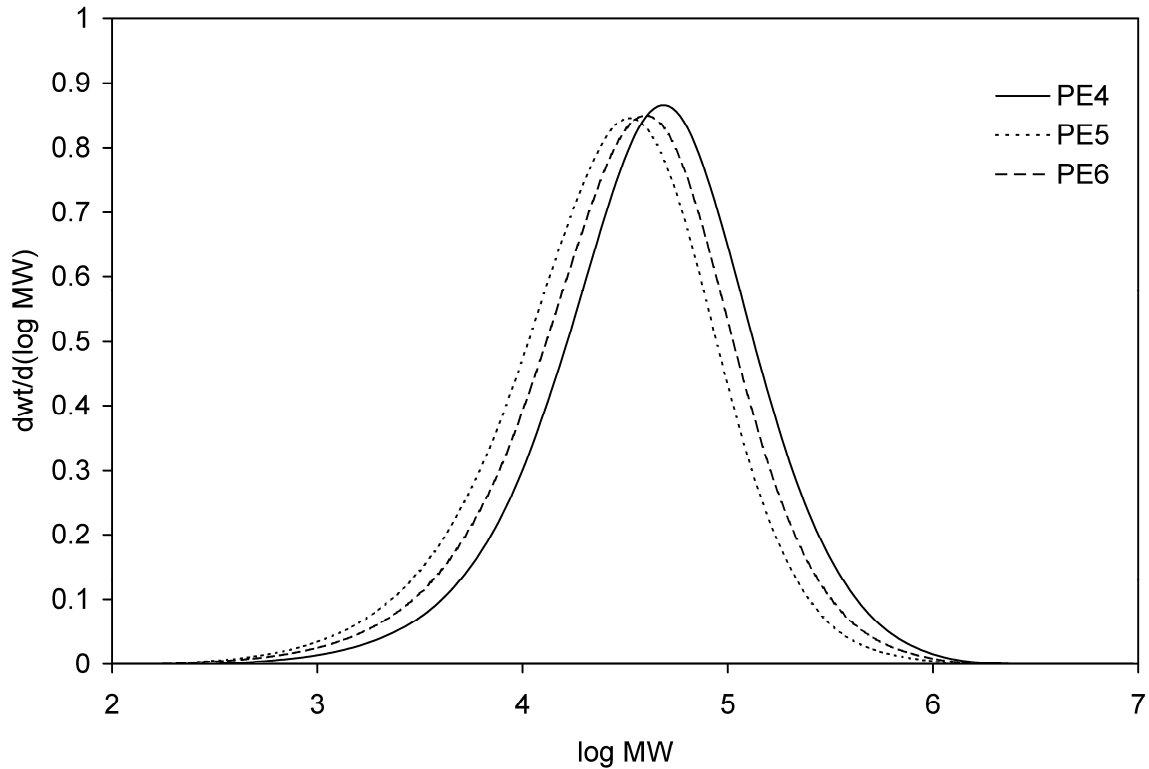


**Figure 4.1: MWD curves of PE 4-6**

The MWD of polyethylene also influences its ESCR. Resins with larger polydispersity index (PDI) values have higher ESCR values (see Tables 4.2 and 4.3). This suggests that resins with broad MWD exhibit higher ESCR. GPC analysis of all resins showed that PE4-6 have the narrowest MWD (Figure 4.1), followed by PE1-3 (Figure 4.2), whereas the pipe resins PE7-10 have the broadest MWD (Figure 4.3). Of the four pipe resins, PE9 and PE10 have bimodal and much broader MWD than all other resins. It is especially worth noting that PE10 shows a much larger fraction of polymer at the high MW tail of the distribution compared to all other resins. Higher content of high MW chains leads to the formation of more inter-lamellar connections, which explains the improved ESCR for the resin.

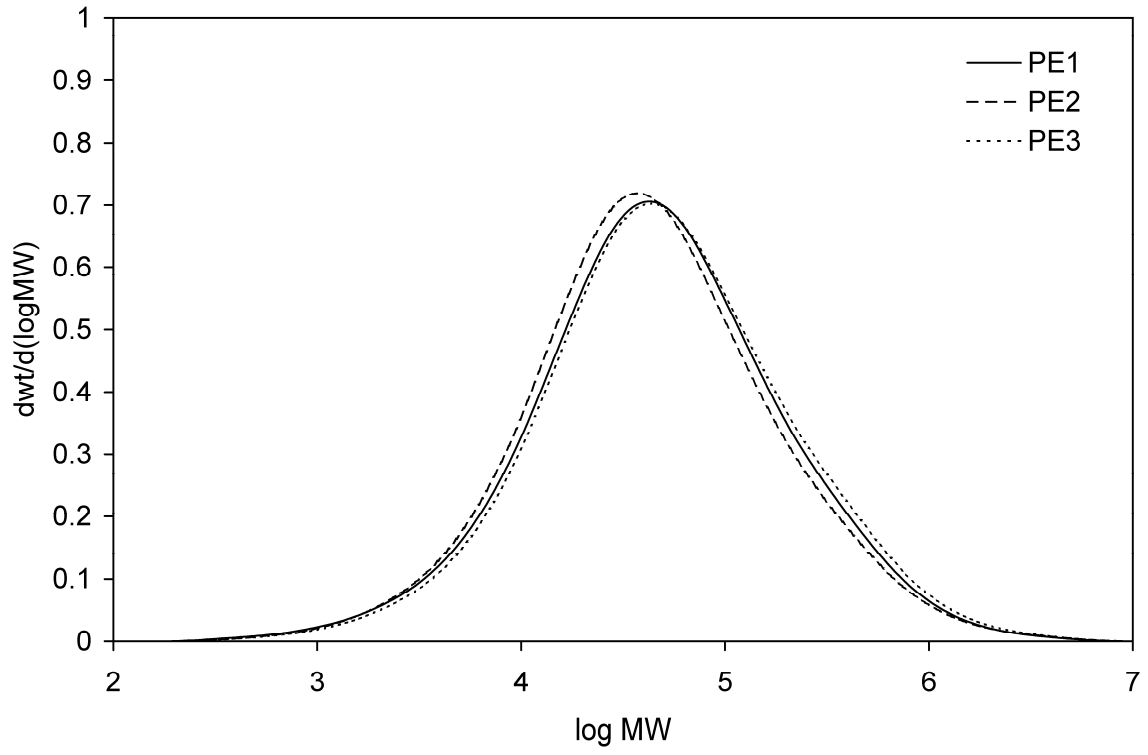


Figure 4.2: MWD curves of PE 1-3

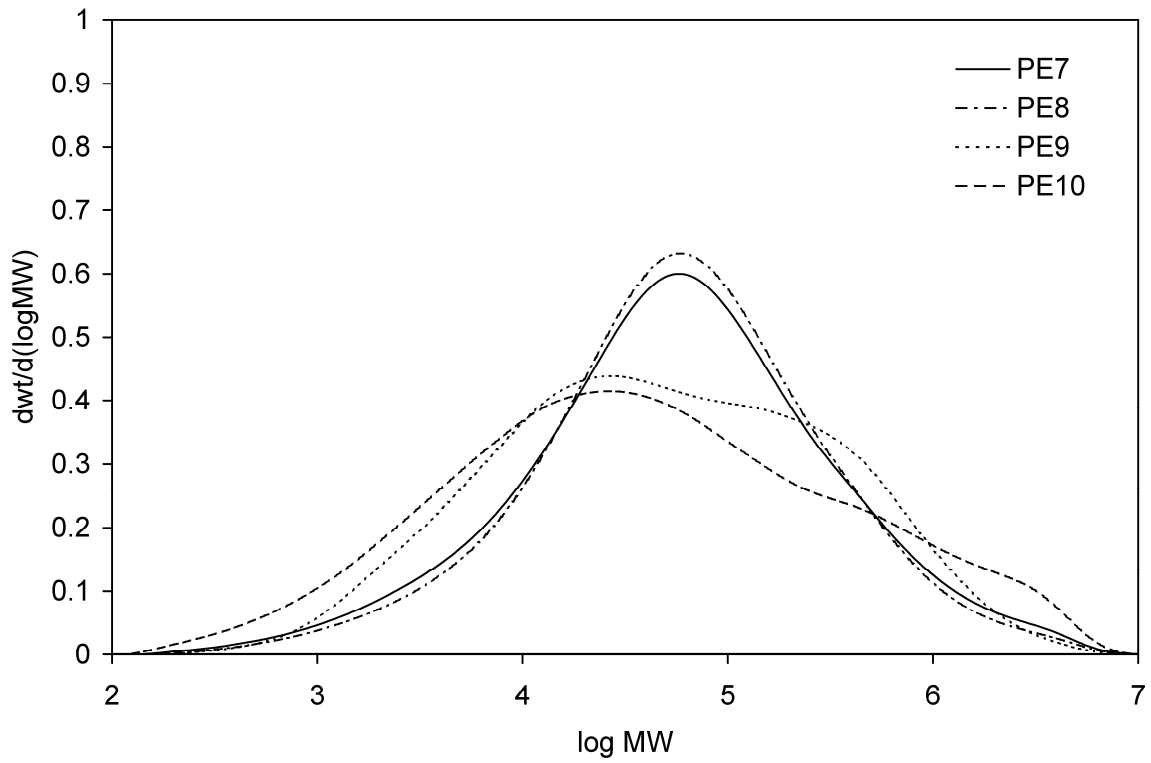


Figure 4.3: MWD curves of PE 7-10

Molecular weight and molecular weight distribution differences alone cannot explain the different ESCR behaviour of the resins. PE 1-3 have similar MW values and MWD shapes (Figure 4.2), yet PE1 has a higher ESCR value than PE2 or PE3. This difference can be attributed to the different SCB content of these resins. All of the resins in this study have butyl branches as the side chain group. PE9 also has a small amount of methyl branches. Table 4.3 lists the number of short branches per 1000 carbon atoms for all resins as measured via  $^{13}\text{C}$ -NMR. Comparing PE1-3, PE1 has almost three times as much SCB compared to PE2 or PE3. As mentioned earlier, an increase in resin SCB content is known to improve ESCR of polyethylene. However, a higher SCB content alone, as in the case of PE5-6, did not result in good ESCR behaviour. Based on the analysis results so far, it is important to point out (and re-emphasize the point from the literature) that high SCB content must be combined with sufficiently high MW values (and appropriate breadth of the MWD) in order to improve ESCR of a resin. In addition to SCB content, short chain branching distributions (SCBD) of resins were determined using Fourier Transform Infrared Spectroscopy (FTIR) coupled with GPC. In general, PE1-6 were found to have higher SCB content in the low MW end of the molecular weight distribution, while PE7-10 had higher SCB content in the high MW end of the MWD. The higher SCB content in the high MW end of the MWD is known to improve ESCR of polyethylene (2), which explains in part the significantly higher ESCR values of PE7-10 compared to PE1-6. More discussion regarding SCBD of resins can be found in Appendix A.

For linear polyethylene, crystallinity increases in a way directly proportional to MW. The presence of SCB interrupts the chain folding process of crystallization and reduces the overall crystallinity of the material. Long chains that are not incorporated into the crystalline lamellae form chain entanglements and tie-molecules that increase ESCR of polyethylene (27). For polymers of similar MW, resins containing higher SCB content would possess lower crystallinity. Comparing PE1-3, PE1 has higher SCB content, lower crystallinity (Table 4.3) and higher ESCR value (Table 4.4). The same trend is also observed for the pipe resins. PE10 has the highest ESCR value with the lowest percent crystallinity. In summary, pipe grade resins take longer to fail in NCLT than non-pipe resins. The differences in measured ESCR values can be explained by current theory and understanding of ESC of polymers.

#### **4.3.1.1 Effect of Notch Depth and Stress Level on NCLT**

The notched constant load test is a standard ASTM method that is widely used by both academia and industry (2, 25) to determine ESCR of a polymer. To investigate whether the test procedure used for NCLT contributes any significant variability to the results, independently replicated tests were conducted.

Tests were replicated starting from step one, sample plate molding. Comparisons were made between samples from different molded plates. Results of the tests were then analyzed using statistical methods to investigate sources of variability. Table 4.5 shows the ANOVA (ANalysis Of VARIance) for replicated tests using PE1. The F-observed value of Table 4.5 is smaller than the F-critical value of 224.58 (based on a 5%

significance level and (4, 1) degrees of freedom). This means that there is no statistically significant difference in variability between the results of the independently replicated tests. Therefore, the test procedure used does not contribute significantly to the variability of the measurements. Independent replicated tests on other resins also demonstrated that the test procedure does not contribute significant variability to the results. Therefore, the main source of variability in NCLT is from the material itself.

**Table 4.5: ANOVA of independent replicated test results for PE1**

	df	SS	MS	F
Same molded plate	4	2.527	0.632	94.33
Different molded plates	1	0.0067	0.0067	
Total	5	2.5337		

In the ASTM method (ASTM D5397) for NCLT, the notch depth is recommended to be at 20% of the thickness of the sample, but there is no recommendation for the applied level of stress. In the literature, various applied stresses are reported. Some take the approach of applying stress as a percentage of the yield strength of the material, while others use a constant stress level for different polymers. In order to clarify the effect that yield stress and notch depth have on the results of NCLT, experiments using a central composite design (28) were carried out. The design matrix of the experiment was given earlier in the experimental section (Table 4.2).

PE1 was again the resin selected for this experiment because it has a reasonable NCLT failure time. The tensile strength at yield for PE1 is 27 MPa. Results from the experiments are presented in Table 4.6. Figure 4.4 is a contour plot of ESCR (in hours) as a function of stress applied (percentage yield strength) and notch depth (percentage

notch depth). The change in ESCR is larger with changes in stress level than with changes in notch depth. Observe the more closely packed contour lines in the decreasing yield strength (stress level) direction, an indication of steeper increase of ESCR values. This shows that NCLT results are more sensitive to changes in stress level than changes in notch depth. When the stress level is low, the effect of notch depth is rather small.

**Table 4.6: NCLT results for PE1 at different levels of notch depth and yield stress**

% notch depth	% yield strength	ESCR (hours)
20%	10%	167.8
20%	25%	1.9
50%	10%	87.9
50%	25%	1.3
19%	15%	32.0
61%	15%	7.0
40%	4%	300.0
40%	26%	1.6
40%	15%	6.0
40%	15%	6.1
60%	23%	2.2
60%	37%	0.4
46%	30%	0.4
74%	30%	1.8
60%	30%	1.4

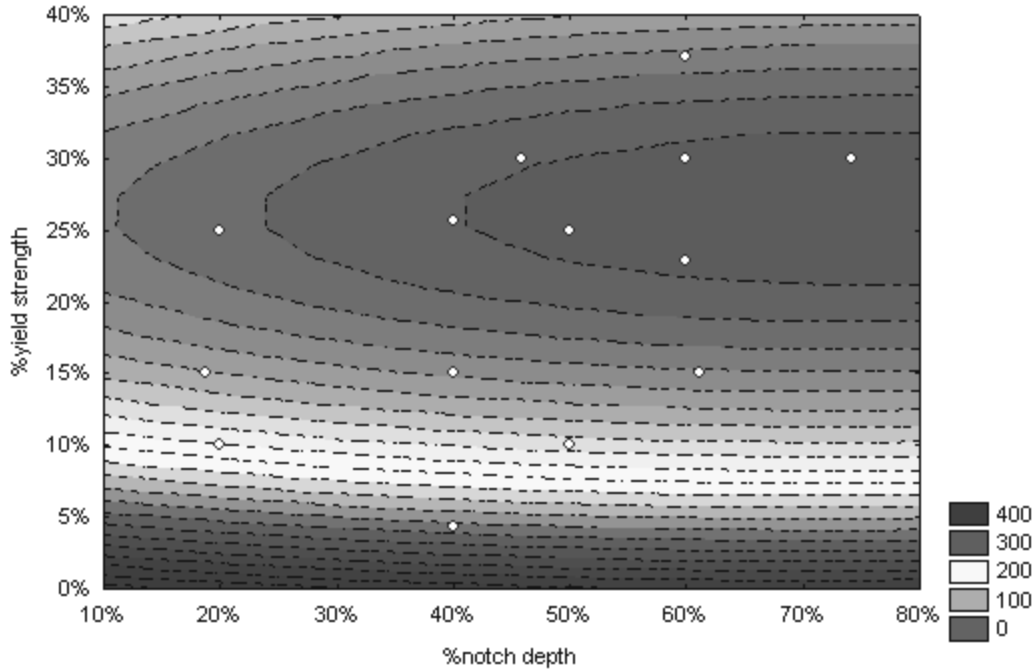


**Figure 4.4: Effect of % yield strength and % notch depth on NCLT results (hours)**

The contour plot of Figure 4.4 is generated using an equation of the following form,

$$z = \beta_0 + \beta_1 x + \beta_2 y + \beta_3 x^2 + \beta_4 y^2 + \beta_5 xy + \varepsilon \quad (4.1)$$

$z$  – NCLT result,  $x$  – % notch depth,  $y$  - % yield stress,  $\varepsilon$  - error

Analysis of variance carried out on Equation 4.1 above gives indications of the influence that each term has on the NCLT results. In Table 4.7, the linear and quadratic terms of % yield strength have the largest F values, which indicate that yield stress used has the greatest influence on NCLT results. The notch depth terms do not have an F value larger than the corresponding F-critical value of 5.32 (with (1,8) degrees of freedom at 5% significance level), hence they do not have a significant influence on NCLT results.

There is also no significant interaction from the combined effect of percentage notch depth and percentage yield stress applied (xy term in Equation 4.1, 1L by 2L in Table 4.7). The ANOVA results indicate that the change from 20% notch depth to 40% notch depth has no significant effect on the NCLT results. At a stress level of 15% of the yield strength, Figure 4.4 also shows that there is no significant change in NCLT values of samples with different notch depths. Therefore, the use of 40% notch depth does not alter the conclusions drawn on ESCR behaviour of polyethylene. Hence, it was decided to adopt 15% of yield stress as the common test stress level (as a compromise), since this level gave consistent results for the wide range of different resins in this study. Since NCLT results are sensitive to the level of stress used, caution should be exercised when comparing test results from different sources.

**Table 4.7: ANOVA of effect of yield strength and notch depth on NCLT results (hours)**

	SS	df	MS	F
Test date (blocks)	742.0	1	742.0	0.422
Notch depth(1L*)	1063.5	1	1063.5	0.605
Notch depth(Q*)	124.9	1	124.9	0.071
%yield strength(2L)	22172.0	1	22172.0	12.617
%yield strength(Q)	20527.3	1	20527.3	11.681
1L by 2L	2.2	1	2.2	0.001
Error	14059.0	8	1757.4	
Total	58690.9	14		

\*L-linear term, Q-quadratic term

### 4.3.2 Strain Hardening and ESCR of Resins

NCLT is a time-consuming test method. As seen in the previous section, sample test times range from a few hours to several thousands of hours. There is a great interest in the development of a faster test for classifying ESCR behaviour of polymers (of course,

in a reliable way). Tensile tests performed on “pre-strain-hardened” samples of polymer have shown promise in correlating ESCR to tensile properties of polyethylene (29, 30). Raman spectroscopy studies of polyethylene at the strain hardening stage have shown that the structures of cold drawn material just before failing and slow crack growth fibrils are very similar (4). Hence, strain hardening behaviour can be related to ESCR of polyethylene. Recently, Kurelec *et al.* (25) proposed the use of strain hardening modulus obtained at 80°C as a possible correlation to ESCR values of polyethylene.

Since most PE applications are under ambient conditions, a method to test the ESCR of resins at room temperature would be practical. With this aim in mind, tensile constant strain rate tests were carried out at room temperature following the general guidelines of the standard tensile test (ASTM D638). Displacement of crosshead and the sample load were measured at constant strain rate. As compared to approaches where true stress and true strain measurements are needed (25, 31), this method does not require any special equipment and can be readily carried out on any tensile tester.

The elongation of sample was observed to follow the typical deformation behaviour of a semi-crystalline polymer (Figure 4.5). Load increases with increasing displacement until the yield point; then the load drops and the test sample undergoes ductile deformation at a relatively constant load value until strain hardening occurs and the load increases again with increasing displacement; finally, the sample breaks. Independent replicated tests were carried out for selected resins to investigate the reproducibility of the strain hardening test. In Figure 4.5 replicates of PE1 and PE7 are shown. The load value for

the strain hardening section of the graph for PE1 is the same for both samples. For PE7 there is a small difference in the load value of 4.3%. The results are well within the acceptable range, demonstrating good reproducibility of the strain hardening test. Detailed statistical analysis of the strain hardening test is presented later in section 4.3.6. Several resins (PE2, PE3, PE5 and PE6) could not be tested using the strain hardening test method. PE5 and 6 are brittle and break before full elongation can be achieved. PE2 and 3 did not achieve strain hardening even at maximum extension of the test apparatus. These resins are excluded from the subsequent discussion.

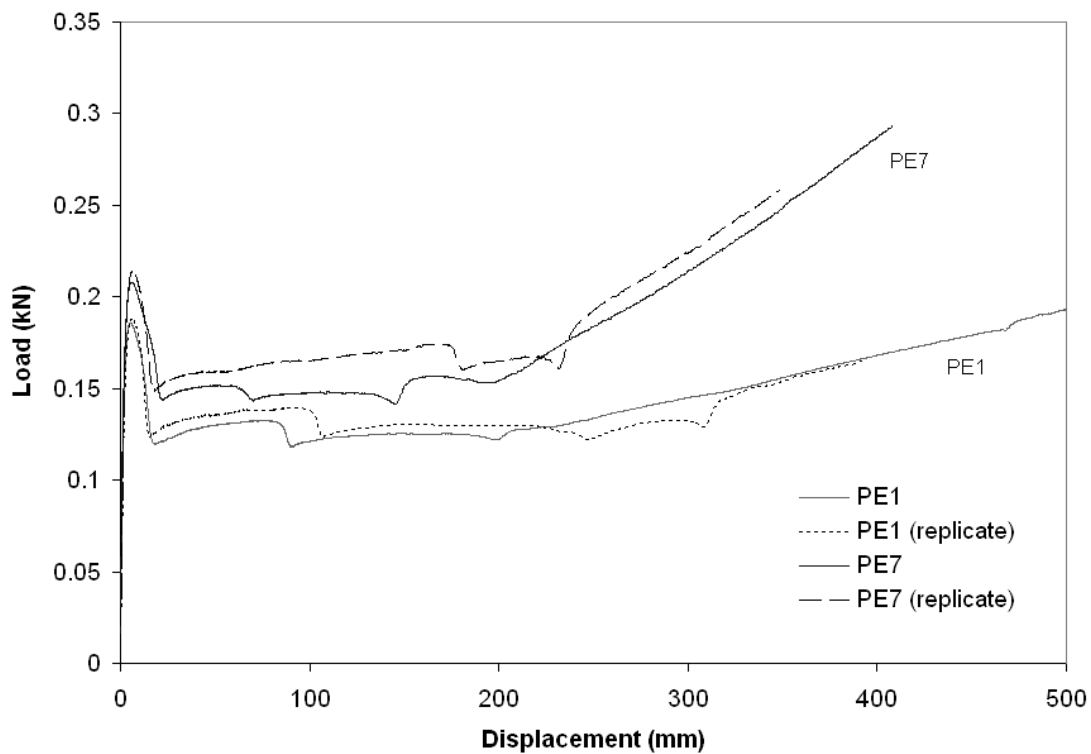


Figure 4.5: Tensile elongation at constant strain rate of 0.5 mm/min

The rate of load increase in the strain hardening stage is faster for high MW material than for low MW material. This can be seen in the behaviour of PE7 and PE1 in Figure 4.5. The strain hardening section of the elongation curve is linear and well-defined. Therefore, a characteristic slope can be determined for each resin. This characteristic slope is a function of applied load over total sample displacement, which could be considered as a definition of “material stiffness” (19). This measurement is related to strain hardening modulus (25), thus, in order to distinguish it from the conventional definition of “stiffness” for a material (related to Young’s modulus in the pre-yield section of the graph), we will call this characteristic slope the “hardening stiffness” (HS). The values of HS and ESCR for each resin tested are listed in Table 4.8.

**Table 4.8: Hardening stiffness (HS) and NDR of polyethylene**

	Strain rate - 0.5 mm/min			Strain rate – 7 mm/min			ESCR (hours)
	Hardening stiffness (N/mm)	Coefficient of variation of HS	NDR	Hardening stiffness (N/mm)	Coefficient of variation of HS	NDR	
PE4	0.183	0.08	9.3	0.287	0.13	10.5	3.6
PE1	0.250	0.08	7.2	0.527	0.003	8.6	4.8
PE8	0.578	0.02	7.0	0.730	0.11	6.3	198
PE9	0.609	N/A	6.4	0.895	0.03	7.1	872
PE7	0.657	N/A	6.1	0.940	0.02	7.1	1396
PE10	0.663	0.02	6.6	1.008	0.01	6.9	>3000

In Figure 4.6 the strain hardening section of the load-displacement graph (Figure 4.5) for all resins is plotted and shifted to the same origin, in order to illustrate more clearly the differences between their slopes. The curves of resins with lower ESCR value have less of a steep slope in Figure 4.6. PE80 grade resin (PE8) has lower ESCR/NCLT value than the PE100 resins (PE7, PE9 and PE10). The differences can be clearly seen in the slopes of the curves. For resins with similar ESCR values, such as PE7 and PE9, the strain

hardening behaviour is similar, which is well reflected by the overlap of the two curves in Figure 4.6. The same trend is observed for PE1 and PE4, which also have similar ESCR values.

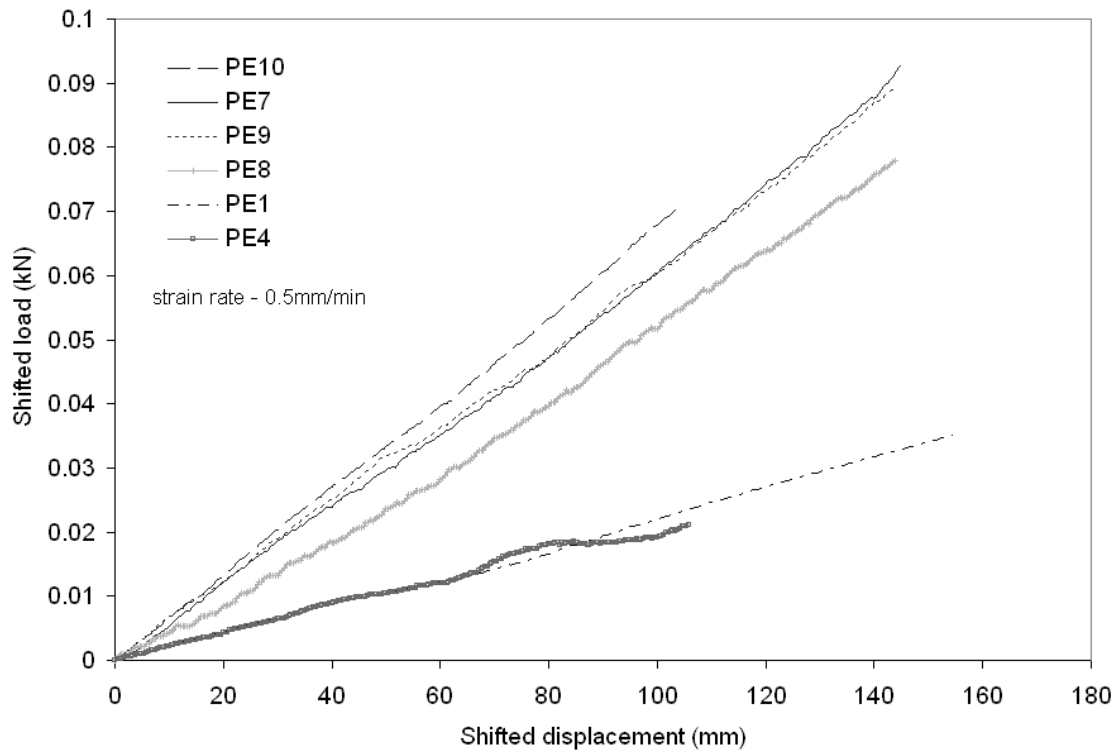


**Figure 4.6: Shifted load-displacement curves of the strain hardening stage; 0.5 mm/min strain rate**

The characteristic slope of curves in Figure 4.6 gives the HS value for each resin. These values are cited in Table 4.8. In Figure 4.7 the ESCR value of each resin is plotted against its hardening stiffness. The plot shows that the stiffer the material during strain hardening the higher its ESCR, and therefore establishes that the hardening stiffness can be used as a measure of the ESCR of polyethylene.

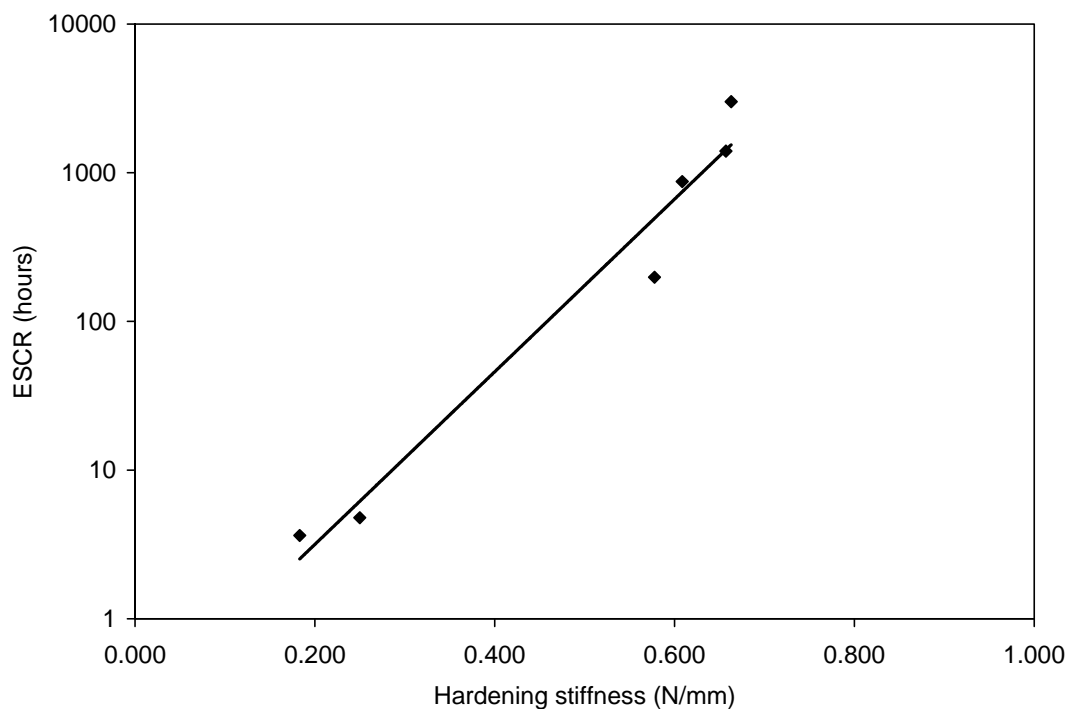


**Figure 4.7: Relation between ESCR and strain hardening stiffness of polyethylene at 0.5 mm/min strain rate**

### 4.3.3 Tensile Yield Point and ESCR

In contrast to the good correlation between ESCR values and strain hardening behaviour (see Figures 4.6 and 4.7), the behaviour at the yield point during tensile tests did not show any correlation to the ESCR of resins. In Figure 4.8 the load-displacement curves of the initial stages of ductile deformation are shown (see Figure 4.5, magnification of area below 50 mm displacement). Neither the yield load nor the point of onset of steady elongation offers any correlation to the resin ESCR value. During the strain hardening stage, the roles of inter-lamellar linkages are emphasized. Since chain entanglements and tie-molecules do not play a major role in the initial stage of ductile deformation, no correlation between ESCR and tensile yield behaviour of polyethylene can be made.

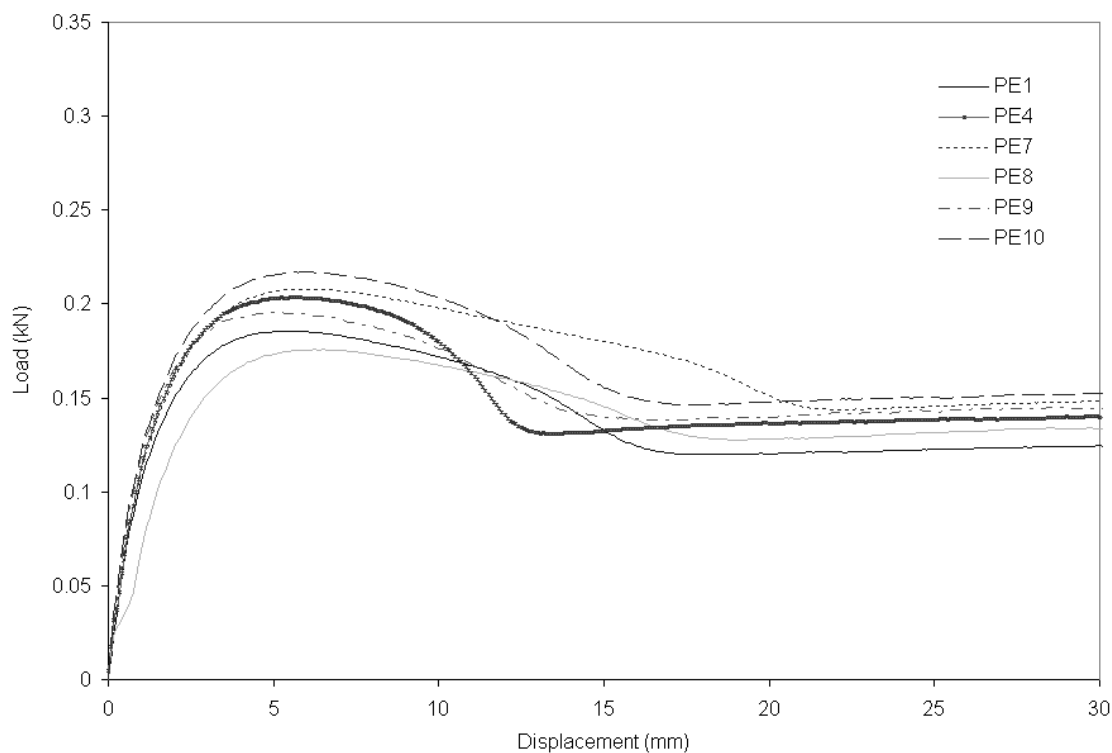


**Figure 4.8: Tensile elongation curves at yield point, 0.5 mm/min strain rate**

#### **4.3.4 Natural Draw Ratio (NDR) and ESCR**

An alternative tensile test measurement that has recently gained attention as a possible property to correlate to ESCR values of polymers is the natural draw ratio (32, 33). NDR has been defined in Equation 3.14. The NDR values of resins in this study are listed in Table 4.8. ESCR of resins is plotted against NDR in Figure 4.1. NDR appears to be inversely proportional to ESCR, which is in agreement with observations reported in the literature. Our test results show that resins with higher ESCR values, such as PE10, have smaller NDR. NDR is a function of the extensibility of the polymer network. As established earlier, resins with higher ESCR have more inter-lamellar linkages. A more

entangled polymer network would have lower extensibility and hence, smaller NDR. Therefore, it should be possible to correlate low NDR to high ESCR.

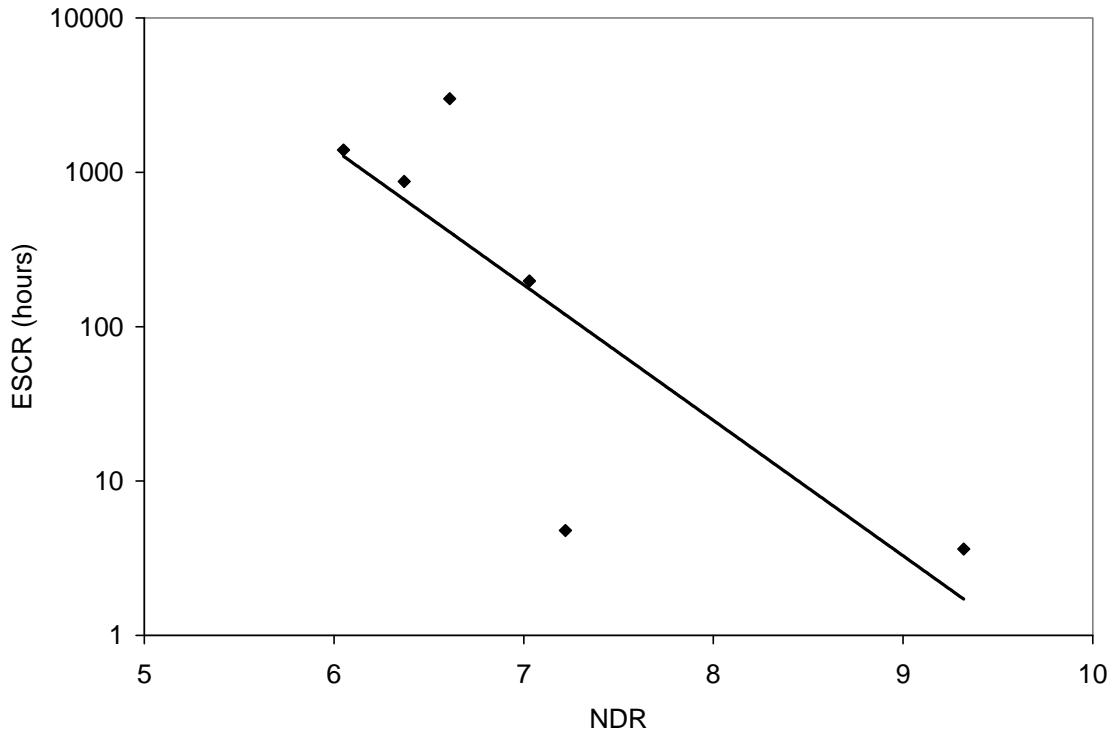


**Figure 4.9: Relationship between ESCR and NDR of polyethylene at 0.5 mm/min strain rate**

In Figure 4.9, it can be seen that the data points are relatively scattered (compared to the points of Figure 4.7). As shown in Figure 4.5, the load-displacement curves of resins are not smooth in the necking section (for example, observe curves in the displacement range of 50 mm to 150 mm). This is because the deformation is not uniform during the necking stage. Once full extension of the dogbone is realized, at the onset of strain hardening, the material deformation becomes uniform and the load-displacement curve is relatively smooth. The fluctuations in the steady elongation section of the load-displacement curve make the determination of the onset of strain hardening difficult (in agreement again with

observations of section 4.3.3), thus effectively resulting in the increased scatter of NDR data.

#### **4.3.5 Effect of Strain Rate**

The reason for developing a tensile test as an indicator of ESCR of polyethylene is because NCLT can be time consuming (and rather imprecise). Therefore, it is worth considering a tensile test at a high strain rate. Previous work done by Kurelec *et al.* was carried out at a 10 mm/min strain rate at 80°C (25). The reason for conducting the test at an elevated temperature was because of the lack of sensitivity in detecting differences in materials at high strain rate and lower temperature. In their opinion, testing at room temperature might be possible (i.e., reliable) if the strain rate is lowered to 0.25 mm/min.

Since increasing the speed of testing is one of the motivations for exploring tensile testing as a method for determination of ESCR of polyethylene, we subsequently investigated the use of higher strain rates at room temperature. The highest strain rate tried was 7 mm/min. In Figure 4.10, the shifted load-displacement curves for samples tested at 7 mm/min are shown. At 7 mm/min, resins exhibit curves with larger slopes compared to the tests done at 0.5 mm/min (compare Figures 4.6 and 4.10, and entries of Table 4.8). The difference between PE100-grade resins, PE80-grade resin and other types of HDPE was more pronounced at the higher strain rate. Within the PE100 resins, PE7 and PE9 curves showed similar slopes, as before.

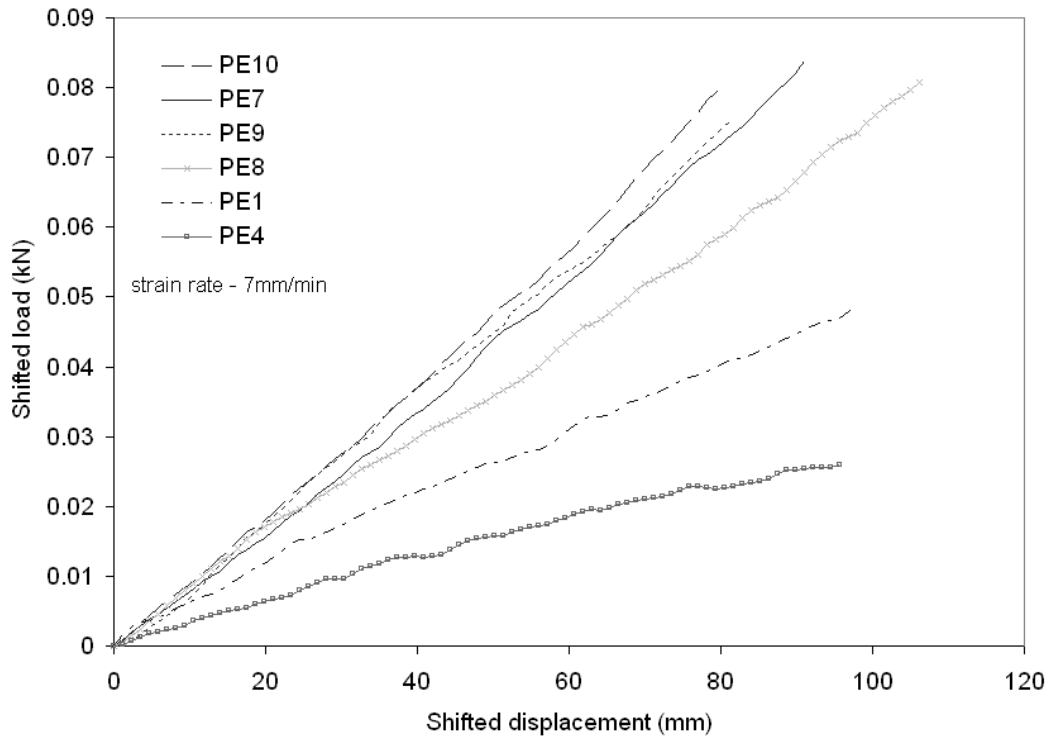


**Figure 4.10: Shifted load-displacement curves of polyethylene; 7 mm/min strain rate**

Let's consider again the values of strain hardening stiffness (HS) and NDR for 7 mm/min strain rate as listed in Table 4.8. The differences in HS values of the resins can be clearly seen. In Figure 4.11, ESCR values are plotted versus hardening stiffness values at 7 mm/min and 0.5 mm/min. The trend in hardening stiffness at 7 mm/min strain rate is the same as tests done at 0.5 mm/min. Higher hardening stiffness values are associated with higher ESCR values. At the higher strain rate, resins show higher hardening stiffness values (the curve for 7 mm/min is shifted to the right of the 0.5 mm/min curve). The difference between ESCR of resins is able to be detected equally well using both strain rates at room temperature. The 7 mm/min strain rate is comparable in magnitude to the 10 mm/min strain rate used by Kurelec *et al.* at 80°C (25). Therefore, this

demonstrates that it is possible to carry out reliable strain hardening tests using a relatively high strain rate (in order to minimize the duration of the test) even at room temperature conditions.

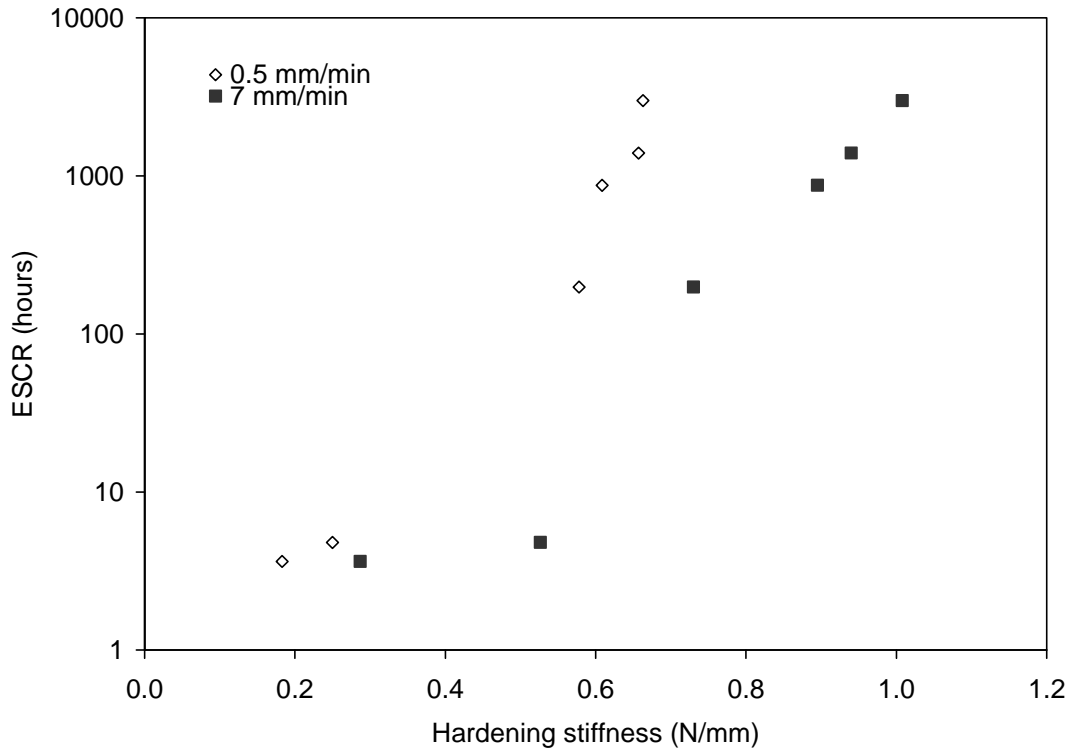


**Figure 4.11: ESCR vs. hardening stiffness at different strain rates**

The NDR values do not seem to be affected by the difference in strain rates as much as the strain hardening stiffness. In Figure 4.12 the NDR values at 0.5 mm/min and 7 mm/min strain rate overlap with each other (with slightly more scatter than the hardening stiffness data). The same issue related to the determination of the onset of strain hardening point persists in tests run at 7 mm/min strain rate as well. NDR is related to the extensibility of the polymer network, and hence the speed of the extension should not have much effect. The results show that NDR can be used as a strain rate-independent

indicator of the ESCR trends of a polymer, albeit with some caution due to the noisier nature of the NDR correlation with ESCR data.

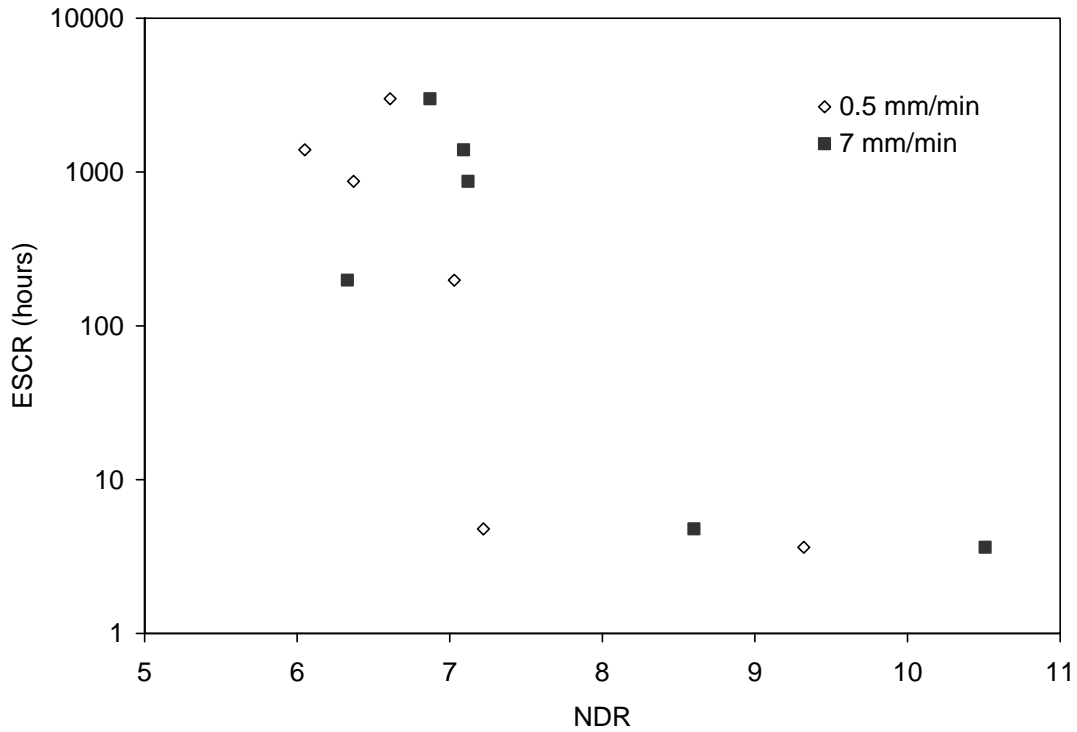


Figure 4.12: ESCR vs. NDR at different strain rates

### 4.3.6 Reproducibility of Strain Hardening Test

One of the main issues of the NCLT method is the large variability associated with its test results. As mentioned in section 4.3.1, the coefficient of variation for NCLT can be as high as 0.5. Therefore, before the strain hardening test can be proposed as a good indicator of ESCR, better reproducibility than NCLT must be demonstrated. If the test method has large variability, then the difference between materials would become hard to

detect. Repeats and independent replicate tests were carried out to investigate the variability (and sensitivity) of the strain hardening test.

The coefficient of variation for hardening stiffness measurements listed in Table 4.8 ranged from 0.003-0.13. The average coefficient of variation for both 0.5 mm/min and 7 mm/min strain rates is 0.05. HS values have smaller coefficient of variation than NCLT results, for which the smallest value is 0.09 and the average value is 0.20 (Table 4.4). The smaller coefficients of variation show that the strain hardening test is more precise than the NCLT.

Once again, independently replicated tests were carried out to determine the contribution of variability by the test procedure, for the strain hardening test. In Table 4.9, results from ANOVA analysis of PE8 are presented. The F-observed value is smaller than the F-critical value of 10.13 (5% significance level and (1,3) degrees of freedom), which indicates that the test procedure does not contribute significant variability to the measurements.

**Table 4.9: ANOVA of PE8 at 7 mm/min strain rate**

	df	SS	MS	F
Samples from different plates	1	0.0131	0.0131	2.259
Samples from same plate	3	0.0174	0.0058	
Total	4	0.0305		

It has been shown above that the variability of the hardening stiffness measurement is relatively small. To verify that there are true differences between the HS measurements

(and hence, to demonstrate that the HS measurements can truly detect differences in ESCR between resins), we employ again the analysis of variance technique. In Table 4.10, ten samples tested at 0.5 mm/min were analysed. The results show that the F-observed value (187.57) is larger than the F-critical value (6.26) at 5% significance level and (5,4) degrees of freedom. This means that there are true differences between the measurements for the resins and these can be detected by (are reflected in the values of) HS. The same analysis is repeated for the 7 mm/min strain rate results with 19 samples (Table 4.11). The F-observed value (86.54) is larger than the F-critical value of 3.03 at 5% significance level and (5,13) degrees of freedom, which indicates again true differences exist between resins. Based on these analyses we conclude that the strain hardening test is indeed sensitive to material differences at both 0.5 mm/min and 7 mm/min strain rates at room temperature.

**Table 4.10: ANOVA of hardening stiffness values at 0.5 mm/min strain rate**

	df	SS	MS	F
Different resins	5	0.4126	0.08253	187.57
Same resin	4	0.0018	0.00044	
Total	9	0.4144		

**Table 4.11: ANOVA of hardening stiffness values at 7 mm/min strain rate**

	df	SS	MS	F
Different resins	5	1.3198	0.26395	86.54
Same resin	13	0.0396	0.00305	
Total	18	1.3594		

### **4.3.7 Other Material Indicators for ESCR**

In this thesis, we also looked at other possible fundamental property indicators for environmental stress cracking resistance of polyethylene. Previous research has proposed to use crystallization analysis fractionation (CRYSTAF) indicators to relate to ESCR of polyethylene (34). Analysis of our resins based on the proposed CRYSTAF method (34) found the method to be unreliable and unclear in its relation (correlation) to ESCR for polyethylene. Our results and a related discussion regarding CRYSTAF analysis and ESCR can be found in Appendix B.

### **4.3.8 Modeling Creep Behaviour of Polyethylene for Structural Applications**

Environmental stress cracking of polyethylene is classified as a type of creep rupture failure. Creep rupture, as the name suggests, is closely related to creep behaviour of PE. Therefore, the studying of creep behaviour of a polymer is a natural step during research on ESCR of polyethylene. In Appendix C, analysis of a creep model that forms part of a practical approach for constitutive modeling of polyethylene is presented. The constitutive modeling approach was proposed to offer an efficient way for calibrating (macro)mechanical models for use in structural analysis of polymers (35, 36).

## **4.4 Concluding Remarks**

In this chapter, it is shown that strain hardening stiffness can be reliably correlated to ESCR of resins. The strain hardening test method proposed is an improvement on work presented by Kurelec *et al.* (25), because hardening stiffness values can be calculated

from simpler load-displacement measurements made under ambient conditions, which eliminates the need for the specialized equipment required to measure true stress and true strain and maintain sample temperature. Kurelec *et al.* (25) suggested that to conduct strain hardening tests at room temperature is only possible at low strain rates of 0.25 mm/min. We showed that the strain hardening test can be extended to detect differences in ESCR of resins even at high strain rates of up to at least 7 mm/min (thus reducing the duration of the test). Strain rate of 7 mm/min is comparable in magnitude to the 10 mm/min strain rate (at 80°C) used by Kurelec *et al.* (25). This provides for much faster and reliable and reproducible results at room temperature than previously reported. The strain hardening test is based on a fundamental polyethylene characteristic, thus, a better way to evaluate ESCR of polyethylene than the more empirical NCLT test.

The measurements of ESCR of high density polyethylene resins via NCLT and strain hardening methods were compared in Table 4.12 using statistical analysis of several independent replicates. In the entries of Table 4.12, a “No” means failure to record a measurement. This is due to the nature of the resin/specimen tested and in no way a limitation of the test. Of the two methods, the strain hardening method was preferred as it was demonstrated to be a faster technique, which could potentially decrease analysis time by up to hundred-fold. In addition, the strain hardening test is much simpler to perform than NCLT as there is no need for sample notching, or a temperature-controlled and concentration-controlled bath. For any good analytical method, efficiency is not the only requirement; good precision and reproducibility are also needed. Statistical analysis of the test results showed that the strain hardening test is more precise than NCLT. For the

strain hardening test the average coefficient of variation is 0.05, which is a significant improvement compared to that of NCLT, which has an average coefficient of variation of 0.20. Therefore, it has been demonstrated that the strain hardening method proposed herein is a simple, precise, reproducible and hence a more practical way to classify ESCR of high density polyethylene. The strain hardening test has the potential to replace the NCLT test, which has been in use for the past 25 years, as the principal means of evaluating ESCR of polyethylene.

**Table 4.12: Resins tested with NCLT and strain hardening test (summary)**

<b>Resin</b>	<b>NCLT</b>	<b>Strain hardening test</b>	<b>Comments</b>
PE1	Yes	Yes	
PE2	Yes	No	Could not reach strain hardening at low strain rate. At high strain rate, specimen failed before fully elongated.
PE3	Yes	No	Could not reach strain hardening at low strain rate. At high strain rate, specimen failed before fully elongated.
PE4	Yes	Yes	
PE5	No	No	Material brittle and can not be “notched” for NCLT. Strain hardening test failure occurs before specimen being fully extended at all strain rates.
PE6	No	No	Material brittle and can not be “notched” for NCLT. Strain hardening test failure occurs before specimen being fully extended at all strain rates.
PE7	Yes	Yes	
PE8	Yes	Yes	
PE9	Yes	Yes	
PE10	Yes	Yes	

## 4.5 References

1. Brostow, Witold and Corneliussen, Roger D.(1986), *Failure of plastics*, Hanser Publishers, New York.
2. Scheirs, J., Böhm, L. L., Boot, J. C., & Leever, P. S. (1996), "PE100 resins for pipe applications: continuing the development into the 21st century", *Trends in Polymer Science*, vol. 4, no. 12, pp. 408-415.
3. Lustiger, A. & Markham, R. L. (1983), "Importance of tie molecules in preventing polyethylene fracture under long-term loading conditions", *Polymer*, vol. 24, pp. 1647-1654.
4. Lagaron, J. M., Dixon, N. M., Reed, W., Pastor, J. M., & Kip, B. J. (1999), "Morphological characterisation of the crystalline structure of cold-drawn HDPE used as a model material for the environmental stress cracking (ESC) phenomenon", *Polymer*, vol. 40, pp. 2569-2586.
5. Ward, A. L., Lu, X., Huang, Y., & Brown, N. (1991), "Mechanism of slow crack growth in polyethylene by an environmental stress cracking agent", *Polymer*, vol. 32, no. 12, pp. 2172-2178.
6. Scheirs, J. (2000), *Compositional and Failure Analysis of Polymers: A practical approach*, John Wiley & Sons, Ltd, Chichester, West Sussex, England.
7. Ferry, J. D. (1980), *Viscoelastic properties of polymers*, 3 edn, Wiley, New York.
8. Bayer, R. K. (1991), "Structure transfer from a polymeric melt to the solid state. Part I: The influence of chain entanglements in linear polyethylene", *Colloid and Polymer Science*, vol. 269, pp. 421-432.
9. Bayer, R. K., Liebentraut, F., & Meyer, T. (1992), "Structure transfer from a polymeric melt to the solid state. Part II: Dependence on molecular weight", *Colloid and Polymer Science*, vol. 270, pp. 331-348.
10. Bayer, R. K. (1994), "Structure transfer from a polymeric melt to the solid state. Part III: Influence of knots on structure and mechanical properties of semicrystalline polymers", *Colloid and Polymer Science*, vol. 272, pp. 910-932.
11. Brown, N. & Ward, I. M. (1983), "The influence of morphology and molecular weight on ductile-brittle transitions in linear polyethylene", *Journal of Materials Science*, vol. 18, pp. 1405-1420.
12. Yeh, J. T. & Runt, J. (1991), "Fatigue crack propagation in high-density polyethylene", *Journal of Polymer Science, Part B: Polymer Physics*, vol. 29, pp. 371-388.

13. Brown, N., Lu, X., Huang, Y., Harrison, I. P., & Ishikawa, N. (1992), "The Fundamental Material Parameters That Govern Slow Crack-Growth in Linear Polyethylenes", *Plastics Rubber and Composites Processing and Applications*, vol. 17, no. 4, pp. 255-258.
14. Capaccio, G. & Ward, I. M. (1981), "Structural studies of ultrahigh-modulus linear polyethylene using nitric acid etching and gel permeation chromatography. I Determination of the crystal size distribution", *Journal of Polymer Science, Part B: Polymer Physics*, vol. 19, pp. 667-675.
15. Huang, Y. & Brown, N. (1988), "The effect of molecular weight on slow crack growth in linear polyethylene homopolymers", *Journal of Materials Science*, vol. 23, pp. 3648-3655.
16. Janimak, J. J. & Stevens, G. C. (2001), "Inter-relationships between tie-molecule concentration, molecular characteristics and mechanical properties in metallocene catalysed medium density polyethylenes", *Journal of Materials Science*, vol. 36, no. 8, pp. 1879-1884.
17. Huang, Y. & Brown, N. (1990), "The dependence of butyl branch density on slow crack growth in polyethylene: kinetics", *Journal of Polymer Science, Part B: Polymer Physics*, vol. 28, pp. 2007-2021.
18. Hosoda, S., Nomura, H., Gotoh, Y., & Kihara, H. (1990), "Degree of branch inclusion into the lamellar crystal for various ethylene/a-olefin copolymers", *Polymer*, vol. 31, pp. 1999-2005.
19. Ward, I. M. (1971), *Mechanical Properties of Solid Polymers*, Wiley-Interscience, Toronto.
20. Hay, I. L. & Keller, A. (1965), "Polymer Deformation in Terms of Spherulites", *Kolloid-Zeitschrift and Zeitschrift fur Polymere*, vol. 204, no. 1-2, pp. 43-74.
21. Geil, P. H. (1964), "Polymer Deformation .3. Annealing of Drawn Polyethylene Single Crystals + Fibers", *Journal of Polymer Science Part A-General Papers*, vol. 2, no. 9, pp. 3835-3855.
22. Peterlin, A. (1965), "Crystalline Character in Polymers", *Journal of Polymer Science Part C-Polymer Symposium* no. 9, pp. 61-89.
23. Alvarado-Contreras, J. A. (2007), *Micromechanical Modelling of Polyethylene*, PhD Thesis, Department of Civil Engineering, University of Waterloo, Waterloo, Canada.
24. Allison, S. W., Pinnock, P. R., & Ward, I. M. (1966), "Cold drawing of poly(ethylene terephthalate)", *Polymer*, vol. 7, no. 1, pp. 66-69.

25. Kurelec, L., Teeuwen, M., Schoffeleers, H., & Deblieck, R. (2005), "Strain hardening modulus as a measure of environmental stress crack resistance of high density polyethylene", *Polymer*, vol. 46, pp. 6369-6379.
26. Cooke, R., Graham, B. A., & Nicholas, J. J. Januray 11, 2008 meeting. private communication. (2008). ExxonMobil Chemical Canada. Ref Type: Generic
27. Hittmair, P. & Ullman, R. (1962), "Environmental stress cracking of polyethylene", *Journal of Applied Polymer Science*, vol. 6, no. 19, pp. 1-14.
28. Box, G. E. P., Hunter, W. G., & Hunter, J. S. (1978), *Statistics for Experimenters: An Introduction to Design, Analysis and Model Building*, Wiley, Toronto.
29. Hubert, L., David, L., Séguéla, R., Vigier, G., Corfias-Zuccalli, C., & Germain, Y. (2002), "Physical and mechanical properties of polyethylene for pipes in relation to molecular architecture. II. short-term creep of isotropic and drawn materials", *Journal of Applied Polymer Science*, vol. 84, pp. 2308-2317.
30. Rose, L. J., Channell, A. D., Frye, C. J., & Capaccio, G. (1994), "Slow crack growth in polyethylene: a novel predictive model based on the creep of craze fibrils", *Journal of Applied Polymer Science*, vol. 54, pp. 2119-2124.
31. Maxwell, A. S. & Pilkington, G. (2008), "Prediction of environmental stress cracking resistance in linear low density polyethylenes", *Polymer Engineering and Science*, vol. 48, no. 2, pp. 360-364.
32. Seguela, R. (2005), "Critical review of the molecular topology of semicrystalline polymers: the origin and assessment of intercrystalline tie molecules and chain entanglements", *Journal of Polymer Science, Part B: Polymer Physics*, vol. 43, no. 14, pp. 1729-1748.
33. DesLauriers, P. J. "Relationship between notched pipe test and NDR", SPE International Polyolefins Conference 2006, Houston, TX, USA.
34. Soares, J. B. P., Abbott, R. F., & Kim, J. D. (2000), "Environmental stress cracking resistance of polyethylene: the use of CRYSTAF and SEC to establish structure-property relationships", *Journal of Polymer Science, Part B: Polymer Physics*, vol. 38, pp. 1267-1275.
35. Liu, H. (2007), *Material modelling for structural analysis of polyethylene*, MASC Thesis, Department of Civil engineering, University of Waterloo, Waterloo, Ontario, Canada.
36. Liu, H., Polak, M. A., & Penlidis, A. (2007), "A practical approach to modeling time-dependent nonlinear creep behaviour of polyethylene for structural applications", *Polymer Engineering and Science*, vol. 48, no. 1, pp. 159-167.

# **CHAPTER 5 AMORPHOUS PHASE STRUCTURE AND MECHANICAL BEHAVIOUR OF POLYETHYLENE**

## **5.1 Introduction\***

Environmental stress cracking (ESC) is a serious problem for polyethylene used in pipe and other structural applications. It is a brittle type of failure that occurs at stress levels below the yield stress of the polymer (1). ESC often goes undetected until the PE pipe has completely failed because there is no visible deformation. The accelerating nature of ESC can often cause polyethylene (PE) pipes that are designed to have a service life of fifty years or more to fail in less than a year (1).

The failure mechanism of ESC is believed to be a process of chain disentanglement during which lamellae remain intact (2). Environmental stress cracking resistance (ESCR) of polyethylene has been shown to be influenced by molecular weight (MW) and short chain branching (SCB). High MW and SCB content have been linked to increasing formations of inter-lamellar links that increase ESCR of polyethylene (3-7). It is also believed that SCB prevents chain slippage from the crystalline lamellae, thereby slowing down the chain disentanglement process (8). Most published work on ESCR focuses on bridging-tie-molecules as the main source of inter-lamellar links that influence ESCR (4, 5, 9, 10). Recently, growing attention is being focused on the influence of physical chain entanglements on ESCR (11-13). Probability studies have shown that high MW chains

---

\* Two paper drafts have been produced based on information in this chapter. They were submitted in Oct. 2008 and are currently under review in *Polymer Engineering and Science* and *Polymer International*, respectively.

that are capable of forming bridging-tie-molecules are twice as likely to form chain entanglements (3, 11, 14). Molecules not long enough to become bridging-tie-molecules, which end up as cilia and loose loops in the amorphous phase, can form entanglements as well. In addition, bridging-tie-molecules can also form entanglements with other chains. Therefore, the number of chain entanglements in a polyethylene network is higher than the number of bridging-tie-molecules (14).

Physical chain entanglements are known to influence the tensile properties of semicrystalline polymers (15-19). An increase in chain entanglement density has been shown to decrease the elongation of polyethylene (15, 20-22). Chain entanglements in an uncrosslinked polymer network affect its natural draw ratio (NDR), which is an indicator of polymer network extensibility (23). Recent work by Zuo *et al.* (24) has also demonstrated that physical chain entanglements rather than bridging-tie-molecules have the most influence on strain hardening behaviour of polypropylene.

Recent research has demonstrated that NDR and tensile strain hardening are linked to ESCR of polyethylene (12, 13, 25, 26). Polyethylene with high strain hardening modulus has been shown to have high ESCR. Decreases in NDR have been associated with increasing ESCR of polyethylene. Since chain entanglements have a strong influence on both strain hardening behaviour and NDR, physical chain entanglements should influence ESCR of polyethylene. Chain entanglements, like bridging-tie-molecules, are expected to form part of the inter-lamellar connections. Since ESC occurs through a process of

disentanglement, a high number of chain entanglements in the polymer system would therefore increase its ESCR.

Direct measurement of entanglements in a polymer solid is not possible with current techniques. However, since entanglements affect chain mobility in the polymer network (27), study of the overall mobility of the network can provide insight into the nature of entanglements. Disentanglement of chains involves movement of the polymer backbone in reptation or primitive-path fluctuation (28-31). Researchers have attempted to link  $\alpha$  and  $\beta$  relaxation processes to chain mobility and ESCR of polyethylene (32-34). However, there are several disadvantages in using material properties in the  $\alpha$  and  $\beta$  temperature range as indicators of polyethylene main chain mobility.  $\beta$ -relaxation occurs at temperatures below the glass transition temperature ( $T_g$ ) of the polymer where, most researchers agree, the movement of the polymer backbone is severely limited and only the movement of short chain branches is prominent (35). The  $\alpha$ -relaxation process occurs at temperatures above  $T_g$  and below the melting temperature of the polymer, a range over which studies have shown that the relaxation of the crystalline phase dominates (36-38). Therefore, it is difficult to isolate the effect of main chain mobility in  $\alpha$  and  $\beta$  relaxation processes.

Chain entanglements can be found in the amorphous phase of semicrystalline polymers, such as polyethylene. The amorphous phase has many characteristics similar to a polymer melt. The movement of the large PE backbones due to disentanglement can be more readily studied in the melt state using rheological techniques (27). Research has

shown that chain entanglements in the melt are largely preserved in the amorphous phase upon solidification (39). As crystal lamellae grow, chain entanglements are pushed into the amorphous phase. Hence, in our study, the entanglement effect in solid PE is based on melt rheological measurements. The relationship between network mobility in the melt state and strain hardening behaviour in the solid state is established. Then the study is extended to examine the influence of chain entanglements on ESCR of polyethylene. Materials studied cover a wide range of MWs and molecular weight distributions (MWDs) for HDPE in structural applications.

## 5.2 Experimental Methods

Three types of characterization experiments were carried out in Chapter 5, namely polymer characterization experiments (such as GPC), rheological experiments, and mechanical tests. Table 5.1 contains the list of experimental methods used and corresponding material property determined. The third column, “Chapter 3 section #”, refers to the sections in Chapter 3 that contain more detailed descriptions of each method.

**Table 5.1: List of experimental methods for Chapter 5**

<b>Method</b>	<b>Property Determined</b>	<b>Chapter 3 section #</b>
GPC	Molecular weight and molecular weight distribution	3.1.3
<sup>13</sup> C NMR	Short chain branch content	3.1.4
Oscillating shear experiments	Rheological characteristics	3.2.1
Tensile test	Strain hardening measurements and NDR	3.3.1
NCLT	ESCR values	3.3.2

## 5.3 Network Mobility and ESCR

### 5.3.1 Rheological Characteristics

Ten industrial high density polyethylene resins (PE1-10) are investigated in this study. Material characteristics of each resin are presented in Table 5.2.  $M_n$ ,  $M_w$  and  $M_z$  stand for number-average, weight-average and z-average molecular weight, respectively. PDI is the polydispersity index ( $M_w/M_n$ ). The number of short chain branches per thousand carbon atoms was measured using  $^{13}\text{C}$ -NMR. All resins were found to have butyl side chains; PE9 also has a small number of methyl side chains.

**Table 5.2: Characteristics of resins**

Resin	ESCR (hours)	$M_n$ (kg/mol)	$M_w$ (kg/mol)	$M_z$ (kg/mol)	PDI	SCB (/1000C)
PE1	4.8	16.3	127.5	814.0	7.8	2.8
PE2	1.2	15.7	118.5	837.1	7.6	1.1
PE3	2.8	17.9	140.1	889.8	7.8	0.9
PE4	3.6	19.7	79.4	239.3	4.0	3.8
PE5	N/A	11.4	49.7	157.8	4.4	7.0
PE6	N/A	14.0	62.0	195.0	4.4	4.7
PE7	1396	11.8	222.8	1593.5	18.9	4.3
PE8	198	14.0	202.1	1398.4	14.4	4.5
PE9	843	10.4	217.9	1244.2	20.9	7.0
PE10	>3000	5.9	315.4	2129.3	53.3	11.8

Dynamic storage ( $G'$ ) and loss modulus ( $G''$ ) values were measured in oscillating shear experiments. Independent replication, using a new disc each time, showed good reproducibility of the results. Calculations of the zero shear viscosity ( $\eta_0$ ) and the steady state compliance ( $J_e^0$ ) were carried out using the NLREG software (40) based on the well known relationship given in Equations 5.1 and 5.2 (27), where  $\omega$  is the frequency. Table

5.3 contains rheological characteristics of the resins (some of the symbols of Table 5.3 will be explained and discussed later in the text). The values of the zero shear viscosity and the steady state compliance are within ranges reported for polyethylene in the literature (27, 41-43).

$$\eta_o = \lim_{\omega \rightarrow 0} \frac{G''(\omega)}{\omega} \quad (5.1)$$

$$J_e^o = \lim_{\omega \rightarrow 0} \frac{G'(\omega)}{\eta_o^2 \omega^2} \quad (5.2)$$

**Table 5.3: Rheological characteristics of resins at 190°C**

	$\eta_o$ (Pa s)	$J_e^o$ (1/Pa)	$G_N^o$ Pa	$M_e$ (g/mole)	LCBI
PE1	3.13E+05	2.22E-03	540.2	5403	0.90
PE2	2.00E+05	3.79E-03	317.0	9208	0.86
PE3	5.42E+05	1.43E-03	838.9	3480	0.96
PE4	1.78E+03	3.68E-03	325.9	8958	-0.02
PE5	2.77E+02	7.37E-02	16.3	179194	-0.01
PE6	6.23E+02	4.14E-02	29	100816	-0.03
PE7	8.19E+05	6.30E-04	1904.3	1533	0.58
PE8	2.03E+06	4.07E-04	2950.1	990	0.96
PE9	1.12E+06	6.51E-04	1843.4	1584	0.69
PE10	6.07E+06	1.34E-04	8951.7	326	0.86

The number of entanglements in a polymer system can be inferred based on the molecular weight between entanglements ( $M_e$ ). For polymer chains of similar chain length (molecular weight), smaller  $M_e$  means more entanglements. According to rheological theories (27), the plateau modulus ( $G_N^o$ ) of a polymer is related to its  $M_e$  through Equation 5.3.

$$G_N^o = \frac{\rho RT}{M_e} \quad (5.3)$$

$\rho$  - melt density at 190°C (0.758 kg/m<sup>3</sup>),  $R$  - gas constant,  $T$  - absolute temperature

Over the years, several approaches for calculation of the plateau modulus ( $G_N^0$ ) have been used (27, 44). These methods were developed based on polymer systems of high MW and narrow MWD. For polyethylene, two methods for obtaining  $G_N^0$  are most frequently reported. The first method is the integration of the terminal zone loss modulus curve when the peak maximum can be defined. The second approach takes the value of  $G'$  as  $G_N^0$  when the  $\tan(\delta)$  curve approaches a minimum. The pros and cons of these and other methods were discussed in detail by Liu *et al.* (45). For polymer systems with a MWD of  $PDI > 2$ , Liu *et al.* (45) showed that none of the methods currently used is significantly better than the other. This may explain the wide range of  $M_e$  values reported, 830 – 2300 g/mole, for polyethylene in the literature (27, 38, 46). In addition, it is not clear if all  $M_e$  values reported are based on PE homopolymer. Polyethylene with short chain branches would have reduced chain flexibility, and thus appear to have higher apparent  $M_e$  values.

Work by Graessley and Edwards (47) showed that the product of  $J_e^0 G_N^0$  is relatively constant for a variety of polymer systems (which is expected since  $G_N^0$  and  $J_e^0$  are both material parameters). Doi and Edwards (44) further showed that a semi-empirical relationship exists between  $G_N^0$  and  $J_e^0$  in the form of Equation 5.4.

$$G_N^0 = \frac{6}{5J_e^0} \quad (5.4)$$

The broad MWD of resins in this study (see PDI values in Table 5.2) makes the determination of the plateau modulus using both the integration method or the  $\tan(\delta)_{\text{minimum}}$  method difficult (45). Due to thermal stability limitations of resins (see section 3.2.1), rheological experiments could not be carried out at temperatures higher than 190°C. With the use of only one test temperature, it is not possible to use the time-temperature superposition principle to gain information regarding the low frequency region, therefore, no direct measurement of  $G_N^0$  is possible. The relationship in Equation 5.4 is admittedly for polymers of narrow molecular weight distribution. For polymers with broad MWD the coefficient of 6/5 does not apply. However, the relationship of  $M_e \propto 1/G_N^0 \propto J_e^0$  is still valid. Since our main interest is in the relative differences of the  $M_e$  values and not in the precise values themselves, we decided to adopt the approach of Doi and Edwards (44) for calculation of  $G_N^0$ . The calculated  $G_N^0$  and  $M_e$  values derived thereof are presented in Table 5.3.

The idea of chain entanglements in uncrosslinked polymers was first suggested by Bueche (48, 49) in order to explain the relationship of  $\eta_0$  vs.  $M_w^{3.4}$  when the polymer MW is higher than a certain critical molecular weight ( $M_c$ , where  $M_c \cong 2M_e$  (27)). It was suggested that the dragging of one polymer chain by the other contributes to the overall viscosity of the polymer system. Higher viscosity means lower mobility for the

network. Hence, the mobility of polymer chains in the melt is controlled by the entanglements in the system.

Comparing resins in this study, PE7-10 have higher  $\eta_0$  values than other resins (Table 5.3). The high MW of PE7-10 (Table 5.2) is the key factor influencing the viscosity of the resins. In Figure 5.1,  $\eta_0$  is plotted against  $M_w$  of resins. The relationship of increasing  $\eta_0$  values as a result of increases in  $M_w$  is shown. Resins in this chapter follow the general relationship of  $\eta_0 \propto M_w^{3.4}$  (as indicated by the solid line in Figure 5.1). High molecular weight means longer polymer chains and more entanglements. These long molecules are less mobile and reduce the overall mobility of the network, resulting in higher  $\eta_0$  values.

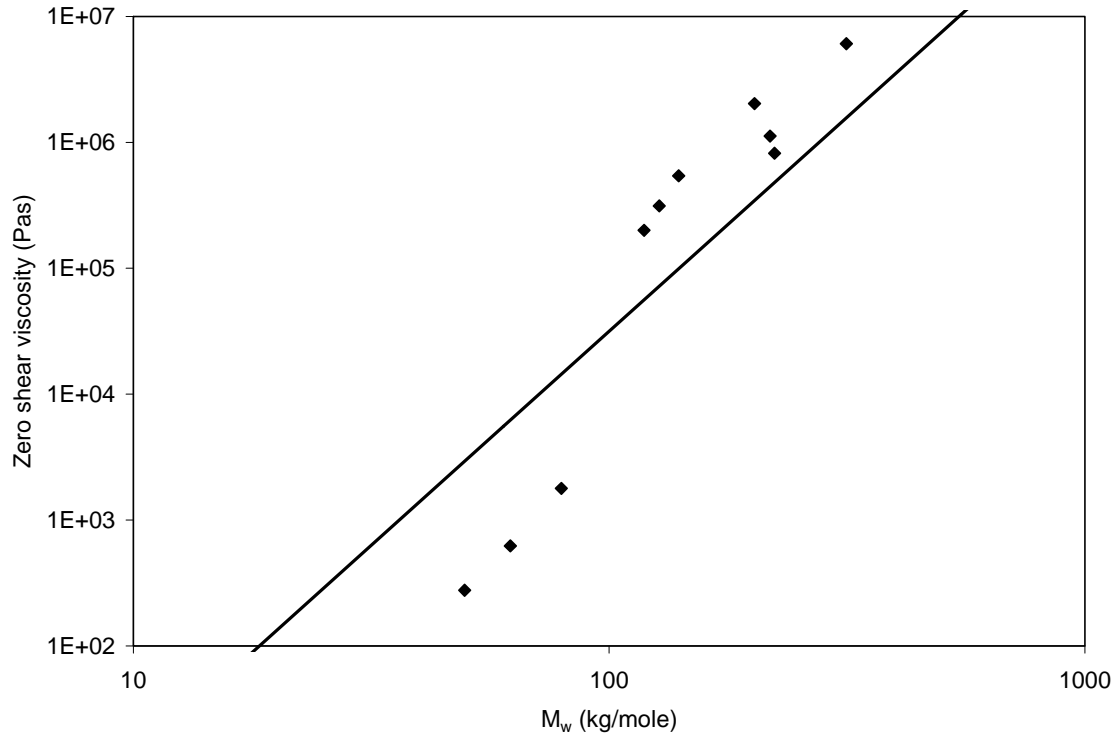


**Figure 5.1: Zero shear viscosity ( $\eta_0$ ) vs.  $M_w$**

In Figure 5.2, the entanglement molecular weights ( $M_e$ ) are plotted against zero shear viscosity. The trend of smaller  $M_e$  values associated with higher  $\eta_0$  values can be seen. Smaller values of  $M_e$  indicates the presence of a higher number of chain entanglements per chain. As mentioned earlier, friction between chain entanglements limits the overall mobility of the polymer network. Higher number of chain entanglements means more friction and lower network mobility. As the network mobility decreases the viscosity of the polymer increases.

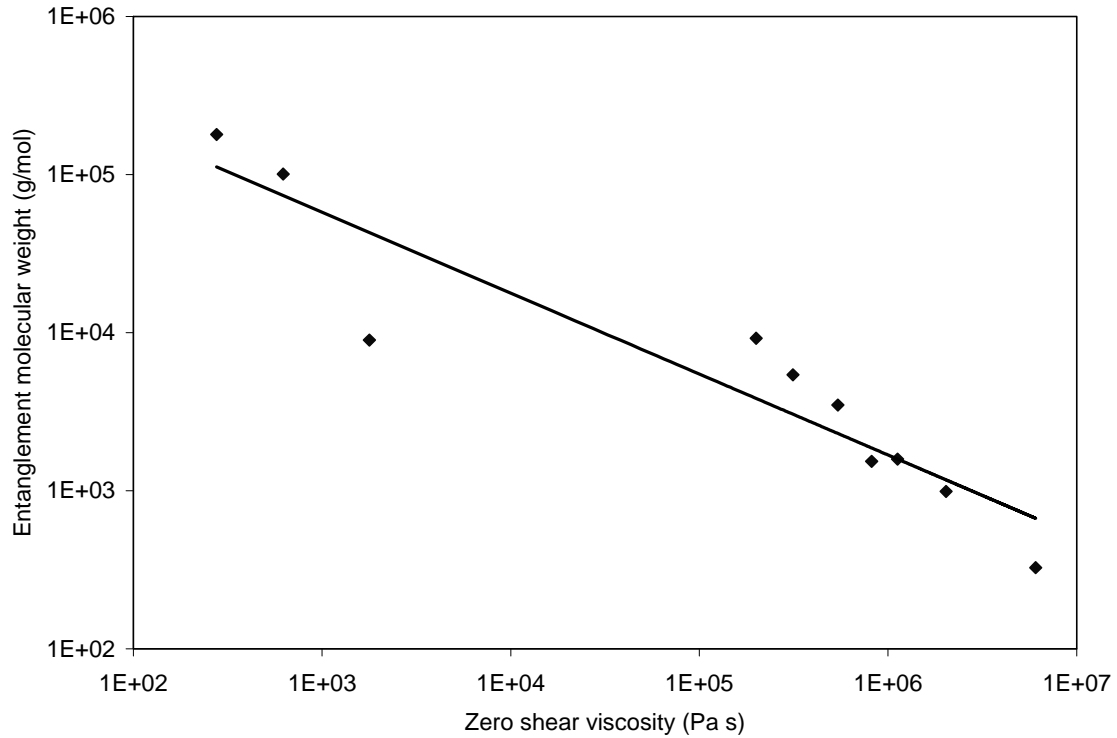


**Figure 5.2: Relationship between entanglement molecular weight ( $M_e$ ) and zero shear viscosity ( $\eta_0$ )**

The exact number of entanglements in a polymer system is in a dynamic equilibrium due to continuously entanglement and disentanglement of chains. The ratio of  $M_w/M_e$  can be taken as an indication of the minimum number of entanglements in a polymer system at any given time. Hence, if one plotted the zero shear viscosity vs. the ( $M_w/M_e$ ) ratio, one would see a trend of increasing zero shear viscosity with an increasing ratio, the same fact as demonstrated in Figure 5.2, namely that increasing number of chain entanglements decreases the network mobility of polyethylene. Therefore,  $M_e$  can be used as an indicator of entanglement concentration without having to measure the actual number of entanglements.

### 5.3.2 Long Chain Branching Effect

In general, the rheological characteristics in Table 5.3 reflect the differences in MW of the resins (Table 5.2). Resins with higher MW have higher  $\eta_0$  and  $G_N^0$  values; and lower  $J_e^0$  and  $M_e$  values. This observation follows current understanding in rheological theories (27). However, PE8 behaves differently from the expected trend. PE7 has higher MW than PE8 (see Table 5.2,  $M_w$  and  $M_z$  values). Yet PE8 shows higher zero shear viscosity and lower  $M_e$  than PE7. Other properties that influence  $\eta_0$  of a polymer are MWD and long chain branching (LCB) (27). Comparing these two resins further, they exhibit MWDs of a similar breadth (see Figure 5.3c). Therefore, the difference in  $\eta_0$  values must be due to a factor other than the MWD.

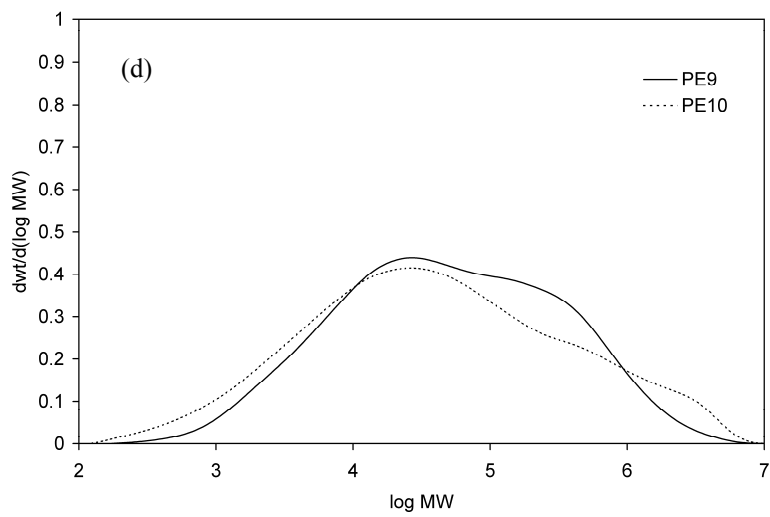
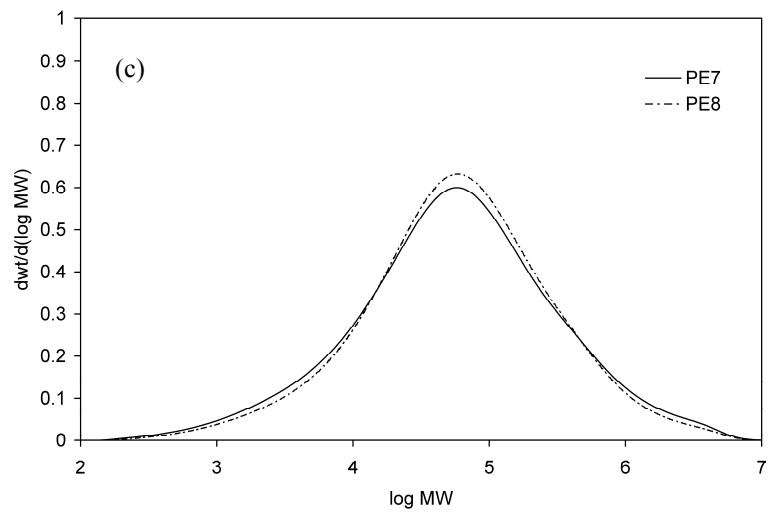
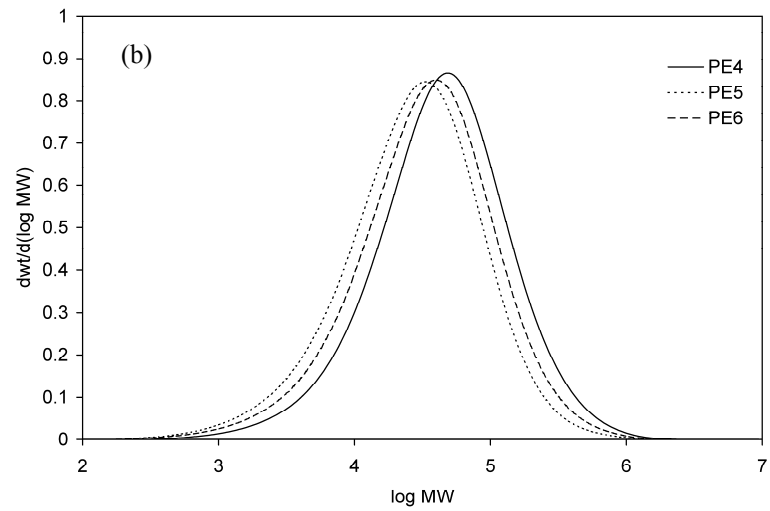
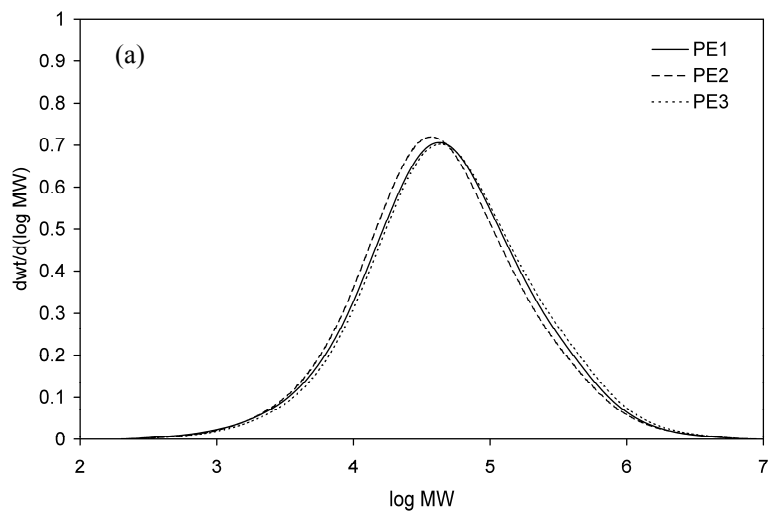
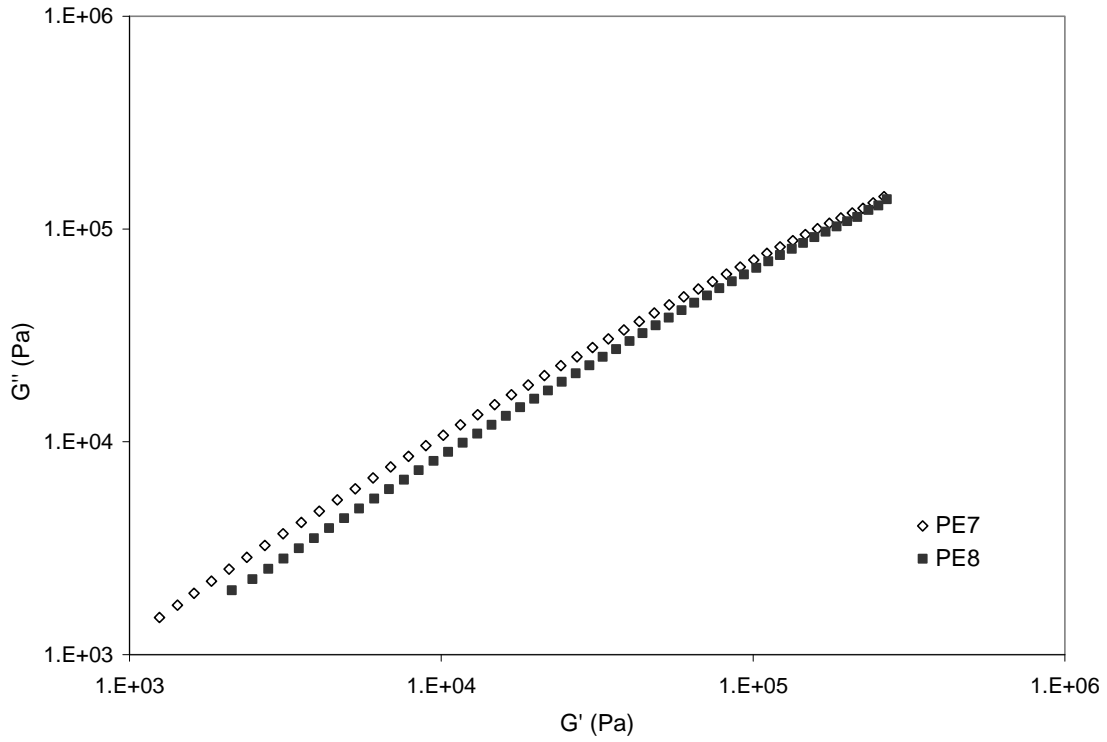
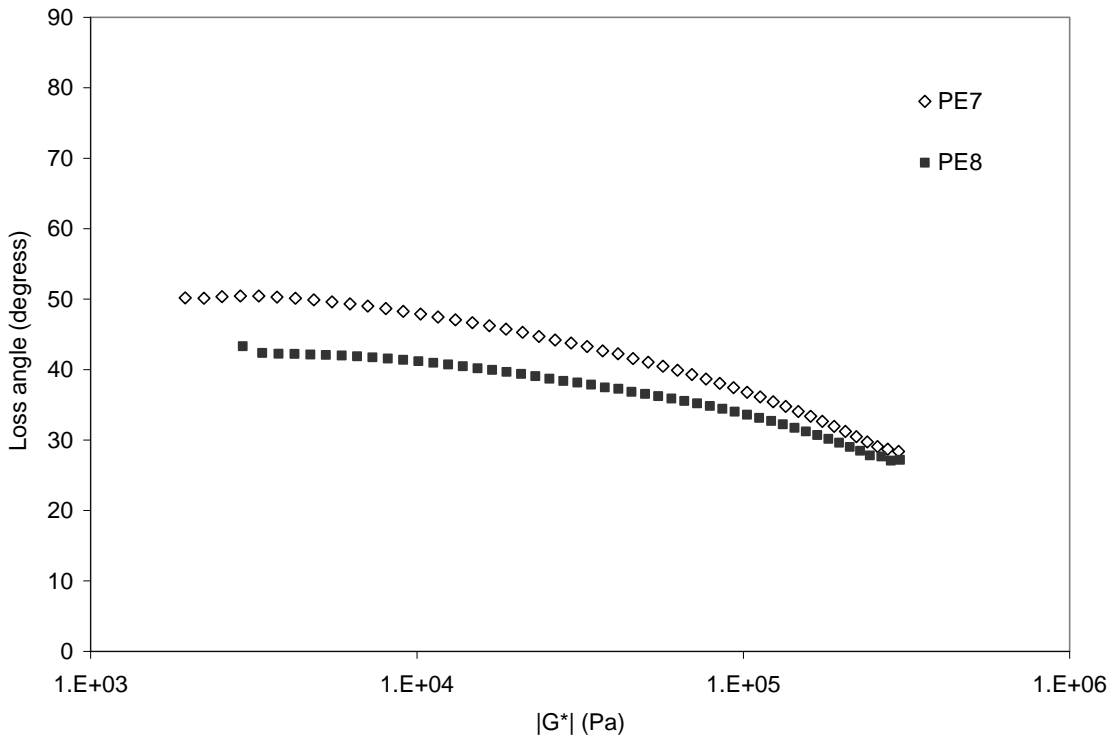


Figure 5.3: MWD curves of resin

It was suspected that the presence of long chain branching was responsible for the observed differences in  $\eta_0$  values between PE7 and PE8. For resins of similar MWD, the Cole-Cole plot can be used to compare potential differences in LCB concentration (50, 51). In Figure 5.4,  $G''$  versus  $G'$  is plotted for PE7 and PE8. The separation of the curves at lower frequency is an indication that PE8 has more LCB than PE7. In addition to the Cole-Cole plot, the Van Gorp-Palmen plot of PE7 and PE8 is presented in Figure 5.5. In the Van Gorp-Palmen plot, polymers with higher LCB will show lower loss angle values at the same  $|G^*|$  values (52, 53).  $|G^*|$  is the absolute value of the complex modulus, which is a vectorial resolution of the  $G'$  and  $G''$  components in the complex plane (27). From Figure 5.5 it is evident that PE8 shows lower loss angle values compared to PE7 at the same  $|G^*|$  values. Hence, Figure 5.5 confirms the indications from Figure 5.4, that resin PE8 has a higher content of LCB than PE7. Another indicator for even very low levels of LCB in a polymer system is the LCBI (long chain branch index) proposed by Shroff and Mavridis (54). In Table 5.3, LCBI values for all resins have been calculated according to the method of Shroff and Mavridis (54). The LCBI values are less than one, indicating very low concentration of LCB. PE8 has larger LCBI (0.96) as compared to PE7 (0.58); a larger LCBI value is an indication of higher LCB content. These three indicators confirm separately that PE8 seems to have a higher LCB content than PE7.



**Figure 5.4: Cole-Cole plot for PE7 and PE8 resins**



**Figure 5.5: Van Gorp-Palmen plot for PE7 and PE8 resins**

The presence of LCB is known to influence the rheological behaviour of polymers. Several studies have shown that at low concentration presence of LCB increases the  $\eta_0$  of high density polyethylene (41, 55-57). Although PE7 has a higher MW value (see Table 5.2), the higher LCB content of PE8 causes it to have higher zero shear viscosity than PE7. Since zero shear viscosity is related to the steady state compliance and the entanglement molecular weight (Equations (5.2-5.4)), the higher zero shear viscosity value of PE8 translates to lower  $J_e^0$  and  $M_e$  values compared to those of PE7. The smaller  $M_e$  value of PE8 would give an appearance of more entanglements in the system than expected.

### **5.3.3 Chain Entanglements and Tensile Elongation**

Strain hardening is a tensile elongation behaviour that has been linked to chain entanglements in a polymer network (23). Physical chain entanglements have been shown to control the extensibility of a polymer network through the behaviour of melt-spun fibres (58). For semi-crystalline polymers, strain hardening behaviour is also postulated to be primarily controlled by the amorphous phase chain entanglements rather than bridging-tie-molecules (24, 59).

Tensile strain hardening experiments, with constant deformation/strain rates of 0.5 mm/min and 7 mm/min, were performed on dogbone shaped samples (see Chapter 3) at room temperature conditions. Strain hardening behaviour was observed for PE1, PE4

and PE7-10. Strain hardening values for PE2 and PE3 could not be reported due to limitations of the test apparatus. The strain hardening stage could not be attained for these two resins even at the maximum extension of the test apparatus. Values are not reported for PE5 and PE6 because their brittle nature caused them to fracture before full extension could be achieved. Therefore, PE2, PE3, PE5 and PE6 are henceforth excluded from the discussion in this section.

Figure 5.6 shows the load-displacement curves for PE1 and PE7 at strain rate of 0.5 mm/min. All resins that achieved strain hardening exhibited similar load-displacement curves to those shown in Figure 5.6, which are typical for tensile deformation behaviour of polyethylene. A maximum load was observed at the yield point. After yield, the sample load holds relatively steady during the stable elongation phase. At the onset of strain hardening (after 200 mm in Figure 5.6), the load increases with increasing displacement again until ultimately the sample breaks. Independent replicate tests were carried out and showed good reproducibility of the results (Figure 5.6).

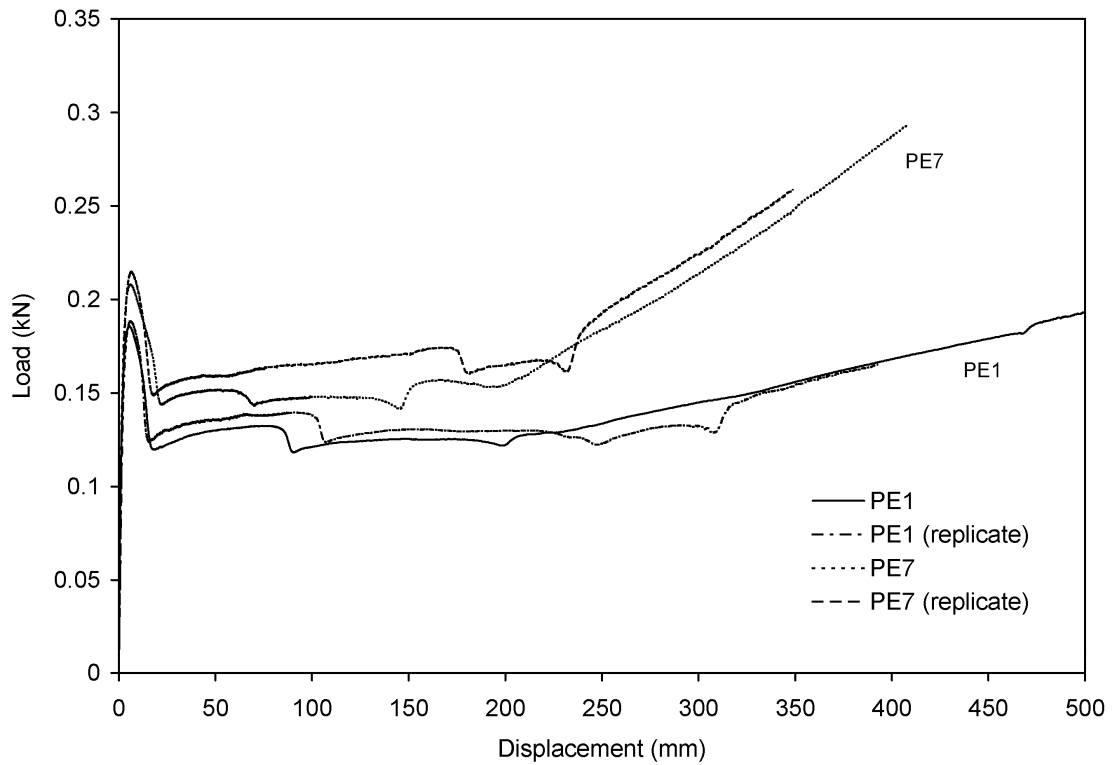


**Figure 5.6: Tensile elongation curves at 0.5 mm/min constant strain rate**

During the strain hardening stage of the elongation which occurs after 200 mm for both resins in Figure 5.6, the load-displacement curves become linear and well defined. The characteristic slope of the strain hardening section of the load-displacement curve is a function of applied load over total sample displacement, which can be considered as a definition of “material stiffness” (23). The strain hardening stiffness (HS) is related to the strain hardening modulus of resins. The hardening stiffness of the resins at both 0.5 mm/min and 7 mm/min strain rates are shown in Table 5.4.

**Table 5.4: Hardening stiffness (HS) and NDR of polyethylene**

	Strain rate 0.5 mm/min		Strain rate 7 mm/min	
	Hardening stiffness (N/mm)	NDR	Hardening stiffness (N/mm)	NDR
PE4	0.183	9.3	0.287	10.5
PE1	0.250	7.2	0.527	8.6
PE8	0.578	7.0	0.730	6.3
PE9	0.609	6.4	0.895	7.1
PE7	0.657	6.1	0.940	7.1
PE10	0.663	6.6	1.008	6.9

From Table 5.4 it can be seen that hardening stiffness values are higher at the faster deformation rate of 7 mm/min than at 0.5 mm/min. For tensile constant strain rate experiments, load responses are known to increase with increasing strain rate (23). Comparing to the MW values in Table 5.2, it can be seen that resins with high MW have higher hardening stiffness values. In Figure 5.7, hardening stiffness values are plotted against the corresponding  $M_e$  values of the resins. For all deformation rates, resins with smaller  $M_e$  values have higher hardening stiffness values. Of course, in the case of PE8, its  $M_e$  value is lowered due to the presence of LCB as discussed in section 5.3.2. In general, smaller  $M_e$  values mean there are more chain entanglements per chain; and the higher number of chain entanglements means there are more restrictions on the polymer network. A more restricted network would have more resistance to deformation and thus, result in a “stiffer” response (and hence a larger value of HS) during the strain hardening stage.

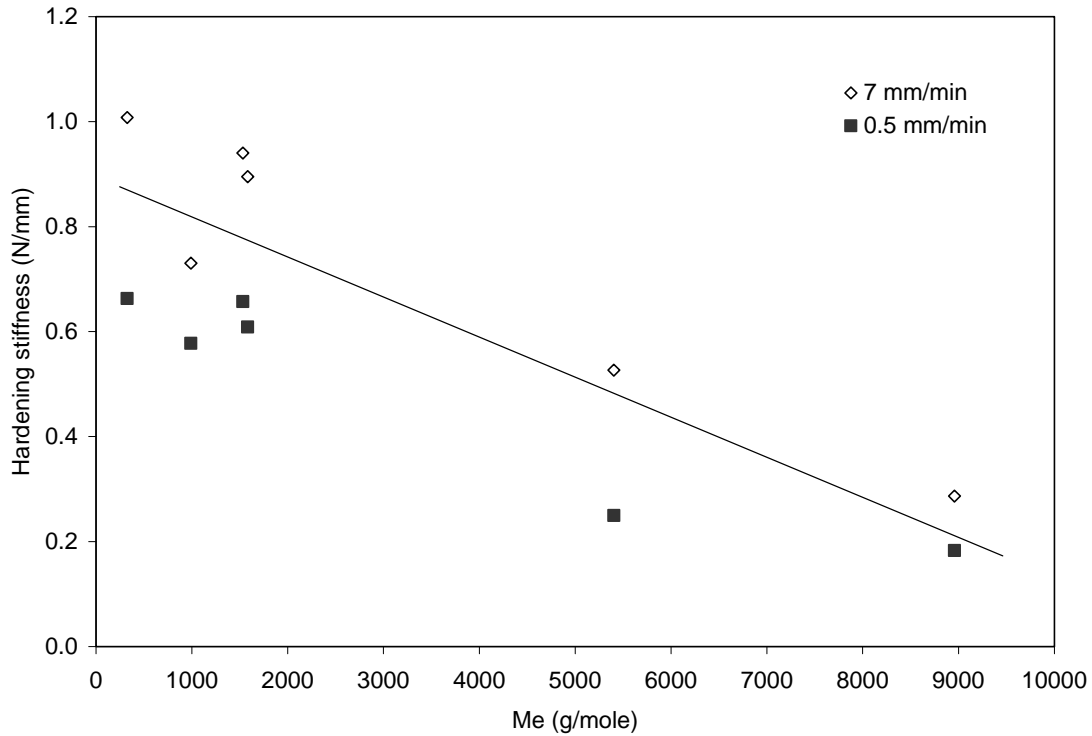


**Figure 5.7: Hardening stiffness vs.  $M_e$  (the line is only a visual guide to the eye)**

Another indicator used to measure the extension behaviour of a polymer network is the NDR. Lower NDR means that the network has less extensibility. Figure 5.8 is a plot of NDR as a function of  $M_e$ . Increases in NDR can be seen with increasing  $M_e$  values. The NDR values of the resins are similar for both 0.5 mm/min and 7 mm/min deformation rates (Table 5.4). The extensibility of the polymer network is relatively insensitive to the speed of the extension, resulting in NDR values being similar for different strain rates. On the other hand, the extensional limit of a polymer network is sensitive to the number of restrictions within the network. High  $M_e$  indicates fewer entanglements per chain. Therefore, less restriction on the extension of the network results in higher NDR values.

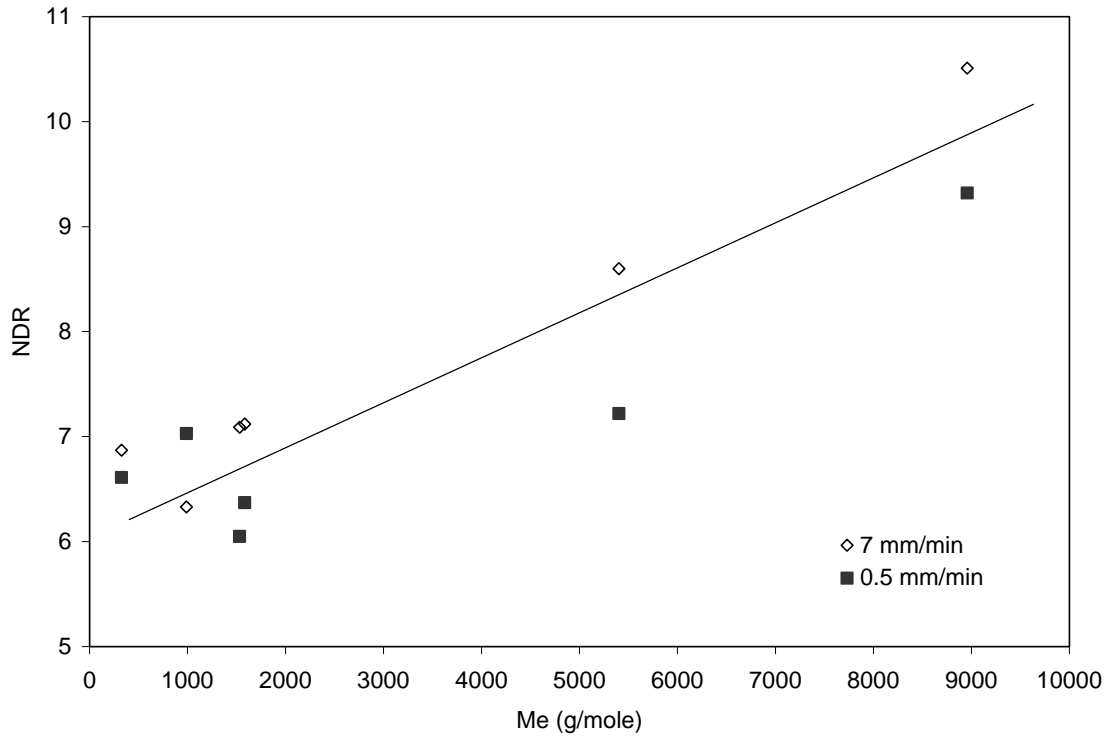


**Figure 5.8: NDR vs.  $M_e$  (the line is for the sole purpose of guiding the eye)**

### 5.3.4 ESCR and Chain Entanglements

Environmental stress cracking occurs through a mechanism of disentanglement. It is believed that a high number of inter-lamellar links is key to the high ESCR of HDPE. Previous work has mainly focused on bridging-tie-molecules as the origin of inter-lamellar connections. However, studies have shown that the number of bridging-tie-molecules is much lower than the number of entanglements in a polymer system (3, 11, 14). Strain hardening has also been shown to be influenced by the number of chain entanglements in a polymer. Recently, strain hardening behaviour of PE has been linked to its ESCR (25, 26, 60). Together, these recent publications suggest that physical chain entanglements must contribute significantly to the number of inter-lamellar connections

that affect the ESCR of HDPE. Therefore it is proposed that the relationship observed in section 5.3.3 between strain hardening behaviour and entanglement molecular weight should hold for ESCR as well.

The ESCR results for the resins herein in number of hours before failure are presented in Table 5.2. The values cited are means (averages) over several independent replicates (usually three dogbones from the same plate, and often two or three independent plates with two to five dogbones per plate). Statistical analysis on independent replicate tests showed that the test procedure does not contribute any statistically significant variability to the results (for details of the statistical analysis see Chapter 4). PE5 and PE6 could not be tested using the NCLT method because they were brittle and could not be notched even at a very slow notching speed.

Of the resins studied, PE7-10 have much higher ESCR than PE1-4. The ESCR of PE7-10 is two to three orders of magnitude larger than the ESCR of PE1-4 (Table 5.2). The difference in ESCR can be attributed to MW differences of the resins. PE7-10 have much higher MW than PE1-6, especially  $M_z$ -average molecular weight. High MW means there are more molecules that can form inter-lamellar links, and thus increase the ESCR of the resin. PE10 has the highest MW and ESCR of all resins. It did not fail even after 3000 hours.

$^{13}\text{C}$ -NMR analysis shed further light on the behaviour of these resins (see Table 5.2). For PE1-4, the differences in ESCR can be correlated to the differences in SCB per thousand

carbon atoms. SCB improves ESCR of HDPE by encouraging the formation of inter-lamellar links and hindering chain slips from crystalline lamellae. Of the four resins (PE1-4), PE2 and PE3 have similar MW as PE1, but lower SCB content (Table 5.2). The low SCB of PE2 and PE3 results in lower ESCR values. The SCB influence on ESCR can also be seen in the behaviour of PE4, which has a similar ESCR to PE1. PE4 would be expected to have lower ESCR because of lower MW than PE1-3. However, the higher SCB content of PE4 makes up for the MW differences, resulting in PE4 having higher ESCR than PE2 and PE3.

In Figure 5.9, ESCR is plotted against  $M_e$  of the resins. High ESCR values are associated with low  $M_e$ , indicating that resins with more chain entanglements have higher ESCR. This result confirms the earlier postulation that chain entanglements affect the ESCR of polyethylene. The number of chain entanglements is influenced by the chain length, whereby larger chains have a greater number of chain entanglements than smaller chains. Comparing all the resins, PE7-10 have much higher  $M_w$  values than PE1-6; and indeed, PE7-10 also have much lower  $M_e$  values than PE1-6 (Table 5.3), signifying once more that PE7-10 have more chain entanglements. A higher number of chain entanglements reduces the mobility of the polymer chains (higher  $\eta_0$ ). Less mobile chains would take longer to disentangle from each other and from the crystal lamellae, thus resulting in higher ESCR. Once again, PE8 exhibits a “deviant” behaviour from that expected (based solely on  $\eta_0$ ) due to the further lowering of  $M_e$  by LCB.

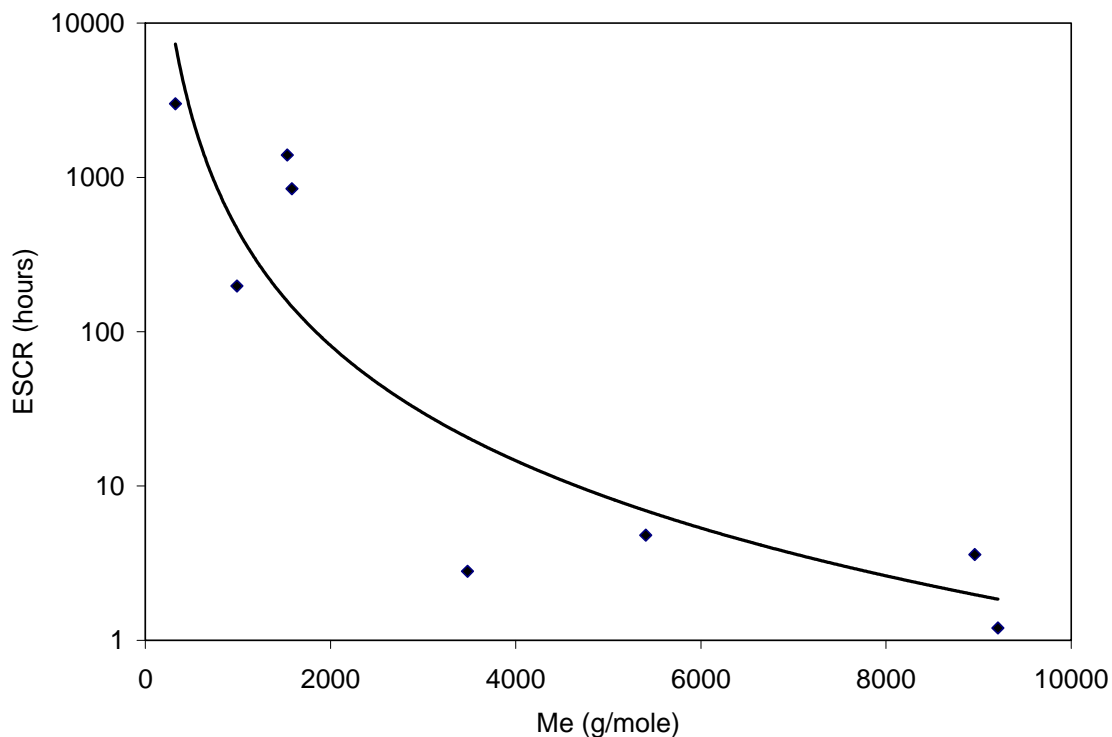


**Figure 5.9: ESCR vs.  $M_e$  for PE1-4 and PE7-10**

Rheological properties in the terminal zone, such as  $\eta_0$  and  $M_e$ , are strongly influenced by the longest molecules in the system (27). On the other hand, resins with high MW due to longer chains are known to have higher (“better”) ESCR values. It can be seen that the connection between rheological properties and ESCR is through the influence of long chains on the polymer system. The influence of MW can be more clearly seen from the  $M_z$ -average molecular weight values of the resins.  $M_z$  emphasizes the high molecular weight part of the MWD more so than  $M_w$ , and therefore, can reflect more of the influence of the largest molecules in the system. From Table 5.2, the  $M_z$  values of PE7-10 are an order of magnitude larger than the  $M_z$  values of PE1-6. The higher  $M_z$  values mean that PE7-10 have more polymer chains in the high molecular weight fraction of the MWD. This is confirmed by the MWD plots of resins in Figure 5.3, which clearly show

that PE7-10 have a larger fraction in the high MW end of the distribution than PE1-6. Observe the larger area under the MWD curve in Figure 5.3(d) for log MW values greater than six in comparison to Figure 5.3(a-c). PE10 has the largest fraction in the high MW end of the MWD as compared to all other resins. The resins with high  $M_z$  value have large  $\eta_0$  and small  $M_e$  values (Table 5.3). Large  $\eta_0$  means that these resins have more entanglements and less network mobility. Hindrances to mobility in the melt are “transferred” into the amorphous phase of HDPE upon solidification, thus becoming hindrances to the disentanglement steps of ESC.

#### **5.4 Micromechanical Modeling**

Ductile deformation behaviour of polyethylene is affected by both the crystalline and amorphous phases of the material (61-64). The onset of strain hardening occurs when the amorphous phase is fully stretched out. In the strain hardening phase, the fully extended amorphous phase becomes the rigid load-bearing element, while crystalline lamellae break apart and unfold to accommodate the change in strain (65). During strain hardening the load-bearing elements in the amorphous phase are the inter-lamellar links. These linkages comprised of both tie-molecules and entanglements (2, 27). Past and recent published work has speculated that physical chain entanglements are more likely to be responsible for the inter-lamellar connection than tie-molecules (3, 11, 14, 24).

There are two main difficulties in studying entanglement effects on strain hardening behaviour of polyethylene. The first difficulty is that the number of entanglements in solid PE cannot be directly measured with any currently available techniques. Physical

chain entanglements are found in the amorphous phase of polyethylene, which has many characteristics similar to its melt. The number of entanglements in the amorphous phase remains relatively constant due to the dynamic equilibrium achieved by the entanglement and disentanglements of chains. Large chain movements (such as entanglement and disentanglement of chains) involves movement of the polymer backbone in reptation or primitive-path fluctuation (28-31). The movement of the large PE backbones can be more readily studied in the melt state using rheological techniques (27). Flory and Yoon has shown that chain entanglements in the melt are largely preserved in the amorphous phase upon solidification (39). Therefore, melt entanglement measurements can be used to represent the state of physical chain entanglement in the solid.

The second obstacle for studying the relationship between chain entanglements and strain hardening experimentally lays in the difficulty of isolating entanglement effect from influence of other structure properties. When dealing with polyethylene resins, change in one material property is connected to changes in other properties. For example, increasing chain entanglements can be achieved with increasing amorphous phase of PE, which would be accompanied by decreasing crystallinity of the material. Crystallinity and lamella characteristics play important roles in polyethylene mechanical behaviour (23, 64), hence any changes can not be ignored. When real resins are involved, it is not possible to keep all other material properties constant and only change entanglement conditions.

In this section, the relationship between physical chain entanglements and strain hardening of polyethylene is first established experimentally, and then experimental results are compared to independent micromechanical modeling of uniaxial tensile deformation for polyethylene. Unlike experimental work, in micromechanical modeling all material properties except the number of entanglements can be held constant, thus isolates the chain entanglement effect has on strain hardening behaviour of PE. Allowing a more controlled and systemic approach in studying the relationship between chain entanglements and strain hardening behaviour of polyethylene.

#### **5.4.1 Chain Entanglements and Strain Hardening – Justification via Micromechanical Modeling**

Strain hardening occurs during ductile deformation of polyethylene under large strains. Ductile deformation involves rearrangement of both the crystalline and amorphous phases of the polymer (64). In experimental work, it is difficult to control the entanglement nature of polyethylene, as alluded to in the introduction. Herein comes into play the role of a valid micromechanical model. Such a model can shed more light on the effects of the number of chain entanglements, by isolating these effects on the strain hardening behaviour of PE, and thus clarifying their relationship. This interaction between a valid mathematical model, independently developed, and empirical observations can offer useful insights into these complex phenomena underlying mechanical behaviour/performance of polymeric materials like polyethylene. Thus, micromechanical modeling work was carried out in parallel, in order to independently verify the observed relationship between physical chain entanglements and strain

hardening of high density polyethylene. The complementarity of the two approaches not only highlighted but also confirmed the speculated entanglements effects on the mechanical response of PE.

The strain hardening of polyethylene under uniaxial tension was revisited using a micromechanical model (65). Micromechanical models are a class of analytical models that emphasize the relationship between the macroscopic mechanical behaviour of a material and its microstructure (66). For polyethylene, micromechanical modeling of large deformations was pioneered by Lee *et al.* (67, 68) and Argon (69). The model in Alvarado-Contreras (65) incorporates Continuum Damage Mechanics Theory into the micromechanical model first developed by Lee *et al.* (67, 68) to describe more realistically the mechanical behaviour of high density polyethylene. Compared to other polyethylene models without damage laws, such as the viscoplastic model developed by Nikolov *et al.* (70), the model with damage (65) offers more successful simulation of the material behaviour, especially when strain is large. Simulation results (solid curve) from (65) are compared with experimental data from G'Sell and Jonas (71) in Figure 5.10. The figure also contains results (see +) from an earlier viscoplastic model (70). One can see the improvement when the equivalent strain becomes larger than 1.5.

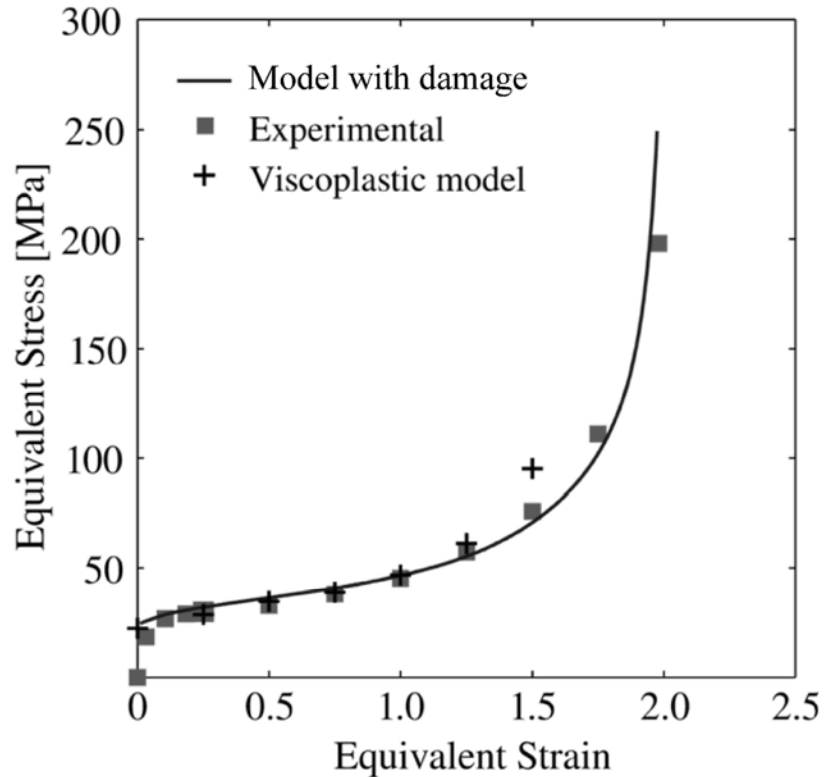


**Figure 5.10: Simulation results of semicrystalline polyethylene (65): equivalent stress vs. equivalent strain behaviour under uniaxial tension**

Polyethylene, being a semicrystalline material, is modeled with the crystalline and amorphous phases as collections of inclusions. Each inclusion is in the shape of a rectangular block with a crystalline layer (lamella) attached to an amorphous layer. The volume fraction of the crystalline layer to the amorphous layer in each inclusion is assigned based on overall material crystallinity. Mechanical loads are transferred from one phase to another through inter-lamellar links. A hundred inclusions, with equal volume fractions, were used in the modeling. For each inclusion, its orientation is numerically generated in a random manner using Euler angles (65). In the micromechanical model, the crystalline phase consisted of polyethylene crystals with eight slip systems to accommodate deformations (see Figure 5.11 ). The amorphous phase was modeled as a random network of entanglements. Each entanglement is an

idealized unit cell (see Figure 5.12) based on the eight chain model (72), whereas each chain has a set number of rigid links (N) representing the C-C bonds in polyethylene. What is relevant for the current investigation is that a small N value means there are less C-C links between entanglements, and hence overall more entanglements in the system.

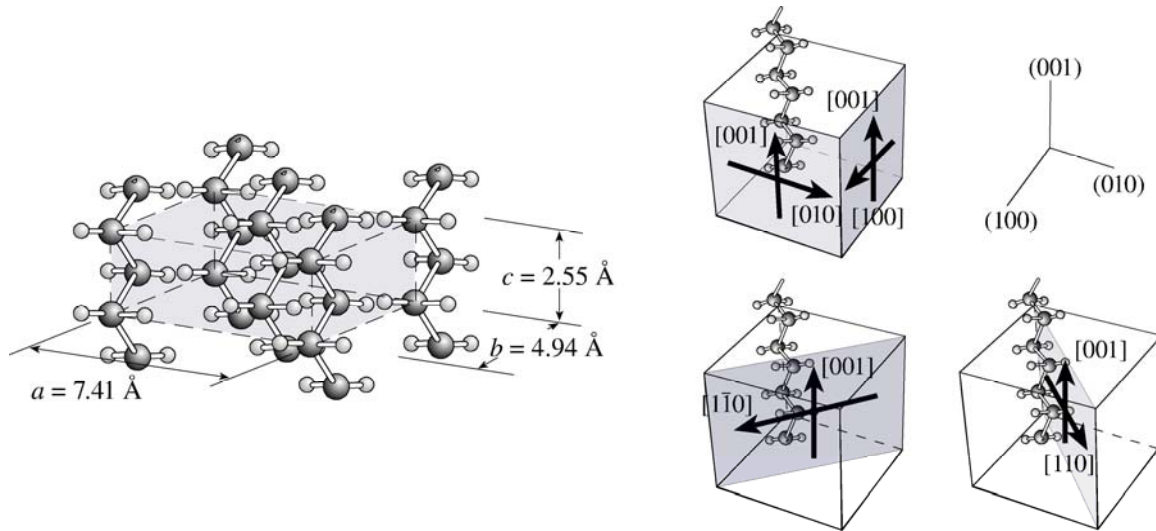


Figure 5.11: Schematic representation of polyethylene crystal and slip system, ref. (65)

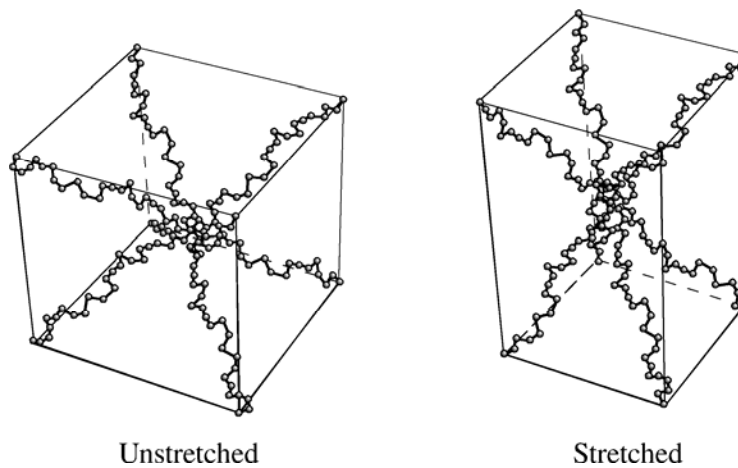


Figure 5.12: Schematic illustration of the eight chain network model for the amorphous phase, ref. (65)

Since the focus of this chapter is not micromechanical modeling itself, the reader can refer to references (65) and (73) for more details on micromechanical modeling combined with damage laws. Mathematical equations and material parameters used in the micromechanical model simulations are presented in Appendix D. For the purpose of this study, the only model parameter changed is the number of rigid links ( $N$ ), while all other model parameters were held constant in order to isolate entanglement effects on deformation behaviour of polyethylene. The number of rigid links or the  $N$  value used ranged from 20-200.

Even though the micromechanical model used was developed earlier independently of experimental results in this study, the mathematical model concept of number of rigid links ( $N$ ) between entanglement points is “equivalent” to the idea of the experimentally determined molecular weight between entanglements ( $M_e$ ). The  $M_e$  value can easily be converted to number of rigid links between entanglements by dividing it by the molecular weight of the repeating unit. Conversely, multiplying the  $N$  value with the molecular weight of the ethylene repeating unit (28 g/mol) results in  $M_e$ , hence the molecular weight between entanglements used in the micromechanical model ranged from 560-5600 g/mol.

In micromechanical modeling it is possible to observe individual mechanical responses of the crystalline and amorphous phases. In Figures 5.13 and 5.14, uniaxial tensile deformation modeling results of the crystalline and amorphous phases are presented,

respectively. The stress-strain curves showed that for the same level of strain during strain hardening, the stress response of the crystalline phase (Figure 5.13) is much smaller than the stress response of the amorphous phase (Figure 5.14). The scale of the y-axis (phase equivalent stress) is much smaller for Figure 5.13 than Figure 5.14. Indeed, the crystalline phase did not seem to show any significant strain hardening until the number of rigid links became 40 and less. These two plots show that the amorphous phase plays a more important role in strain hardening of polyethylene.

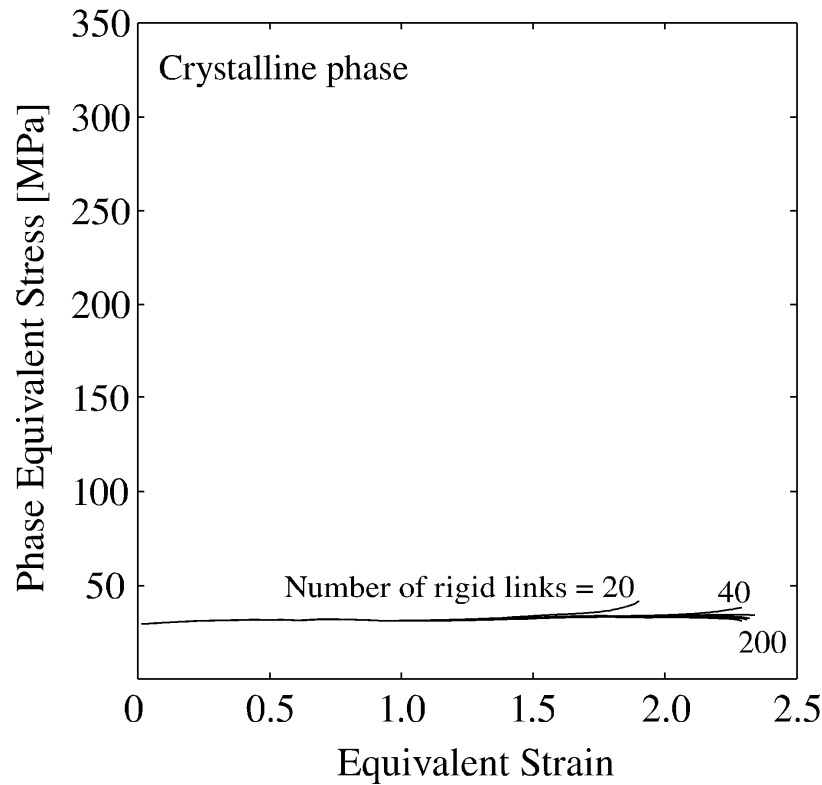


**Figure 5.13: Influence of the number of rigid links on the stress-strain response of the crystalline phase**

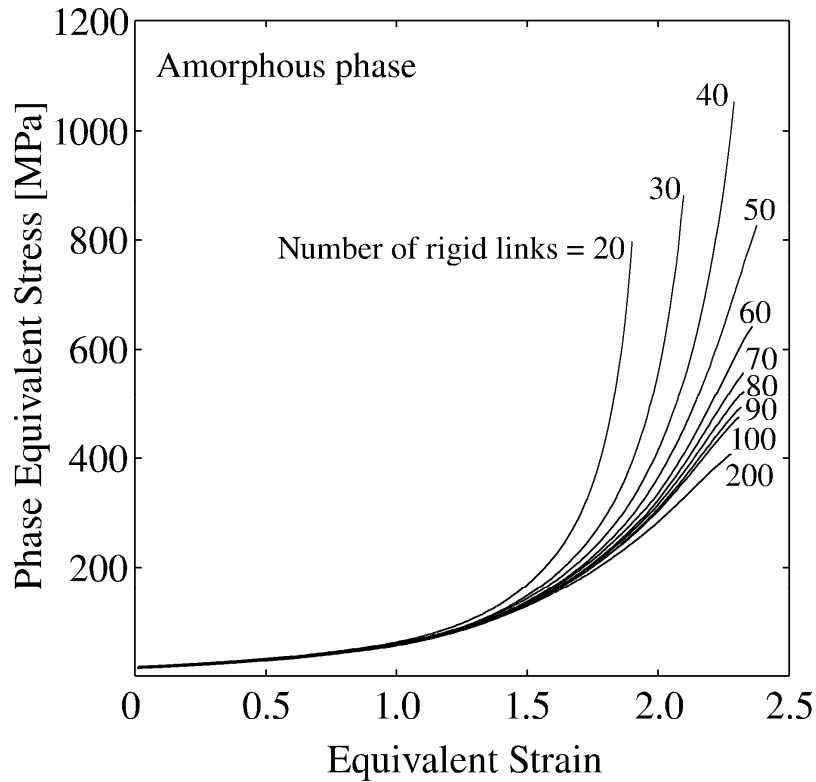


**Figure 5.14: Influence of the number of rigid links on the stress-strain response of the amorphous phase**

In Figure 5.15, uniaxial tension deformation modeling results for semicrystalline polyethylene are shown. The stress-strain relationship is plotted as a function of the number of rigid links between entanglements based on the eight chain model. The stress-strain curves show a step increase after an equivalent strain of 1, at which point strain hardening behaviour is observed. Simulations with smaller numbers of rigid links between entanglements ( $N$ ) exhibit more strain hardening, manifested by the larger slope of the stress-strain curves. The stress-strain curve with  $N=20$  has the most strain hardening in Figure 5.15. A smaller  $N$  value translates into more entanglements in the polymer system.

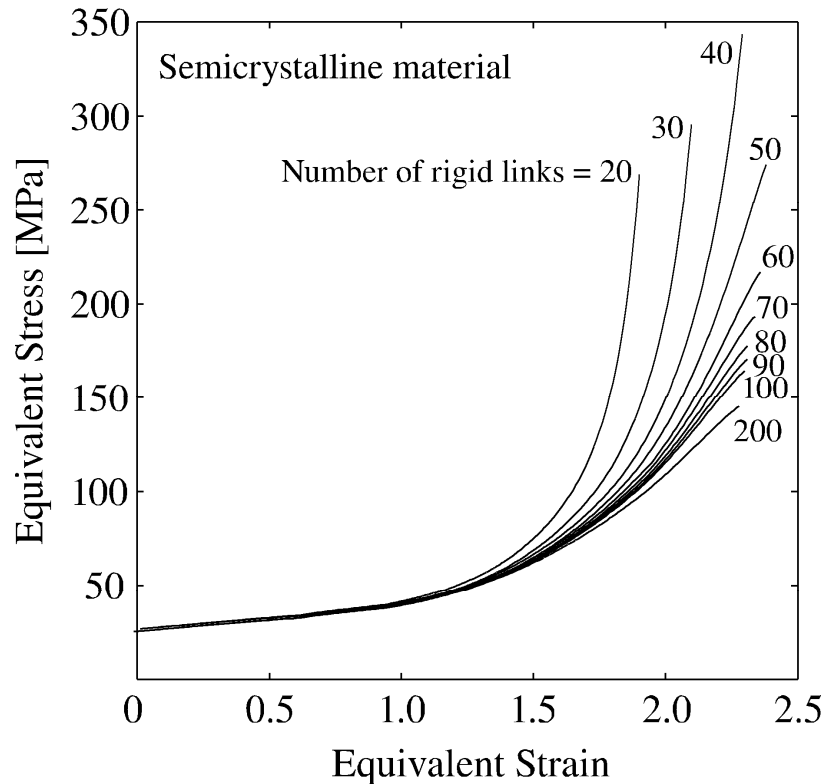


**Figure 5.15: Influence of the number of rigid links on stress-strain response for semicrystalline polyethylene**

The load-displacement curves in Figure 5.16 are based on tensile strain hardening experiments at 0.5 mm/min deformation rate. The sequence of PE samples in the graph is in order of decreasing strain hardening. The same trend in curves and strain hardening ranking was observed for experiments carried out at 7 mm/min deformation rate (see Chapter 4 for more details). The load-displacement curves in Figure 5.16 are based on experiments at 0.5 mm/min deformation rate. The sequence of PE samples in the graph is in order of decreasing strain hardening. The same trend in curves and strain hardening ranking was observed for experiments carried out at 7 mm/min deformation rate. However, PE8 seems to deviate from this trend. PE8 showed less strain hardening than PE7 and PE9 even though it has a smaller  $M_c$  value than either of these two resins. It is believed that PE8 contains a small amount of long chain branches (LCB) that increased

its  $\eta_0$  (41, 55-57), thus resulting in a smaller calculated  $M_e$  value, and hence giving the appearance of more chain entanglements. The influence of LCB on rheological properties of resins was discussed in more detail in section 5.3.2.

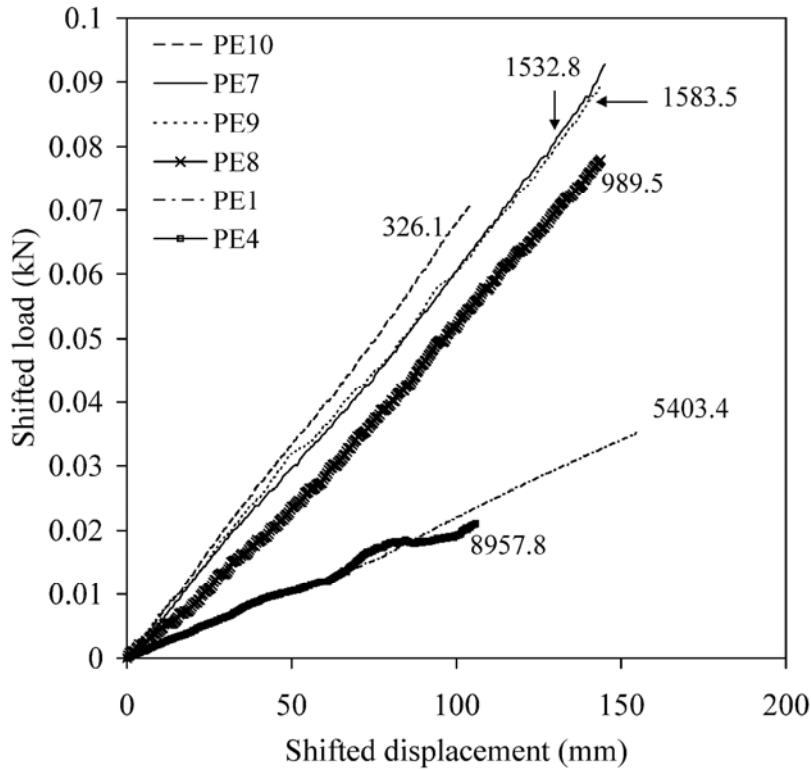


**Figure 5.16: Shifted load-displacement curves of the strain hardening stage and corresponding  $M_e$  of resins; deformation rate 0.5 mm/min**

The strain hardening ranking of the stress-strain curves in Figure 5.15 shows the same trend as the load-displacement curves in Figure 5.16. In Figure 5.15, the  $N=20$  ( $M_e=560$  g/mol) curve showed the most strain hardening, while the  $N=200$  ( $M_e=5600$  g/mol) curve showed the least strain hardening. In Figure 5.16, the resin with  $M_e=326.1$  g/mol (PE10) has the most strain hardening, whereas the resin with  $M_e=8957.8$  g/mol (PE4) has the least strain hardening (see also the hardening stiffness values in Table 5.4). The plots of Figures 5.15 and 5.16 exhibit the sample overall pattern. Thus, by describing the same

trends in material response as the experimental results, the micromechanical model simulations independently confirm the postulate that physical chain entanglements are the key structural feature affecting strain hardening behaviour of polyethylene.

## **5.5 Concluding Remarks**

Viscosity is a measure of polymer network mobility and is known to increase with increasing number of physical chain entanglements in the system. In this chapter, melt state chain entanglement behaviour is used to make inferences regarding the nature of entanglements in solid state PE. Physical chain entanglements are known to control tensile strain hardening behaviour of a polymer. Experimental results showed that the resistance of network extension (the strain hardening stiffness) increases with decreasing value of entanglement molecular weight of the resin and hence, demonstrated that the  $M_e$  determination in the melt phase is directly related to the entanglement state of the solid PE. The above conclusion was further confirmed by the observation that increases in the extensibility of the network (NDR) are associated with increasing  $M_e$ .

The success of relating a rheological indicator of entanglements to the strain hardening behaviour of solid PE subsequently led to the investigation of the relationship between chain entanglements and ESCR. Previous research and Chapter 4 of this thesis have established that strain hardening behaviour and ESCR of polyethylene are related. In this chapter, experiments showed that the entanglement molecular weight is inversely proportional to ESCR. A resin with smaller  $M_e$ , hence a higher number of entanglements, exhibits a higher ESCR. The correlation between  $M_e$  and ESCR demonstrated that, in

addition to bridging-tie-molecules, physical chain entanglements contribute significantly to the formation of inter-lamellar connections that improve ESCR of HDPE.

In this chapter, the relationship between physical chain entanglements and strain hardening behaviour of polyethylene is studied using both an experimental approach and micromechanical modeling. In the experimental approach, tensile deformation experiments and rheological tests were carried out. Increasing tensile strain hardening is associated with decreasing molecular weight between entanglements ( $M_e$ ) values of polyethylene resins. Smaller molecular weight between entanglements means there are more chain entanglements in the polymer.

In a complementary micromechanical modeling step, the number of rigid links between entanglements ( $N$ ) was studied in parallel. As the  $N$  value decreases, the number of entanglements in the system increases, hence making  $N$  and  $M_e$  “equivalent”. The modeling results showed that as the number of entanglements increased, stress-strain responses of polyethylene showed increasing strain hardening. In addition, the micromechanical model also confirmed that in tensile strain hardening the amorphous phase of polyethylene plays a more dominant role than its crystalline phase. The micromechanical modeling work independently demonstrated the same relationship between physical chain entanglements and strain hardening as the experimental approach. These two approaches established separately that physical chain entanglements are key microstructural characteristics that influence tensile strain hardening of polyethylene.

## 5.6 References

1. Brostow, W. and Corneliussen, R. D. (1986), *Failure of Plastics*, Hanser Publishers, New York.
2. Lustiger, A. & Markham, R. L. (1983), "Importance of tie molecules in preventing polyethylene fracture under long-term loading conditions", *Polymer*, vol. 24, pp. 1647-1654.
3. Brown, N., Lu, X., Huang, Y., Harrison, I. P., & Ishikawa, N. (1992), "The Fundamental Material Parameters That Govern Slow Crack-Growth in Linear Polyethylenes", *Plastics Rubber and Composites Processing and Applications*, vol. 17, no. 4, pp. 255-258.
4. Huang, Y. & Brown, N. (1988), "The effect of molecular weight on slow crack growth in linear polyethylene homopolymers", *Journal of Materials Science*, vol. 23, pp. 3648-3655.
5. Huang, Y.-L. & Brown, N. (1991), "Dependence of slow crack growth in polyethylene on butyl branch density: morphology and theory", *Journal of Polymer Science, Part B: Polymer Physics*, vol. 29, pp. 129-137.
6. Yeh, J. T. & Hong, H. S. (1994), "Effect of branch frequency on dynamic fatigue behaviour of slowly notched polyethylene polymers", *Journal of Polymer Research*, vol. 1, no. 4, pp. 375-383.
7. Janimak, J. J. & Stevens, G. C. (2001), "Inter-relationships between tie-molecule concentration, molecular characteristics and mechanical properties in metallocene catalysed medium density polyethylenes", *Journal of Materials Science*, vol. 36, no. 8, pp. 1879-1884.
8. Yeh, J. T., Chen, C. Y., & Hong, H. S. (1994), "Static fatigue behaviour of linear low-density polyethylene", *Journal of Materials Science*, vol. 29, pp. 4104-4112.
9. Schellenberg, J. & Fienhold, G. (1998), "Environmental stress cracking resistance of blends of high-density polyethylene with other polyethylenes", *Polymer Engineering and Science*, vol. 38, no. 9, pp. 1413-1419.
10. Ward, A. L., Lu, X., Huang, Y., & Brown, N. (1991), "Mechanism of slow crack growth in polyethylene by an environmental stress cracking agent", *Polymer*, vol. 32, no. 12, pp. 2172-2178.
11. Brown, N. & Ward, I. M. (1983), "The influence of morphology and molecular weight on ductile-brittle transitions in linear polyethylene", *Journal of Materials Science*, vol. 18, pp. 1405-1420.

12. DesLauriers, P. J. "Relationship between notched pipe test and NDR", SPE International Polyolefins Conference 2006, Houston, TX, USA.
13. Seguela, R. (2005), "Critical review of the molecular topology of semicrystalline polymers: the origin and assessment of intercrystalline tie molecules and chain entanglements", *Journal of Polymer Science, Part B: Polymer Physics*, vol. 43, no. 14, pp. 1729-1748.
14. Yeh, J. T. & Runt, J. (1991), "Fatigue crack propagation in high-density polyethylene", *Journal of Polymer Science, Part B: Polymer Physics*, vol. 29, pp. 371-388.
15. Baltá Calleja, F. J., Santa Cruz, C., Bayer, R. K., & Kilian, H. G. (1990), "Microhardness and surface free energy in linear polyethylene: the role of entanglements", *Colloid and Polymer Science*, vol. 268, pp. 440-446.
16. Bartczak, Z. (2005), "Effect of chain entanglement on plastic deformation behaviour of linear polyethylene", *Macromolecules*, vol. 38, pp. 7702-7713.
17. Huang, B., Ito, M., & Kanamoto, T. (1994), "Deformation mechanism of amorphous poly(ethylene terephthalate) as a function of molecular weight and entanglements", *Polymer*, vol. 35, no. 6, pp. 1210-1215.
18. Men, Y. & Rieger, J. (2003), "Role of the entangled amorphous network in tensile deformation of semicrystalline polymers", *Physical Review Letters*, vol. 91, no. 9, pp. 095502-1-095502-4.
19. Plummer, C. J. G. & Kausch, H.-H. (1996), "Deformation and entanglement in semicrystalline polymers", *Journal of Macromolecular Science: Physics*, vol. B35, pp. 637-657.
20. Bayer, R. K. (1991), "Structure transfer from a polymeric melt to the solid state. Part I: The influence of chain entanglements in linear polyethylene", *Colloid and Polymer Science*, vol. 269, pp. 421-432.
21. Bayer, R. K. (1994), "Structure transfer from a polymeric melt to the solid state. Part III: Influence of knots on structure and mechanical properties of semicrystalline polymers", *Colloid and Polymer Science*, vol. 272, pp. 910-932.
22. Bayer, R. K., Baltá Calleja, F. J., & Kilian, H. G. (1997), "Crystal hardness and average distance between stable entanglements in melt crystallized polyethylene", *Colloid and Polymer Science*, vol. 275, pp. 432-439.
23. Ward, I. M. (1971), *Mechanical Properties of Solid Polymers*, Wiley-Interscience, Toronto.

24. Zuo, F., Keum, J. K., Chen, X., Hsiao, B. S., Chen, H., Lai, S.-Y., Wevers, R., & Li, J. (2007), "The role of interlamellar chain entanglement in deformation-induced structural changes during uniaxial stretching of isotactic polypropylene", *Polymer*, vol. 48, no. 23, pp. 6867-6880.
25. Kurelec, L., Teeuwen, M., Schoffeleers, H., & Deblieck, R. (2005), "Strain hardening modulus as a measure of environmental stress crack resistance of high density polyethylene", *Polymer*, vol. 46, pp. 6369-6379.
26. Maxwell, A. S. & Pilkington, G. (2008), "Prediction of environmental stress cracking resistance in linear low density polyethylenes", *Polymer Engineering and Science*, vol. 48, no. 2, pp. 360-364.
27. Ferry, J. D. (1980), *Viscoelastic Properties of Polymers*, 3 edn, Wiley, New York.
28. de Gennes, P. G. (1971), "Reptation of a polymer chain in the presence of fixed obstacles", *Journal of Chemical Physics*, vol. 55, no. 2, pp. 572-579.
29. Brochard, F. & de Gennes, P. G. (1986), "Polymer-polymer interdiffusion", *Europhysics Letters*, vol. 1, no. 5, pp. 221-224.
30. de Gennes, P. G. (1975), "Reptation of stars", *Journal de Physique*, vol. 36, pp. 1199-1203.
31. Doi, M. & Kuzuu, N. Y. (1980), "Nonlinear elasticity of rodlike macromolecules in condensed state", *Journal of Polymer Science, Polymer Physics Edition*, vol. 18, no. 3, pp. 409-419.
32. Men, Y. F., Rieger, J., Enderle, H.-F., & Lilge, D. (2004), "The mobility of the amorphous phase in polyethylene as a determining factor for slow crack growth", *European Physical Journal E: Soft Matter*, vol. 15, no. 4, pp. 421-425.
33. Munaro, M. & Akcelrud, L. (2008), "Polyethylene blends: a correlation study between morphology and environmental resistance", *Polymer Degradation and Stability*, vol. 93, pp. 43-49.
34. Lear, J. J. & Geil, P. H. (1991), "Slow crack growth and molecular mobility in commercial gas pipe resins", *International Journal of Polymeric Materials*, vol. 15, no. 3-4, pp. 147-170.
35. Menard, K. P. (1999), *Dynamic Mechanical Analysis: A Practical Introduction*, CRC Press, New York.
36. Simanke, A. G., Galland, G. B., Neto, R. B., Quijada, R., & Mauler, R. S. (1999), "Influence of the type and the comonomer contents on the mechanical behavior of ethylene/alpha-olefin copolymers", *Journal of Applied Polymer Science*, vol. 74, no. 5, pp. 1194-1200.

37. Simanke, A. G., Galland, G. B., Freitas, L., da Jornada, J. A. H., Quijada, R., & Mauler, R. S. (1999), "Influence of the comonomer content on the thermal and dynamic mechanical properties of metallocene ethylene/1-octene copolymers", *Polymer*, vol. 40, no. 20, pp. 5489-5495.
38. Stadler, F. J., Kaschta, J., & Muenstedt, H. (2005), "Dynamic-mechanical behavior of polyethylenes and ethene-/alpha-olefin-co-polymers. Part I. alpha '-relaxation", *Polymer*, vol. 46, no. 23, pp. 10311-10320.
39. Flory, P. J. & Yoon, D. Y. (1978), "Molecular morphology in semicrystalline polymers", *Nature*, vol. 272, no. 16, pp. 226-229.
40. Honerkamp, J. & Weese, J. (1993), "A nonlinear regularization method for the calculation of relaxation spectra", *Rheol Acta*, vol. 32, pp. 65-73.
41. Muenstedt, H. & Auhl, D. (2005), "Rheological measuring techniques and their relevance for the molecular characterization of polymers", *Journal of Non-Newtonian Fluid Mechanics*, vol. 128, no. 1, pp. 62-69.
42. Stadler, F. J., Piel, C., Klimke, K., Kaschta, J., Parkinson, M., Wilhelm, M., Kaminsky, W., & Muenstedt, H. (2006), "Influency of type and content of various comonomers on long-chain branching of ethene/-a-olefin copolymers", *Macromolecules*, vol. 39, no. 4, pp. 1474-1482.
43. Peón, J., Vega, J. F., Del Amo, B., & Martínez-Salazar, J. (2003), "Phase morphology and melt viscoelastic properties in blends of ethylene/vinyl acetate copolymer and metallocene-catalysed linear polyethylene", *Polymer*, vol. 44, pp. 2911-2918.
44. Doi, M. & Edwards, S. F. (1986), *The Theory of Polymer Dynamics*, Clarendon Press, Oxford.
45. Liu, C., He, J., van Ruymbek, E., Keunings, R., & Bailly, C. (2006), "Evaluation of different methods for the determination of the plateau modulus and entanglement molecular weight", *Polymer*, vol. 47, pp. 4461-4479.
46. Fetters, L. J., Lohse, D. J., & Colby, R. H. (1996), "Chain dimensions and entanglement spacings," in *Physical properties of polymers handbook*, J. E. Mark, ed., American Institute of Physics, Woodbury, New York, pp. 335-340.
47. Graessley, W. W. & Edwards, S. F. (1981), "Entanglement interactions in polymers and the chain contour concentration", *Polymer*, vol. 22, pp. 1329-1334.
48. Bueche, F. (1962), *Physical Properties of Polymers*, Interscience Publishing, New York.
49. Bueche, F. (1952), "Mobility of molecules in liquids near the glass temperature", *Journal of Chemical Physics*, vol. 30, pp. 748-752.

50. Harrell, E. R. & Nakajima, N. (1984), "Modified Cole-Cole plot based on viscoelastic properties for characterizing molecular architecture of elastomers", *Journal of Applied Polymer Science*, vol. 29, no. 3, pp. 995-1010.
51. Shroff, R. & Mavridis, H. (1995), "New measures of polydispersity from rheological data on polymer melts", *Journal of Applied Polymer Science*, vol. 57, pp. 1605-1626.
52. Trinkle, S., Walter, P., & Friedrich, C. (2002), "Van Gulp-Palmen plot II - classification of long chain branched polymers by their topology", *Rheol.Acta*, vol. 41, pp. 103-113.
53. Trinkle, S. & Friedrich, C. (2001), "Van Gulp-Palmen-plot: a way to characterize polydispersity of linear polymers", *Rheol.Acta*, vol. 40, pp. 322-328.
54. Shroff, R. N. & Mavridis, H. (1999), "Long-chain-branching index for essentially linear polyethylenes", *Macromolecules*, vol. 32, pp. 8454-8464.
55. Janzen, J. & Colby, R. H. (1994), "Diagnosing long-chain branching in polyethylenes", *Journal of Molecular Structure*, vol. 485-486, pp. 569-584.
56. Wood-Adams, P. M. (2001), "The effect of long chain branches on the shear flow behavior of polyethylene", *Journal of Rheology*, vol. 45, no. 1, pp. 203-210.
57. Vega, J. F. & Martínez-Salazar, J. (2003), "Rheological features and molecular architecture of polyethylenes", *Polymer Bulletin*, vol. 50, pp. 197-204.
58. Allison, S. W., Pinnock, P. R., & Ward, I. M. (1966), "Cold drawing of poly(ethylene terephthalate)", *Polymer*, vol. 7, no. 1, pp. 66-69.
59. Schrauwen, B. A. G., Janssen, R. P. M., Govaert, L. E., & Meijer, H. E. H. (2004), "Intrinsic deformation behaviour of semicrystalline polymers", *Macromolecules*, vol. 37, pp. 6069-6078.
60. Hubert, L., David, L., Séguéla, R., Vigier, G., Corfias-Zuccalli, C., & Germain, Y. (2002), "Physical and mechanical properties of polyethylene for pipes in relation to molecular architecture. II. short-term creep of isotropic and drawn materials", *Journal of Applied Polymer Science*, vol. 84, pp. 2308-2317.
61. Hay, I. L. & Keller, A. (1965), "Polymer Deformation in Terms of Spherulites", *Kolloid-Zeitschrift and Zeitschrift fur Polymere*, vol. 204, no. 1-2, pp. 43-74.
62. Geil, P. H. (1964), "Polymer Deformation .3. Annealing of Drawn Polyethylene Single Crystals + Fibers", *Journal of Polymer Science Part A-General Papers*, vol. 2, no. 9, pp. 3835-3855.
63. Peterlin, A. (1965), "Crystalline Character in Polymers", *Journal of Polymer Science Part C-Polymer Symposium* no. 9, pp. 61-89.

64. Lin, L. & Argon, A. S. (1994), "Structure and plastic deformation of polyethylene", *Journal of Materials Science*, vol. 29, pp. 294-323.
65. Alvarado-Contreras, J. A. (2007), *Micromechanical Modelling of Polyethylene*, PhD Thesis, Department of Civil Engineering, University of Waterloo, Waterloo, Ontario, Canada.
66. Budiansky, B. (1983), "Micromechanics", *Computers and Structures*, vol. 16, no. 1-4, pp. 3-12.
67. Lee, B. J., Argon, A. S., Parks, D. M., Ahzi, S., & Bartczak, Z. (1993), "Simulation of Large-Strain Plastic-Deformation and Texture Evolution in High-Density Polyethylene", *Polymer*, vol. 34, no. 17, pp. 3555-3575.
68. Lee, B. J., Parks, D. M., & Ahzi, S. (1993), "Micromechanical Modeling of Large Plastic-Deformation and Texture Evolution in Semicrystalline Polymers", *Journal of the Mechanics and Physics of Solids*, vol. 41, no. 10, pp. 1651-1687.
69. Argon, A. S. (1997), "Morphological mechanism and kinetics of large-strain plastic deformation and evolution of texture in semicrystalline polymers", *Journal of Computer-Aided Materials Design*, vol. 4, no. 2, pp. 75-98.
70. Nikolov, S., Lebensohn, R. A., & Raabe, D. (2006), "Self-consistent modeling of large plastic deformation, texture and morphology evolution in semi-crystalline polymers", *Journal of the Mechanics and Physics of Solids*, vol. 54, no. 7, pp. 1350-1375.
71. G'Sell, C. & Jonas, J. J. (1981), "Yield and transient effects during the plastic deformation of solid polymers", *Journal of Materials Science*, vol. 16, no. 7, pp. 1956-1974.
72. Arruda, E. M. & Boyce, M. C. (1993), "A 3-Dimensional Constitutive Model for the Large Stretch Behavior of Rubber Elastic-Materials", *Journal of the Mechanics and Physics of Solids*, vol. 41, no. 2, pp. 389-412.
73. Alvarado-Contreras, J. A., Polak, M. A., & Penlidis, A. (2007), "Micromechanical approach to Modeling damage in crystalline polyethylene", *Polymer Engineering and Science*, vol. 47, no. 4, pp. 410-420.

## **CHAPTER 6 PHASE INTERCONNECTIVITY AND ESCR**

### **6.1 Introduction\***

Polyethylene (PE) is one of the most versatile commercial polymers today. The semi-crystalline nature of PE allows it to operate over a wide range of temperatures. The crystalline phase of the polymer gives it strength, while the amorphous phase allows PE to be flexible. High density polyethylene (HDPE) is used in the manufacturing of a variety of products, from paint containers to gas line pipes. Compared to pipes of other materials, HDPE pipes have the advantages of being light-weight, corrosion-resistant and easy to install. However, one of the major problems for polyethylene in pipe and other structural applications is environmental stress cracking (ESC). HDPE pipes that should have a service life of fifty years can fail in just one year due to ESC (1). Therefore, environmental stress cracking resistance (ESCR) of polyethylene is of key interest to manufacturers and researchers alike.

The semicrystalline nature of PE influences many of its mechanical properties (2). Melt-crystallized polyethylene has a spherulite morphology, where lamellae made up of spherulites are embedded in a matrix of amorphous material (3-5). The structure of lamellae generally consists of regular chain-folding arrangements with the molecular chains perpendicularly aligned to the lateral lamellar surfaces (6, 7). The regular chain-

---

\* The contents of this chapter form the basis of a paper that has conditionally been accepted by the Journal of Applied Polymer Science, "Phase interconnectivity and environmental stress cracking resistance of polyethylene: a crystalline phase investigation", submitted Aug. 2008.

folding growth of a lamella results in crystals with lateral direction dimensions (1-50  $\mu\text{m}$ ) being much larger than their thickness (2-25 nm) (6-9).

The bulk crystallinity of polyethylene is largely influenced by the processing conditions. Slow cooled and annealed materials have higher crystallinity than quenched PE (10-13). Under the same processing conditions, the crystallinity of PE is influenced by molecular weight and chain structure. The crystallinity of PE increases with increasing molecular weight (11) because longer polymer chains can form larger lamellae. The presence of short chain branching (SCB) hinders the lamella formation process, because chains with SCB cannot be readily incorporated into the lamellar structure. Thus, smaller lamellae are formed and the crystallinity of PE is decreased (14-16). Research has shown that side branches longer than two-carbon atoms cannot be incorporated into the lamella (14). Linear low density polyethylene (LLDPE) with its many side chain groups is known to have lower crystallinity than high density polyethylene, which has fewer side chains (12).

Environmental stress cracking is a form of brittle fracture (17). The mechanism of failure is believed to be a process of disentanglement of inter-lamellar linkages/connections (tie-molecules (17) and entanglements (18)) from the crystalline phase. Research has shown that ESCR of HDPE increases with increasing molecular weight (MW) and SCB content. High MW indicates the presence of long polymer chains that can crystallize into two or more lamellae and form inter-lamellar connections that improve ESCR (13, 19, 20). High SCB content disrupts the formation of the crystalline phase and forces polymer chains into the amorphous phase. Increase in amorphous phase material is believed to

lead to formation of more tie-molecules (21-23). SCB also hinders chain slippage from a lamella by acting as an “anchor point” (24). Since inter-lamellar linkages are an important factor influencing ESCR of polyethylene, most research on ESCR in the past has traditionally focused on the amorphous phase of the material.

Published work on the effect of the crystalline phase of PE on ESCR has revealed unclear relationships. Earlier work by Hittmair and Ullman (25) showed an increase in ESCR with increase in crystallinity. A probabilistic approach to the calculation of tie-molecule concentration, as developed by Huang and Brown (19, 26), stated that ESCR of polyethylene is inversely proportional to the thickness of the lamella, because more lower MW chains can act as tie-molecules when the lamellae are thinner. This implies an increase in ESCR with decreasing crystallinity. Lu *et al.* (10) observed that annealing of PE below 113°C improves its slow crack growth resistance (SCGR). At annealing temperatures above 113°C, the SCGR of PE decreases with increasing anneal temperature. Lu *et al.* (10) attributed the former observation to an increase in crystal perfection with annealing. The latter observation was concluded to be caused by a decrease in tie-molecules due to increased incorporation of chains into the crystalline phase. Most experimental observations of the relationship between PE crystallinity and ESCR were made as a side note on research about the effect that molecular characteristics have on tie-molecule concentration (24, 27-29). These publications generally show that a decrease in crystallinity is merely a side effect of an increase in inter-lamellar links due to an increasing SCB content.

There is no doubt that the influence of crystallinity on ESCR of polyethylene is complicated and further clarification is needed. Previous work on crystallinity and ESCR was mostly restricted to a few resins of limited MW and molecular weight distribution (MWD) range. In the work presented herein, high density polyethylene resins of a wide range of MW and MWD are studied to investigate and quantify the effect of crystalline phase on ESCR. ESCR of resins is associated to classical crystalline phase property indicators, such as crystallinity and lamella thickness. In addition to these indicators, a lamella lateral surface analysis and its effect on ESCR is pursued further.

## 6.2 Experimental Methods

Experimental methods for this chapter have been discussed in Chapter 3 of the thesis. Table 6.1 contains a summary, as in previous chapters, referring back to the appropriate sections of Chapter 3.

**Table 6.1: List of experimental methods for Chapter 6**

<b>Method</b>	<b>Property Determined</b>	<b>Chapter 3 section #</b>
DSC	Crystallinity and lamella thickness	3.1.1
GPC	Molecular weight and molecular weight distribution	3.1.3
<sup>13</sup> C NMR	Short chain branch content	3.1.4
X-Ray diffraction	Crystallinity and lamella thickness	3.1.5
NCLT	ESCR values	3.3.2

### 6.3 Material Characteristics

Different resin characteristics are listed again in Table 6.2.  $M_n$ ,  $M_w$ , and  $M_z$  stand for number-average, weight-average and z-average molecular weights, respectively. PDI is the polydispersity index based on  $M_w/M_n$ . The SCB column gives the number of short chain branches per one thousand carbon atoms for the resins. All resins were copolymers with the butyl group as a side chain. Detailed discussion of environmental stress cracking resistance (ESCR) of resins can be found in section 4.3.1.

**Table 6.2: Material characteristics of resins**

Resin	ESCR (hours)	$M_n$ (kg/mol)	$M_w$ (kg/mol)	$M_z$ (kg/mol)	PDI	SCB (/1000C)
PE1	4.8	16.3	127.5	814.0	7.8	2.8
PE2	1.2	15.7	118.5	837.1	7.6	1.1
PE3	2.8	17.9	140.1	889.8	7.8	0.9
PE4	3.6	19.7	79.4	239.3	4.0	3.8
PE5	N/A	11.4	49.7	157.8	4.4	7.0
PE6	N/A	14.0	62	195.0	4.4	4.7
PE7	1396	11.8	222.8	1593.5	18.9	4.3
PE8	198	14.0	202.1	1398.4	14.4	4.5
PE9	843	10.4	217.9	1244.2	20.9	7.0
PE10	>3000	5.9	315.4	2129.3	53.3	11.8

#### 6.3.1 Crystallinity and Lamella Thickness

Crystalline phase characteristics of resins were investigated using DSC and X-ray diffraction methods. Since percentage crystallinity and lamella thickness values were obtained using both techniques, in order to avoid confusion a definition of certain terms is in order from the outset of this section. In the following, DSC-crystallinity refers to the percentage crystallinity of polymer obtained using the DSC method outlined in section

3.1.1; WAXS-crystallinity is the percentage resin crystallinity based on Equation 3.6 in section 3.1.5. DSC-lamella thickness is calculated using Equation 3.3 and the peak melting temperature from the DSC curve. On the other hand, SAXS-lamella thickness refers to lamella thickness based on the long period information from SAXS and Equation 3.8.

### 6.3.2 Resin Crystallinity Measurements

Information regarding percentage crystallinity of resins is presented in Table 6.3. All resins have crystallinity values that are 50% or higher, characteristic of HDPE. Crystallinity values of resins in this chapter mainly reflect the SCB influence. Presence of SCB is known to interrupt formation of crystalline lamellae; hence, higher SCB content decreases the overall crystallinity of polymer (14). PE10 has lower crystallinity than other resins because of higher SCB content (see Table 6.2). In contrast, PE2 and PE3 have higher crystallinity than all other resins because of their low SCB content.

**Table 6.3: Crystallinity and lamella thickness of resins**

	DSC	WAXS	DSC		SAXS	
	%crystallinity	%crystallinity	Melt temperature (°C)	Lamella thickness (nm)	L - long period (nm)	Lamella thickness (nm)
PE1	55.4%	61.9%	130.5	15.3	24.27	13.3
PE2	58.8%	70.2%	135.5	26.8	28.68	16.7
PE3	57.9%	66.4%	134.1	22.3	25.53	14.7
PE4	55.1%	60.2%	130.1	14.7	23.31	12.7
PE5	53.9%	61.1%	129.1	13.6	19.94	10.7
PE6	56.6%	63.0%	129.8	14.4	21.60	12.1
PE7	53.3%	60.0%	130.7	15.5	24.75	13.1
PE8	56.2%	60.3%	128.6	13.1	26.61	14.8
PE9	61.5%	63.3%	129.9	14.6	24.27	14.9
PE10	51.1%	59.5%	127.0	11.7	24.54	12.4

From Table 6.3, it is observed that the WAXS-crystallinity values are systematically higher than the DSC-crystallinity values. Other published work also observed that the WAXS method tended to give a higher measured crystallinity value than that from the DSC method (30-32). The differences between crystallinity determinations obtained using the two methods are believed to be due to the different nature of the two methods. DSC-crystallinity is based on the enthalpy of fusion of polymer crystals, whereas WAXS-crystallinity is based on scattering intensity peaks. Thus, the two methods reflect aspects of the crystalline phase that are fundamentally different from each other. Therefore, differences between the DSC-crystallinity and WAXS-crystallinity values can be expected. In Figure 6.1, the crystallinity values of resins are plotted in ascending order. The linear regression confirmed (as expected) that the DSC-crystallinity and WAXS-crystallinity have similar slope values, but different intercepts. The WAXS-crystallinity has a larger intercept value (58.18%) than the DSC-crystallinity (50.61%). This result indicates that despite the differences in actual crystallinity values between the two methods, the trend in resin crystallinity is the same from both methods. This consistent trend (Figure 6.1) confirms the real crystallinity differences between the resins.

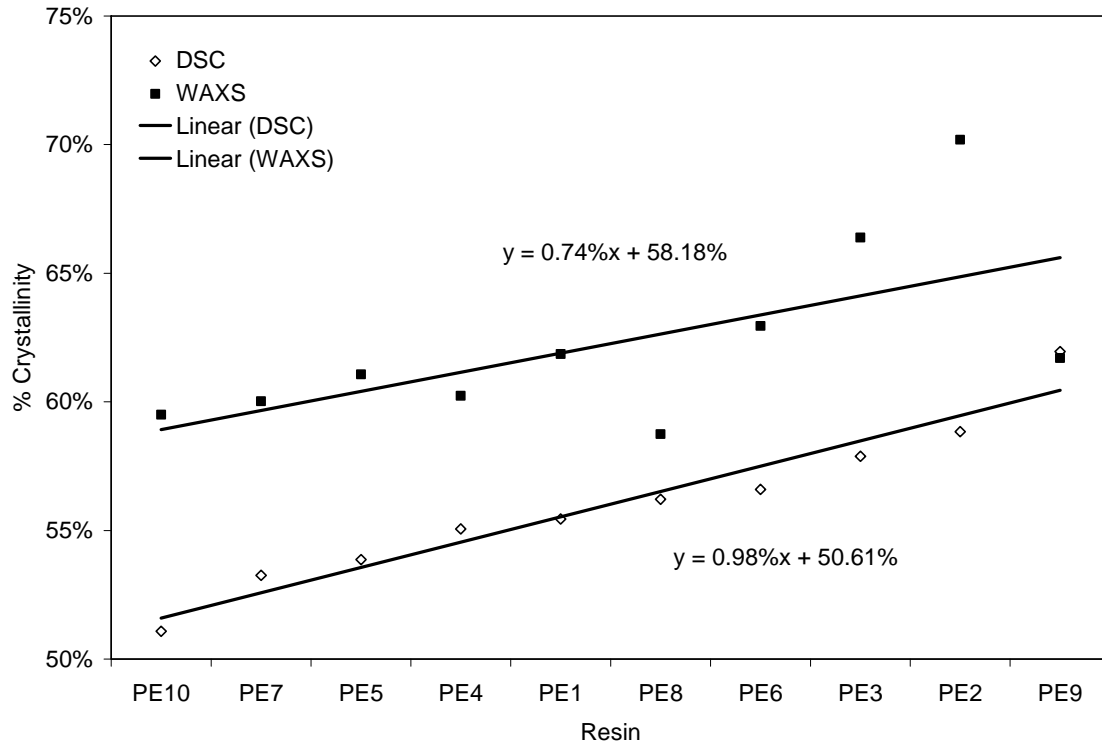


**Figure 6.1: Percentage crystallinity of resins by DSC and WAXS**

Independently replicated tests and repeats were carried out on both DSC and WAXS determinations in order to investigate further the precision of the measurements. For DSC, the average coefficient of variation (standard deviation/mean) for the measurements was 0.059, based on an average of 10 independently replicated measurements per resin, thus demonstrating the good reproducibility of the DSC measurements. For WAXS experiments, being not such a commonly used or studied technique, independent replication with selective resins started with step one, namely the molding of plates. ANOVA (ANalysis Of VAriance) technique was used to investigate different sources of variability. In Table 6.4, ANOVA of PE9 is presented. The F-observed value is smaller than the F-critical value of 7.71 according to a 5% significance level and (1,4) degrees of freedom. This means that the test procedure does not

contribute statistically significant variability to the measurements. Therefore, the WAXS measurements can be trusted to reflect material property differences.

**Table 6.4: ANOVA of WAXS measurements for PE9**

	<b>df</b>	<b>SS</b>	<b>MS</b>	<b>F</b>
Different molding of plates	1	0.00144	0.00144	6.26
Same molding of plates	4	0.00094	0.00023	
Total	5	0.00238		

### 6.3.3 Lamella Thickness Measurements

Lamella thickness (DSC and SAXS) information of resins is also presented in Table 6.3. The values of lamella thickness are within the range of reported lamella thickness values for polyethylene (9). The differences in lamella thickness values seem to follow the differences in SCB content of resins. Resins with lower SCB content (PE2 and PE3) have thicker lamellae.

Overall, the lamella thickness values obtained from DSC and SAXS are similar. This can be seen in Figure 6.2, where the ratio of the DSC-lamella thickness value to the SAXS-lamella thickness value fluctuates about 1. However, for PE2 and PE3 the DSC method gives a much higher lamella thickness value than the SAXS method (see Table 6.3). SAXS long period is a measurement of the average periodic spacing in a polymer system (33). Therefore, SAXS-lamella thickness is a measurement of the average lamella thickness of the system. On the other hand, the DSC result is based on the peak melting temperature, which is associated with the most abundant lamella thickness present in a polymer system. The SAXS-lamella thickness is analogous to the mean of a data set,

while the DSC-lamella thickness is the mode of the data set. Therefore, some difference between the most abundant lamella thickness value and the average lamella thickness value can be understood.

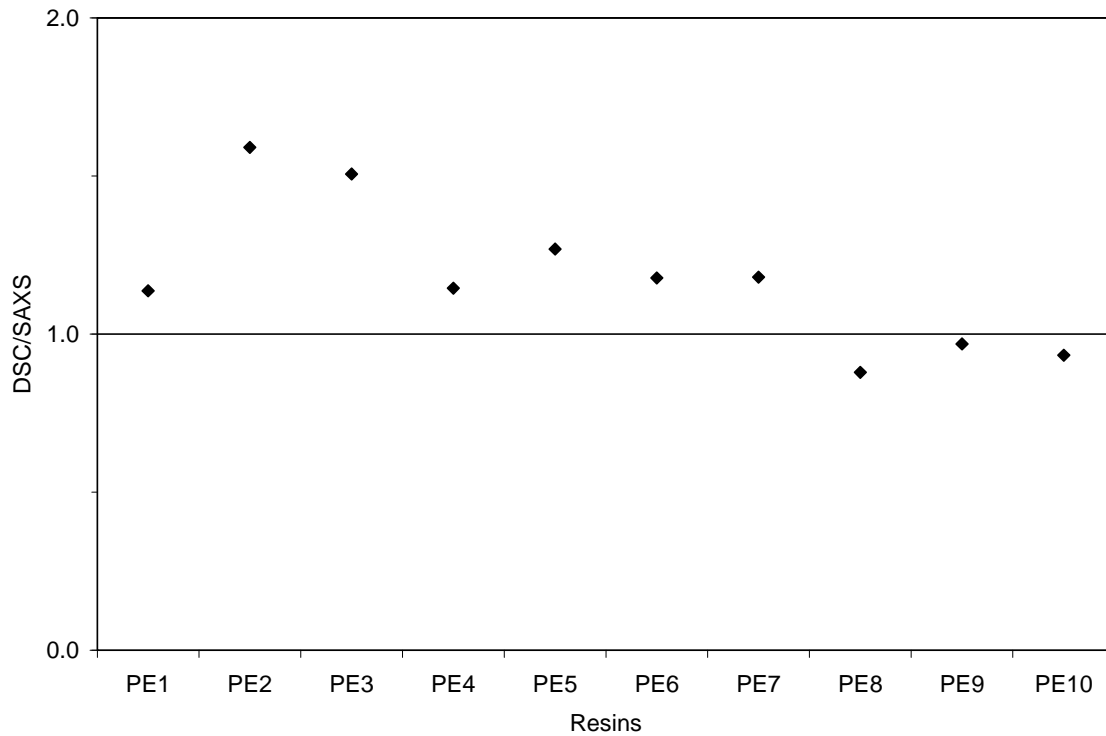


**Figure 6.2: Ratio of DSC-lamella thickness value to SAXS-lamella thickness value**

SAXS-lamella thickness values are calculated using the SAXS long period information and the percentage crystallinity of the resin (Equation 3.8). In this chapter, resin crystallinity was obtained from both the DSC and WAXS methods. SAXS-lamella thickness values presented in Table 6.3 are calculated using DSC-crystallinity. It was established in section 6.3.2 that the DSC-crystallinity and the WAXS-crystallinity showed the same trends. Therefore, regardless of which crystallinity measurement is used, the calculated SAXS-lamella thickness would show the same trend. This fact is

confirmed by Figure 6.3, where the ratio of SAXS-lamella thickness calculated based on DSC-crystallinity and WAXS-crystallinity is plotted. The ratio is about 1, thus indicating that lamella thickness values are in good agreement regardless of which crystallinity determination alternative is used. Henceforth, in the rest of the chapter, discussions regarding SAXS-lamella thickness values are based on DSC-crystallinity.

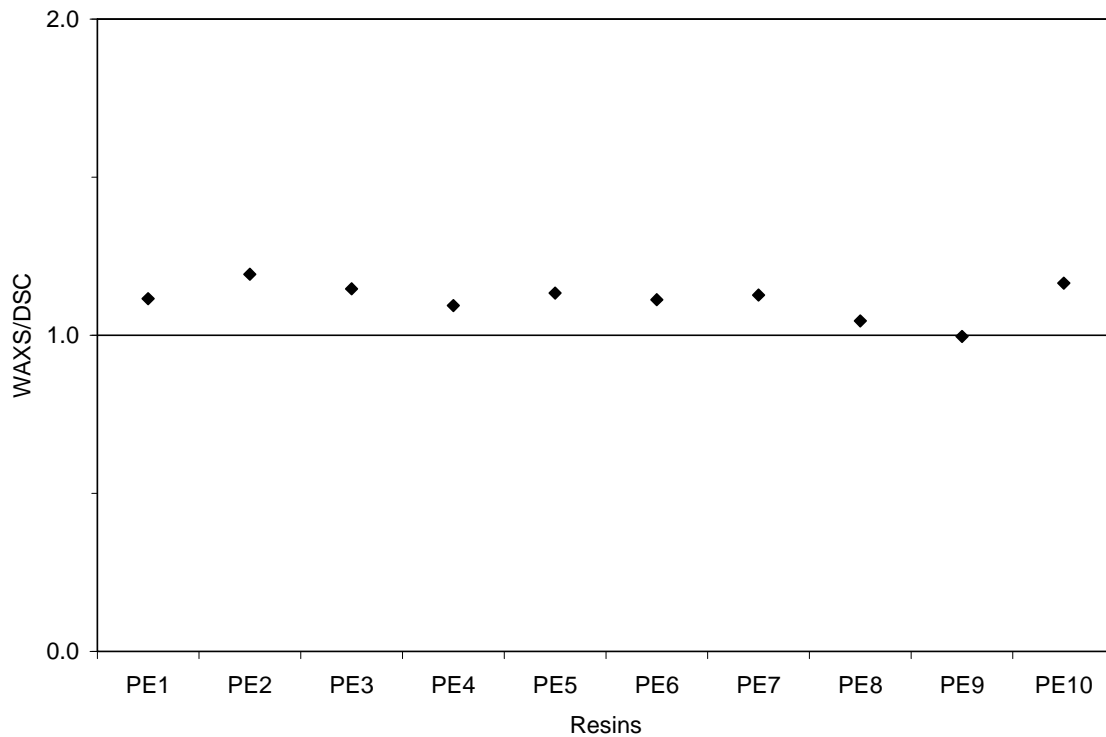


**Figure 6.3: Ratio of lamella thickness calculated using WAXS-crystallinity and DSC-crystallinity**

Lamella thickness values for PE are reported in nanometers. Therefore, the precision of these determinations is important. For DSC peak melting temperature, the average coefficient of variation is 0.009, based on an average of 10 independent replicate measurements per resin. Therefore, once again, the precision of SAXS experiments was explored using selective independently replicated tests and ANOVA. Independent

replication started again from the sample molding step. For comparative purposes, the analysis results for PE9 are presented (Table 6.5). The F-observed value in Table 6.5 is smaller than the F-critical value of 224.6 (based on a 5% significance level and (4,1) degrees of freedom), indicating again that there is no significant contribution to the measurement variability by the test procedure.

**Table 6.5: ANOVA of SAXS measurements for PE9**

	<b>df</b>	<b>SS</b>	<b>MS</b>	<b>F</b>
Same molding of plates	4	0.22803	0.05700	8.333
Different molding of plates	1	0.00684	0.00684	
Total	5	0.23487		

## **6.4 Crystalline Phase Characteristics and ESCR**

### **6.4.1 Crystallinity and ESCR**

The co-existence of crystalline and amorphous phases gives rise to the semicrystalline nature of polyethylene. Mechanical behaviour of PE is influenced by both phases. ESCR of polyethylene is believed to be mainly controlled by the amorphous phase of the material. PE resins with more inter-lamellar linkages have higher ESCR. However, the number of inter-lamellar links in the amorphous phase does not matter if their ends could not be fixed in the crystalline phase. This is a relationship of “anchors” and “ropes”. The precise number of inter-lamellar connections in the amorphous phase cannot be directly measured despite a variety of approaches that have been attempted (9, 34). Since the number of “ropes” cannot be measured, we decided to look at the nature of the “anchor”.

It is well established that an increase in crystallinity increases the tensile yield strength of polyethylene (12). Weight percentage crystallinity is the most often quoted crystalline phase measurement for polyethylene. In Figure 6.4, log ESCR is plotted against the DSC-crystallinity for all resins in this chapter. Log ESCR is used because of the large differences in ESCR values of the resins (see Table 6.2). The data points are rather scattered in Figure 6.4, indicating that no clear correlation exists between percentage crystallinity and ESCR. The lack of an established correlation pattern is most likely due to major MW differences between resins (see Table 6.2). PE crystallinity is strongly influenced by SCB content. On the other hand, ESCR of polyethylene is influenced first by MW, and only secondarily influenced by SCB content. This lack of correlation pattern when the MW range is wide may explain the inconsistent observations reported regarding crystallinity and ESCR in the literature.

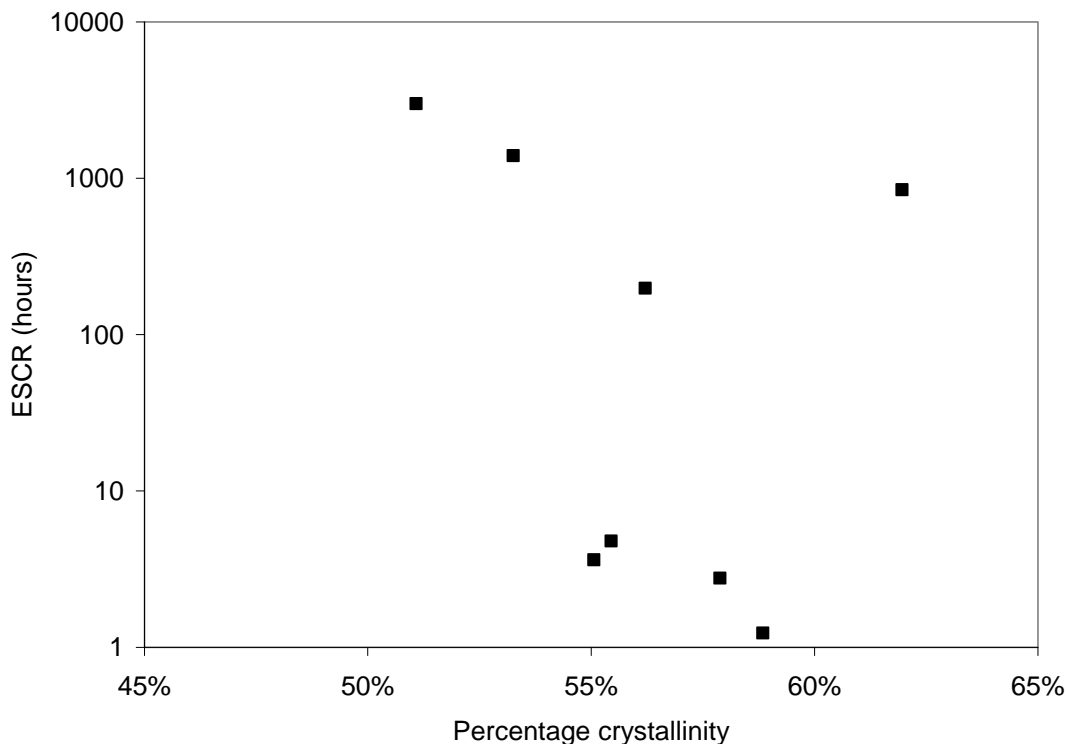


**Figure 6.4: ESCR vs. DSC-crystallinity for PE1-4 and PE7-10**

On closer inspection of the lower MW resins (PE1-4 in Table 6.2), there exists a trend of lower crystallinity (both DSC-crystallinity and WAXS-crystallinity) associated with higher ESCR (see Table 6.3). PE1 and PE4 have lower crystallinity compared to PE2 and PE3 because of higher SCB content (Table 6.2). SCB is known to disrupt lamella formation and decrease crystallinity (14). Lower crystallinity means there is a higher percentage of amorphous phase, and this higher percentage of amorphous material could lead in its turn to formation of more inter-lamellar linkages, which is known to increase ESCR (19).

For the high MW range HDPE resins in this chapter (PE7-10), the relationship between crystallinity and ESCR is more complicated. PE9 has one of the highest crystallinity

values of all resins, yet its ESCR is high (see Tables 6.1 and 6.2). It seems that when MW is high, an increase in crystallinity does not result in large reduction of chains in the amorphous phase because the chains are of sufficient length to form crystalline lamellae and amorphous links. When there is a sufficient number of inter-lamellar links, large crystals may in fact improve ESCR of the material because the crystals are stronger. This confirms observations by Lu *et al.* (10) on the annealing effect on slow crack growth of PE. It needs to be noted that this postulation only applies to polyethylene copolymers, because high MW high crystallinity PE homopolymer is known to have poor/lower ESCR (35).

#### **6.4.2 Lamella Thickness and ESCR**

Lamella thickness is another frequently used crystalline phase indicator for polyethylene. For resins in this chapter, DSC-lamella thickness and SAXS-lamella thickness values were presented in Table 6.3. Lamella thickness has been proposed to be inversely related to formation of tie-molecules (19), therefore, inversely related to ESCR of PE. For resins of similar MW (PE1-3), smaller lamella thickness values can be seen to correlate with higher ESCR values (Tables 6.1 and 6.2). PE1 has thinner lamellae and higher ESCR than PE2-3 because of its higher SCB content than the other two resins. However, when the same analysis is extended to all resins in this chapter, no significant correlation can be observed between lamella thickness and ESCR of resins. In Figure 6.5, a plot of log ESCR and SAXS-lamella thickness is presented. SAXS-lamella thickness values are used because they represent average lamella thickness as discussed in section 6.3.3. The lack of trend for the data points in Figure 6.5 indicates that when MW differences of

materials are large there is no easily established correlation between lamella thickness and ESCR of polyethylene.

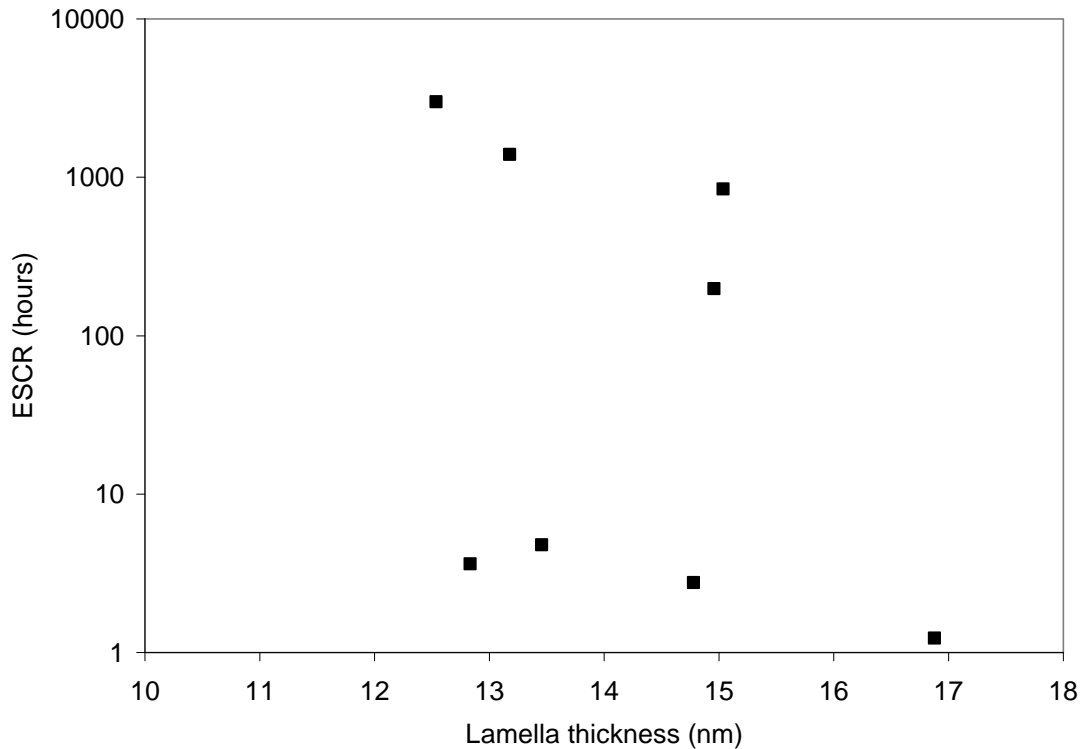
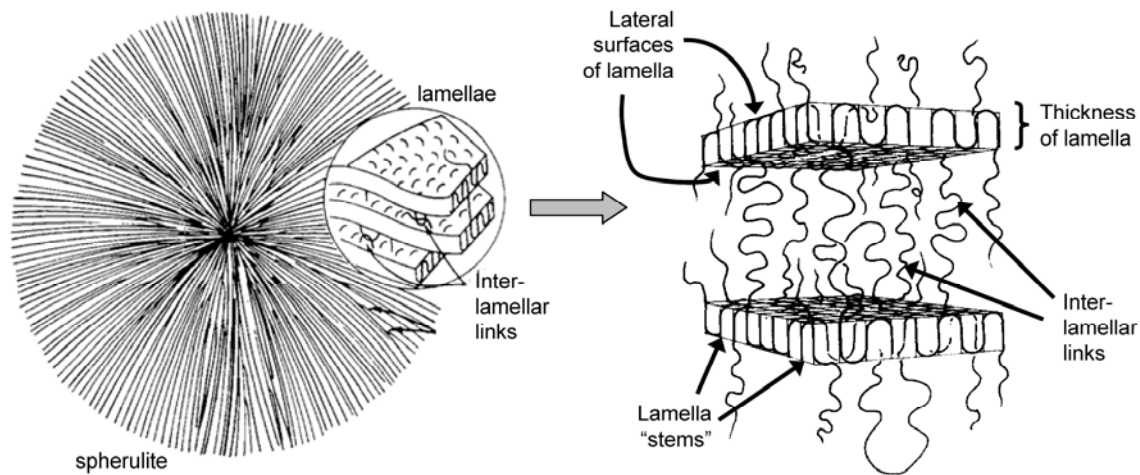


Figure 6.5: ESCR vs. SAXS-lamella thickness for PE1-4 and PE7-10

### 6.4.3 Lamellar Lateral Surface and ESCR

A tough polymer has superior brittle crack resistance. It was recently proposed that the toughness of semicrystalline polyester films depends on the interconnectivity of their crystalline and amorphous phases (36). It seems that changes in phase interconnectivity could not be adequately reflected in changes in crystallinity and lamella thickness of resins. Inter-lamellar links reside predominantly at the lateral lamella surface (37), as illustrated in Figure 6.6, therefore changes in lamella lateral surface area should reflect changes in phase interconnectivity.



**Figure 6.6: Schematic illustration of spherulite and lamella, adapted from ref. (17, 38)**

The crystalline phase of polyethylene consists of spherulites made up of flat shape lamellae (Figure 6.6), where the lateral dimensions of the crystals are much larger than their thickness. Researches have shown that inter-lamellar links form part of the lamella “stems” and protrude from the crystal surfaces more or less perpendicular to the lateral dimensions (6, 9). It has also been reported that 10% or more of lamella “stems” consist of inter-lamellar connections (9, 39). Therefore, it is reasonable to presume that PE with larger lamella lateral surface areas will have more inter-lamellar linkages and higher phase interconnectivity.

Unlike a solid catalyst, the surface area of polyethylene lamellae cannot be measured using a technique such as BET surface analysis. However, the total lateral surface area of lamellae can be calculated based on some understanding of polyethylene microstructure. Since its lateral dimensions are much larger than its thickness, a lamella can be viewed as a thin flat crystal. PE lamellae are often represented by rectangular blocks in

micromechanical simulations for mechanical response studies (40). In this chapter lamellae are also viewed as thin rectangular prisms (see Figure 6.7). For a prism of known volume, its cross-sectional area can be calculated based on its height. The same idea can be applied to rectangular lamella crystals as well. Then the total lamella lateral surface area would be equal to twice that of its cross-sectional area because a lamella has two lateral surfaces. However, inter-lamellar links extended from the lower lateral surface of one crystal are associated with links anchored in the upper lateral surface of the lamella below (see Figure 6.6). Therefore, when calculating lamella lateral surface area in relation to phase interconnectivity only one side of the lamella should be accounted for. The lamella lateral surface area per mole, henceforth referred to simply as lamella area, can be calculated from the following equation:

$$\text{lamella area [m}^2/\text{mole]} = \frac{\text{specific volume of crystal [m}^3/\text{kg]} \cdot \text{MW of crystal [kg/mole]}}{\text{lamella thickness [m]}} \quad (6.1)$$

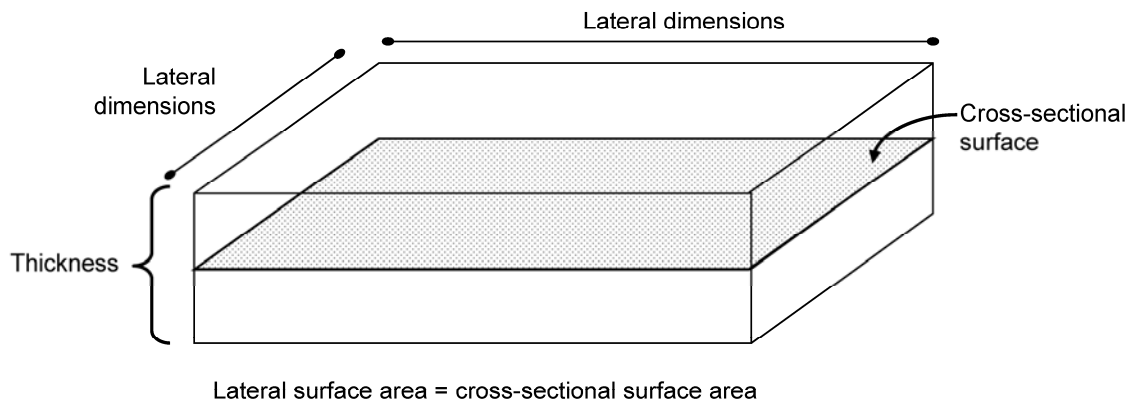


**Figure 6.7: Rectangular prism representation of lamella**

The packing of chains in the crystalline lamella is governed by the steric interaction of molecules (9). Therefore, PE crystals can be considered to be incompressible and of constant density. The lamella density is very nearly equal to the unit-cell density of a perfect polyethylene crystal, which is equal to  $1 \text{ kg/m}^3$  (41). Therefore, the specific volume of a PE crystal is  $1 \text{ m}^3/\text{kg}$ .

The lamella thickness value can be obtained from either DSC or SAXS measurements (see Table 6.3). To simplify calculations, it is assumed that there is no variation of thickness within each lamella crystal, and hence lamella thickness values can be applied to the entire crystal. As with other properties of a polymer, such as MW, there is a distribution of lamella thickness in a polymer system. In our calculations the lamella thickness distribution is assumed to be uniform because the average lamella thickness value (SAXS-lamella thickness) and most abundant lamella thickness value (DSC-lamella thickness) for resins were shown to be similar (see section 6.3.3).

The MW of a crystal for a resin is taken as its  $M_w$  (Table 6.2) multiplied by its percentage crystallinity (Table 6.3). The DSC-crystallinity and WAXS-crystallinity values have been shown to exhibit the same trends in section 6.3.2. Separate crystal-MW calculations based on these two crystallinity measurements would only be different by a scaling factor, therefore, only DSC-crystallinity values were used in subsequent calculations.

The lamella area calculated based on Equation 6.1 is an aggregate representation of the total lamella lateral surface area in a polymer system. In Table 6.6, lamella thickness

values are shown based on calculations done using SAXS-lamella thickness values and DSC-lamella thickness values. As mentioned in section 6.3.3, SAXS-lamella thickness is a measure of the average lamella thickness, while DSC-lamella thickness values represent the most abundant lamella thickness. The pipe resins (PE7-10) have larger lamella area values than non-pipe resins (PE1-6). PE10 has the largest lamella area value of all resins. In Figure 6.8, the lamella area values calculated based on SAXS-lamella thickness and DSC-lamella thickness are plotted against each other. It can be seen that lamella area values based on DSC and SAXS methods align at the  $y = x$  line, indicating that both type of thickness measurements give exactly the same trends.

**Table 6.6: Lamella area estimates of resins**

	Lamella area based on DSC-lamella thickness (m <sup>2</sup> /mole)	Lamella area based on SAXS-lamella thickness (m <sup>2</sup> /mole)
PE1	4.62E+09	5.25E+09
PE2	2.60E+09	4.13E+09
PE3	3.64E+09	5.49E+09
PE4	2.97E+09	3.41E+09
PE5	1.96E+09	2.49E+09
PE6	2.44E+09	2.87E+09
PE7	7.63E+09	9.00E+09
PE8	8.64E+09	7.59E+09
PE9	9.27E+09	8.98E+09
PE10	1.38E+10	1.29E+10

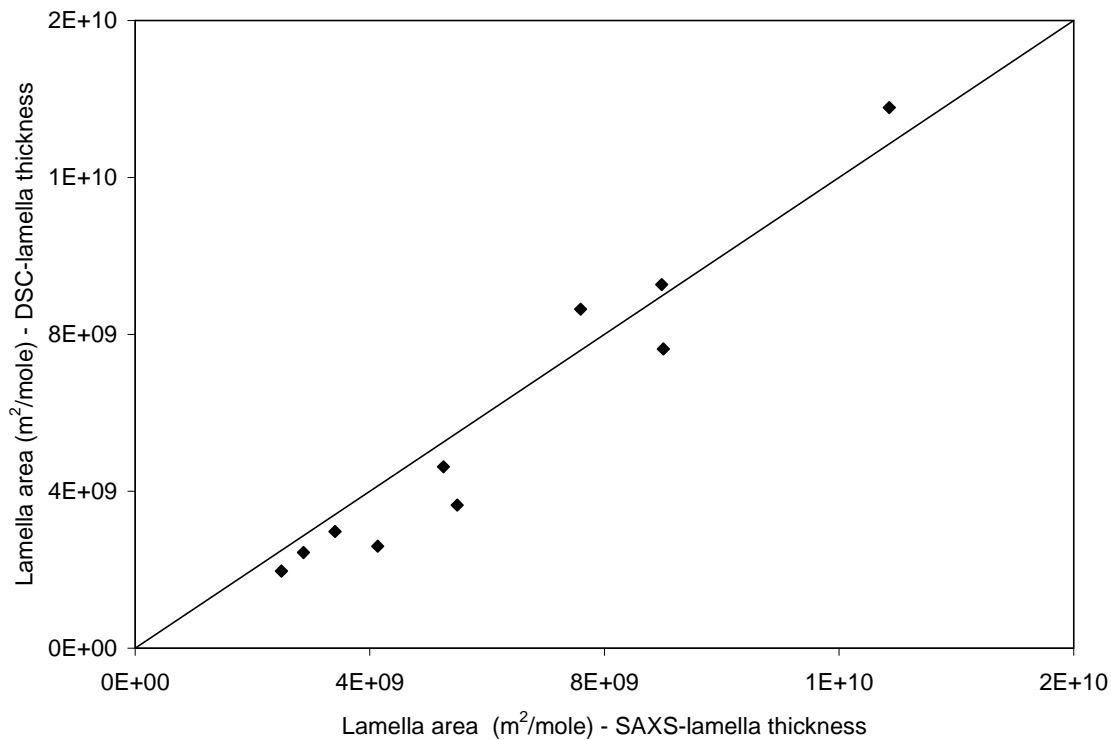


**Figure 6.8: Lamella area estimates based on SAXS-lamella thickness and DSC-lamella thickness measurements**

The lamella area estimate is affected by the lamella thickness value, and hence strongly influenced by the SCB content of the resin. In Figure 6.9, lamella thickness and lamella area are plotted together as a function of changes in SCB/1000 carbon atoms for PE1-3. PE1-3 are used to illustrate this point because they have similar MW, consequently the effect of SCB can be seen with minimum influence from MW differences. Among the three resins, as the SCB content of the resins increases (Figure 6.9), lamella thickness values decrease while lamella area values increase.

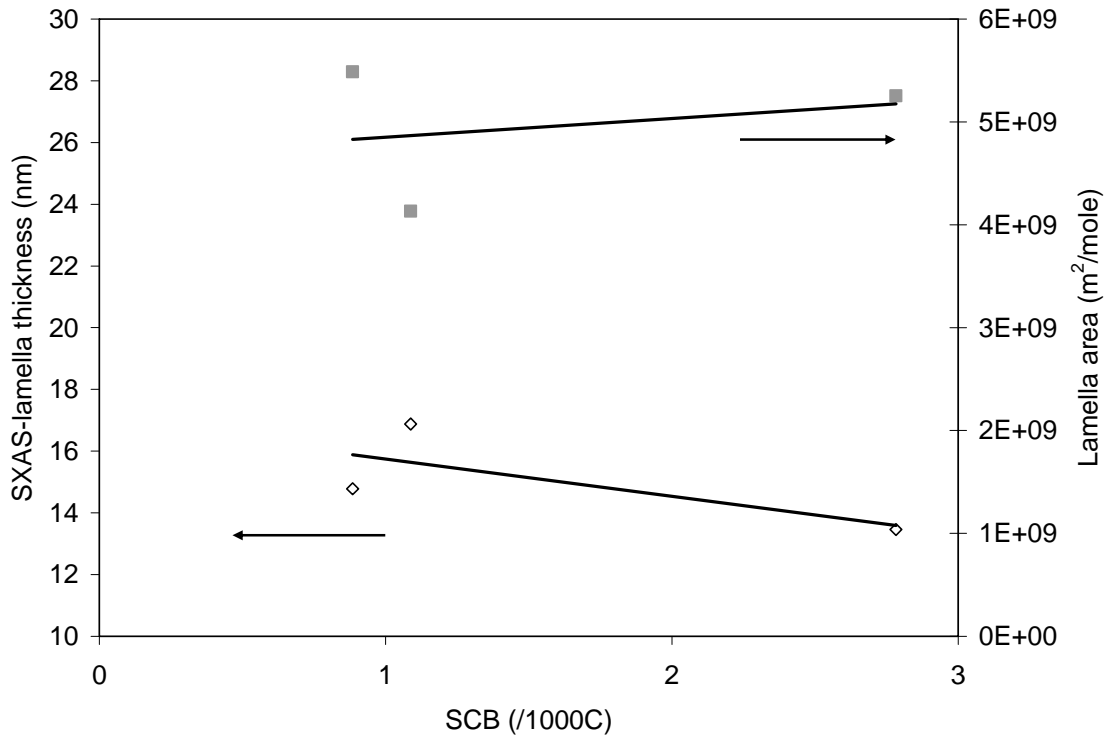


**Figure 6.9: SCB influence on lamella thickness and lamella area for PE1-3**

In earlier sections, plots between crystallinity, lamella thickness and ESCR did not show any meaningful correlations. Resins, such as PE1 and PE7 that have similar SAXS-lamella thickness values, have significantly different ESCR values (see Tables 6.1 and 6.2). In Figure 6.10, log ESCR is plotted against the lamella area of resins (based on SAXS-lamella thickness values). The graph shows an increasing ESCR with increasing lamella area values, thus verifying the postulation that larger lamella area means a higher probability for occurrence of inter-lamellar linkages, which eventually improves ESCR. By taking into account both MW and SCB influences on the crystalline phase, lamella area values more accurately reflect changes in phase interconnectivity, thus offering a better correlation to ESCR of the resins than simply crystallinity or lamella thickness values.

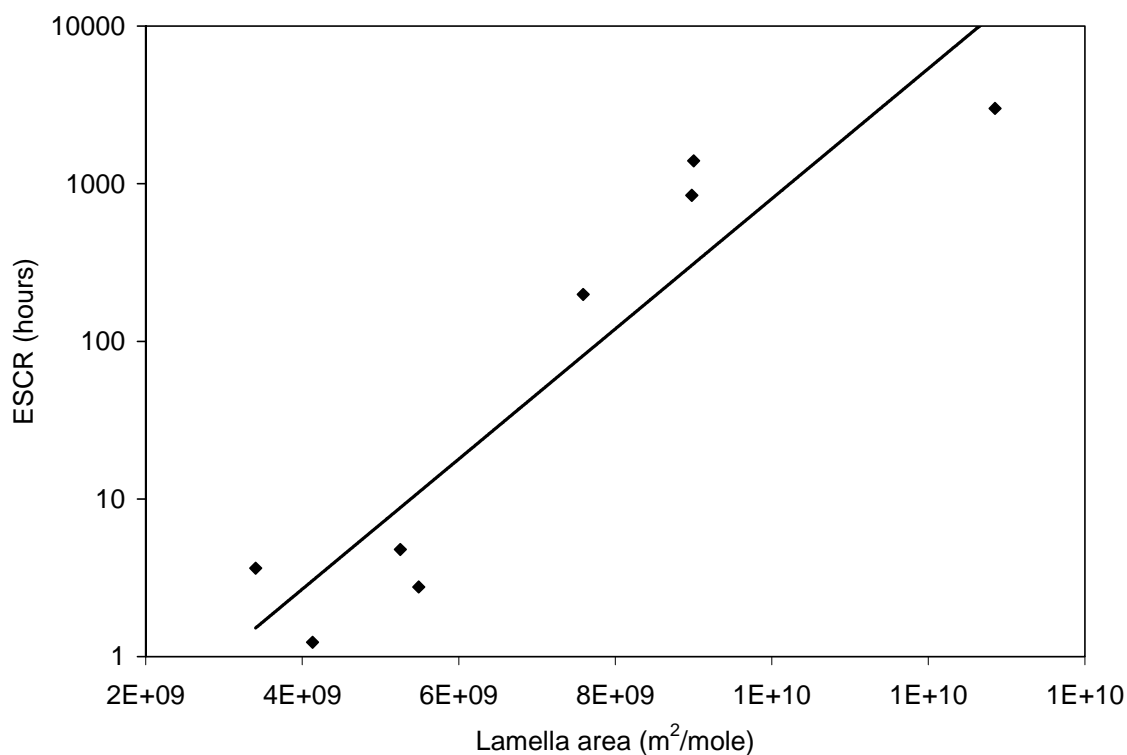


**Figure 6.10: ESCR vs. lamella area of resins based on SAXS-lamella thickness values**

## 6.5 Concluding Remarks

A large body of research exists on crystalline phase influences on ductile deformation behaviour of polyethylene. For brittle fracture behaviour, the effect of crystallinity on ESCR of polyethylene has remained unclear. It is generally accepted that an increase in the number of inter-lamellar linkages in the amorphous phase would result in decreases in PE crystallinity. Therefore, PE with high ESCR should have low crystallinity. In this chapter, behaviour of resins with similar MW (PE1-3) confirmed this observation. However, correlations between crystallinity and ESCR over resins of different MW showed no meaningful results. Resins with very different ESCR values, such as PE4 and

PE8, can have similar crystallinity values. Based on the resins in this chapter, we conclude that when MW differences are large, overall crystallinity cannot be correlated to ESCR of PE. Attempts to correlate lamella thickness to ESCR showed a similarly ambiguous relationship as that between crystallinity and ESCR.

Inter-lamellar links, which are critical to ESCR of PE, must “anchor” in lamellae as the term suggests. Theorization on the ESCR behaviour from the point of interconnectivity between crystalline and amorphous phases leads to the study of the relationship between lamella lateral surface area and ESCR. Unlike crystallinity and lamella thickness that predominantly show SCB effects, lamella area calculations take into account both SCB and MW influences. Our work showed that increasing ESCR is associated with an increasing lamella lateral surface area of PE. Larger lamella lateral surface area increases the probability of inter-lamellar linkage formations, which leads to improved phase interconnectivity and hence higher ESCR for polyethylene.

## 6.6 References

1. Brostow, W. and Corneliussen, R. D. (1986), *Failure of Plastics*, Hanser Publishers, New York.
2. Ward, I. M. (1971), *Mechanical Properties of Solid Polymers*, Wiley-Interscience, Toronto.
3. Keith, H. D. & Padden, F. J. (1959), "The Optical Behavior of Spherulites in Crystalline Polymers .1. Calculation of Theoretical Extinction Patterns in Spherulites with Twisting Crystalline Orientation", *Journal of Polymer Science*, vol. 39, no. 135, pp. 101-122.
4. Keith, H. D. & Padden, F. J. (1959), "The Optical Behavior of Spherulites in Crystalline Polymers .2. the Growth and Structure of the Spherulites", *Journal of Polymer Science*, vol. 39, no. 135, pp. 123-138.
5. Keller, A. (1959), "Investigations on banded spherulites", *Journal of Polymer Science*, vol. 39, pp. 151-173.
6. Keller, A. (1957), "A Note on Single Crystals in Polymers - Evidence for A Folded Chain Configuration", *Philosophical Magazine*, vol. 2, no. 21, pp. 1171-1175.
7. Fischer, E. W. (1957), "Step and spiral crystal growth of high polymers", *Zeitschrift fuer Naturforschung*, vol. 12a, pp. 753-754.
8. Till, P. H. (1957), "The Growth of Single Crystals of Linear Polyethylene", *Journal of Polymer Science*, vol. 24, no. 106, pp. 301-306.
9. Lin, L. & Argon, A. S. (1994), "Structure and plastic deformation of polyethylene", *Journal of Materials Science*, vol. 29, pp. 294-323.
10. Lu, X., Qian, R., Mcghe, A. R., & Brown, N. (1992), "The Effect of Annealing on Slow Crack-Growth in An Ethylene-Hexene Copolymer", *Journal of Polymer Science, Part B: Polymer Physics*, vol. 30, no. 8, pp. 899-906.
11. Stadler, F. J., Kaschta, J., & Muenstedt, H. (2005), "Dynamic-mechanical behavior of polyethylenes and ethene-/alpha-olefin-co-polymers. Part I. alpha '-relaxation", *Polymer*, vol. 46, no. 23, pp. 10311-10320.
12. Lu, X., Qian, R., & Brown, N. (1995), "The Effect of Crystallinity on Fracture and Yielding of Polyethylenes", *Polymer*, vol. 36, no. 22, pp. 4239-4244.
13. Capaccio, G. & Ward, I. M. (1981), "Structural studies of ultrahigh-modulus linear polyethylene using nitric acid etching and gel permeation chromatography. I Determination of the crystal size distribution", *Journal of Polymer Science, Part B: Polymer Physics*, vol. 19, pp. 667-675.

14. Hosoda, S., Nomura, H., Gotoh, Y., & Kihara, H. (1990), "Degree of branch inclusion into the lamellar crystal for various ethylene/ $\alpha$ -olefin copolymers", *Polymer*, vol. 31, pp. 1999-2005.
15. Bodor, G., Dalcolmo, H. J., & Schroeter, O. (2008), "Structural and property correlations of ethylene- $\alpha$ -olefin copolymers", *Colloid and Polymer Science*, vol. 267, no. 6, pp. 480-493.
16. Sindelar, P., Nezbedova, E., Simkova, P., Buran, Z., & Bohaty, P. (2005), "Effect of structural parameters on rapid crack propagation and slow crack growth in high density polyethylene pipeline materials", *Plastics, Rubber and Composites*, vol. 34, no. 7, pp. 329-333.
17. Lustiger, A. & Markham, R. L. (1983), "Importance of tie molecules in preventing polyethylene fracture under long-term loading conditions", *Polymer*, vol. 24, pp. 1647-1654.
18. Ferry, J. D. (1980), *Viscoelastic Properties of Polymers*, 3 edn, Wiley, New York.
19. Huang, Y. & Brown, N. (1988), "The effect of molecular weight on slow crack growth in linear polyethylene homopolymers", *Journal of Materials Science*, vol. 23, pp. 3648-3655.
20. Yeh, J. T. & Runt, J. (1991), "Fatigue crack propagation in high-density polyethylene", *Journal of Polymer Science, Part B: Polymer Physics*, vol. 29, pp. 371-388.
21. Brown, N., Lu, X., Huang, Y., Harrison, I. P., & Ishikawa, N. (1992), "The Fundamental Material Parameters That Govern Slow Crack-Growth in Linear Polyethylenes", *Plastics Rubber and Composites Processing and Applications*, vol. 17, no. 4, pp. 255-258.
22. Janimak, J. J. & Stevens, G. C. (2001), "Inter-relationships between tie-molecule concentration, molecular characteristics and mechanical properties in metallocene catalysed medium density polyethylenes", *Journal of Materials Science*, vol. 36, no. 8, pp. 1879-1884.
23. Huang, Y. & Brown, N. (1990), "The dependence of butyl branch density on slow crack growth in polyethylene: kinetics", *Journal of Polymer Science, Part B: Polymer Physics*, vol. 28, pp. 2007-2021.
24. Yeh, J. T., Chen, J.-H., & Hong, H.-S. (1994), "Environmental stress cracking behavior of short-chain branch polyethylenes in Igepal solution under a constant load", *Journal of Applied Polymer Science*, vol. 54, no. 13, pp. 2171-2186.
25. Hittmair, P. & Ullman, R. (1962), "Environmental stress cracking of polyethylene", *Journal of Applied Polymer Science*, vol. 6, no. 19, pp. 1-14.

26. Huang, Y.-L. & Brown, N. (1991), "Dependence of slow crack growth in polyethylene on butyl branch density: morphology and theory", *Journal of Polymer Science, Part B: Polymer Physics*, vol. 29, pp. 129-137.
27. Munaro, M. & Akcelrud, L. (2008), "Polyethylene blends: a correlation study between morphology and environmental resistance", *Polymer Degradation and Stability*, vol. 93, pp. 43-49.
28. Zhou, Z., Lu, X., & Brown, N. (1993), "The effect of blending high-density and linear low-density polyethylenes on slow crack growth", *Polymer*, vol. 34, no. 12, pp. 2520-2523.
29. Yeh, J. T. & Hong, H. S. (1994), "Effect of branch frequency on dynamic fatigue behaviour of slowly notched polyethylene polymers", *Journal of Polymer Research*, vol. 1, no. 4, pp. 375-383.
30. Simanke, A. G., Galland, G. B., Neto, R. B., Quijada, R., & Mauler, R. S. (1999), "Influence of the type and the comonomer contents on the mechanical behavior of ethylene/alpha-olefin copolymers", *Journal of Applied Polymer Science*, vol. 74, no. 5, pp. 1194-1200.
31. Cramez, M. C., Oliveira, M. J., Fakirov, S., Crawford, R. J., Apostolov, A. A., & Krumova, M. (2001), "Rotationally molded polyethylene: Structural characterization by x-ray and microhardness measurements", *Advances in Polymer Technology*, vol. 20, no. 2, pp. 116-124.
32. Manzur, A. (2008), "Strain rate effect on crystallinity variations in the double yield region of polyethylene", *Journal of Applied Polymer Science*, vol. 108, no. 3, pp. 1574-1581.
33. Kakudo, M. & Kasai, N. (1972), *X-ray Diffraction by Polymers*, Kodansha LTD. and Elsevier Publishing Company, Tokyo, Amsterdam, New York.
34. Seguela, R. (2005), "Critical review of the molecular topology of semicrystalline polymers: the origin and assessment of intercrystalline tie molecules and chain entanglements", *Journal of Polymer Science, Part B: Polymer Physics*, vol. 43, no. 14, pp. 1729-1748.
35. Men, Y. F., Rieger, J., Enderle, H.-F., & Lilge, D. (2004), "The mobility of the amorphous phase in polyethylene as a determining factor for slow crack growth", *European Physical Journal E: Soft Matter*, vol. 15, no. 4, pp. 421-425.
36. Rao, Y., Greener, J., Avila-Orta, C. A., Hsiao, B. S., & Blanton, T. N. (2008), "The relationship between microstructure and toughness of biaxially oriented semicrystalline polyester films", *Polymer*, vol. 49, pp. 2507-2514.
37. Keller, A. (1969), "Solution grown polymer crystals. A survey of some problematic issues", *Colloid and Polymer Science*, vol. 231, no. 1-2, pp. 386-421.

38. Hoffman, J. D., Davis, G. T., & Lauritzen, J. I. Hannay, N. B.(1976), *Treatise on Solid State Chemistry*, Plenum, New York.
39. Bassett, D. C. (2007), "The essential novelty brought to crystallization by molecular length", *Polymer*, vol. 48, pp. 3384-3387.
40. Alvarado-Contreras, J. A. (2007), *Micromechanical Modelling of Polyethylene*, Phd Thesis, Department of Civil Engineering, University of Waterloo, Waterloo, Ontario, Canada.
41. van Krevelen, D. W. (1990), *Properties of Polymers*, 3 edn, Elsevier Scientific Publishing Company, New York.

## **CHAPTER 7 LIFETIME PREDICTION BASED ON SHORT-TERM ESCR TEST FOR POLYETHYLENE**

### **7.1 Introduction**

Environmental stress cracking (ESC) has been a well observed mechanical phenomenon in polyethylene (PE). The bent strip test, the notched constant load (NCLT) and even the strain hardening test developed in this work (see Chapter 4) all represent attempts at ranking environmental stress cracking resistance (ESCR) of the polymeric material. One can qualitatively state that a particular polymer resin may have “better” (higher) ESCR than another resin based on relatively short-term tests, such as the NCLT, but currently there is no method available for quantitatively predicting the long-term ESC behaviour of polyethylene based on short-term tests results.

Environmental stress cracking is a type of slow crack growth (SCG). The rate of SCG in a polymer is determined by the growth rate of the initial damage through the entire material. The initial damage could be an imperfection on the polymer surface from processing or an intentionally introduced notch. Craze is formed at the tip of the damage as a result of stress concentration; it consists of stretched polymer fibrils and voids (see Figure 7.1a) (1). For polyethylene under tensile stress (Figure 7.1b), disentanglements of inter-lamellar linkages at the base of the craze lead to growth of the crack. As the crack opens, the tip of the craze grows and the cycle continues, ultimately leading to failure of the polymer (1-3). The presence of Igepal (surfactant) solution accelerates the SCG/ESC

process by lubricating chain disentanglements, hence SCG of polyethylene in Igepal is faster as compared to that in air (4-6).

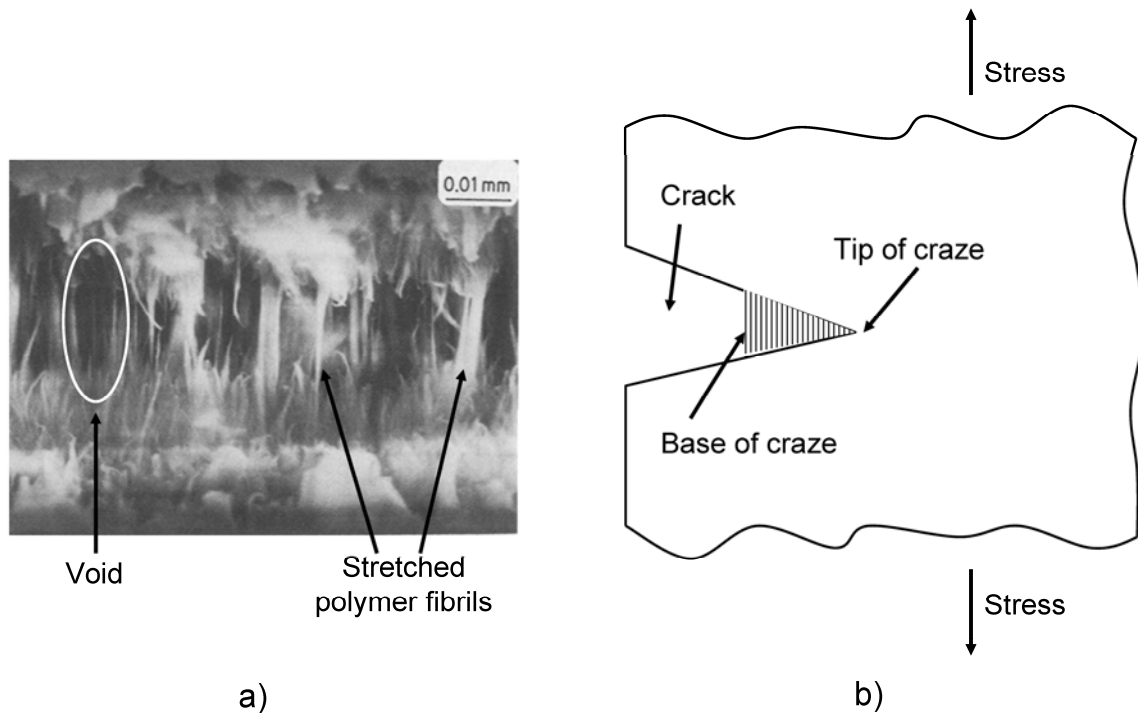


**Figure 7.1: a) SEM view of craze, ref. (1), b) schematic illustration of crack and craze in polymer under tension.**

The slow crack growth resistance (SCGR) of a polymer material is measured by the PENT test (ASTM F1473). The PENT test method is similar to the NCLT for ESCR of polymer. In both cases a tensile static load is applied to a notched polymer sample until it breaks. The main difference is that the PENT test is carried out in air, while NCLT is run in solution of the surfactant Igepal. Similar to ESCR of polymer as measured by the NCLT method, the PENT test evaluates SCGR of polymer according to how quickly the test sample fails; the shorter the failure time, the less the SCGR of the material. Under ambient conditions slow crack growth can take a long time. Research has shown that as

the stress and temperature increases, the rate of SCG increases as well (4, 7, 8). In order to obtain results quickly, the PENT test accelerates the SCG process of samples by testing at elevated temperature. Tests on polyethylene are usually carried out at 80°C.

Recently, Brown (9) proposed a method for quantitative prediction of the long-term failure time of polyethylene undergoing slow crack growth. He theorized that the time to failure by slow crack growth is a function of five variables, the stress (S), the temperature (T), the size of the initial damage (*a*), the geometry correction factor for the shape of damage (Y) (10), and the material resistance (R'). The slow crack growth failure time of the polymer is described by a semi-empirical model, Equation 7.1, which is developed based on experimental observations (1, 7-9, 11-14). In this equation, R is the universal gas constant, while Q is the crack activation energy, constant for a specific polymer. For the crack activation energy of polyethylene Brown (9) suggested using Q = 90 kJ/mole.

$$t = R' (Y S a^{1/2})^{-n} \exp \left[ \frac{Q}{RT} \right] \quad (7.1)$$

In order to predict the ultimate lifetime of a polyethylene material under SCG, Brown (9) suggested to first obtain a sample of the PE material in question and measure its SCG failure time by the PENT test. Under the experimental conditions of the PENT test, the stress (S), temperature (T), damage size or notch depth (*a*) and the geometry correction factor (Y) are all known, and therefore, the material resistance (R') can be calculated using Equation 7.1. Once the material resistance is known from the PENT test, it is then applied to the original polyethylene material. Depending on the shape and application of

the PE material, the remaining variables can be determined from other measurements, and thus the ultimate lifetime of the PE can subsequently be estimated (or, rather, speculated) using Equation 7.1. The key feature in this approach is the assumption that the material resistance as measured by the short-term PENT test is consistent and can be applied to long-term behaviour of polyethylene. The approach has been applied by Brown (9), who estimated that pipe resin that has exhibited a 1-hour PENT test failure time would have a 13-year SCG lifetime. Of course, since this was done in 2007, it still remains an unverified speculation.

Bearing in mind that polymer environmental stress cracking is related to slow crack growth, we herein attempt to develop a predictive model for estimating long-term environmental stress cracking failure time of polyethylene using a model analogous to the SCG model described by Equation 7.1. This ESCR lifetime model would be the first of its kind. Thus, there are several objectives for the work in this chapter. The first is to establish model parameters based on ESCR experiments. The second objective is to investigate the major factors of influence on the model (and hence, model predictions). Lastly, work is carried out to investigate the possible duality between activation energy ( $Q$ ) of environmental stress cracking growth and the  $\alpha$ -relaxation energy of polyethylene, speculated in earlier research (9, 12).

## 7.2 Experimental Methods

Table 7.1 contains the list of experimental methods used for determining material properties of interest for Chapter 7, as done previously for other chapters, referring back to Chapter 3.

**Table 7.1: List of experimental methods for Chapter 7**

<b>Method</b>	<b>Property Determined</b>	<b>Chapter 3 section #</b>
DSC	Crystallinity and lamella thickness	3.1.1
GPC	Molecular weight and molecular weight distribution	3.1.3
<sup>13</sup> C NMR	Short chain branch content	3.1.4
DMA	$\alpha$ -relaxation behaviour	3.2.2
NCLT	ESCR values	3.3.2

## 7.3 Environmental Stress Cracking Model

The main difference between ESC and SCG is the presence of the aggressive environment that accelerates the crack growth process. The rate of environmental stress cracking is affected by the concentration of the environmental agent (oil or soap, as in Igepal solutions). Research has shown that environmental stress cracking of a polymer becomes faster as the Igepal concentration increases from 0% to 10% by volume (15). When exposed to the same environmental conditions (i.e, the same concentration Igepal solution), the rate of ESC for polyethylene would be affected mainly by the applied stress, the size of the initial damage and temperature; effectively, the same factors influencing SCG of polyethylene. Therefore, for ESC under the same environmental conditions a model analogous to Equation 7.1 can be used for estimating environmental stress cracking failure time (t) of polyethylene.

The ESC model has the following form:

$$t = C(YSa^{1/2})^{-n} \exp\left[\frac{Q}{RT}\right] \quad (7.2)$$

In Equation 7.2,  $t$  is the time of ESC failure;  $Y$  is the geometry correction factor of the test sample (10);  $S$  is the applied stress;  $a$  is the size of the initial damage, which is the size of the initial notch in NCLT;  $T$  is temperature in degrees Kelvin; and  $R$  is the universal gas constant.  $C$ ,  $n$  and  $Q$  are material constants.  $C$  is material resistance to environmental stress cracking;  $n$  is a unitless constant empirically observed; and lastly,  $Q$  is the activation energy of crack growth.

In fracture mechanics (10), the stress intensity factor ( $K$ ) is defined as a function of the geometry correction factor, the applied stress and size of the damage (Equation 7.3). The substitution of the stress intensity factor into Equation 7.2 simplifies the ESC model to the form of Equation 7.4.

$$K = YSa^{1/2} \quad (7.3)$$

$$t = CK^{-n} \exp\left[\frac{Q}{RT}\right] \quad (7.4)$$

The Arrhenius form of Equation 7.4 allows for the calculation of ESC failure time at different temperatures. This is very handy because material constants obtained in NCLT tests run at 50°C can then be applied to polyethylene samples operating at room-temperature conditions, which is the normal operating temperature of most polyethylene

materials. This application is based on an important assumption that material parameters (C, n and Q) do not vary with temperature. For smaller temperature differences that do not cross polymer transition temperatures the assumption of material “constants” (parameters) being independent of temperature should hold true. Lu and Brown (7) made a similar assumption in their work on SCG of polyethylene. In addition, polyethylene is not known to exhibit any major morphological changes between ambient temperature and 50°C (16), therefore, material constants measured at 50°C should be able to be applicable to polyethylene at typical operating temperatures.

## **7.4 ESC Model Analysis**

Steps will be carried out first to estimate model parameters based on NCLT results. The material resistance to ESC will then be determined and related to molecular properties of polyethylene. In order to estimate model parameters, multiple NCLT experiments at different temperatures and stress levels are needed. The NCLT test is a time consuming ESCR method. PE1-4 and PE8 (see Table 7.2) have relatively short NCLT times, so they were chosen for the first attempt at developing the ESC model. The high ESCR resins, PE7 and PE9-10, were reserved for verifying the model. NCLT experiments followed the procedures outlined earlier in Chapter 3.

### **7.4.1 Resin Characteristics**

Table 7.2 contains experimentally determined data on ESCR and other material properties.  $M_n$  stands for number-average molecular weight,  $M_w$  is weight-average molecular weight and  $M_z$  is z-average molecular weight. PDI is the polydispersity index

( $M_w/M_n$ ). Short chain branching (SCB) content is expressed in terms of number of short chain branches per thousand carbon atoms (determined by  $^{13}\text{C}$  NMR). The percentage crystallinity and lamella thickness of resins obtained from DSC analysis are also presented in Table 7.2. Procedures and methods for obtaining the data have already been presented in detail in Chapters 2-6. The information is summarized again in Table 7.2 in order to give some background information on the resins and to facilitate subsequent discussion.

**Table 7.2: Resin characteristics**

Resin	ESCR (hours)	Crystallinity %	Lamella thickness (nm)	$M_n$ (kg/mol)	$M_w$ (kg/mol)	$M_z$ (kg/mol)	PDI	SCB (/1000C)
PE1	4.8	55.4%	15.3	16.3	127.5	814.0	7.8	2.8
PE2	1.2	58.8%	26.8	15.7	118.5	837.1	7.6	1.1
PE3	2.8	57.9%	22.3	17.9	140.1	889.8	7.8	0.9
PE4	3.6	55.1%	14.7	19.7	79.4	239.3	4.0	3.8
PE5	N/A	53.9%	13.6	11.4	49.7	157.8	4.4	7.0
PE6	N/A	56.6%	14.4	14.0	62.0	195.0	4.4	4.7
PE7	1396	53.3%	15.5	11.8	222.8	1593.5	18.9	4.3
PE8	198	56.2%	13.1	14.0	202.1	1398.4	14.4	4.5
PE9	843	61.5%	14.6	10.4	217.9	1244.2	20.9	7.0
PE10	>3000	51.1%	11.7	5.9	315.4	2129.3	53.3	11.8

#### 7.4.2 Geometry Correction Factor - Y

The NCLT is a tensile creep rupture test using single sided notched dogbones. In fracture mechanics NCLT (standard) specimens are classified under tensile single-sided notch geometry, and the geometry correction factor (Y) is given by Equation 7.5 (10). In this equation,  $a$  is the notch depth and  $D$  is the sample thickness. For example, a specimen with an  $a/D$  ratio of 0.4 (40% notch depth) has a Y value of 3.73 as based on Equation 7.5.

$$Y = 1.99 - 0.410 * \left(\frac{a}{D}\right) + 18.70 * \left(\frac{a}{D}\right)^2 - 38.48 * \left(\frac{a}{D}\right)^3 + 53.85 * \left(\frac{a}{D}\right)^4 \quad (7.5)$$

### 7.4.3 Determination of n

The n constant (parameter) for a specific resin can be calculated based on NCLT results at the same temperature and different stress levels. For the same resin at two different applied stress levels, the stress intensity factors are  $K_1$  and  $K_2$ , and correspondingly the final failure times are  $t_1$  and  $t_2$ . The exponential term in the ESC model (Equation 7.4) would remain the same when the test temperature does not change because the crack activation energy is a material constant and R is the universal gas constant. Therefore, and since C is considered a material constant, when  $t_1$  is divided by  $t_2$ , the exponential terms and C values cancel each other and the result is Equation 7.6. The n constant can then be calculated by a simple logarithmic transformation of both sides of the equation.

$$\frac{t_1}{t_2} = \left(\frac{K_1}{K_2}\right)^{-n} \quad (7.6)$$

For PE1-4 and PE8 NCLT experiments carried out at 50°C, stress levels and corresponding failure times are shown in Table 7.3, along with the calculated n constant for the resins. In the literature, the slow crack growth n constants range from 2.5-4.8 (9), with n = 3 being the most frequently reported/used value. In this study the n constant for ESC is in the range of 1.97 – 5.12 with a mean value of 3.12. For ductile failure the

failure time ( $t$ ) is proportional to stress to the power of  $-25$  ( $n=25$ ), whereas in brittle failure  $t$  is proportional to stress to the power of  $-3$  ( $n=3$ ) (9). The value of ESC  $n$  constant confirms that environmental stress cracking is a type of brittle failure.

The ESC  $n$  constant value range is similar to the SCG  $n$  constant value range reported. Since slow crack growth and environmental stress cracking are related mechanical phenomena, the similarities in  $n$  value are understandable. The similarity in  $n$  values also points out that the  $n$  constant is likely not affected by the test environment; the experiments in Igepal solution did not significantly alter the  $n$  constant values compared to these obtained from SCG experiments in air. The slightly broader ESC  $n$  constant range can be contributed to the large variability of NCLT results, as discussed in Chapter 4.

**Table 7.3: NCLT stress level, ESCR time, and  $n$  constant of PE1-4 and PE8**

	Stress 1 (MPa)	Stress 2 (MPa)	Time 1 (hours)	Time 2 (hours)	$n$
PE1	6.91	4.05	1.6	4.8	2.06
PE2	6.4	4.8	0.7	1.2	1.97
PE3	6.2	4.65	1.2	2.8	2.90
PE4	4.66	3.51	1.3	3.6	3.54
PE8	4.5	3.3	198.0	968.0	5.12

#### 7.4.4 Crack Activation Energy

For NCLT experiments run at different temperatures ( $T_1$  and  $T_R$ ) using the same applied stress (hence, the same  $K$  value), failure times  $t_1$  and  $t_R$  are obtained. The division of  $t_1$  by  $t_R$ , both in the form of Equation 7.4, cancels out constant terms such as the material resistance ( $C$ ) and the stress intensity factor ( $K$ ). By taking natural logs of both sides of

the ratio ( $t_1/t_R$ ) based on Equation 7.4, Equation 7.7 is obtained. In Figure 7.2, the natural log of the failure time ratio is plotted against the inverse of test temperature for PE1 and PE4. The graph shows a linear relationship between  $\ln(t_1/t_R)$  and  $1/T$ , therefore, the crack activation energy (Q) can be calculated based on the slope of the line and Equation 7.7.

$$\ln\left(\frac{t_1}{t_R}\right) = \frac{Q}{R}\left(\frac{1}{T_1} - \frac{1}{T_R}\right) \quad (7.7)$$

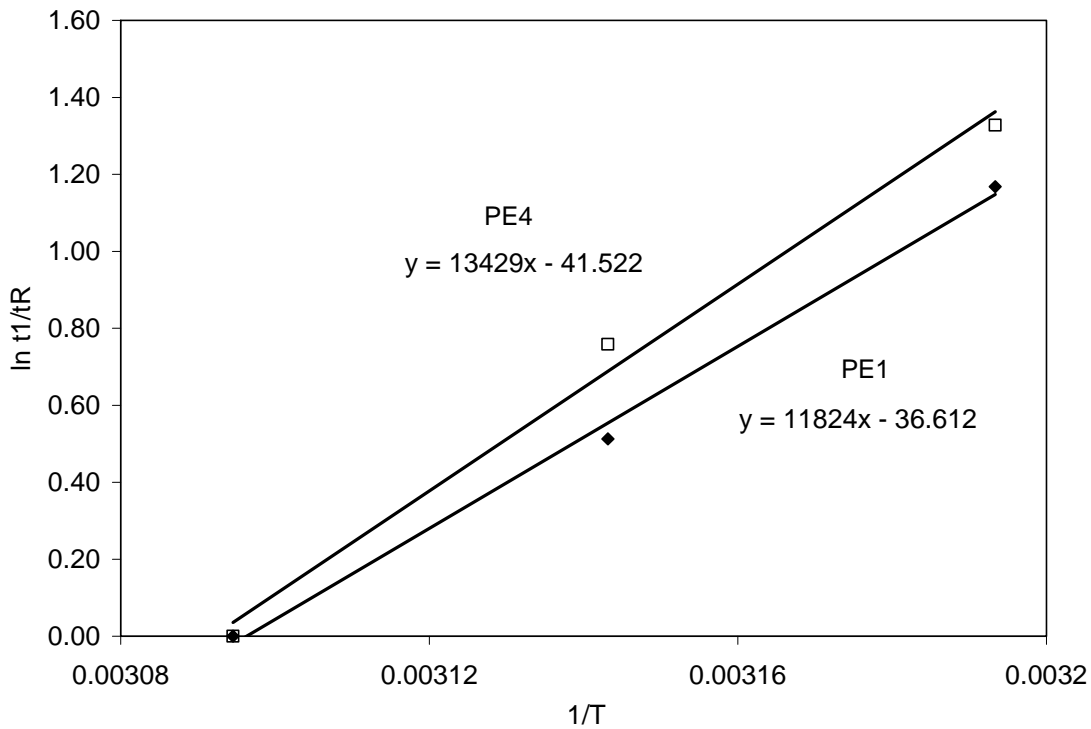


**Figure 7.2: Arrhenius plot for determination of Q for PE1 and PE4**

When determining the Q value in Equation 7.7, experiments should be preformed at both above and below the normal operating temperature of the test ( $T_R$ ) according to standard

practice. The normal temperature for NCLT specified by ASTM is 50°C, therefore  $T_1 < 50^\circ\text{C}$  ( $T_R$ )  $< T_2$  with  $T_R - T_1$  and  $T_2 - T_R$  being at least 5°C for good resolution of results. However, when the temperature of the NCLT bath was increased above 52°C the Igepal solution turned white and two phases were observed. The cloud point of a 1% Igepal solution ranges from 52.5°C-55.5°C (17) and the observed phase separation in the Igepal solution means that the cloud point of the solution was reached. Since Igepal accelerates the brittle fracture by diffusing into the cracks and thus lubricating chain slippage (4), the separation of the Igepal solution at 52°C brings into question whether the diffusion properties of the solution remain the same as at 50°C. In addition, morphological change of polyethylene is more likely to occur at temperatures above 50°C, which could make comparisons between test results from different temperatures less valid (16). On the other hand, at temperatures below 40°C the Igepal solution is in danger of approaching its Kraft point, where properties of a surfactant solution change. With these constraints in mind, the test temperatures for experiments to determine the crack activation energy of environmental stress crack resistance were chosen to be  $T_1=40^\circ\text{C}$ ,  $T_2=45^\circ\text{C}$  and  $T_R=50^\circ\text{C}$ .

The NCLT failure time for PE1-4 and PE8 at different temperatures are shown in Table 7.4. In the table, “Time at a specific temperature level” is in hours and refers to the measured ESCR failure time. The plot of  $\ln(t_1/t_R)$  vs.  $1/T$  for PE2, PE3 and PE8 showed similar linear relationships as those shown in Figure 7.2 for PE1 and PE4. The crack activation energy values calculated based on Equation 7.7 are presented in Table 7.4. In slow crack growth studies of polyethylene, the crack activation energy was reported to have a value in the range of 85-115 kJ/mole (7, 9, 12, 13). The ESC Q values

of the resins in this study are similar in orders of magnitude to these reported values, once again demonstrating that ESC and SCG are related mechanical processes.

**Table 7.4: NCLT results at different temperatures and Q value of PE1-4 and PE8**

	Time at 40°C (hours)	Time at 45°C (hours)	Time at 50°C (hours)	Slope	Q (kJ/mol)
PE1	15.4	8.0	4.8	11824	98.3
PE2	3.0	1.6	1.2	9041.1	75.2
PE3	5.2	3.6	2.8	6379.3	53.0
PE4	13.7	7.8	3.6	13429	111.6
PE8	-	454.9	198.3	17076	142.0

## 7.5 Relationship Between the $\alpha$ -Relaxation Energy and ESC Crack Activation Energy of Polyethylene

The NCLT test is a time consuming test method. Even at the relatively elevated temperature of 50°C, NCLT experiments can take hundreds or thousands of hours, as was shown in this study (Table 7.2). In Table 7.4, the ESC failure time of resins increased on average by a factor of two when the test temperature was lowered by 5°C. This poses a challenge when attempting to determine the crack activation energy of high ESCR polyethylene resins, such as PE10 (see Chapter 4). In addition, NCLT results also tend to have large variability that could reduce the precision of crack activation energy estimations. It would be desirable if another more efficient, reliable, practical and precise method could be found for determination of the crack activation energy.

For polyethylene, the reported slow crack growth activation energy is in the range of 85-115 kJ/mole (7, 9, 12, 13). The SCG crack activation energy shows a similar order of magnitude to that of the reported  $\alpha$ -relaxation energy, 97-208 kJ/mole (18-20), for

polyethylene. More details regarding the  $\alpha$ -relaxation of polyethylene are presented in section 7.5.1. In slow crack growth studies, it was speculated that the SCG crack activation energy and the  $\alpha$ -relaxation energy of polyethylene are closely related, if not equal (9, 12). The environmental stress cracking activation energy of resins in this study ranged from 53-142 kJ/mole, also in a similar range to that of the  $\alpha$ -relaxation energy of polyethylene. In the following section an investigation is undertaken to study the potential relationship between the  $\alpha$ -relaxation energy and the ESC crack activation energy of polyethylene.

### **7.5.1 The $\alpha$ -Relaxation Energy of Polyethylene**

The  $\alpha$ -relaxation of polyethylene occurs at temperatures above the glass transition temperature ( $T_g$ ) but below the melting point of the polymer. Dynamic mechanical analysis (DMA) is the method commonly used to study  $\alpha$ -relaxation behaviour of polymers. In this study, dynamic oscillating experiments in tensile mode were carried out at different temperatures. During DMA sample analysis, storage ( $E'$ ) and loss ( $E''$ ) modulus are measured and  $\tan(\delta)$  determined (see also Chapter 3). Figure 7.3 shows a typical DMA plot of  $\tan(\delta)$  vs. frequency at different temperatures. Similar curves and trends were obtained for the other samples. With increasing temperature, from 80°C to 120°C, the peak of the  $\tan(\delta)$  curve is shifted towards higher frequency. In Figure 7.4, independent replicates are presented for PE1. For the purpose of clarity, only the 90°C and the 110°C curves are shown. The close alignment of the curves indicates good reproducibility of the DMA experiments.

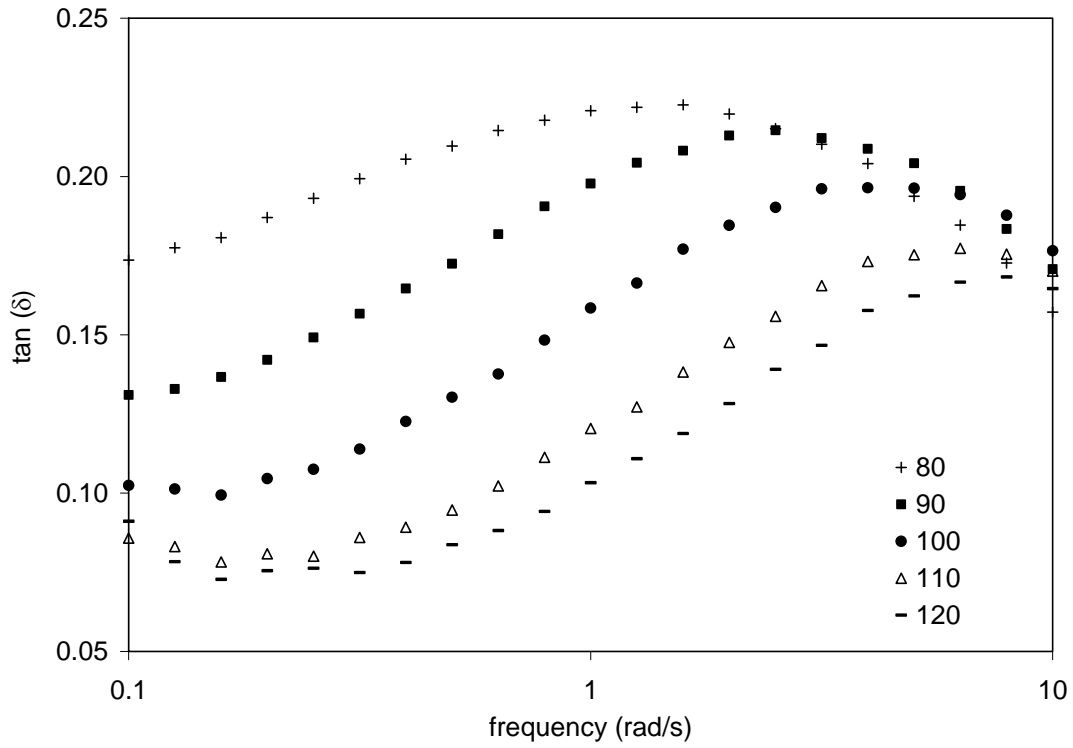


Figure 7.3: Curves for  $\tan(\delta)$  vs. frequency for PE1

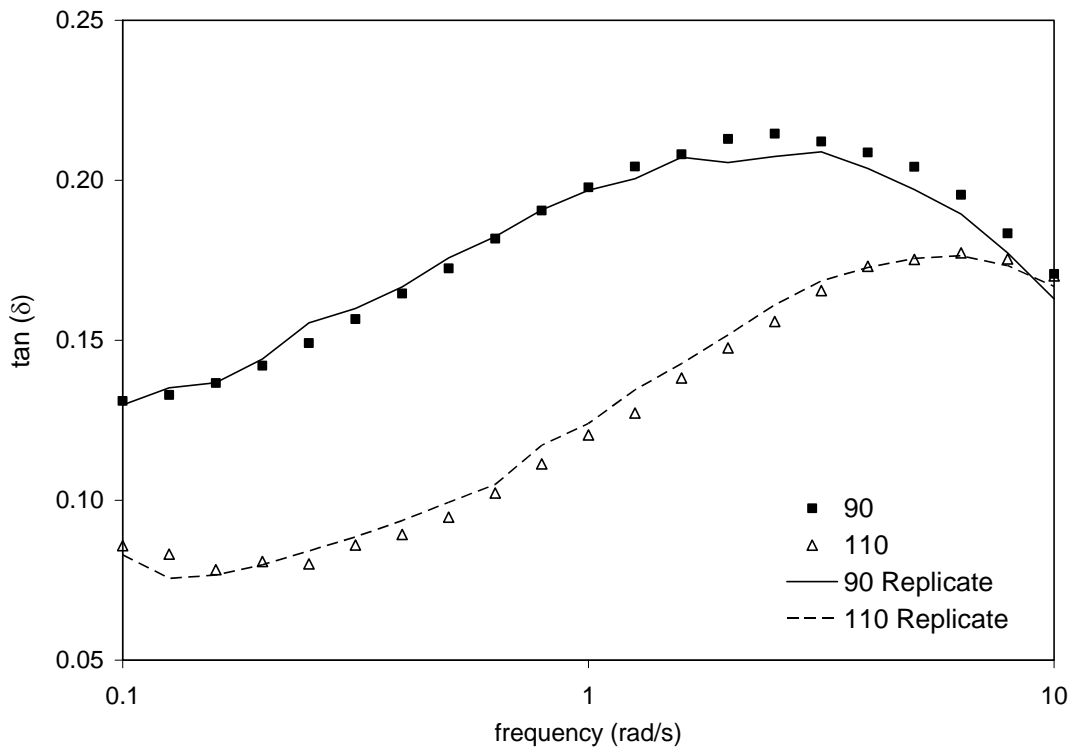
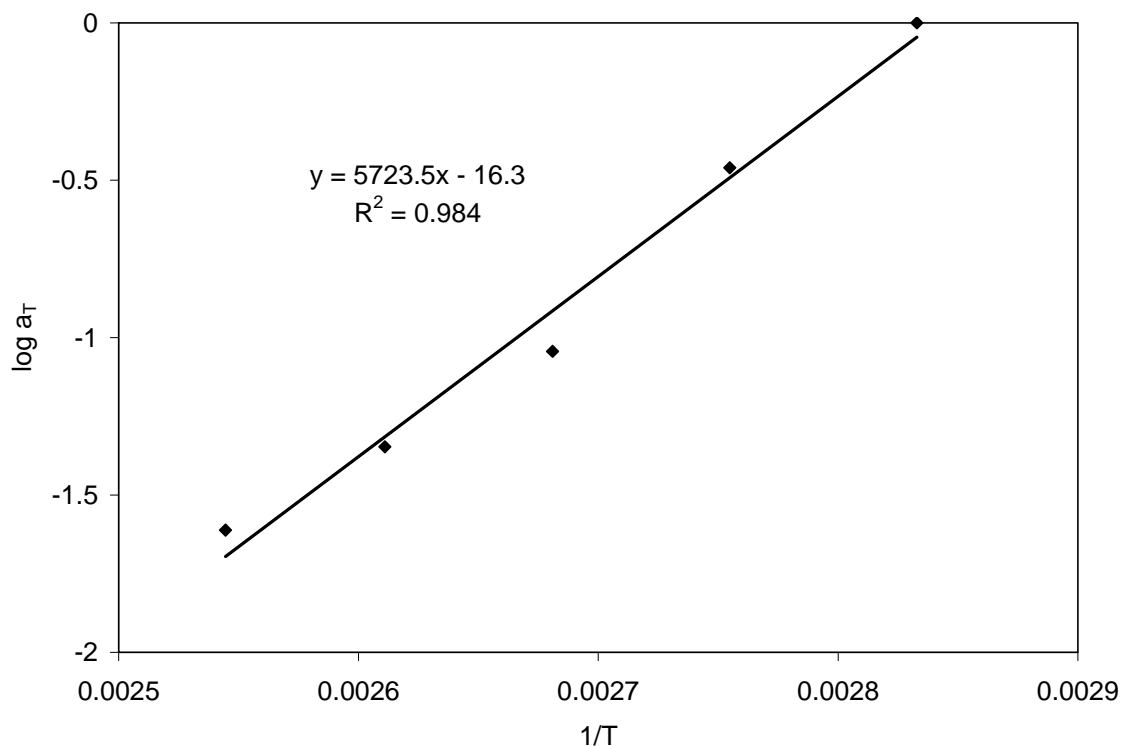


Figure 7.4:  $\tan(\delta)$  vs. frequency curves for PE1 with independent replication

The shifting peak of the  $\tan(\delta)$  curves in Figure 7.3 evidently results in a different peak frequency for each temperature. According to the time-temperature superposition principle (21, 22), the shift in the  $\tan(\delta)$  curve peak with a change in temperature can be described by a shift factor ( $\log a_T$ ) in the form of Equation 7.8, where  $\nu_1$  and  $\nu_2$  represent peak frequency at  $T_1$  and  $T_2$ , respectively. In this equation  $\Delta H$  is the  $\alpha$ -relaxation energy and  $R$  is again the universal gas constant. The constant 2.3 is a correction factor for semicrystalline polymers (23, 24).

$$\log a_T = \frac{\log \nu_1}{\log \nu_2} = \frac{\Delta H}{2.3R} \left\{ \frac{1}{T_2} - \frac{1}{T_1} \right\} \quad (7.8)$$

The shift factor ( $\log a_T$ ) calculated based on the  $\tan(\delta)$  curves in Figure 7.3 is shown in Figure 7.5 as a plot of  $\log a_T$  vs.  $1/T$ . The linear relationship between  $\log a_T$  and  $1/T$  indicates that  $\Delta H$  can be calculated from the slope of the fitted line and Equation 7.8. The  $\alpha$ -relaxation energies for all resins in this study were obtained following the procedure just described and results are presented in Table 7.5. The values cited in Table 7.5 for  $\Delta H$  are the mean values over three repeats including selective independent replicates. The average coefficient of variation of the measurements is 0.05, thus demonstrating good reproducibility of the DMA experiments. The  $\alpha$ -relaxation energies of resins in this study are comparable to values reported in the literature for polyethylene (97-208 kJ/mole (18-20)). The  $\alpha$ -relaxation energy values of PE5-7 and PE9-10 were determined following the same procedure as described in this section and results are shown in Appendix E.



**Figure 7.5: Shift factor vs. inverse temperature for PE1**

**Table 7.5:  $\alpha$ -relaxation energy values for PE1-4 and PE8**

	$\Delta H$ (kJ/mol)	Coefficient of Variation
PE1	109.90	0.03
PE2	112.15	0.02
PE3	115.14	0.07
PE4	123.86	0.06
PE8	150.48	0.05

The  $\Delta H$  values are influenced by differences in the SCB content of the resins. The  $\alpha$ -relaxation process of polyethylene can occur via two suggested mechanisms, namely inter-lamellar slip and intra-crystalline C-shear (19, 25-27). For high density polyethylene of low SCB content (PE1-3), the intra-crystalline C-shear mechanism dominates (19). C-shear involves the slip of the lamella stems and the forces needed to be overcome in this process are the hydrogen bonds between adjacent carbon chains.

Figure 7.6 illustrates how polymer chains are arranged in the lamella, as well as the different crystal slip systems in C-shear. PE1-3 have less than three short chain branches per thousand carbon atoms (see Table 7.2). The lower SCB content of PE2 and PE3 compared to PE1 results in thicker lamellae for PE2 and PE3. As the lamella thickness grows the number of carbon units in the crystalline stems grows as well. Hence, PE2 and PE3 have higher  $\Delta H$  values than PE1 (Table 7.5) because the energy needed for C-shear would increase with increasing number of hydrogen bonds (27).

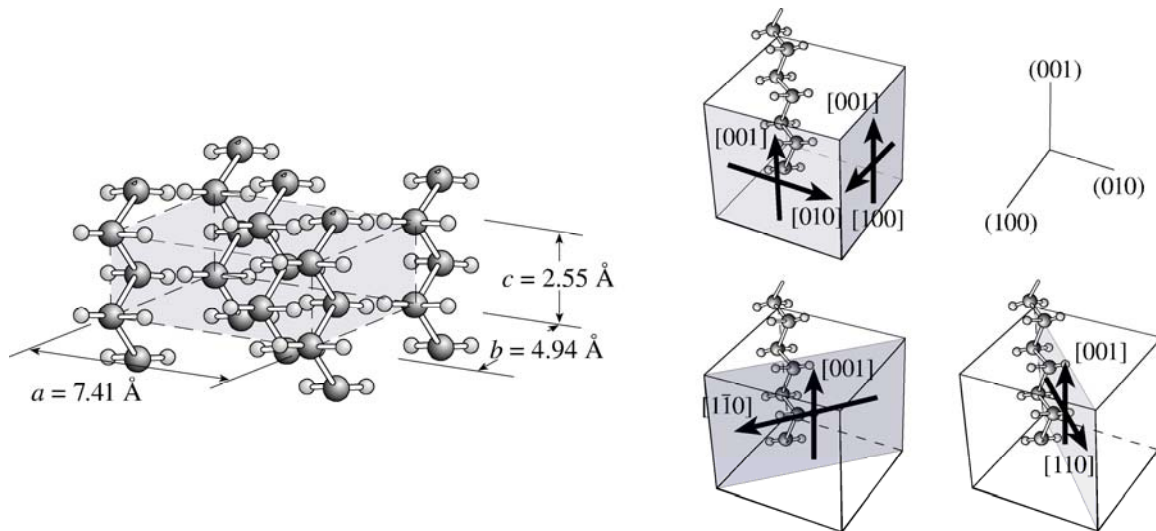


**Figure 7.6: Schematic representation of polyethylene crystal and slip systems, ref. (28)**

The crystallinity of polyethylene decreases with increasing SCB content. The contribution of the intra-crystalline C-shear process to the  $\alpha$ -relaxation energy decreases as the crystal lamellae become thinner due to the interference of short chain branching. On the other hand, increasing SCB content and decreasing crystallinity contribute to more chain entanglements in the polymer. The reduction in network mobility due to increasing chain entanglements hinders the process of inter-lamellar slip. As inter-

lamellar slip becomes more difficult the  $\alpha$ -relaxation energy of polyethylene increases (19), hence resins with higher SCB content (PE4 and PE8) are expected to have larger  $\Delta H$  values than resins with lower SCB content (PE1-3). For PE8, the higher molecular weight (see Table 7.2) of the resin would contribute even more to chain entanglements and result in even higher  $\alpha$ -relaxation energy values.

### **7.5.2 Comparison of Activation Energies**

In both the  $\alpha$ -relaxation and environmental stress cracking of polyethylene, the inter-lamellar movement of polymer chains is a key mechanism. The suspected possible duality between the  $\alpha$ -relaxation energy ( $\Delta H$ ) and crack activation energy ( $Q$ ) could be due to the fact that decreasing network mobility, due to decreases in inter-lamellar movement, is known to increase both the  $\alpha$ -relaxation energy and ESCR of polyethylene.

For PE1-4 and PE8, the environmental stress cracking activation energy and the  $\alpha$ -relaxation energy are presented together in Table 7.6. The orders of magnitude of both types of activation energies are very similar to each other. The ratio of  $Q/\Delta H$  is also shown in Table 7.6, as well as in Figure 7.7. For PE1, PE4 and PE8 the  $Q/\Delta H$  ratios are close to unity, indicating that the values of  $Q$  and  $\Delta H$  are nearly the same for these resins. The similarity of  $Q$  and  $\Delta H$  values supports the postulation that the  $\alpha$ -relaxation energy is the same as the crack activation energy for polyethylene.

**Table 7.6: Crack activation energy (Q) and  $\alpha$ -relaxation energy ( $\Delta H$ ) of PE1-4 and PE8**

	$\Delta H(\text{kJ/mol})$	$Q(\text{kJ/mol})$	$Q/\Delta H$
PE1	109.90	98.3	0.89
PE2	112.15	75.2	0.67
PE3	115.14	53.0	0.46
PE4	123.86	111.6	0.90
PE8	150.48	142.0	0.94

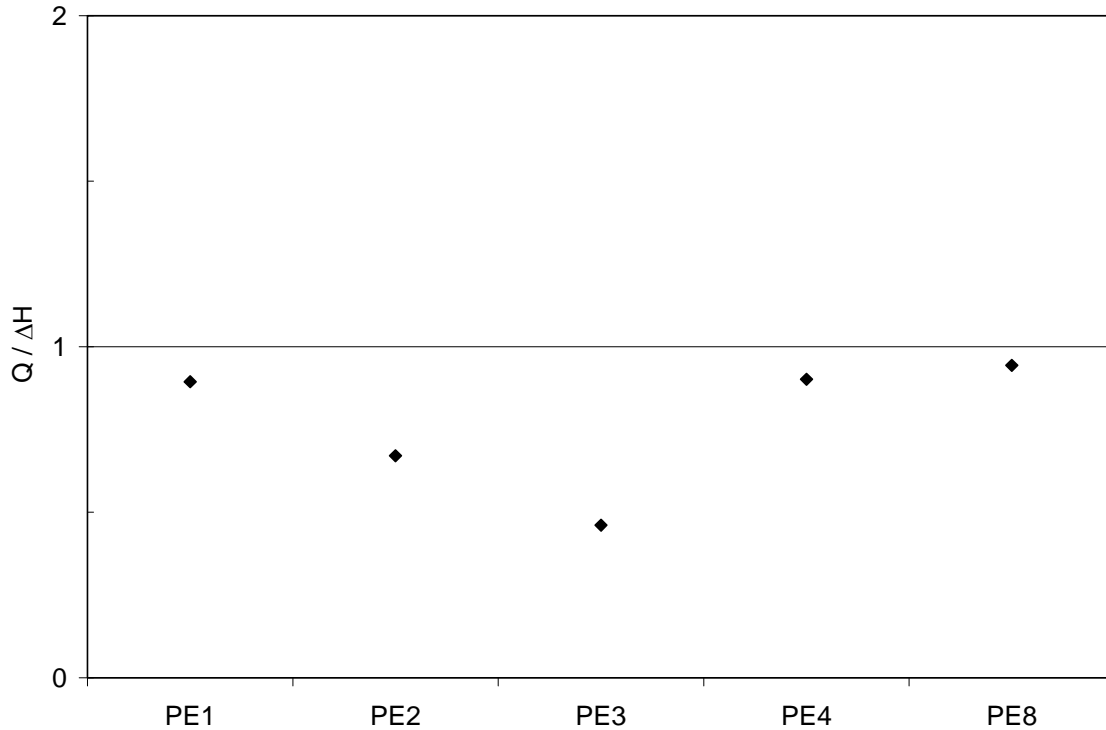


**Figure 7.7: Ratio of  $Q/\Delta H$  for PE1-4 and PE8**

For PE2 and PE3, the value of  $Q/\Delta H$  ratio is not close to unity (see Figure 7.7 and Table 7.6). Compared to the  $\alpha$ -relaxation energy of these resins, PE2 and PE3 exhibit smaller crack activation energy values. In the case of PE3, its crack activation energy ( $Q$ ) is about 50% smaller than its  $\alpha$ -relaxation energy ( $\Delta H$ ). The reduction of crack growth activation energy in the case of PE2 and PE3 could be due to the presence of the

aggressive environment (Igepal solution at 50°C). Ward *et al.* (4) observed that the crack activation energy of polyethylene in Igepal is lower than that of crack activation energy in air, due to the “lubrication” effect that Igepal has on the chain disentanglement process. The  $\alpha$ -relaxation energy was first proposed to be similar to SCG of polyethylene in air, therefore, it is possible that the observed differences between  $Q$  and  $\Delta H$  are the result of the effect of the aggressive environment.

The focus of Ward *et al.* (4) was to establish a possible mechanism for the accelerated failure in Igepal solution compared to failure in air. Only one PE resin was used in their study and little explanation was offered as to which material properties are primarily responsible for the reduction in the value of  $Q$ . Looking at Table 7.6 and Figure 7.7, it is evident that the reduction in crack activation energy is not systemic for all resins. In addition, though PE2 and PE3 have similar values of  $\alpha$ -relaxation energy, the difference between  $\Delta H$  and  $Q$  is not the same for the two resins. These observations indicate that the  $Q$  activation energy reduction may be affected by some other, unaccounted, structural differences of the resins.

Molecular weight is known to have a large influence on the environmental stress cracking resistance of polyethylene; increasing ESCR is associated with increasing MW of the polymer (see Chapters 4-6). In this study, resins with high MW also have high ESCR values (Table 7.2). Figure 7.8 presents the activation energy ratio ( $Q/\Delta H$ ) as a function of  $M_w$  (weight-average molecular weight) of the resins. The data are relatively scattered in the graph with no significant correlation pattern, and so the MW of the resins does not

appear to correlate well with (and hence influence) the reduction of crack activation energy for polyethylene.

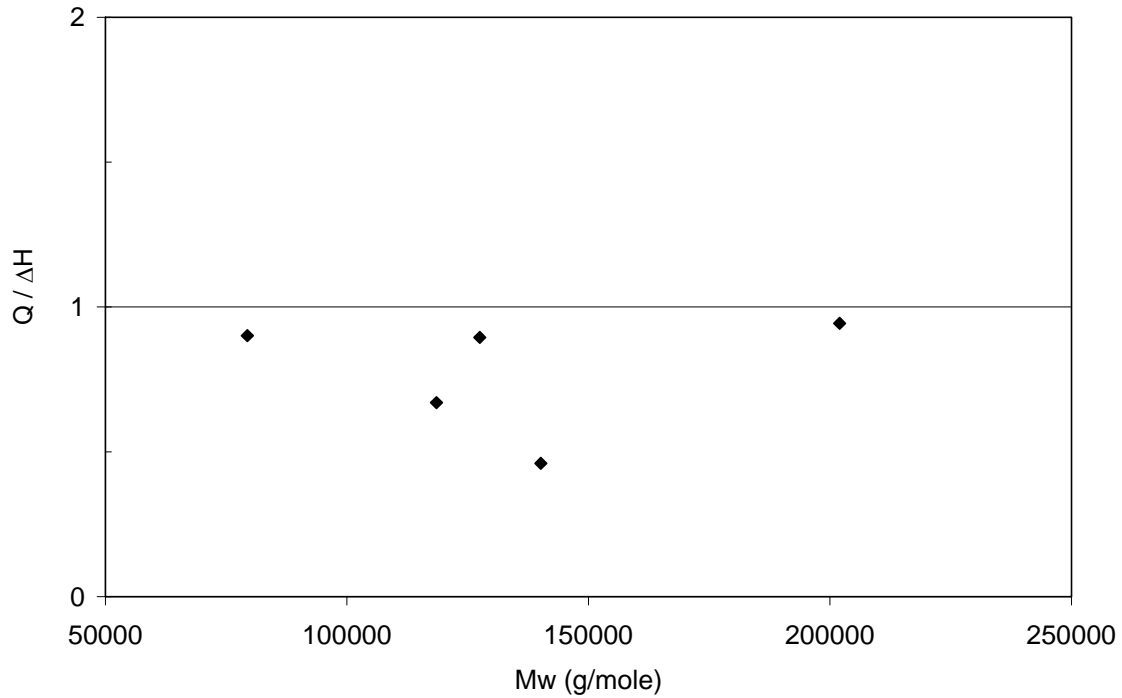


**Figure 7.8: Q/ΔH ratio and Mw for PE1-4 and PE8**

The  $\alpha$ -relaxation is influenced by the crystalline phase characteristics of polyethylene (25, 26, 29, 30). Brown and Lu (12) also proposed that crystalline phase viscosity could be a factor in SCG of polyethylene. In Figure 7.9, the ratio of Q/ΔH is plotted against the percentage crystallinity of resins. The data seem to cluster in two groups, with the lower crystallinity group having a Q/ΔH ratio close to unity, while the higher crystallinity group values show a reduction in crack activation energy.

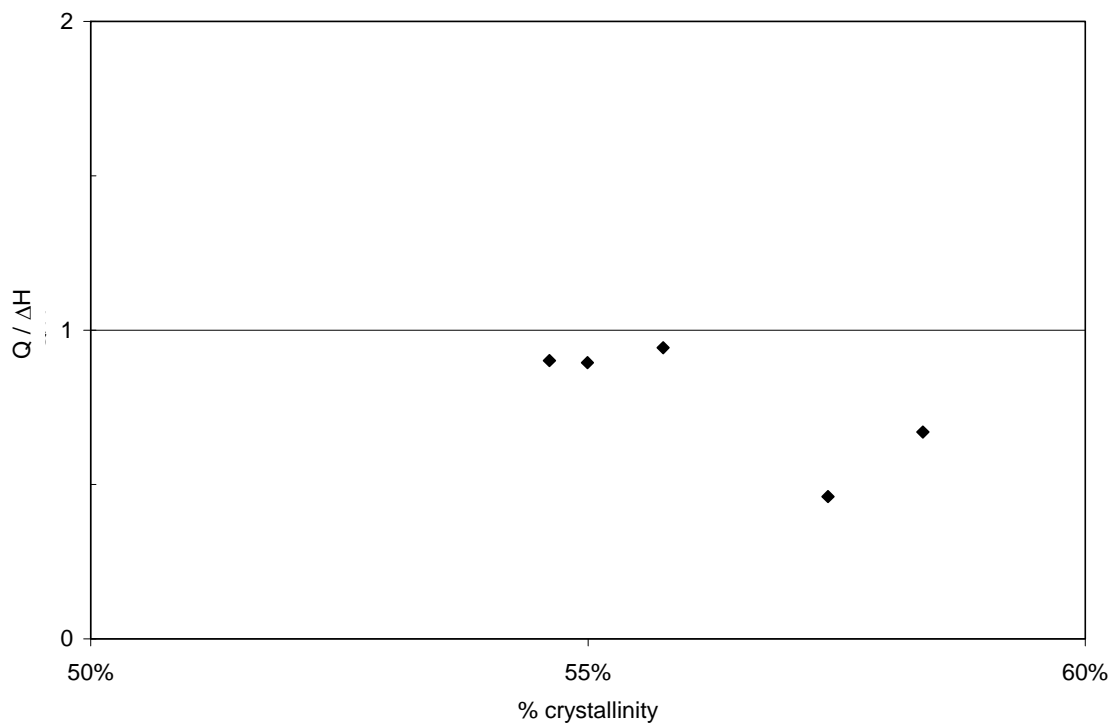


**Figure 7.9: Q/ΔH ratio vs. percentage crystallinity for PE1-4 and PE8**

Short chain branching content influences the crystallinity as well as the ESCR of polyethylene (31-36). With these relationships and the observation from Figure 7.9 in mind, the effect of SCB content has on crack activation energy reduction was investigated. In Figure 7.10, the ratio of Q/ΔH is plotted as a function of the number of SCB per thousand carbon atoms. A trend of increasing Q/ΔH is observed with increasing SCB content of the resins. When the short chain branching content of resins became higher than 2.5 SCB per thousand carbons, the Q/ΔH ratio remained relatively constant and near unity.

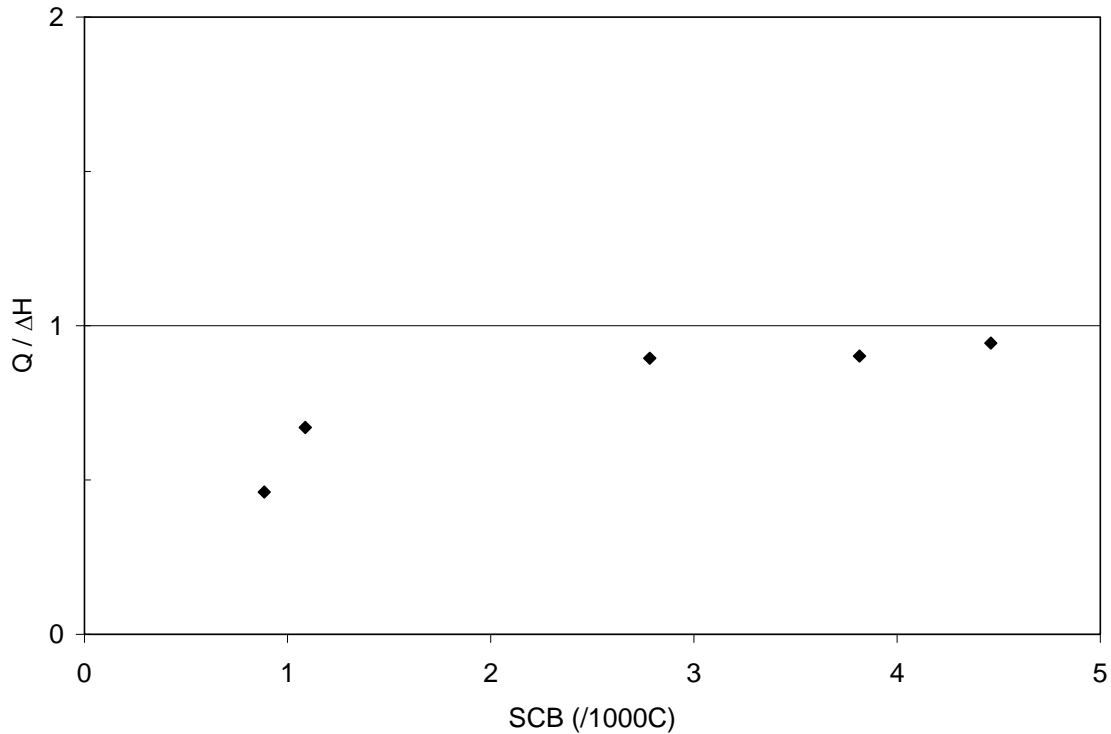


**Figure 7.10: Q/ΔH ratio and SCB per 1000C for PE1-4 and PE8**

Lower crystallinity can be interpreted as a reflection of the higher SCB content of the resins, therefore, Figure 7.9 indirectly showed that increases in SCB content decreased Q and ΔH differences. On the other hand, Figure 7.10 illustrated a relationship between diminishing differences between Q and ΔH with increasing SCB content. Thus, both figures confirmed the same fact, namely that resins with high SCB content do not show a reduction in crack activation energy Q when exposed to Igepal solution. The presence of SCB is known to hinder chain slippages from the crystalline lamellae (37), which would reduce the mobility of PE chains. With high SCB content, the lubrication effect of Igepal is reduced, and hence less reduction is expected of the crack activation energy for polyethylene.

The results of the investigation showed that the  $\alpha$ -relaxation energy ( $\Delta H$ ) and the ESC crack activation energy ( $Q$ ) of polyethylene are related. It would be in haste to conclude that the two are exactly the same, especially in light of the observed reduction in crack activation energy as compared to  $\Delta H$  when SCB content is low. However,  $\Delta H$  values may still be used in place of  $Q$  values in ESC modeling when  $Q$  cannot be readily obtained. Brown (9) proposed to apply a  $Q = 90$  kJ/mole for SCG modeling of all high density polyethylene. This approach seems a little broad-stroked considering the many different types of HDPE in use today. The use of the  $\alpha$ -relaxation energy in place of  $Q$  may offer a more tailored approximation of the true crack activation energy of PE material. A sample calculation of  $\Delta H$  used in ESC modeling is presented and further discussed in Appendix E. In addition, the DMA method also has the advantage of being faster and more precise than the NCLT test. The restriction would be that  $\Delta H$  can more safely be used as  $Q$  when the SCB content of the PE resin is 2.5 SCB per thousand carbon atoms or higher.

## **7.6 Material Resistance to ESC**

In Brown's (9) work on predicting the long-term service life of PE pipelines based on the PENT test (ASTM F1473), he suggested that the failure time of pipeline is directly proportional to the crack resistance of the pipe material, but no resistance value was offered. In work on the relationship between molecular weight and ESCR of polyethylene, Huang and Brown (13) similarly theorized that the resistance to crack growth should be directly proportional to the material failure time. In Equation 7.4, the

ESC time to failure is also formulated to be directly proportional to the material resistance ( $C$ ) to crack growth. In the preceding sections ESC model parameters other than  $C$  were estimated. In this section results from the determination of the material resistance to crack growth are presented.

With knowledge of the geometry correction factor ( $Y$ ), the initial damage size ( $a$ ), the applied stress ( $S$ ),  $n$  constant values, temperature ( $T$ ), crack activation energy ( $Q$ ), and the environmental stress cracking failure time ( $t$ ), the material resistance ( $C$ ) to ESC can be calculated for PE1-4 and PE8 using Equation 7.4. For the estimation of  $C$ , the assumption of material constants being independent of temperature is used. In this calculation, the ESC failure time is the failure time measured in the NCLT test at 50°C. The value of the universal gas constant  $R$  used is 8.314 J/mol K and the temperature of the test condition was 50°C or 323.15K. The applied stress was 15% of the yield stress of the resin (see discussion in Chapters 3 and 4). The value of the initial notch/damage is 40% of the thickness of samples and the geometry correction factor ( $Y$ ) is 3.73 (as shown in section 7.4.2). In Table 7.7 the material resistance is presented along with  $Q$  and  $n$  values of individual resins. The value of material resistance to crack growth is calculated in two ways, one using the individual value of  $n$  constant for each resin, and the other using the mean  $n = 3.12$  for all resins.

**Table 7.7: Material resistance (C) to environmental stress cracking for PE1-4 and PE8**

	Q (kJ/mol)	n	Material resistance to ESC	
			Based on individual n values (hour MPa <sup>n</sup> m <sup>0.5n</sup> )	Based on average n=3.12 (hour MPa <sup>3.12</sup> m <sup>1.56</sup> )
PE1	98.3	2.06	9.8E-17	3.8E-17
PE2	75.0	1.97	2.2E-13	9.4E-14
PE3	53.0	2.90	8.2E-10	7.0E-10
PE4	111.7	3.54	7.8E-20	1.2E-19
PE8	142.0	5.12	3.9E-23	1.9E-22

According to Equation 7.4, the material resistance has complex units in the form of  $[\text{time stress}^n \text{ length}^{0.5n}]$ . Depending on the value of the individual n constant for each resin, the material resistance values have slightly different units, which complicates further comparison between resins. In Figure 7.11, material resistance calculated based on the individual n value is plotted against material resistance calculated using the mean n value. The aligning of data points at the  $y = x$  line indicates that material resistance factors calculated based on the two different n constants have the same trend. Hence, for simplification purposes, from here on all material resistance values presented will be based on calculations done with the average n value.

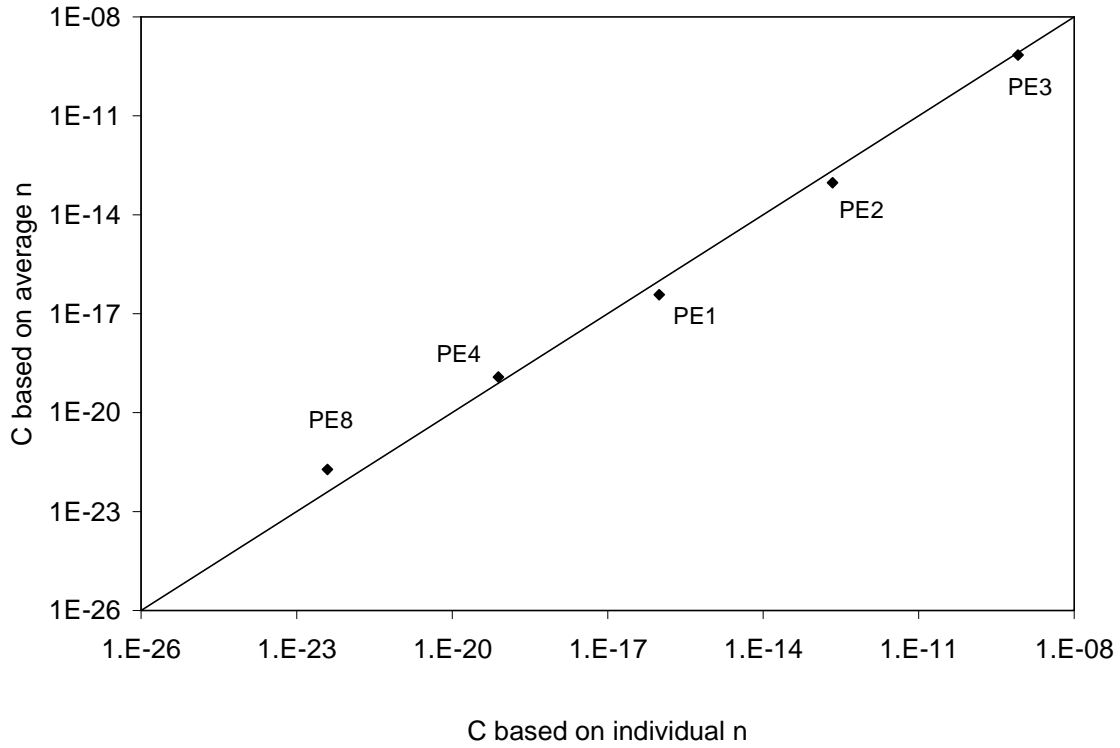


**Figure 7.11: Material resistance to ESC based on average n value and individual n value**

In Figure 7.12, the material resistance to ESC for each resin is plotted against its ESCR value. Figure 7.12 shows a relationship of decreasing material resistance with increasing ESCR. This trend is different from the expected directly proportional relationship between ESCR and resistance to crack growth. Polyethylene material with high ESCR should not have low resistance to ESC.

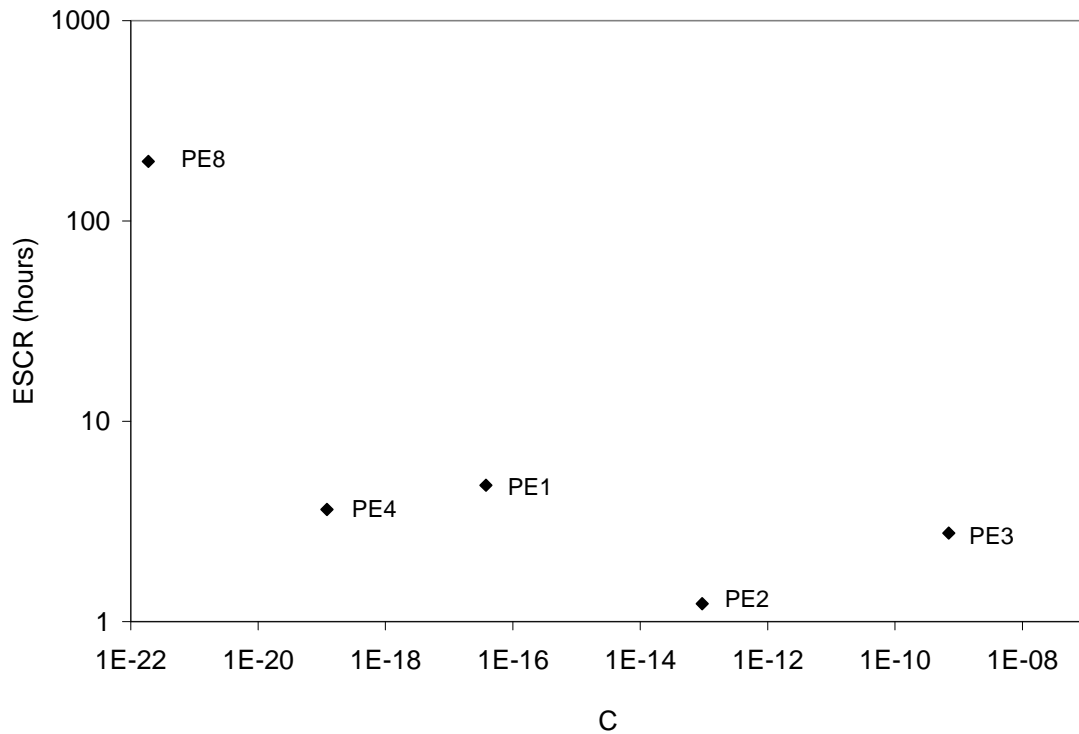


**Figure 7.12: Log ESCR vs. material resistance to ESC for PE1-4 and PE8**

Further investigation revealed that the value of the crack activation energy ( $Q$ ) used with Equation 7.4 may be the reason for the observed relationship in Figure 7.12. In the slow crack growth lifetime estimation model (9), one value of slow crack growth activation energy was used, making the exponential term in the model a constant at a given temperature, and thus, minimizing the influence of the exponential term. To test this postulate, material resistance to ESC for PE1-4 and PE8 was recalculated based on  $Q = 90$  kJ/mol (9) while all other values used in the calculation were kept the same. In Figure 7.13 the plot of  $C$  vs. ESCR showed a relationship of increasing ESCR with increasing material resistance, as was expected. This result confirmed the speculation that the observed inversely proportional behaviour between  $C$  and ESCR in Figure 7.12 is an artifact due to the differences in  $Q$  of the individual resins. This also reveals that

calculations based on the model and estimates of model terms based on experimental observations are vary sensitive to the value of  $Q$  employed (and hence, to the experimental error/noise from the NCLT test; see section 0). This sensitivity may of course be accentuated if  $\Delta H$  is used to replace, as discussed in section 7.5.

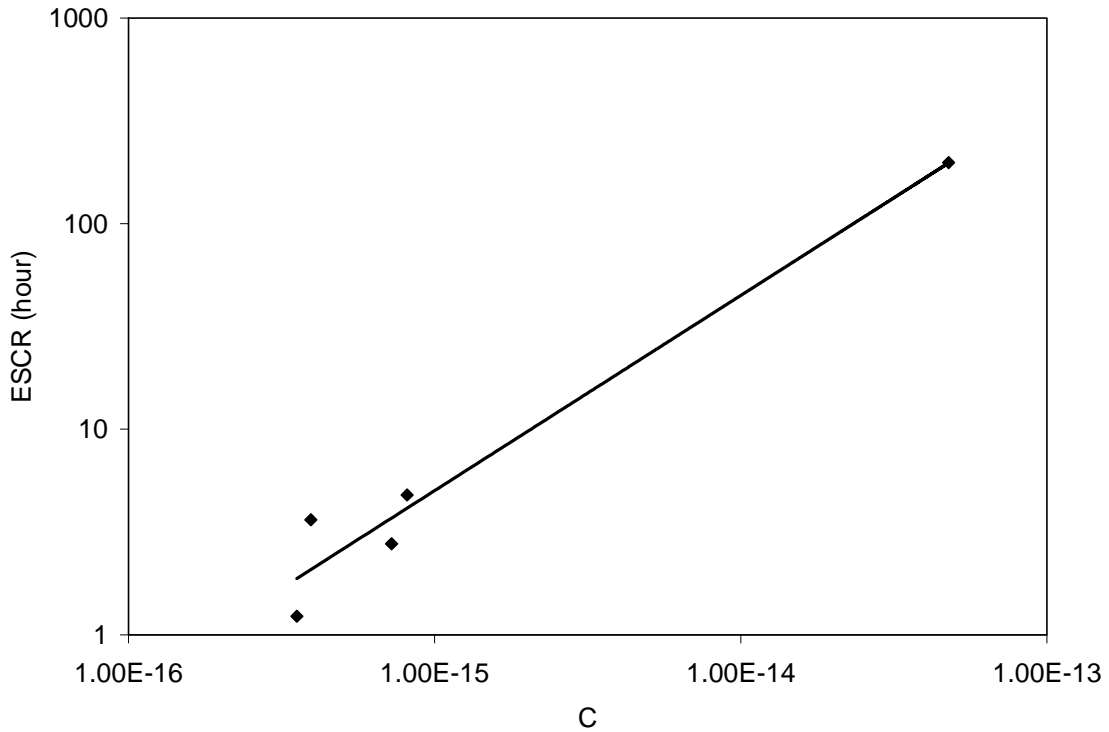


**Figure 7.13: Log ESCR vs. material resistance calculated based on  $Q = 90\text{kJ/mol}$  (9) for PE1-4 and PE8**

As discussed in section 7.5.2, the crack activation energy is influenced by the SCB content of the resins. In Figure 7.14, the crack activation energy (black symbols) is expressed as a function of the SCB content. In the same graph the material resistance to ESC (white symbols) is also shown as a function of SCB content for PE1-4 and PE8. The decreasing trend of  $C$  with increasing SCB content corresponds to the increasing trend of  $Q$  with increasing SCB content. The two data sets behave like mirror images of

one another, thus demonstrating the large influence of the exponential term on the ESC model output. Due to the fact that no reliable material resistance to ESC can be estimated with Equation 7.4, ESCR lifetime estimation for polyethylene is not safe with the current model. Even though the ESC model can not be used to estimate ESCR lifetime of polyethylene over a wide range, the model may still be useful for resins over narrow application ranges. Resins intended for a specific application are more likely to have similar Q activation energy values and the environmental stress cracking model estimate of these resins would be less influenced by the exponential term in the model, thus giving more reliable ESC lifetime predictions.

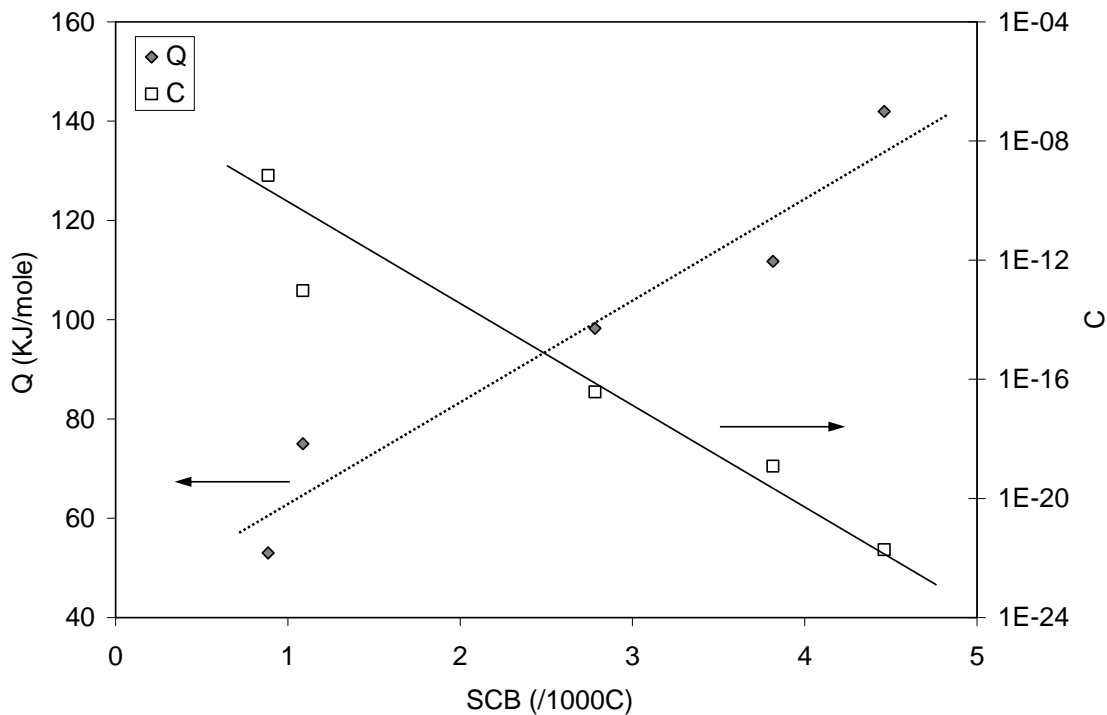


**Figure 7.14: Relationship between Q, C and SCB content of polyethylene for PE1-4 and PE8 (the lines are only a visual guide to the eye)**

## 7.7 Concluding Remarks

The goal of this chapter was to attempt to develop a possible predictive model for quantitative estimation of the long-term environmental stress cracking behaviour of high density polyethylene based on the short-term NCLT test. Since ESC is a form of slow crack growth, the ESC model developed is analogous to the SCG model (9). During model analysis, it was found that the ESC model is very sensitive to the crack activation energy ( $Q$ ), appearing in the exponential term of the model. This sensitivity was hidden in the SCG model (9) because one single value of crack activation energy was applied to all polyethylenes. In ESC, polyethylene resins have different  $Q$  values because of differences in the SCB content. Due to differences in crack activation energy, the estimated material resistance to ESC appears to be inversely proportional to ESCR of polyethylene. With no meaningful correlation of material resistance to ESC, the ESC model cannot be used for estimation of the long-term ESCR lifetime of PE in the current form. When polyethylene resins of narrow application range are considered, however, the ESC model may still offer insights because these resins are likely to have similar crack activation energy values and the model sensitivity to  $Q$  would be reduced.

However, the modeling investigation was very fruitful for many other insights gained, as discussed in sections 7.4 and 7.5. More particularly, the relationship between the ESC crack activation energy ( $Q$ ) and the  $\alpha$ -relaxation energy ( $\Delta H$ ) of polyethylene was studied. The  $\alpha$ -relaxation energy was been shown to be of the same order of magnitude as the ESC crack activation energy for all resins. For PE with 2.5 SCB per thousand carbons or higher, the ratio between  $Q/\Delta H$  is close to unity, indicating that the two

activation energies represent analogous processes and hence have similar information content. For resins with lower SCB content (less than 2.5 SCB/1000C), their crack activation energy is found to be smaller than their  $\alpha$ -relaxation energy. PE resins with lower crack activation energy have faster crack growth, which may provide a possible explanation for why resins of lower SCB content have lower ESCR. The study showed that there is a relationship between the ESC crack activation and the  $\alpha$ -relaxation energy of polyethylene, however further study is needed to clarify the behaviour of why a reduction in Q is observed when the SCB content is low. One possible explanation for the lowering of crack activation energy is the presence of the Igepal solution which lubricates chain movements. The lubrication effect is more prominent in resins with low SCB content because there are less short chain branches to hinder chain movements, which is a key requirement for environmental stress crack of polyethylene. In closing, increasing ESC crack activation energy (Q) with increasing short chain branch content of resins was observed for the first time. This behaviour may explain, at least in part, the reason that PE resins with higher SCB content have “better” ESCR.

## 7.8 References

1. Lu, X. & Brown, N. (1986), "The relationship of the initiation stage to the rate of slow crack growth in linear polyethylene", *Journal of Materials Science*, vol. 21, pp. 2423-2429.
2. Lustiger, A. & Markham, R. L. (1983), "Importance of tie molecules in preventing polyethylene fracture under long-term loading conditions", *Polymer*, vol. 24, pp. 1647-1654.
3. Lagarón, J. M., Dixon, N. M., Reed, W., Pastor, J. M., & Kip, B. J. (1999), "Morphological characterisation of the crystalline structure of cold-drawn HDPE used as a model material for the environmental stress cracking (ESC) phenomenon", *Polymer*, vol. 40, pp. 2569-2586.
4. Ward, A. L., Lu, X., Huang, Y., & Brown, N. (1991), "The mechanism of slow crack growth in polyethylene by an environmental stress cracking agent", *Polymer*, vol. 32, no. 12, pp. 2172-2178.
5. Lagarón, J. M., Pastor, J. M., & Kip, B. J. (1999), "Role of an active environment of use in an environmental stress crack resistance (ESCR) test in stretched polyethylene: A vibrational spectroscopy and a SEM study", *Polymer*, vol. 40, pp. 1629-1636.
6. Scheirs, J. (2000), *Compositional and Failure Analysis of Polymers: A Practical Approach*, John Wiley & Sons, Ltd, Chichester, West Sussex, England.
7. Lu, X. & Brown, N. (1990), "The ductile-brittle transition in a polyethylene copolymer", *Journal of Materials Science*, vol. 25, pp. 29-34.
8. Lu, X. & Brown, N. (1991), "Unification of Ductile Failure and Slow Crack-Growth in An Ethylene-Octene Copolymer", *Journal of Materials Science*, vol. 26, no. 3, pp. 612-620.
9. Brown, N. (2007), "Intrinsic lifetime of polyethylene pipelines", *Polymer Engineering and Science*, vol. 47, pp. 477-480.
10. Williams, J. G. (1984), *Fracture Mechanics of Polymers*, Ellis Horwood Limited, Chichester, West Sussex, England.
11. Chan, M. K. V. & Williams, J. G. (1983), "Slow stable crack growth in high density polyethylenes", *Polymer*, vol. 24, pp. 234-244.
12. Brown, N. & Lu, X. (1995), "A fundamental theory for slow crack growth in polyethylene", *Polymer*, vol. 36, no. 3, pp. 543-548.

13. Huang, Y. & Brown, N. (1988), "The effect of molecular weight on slow crack growth in linear polyethylene homopolymers", *Journal of Materials Science*, vol. 23, pp. 3648-3655.
14. Lu, X. & Brown, N. (1986), "Predicting failure from the initiation stage of slow crack growth in polyethylene", *Journal of Materials Science*, vol. 21, pp. 4081-4088.
15. Qian, R., Lu, X., & Brown, N. (1993), "The Effect of Concentration of An Environmental-Stress Cracking Agent on Slow Crack-Growth in Polyethylenes", *Polymer*, vol. 34, no. 22, pp. 4727-4731.
16. Wright, D. (1996), *Environmental Stress Cracking of Plastics*, Rapra Technology Ltd., Shawbury, United Kingdom.
17. Windholz, Martha ,(1983), *The Merck Index: An Encyclopedia of Chemicals, Drugs, and Biologicals*, 10 edn, Merck & Co., Rahway, N.J., U.S.A.
18. Matsuo, M., Bin, Y., Xu, C., Ma, L., Nakaoki, T., & Suzuki, T. (2003), "Relaxation mechanism in several kinds of polyethylene estimated by dynamic mechanical measurements, positron annihilation, X-ray and <sup>13</sup>C solid-state NMR", *Polymer* no. 4325, p. 4340.
19. Guan, X. & Phillips, P. J. (2007), "Dynamic mechanical properties of random ethylene/1-octene copolymers prepared by rapid cooling", *European Polymer Journal*, vol. 43, pp. 1219-1233.
20. Stadler, F. J., Kaschta, J., & Muenstedt, H. (2005), "Dynamic-mechanical behavior of polyethylenes and ethene-/alpha-olefin-co-polymers. Part I. alpha '-relaxation", *Polymer*, vol. 46, no. 23, pp. 10311-10320.
21. Ward, I. M. (1971), *Mechanical Properties of Solid Polymers*, Wiley-Interscience, Toronto.
22. McCrum, N. G., Buckley, C. P., & Bucknall, C. B. (1997), *Principles of Polymer Engineering*, 2 edn, Oxford University Press, Oxford, New York, Tokyo.
23. van Krevelen, D. W. (1990), *Properties of Polymers*, 3 edn, Elsevier Scientific Publishing Company, New York.
24. Seitz, J. T. & Balazs, C. F. (1968), "Application of time-temperature superposition principle to long term engineering properties of plastic materials", *Polymer Engineering and Science*, vol. 8, no. 2, pp. 151-160.

25. Matthews, R. G., Unwin, A. P., Ward, I. M., & Capaccio, G. (1999), "A comparison of the dynamic mechanical relaxation behavior of linear low- and high-density polyethylenes", *Journal of Macromolecular Science-Physics*, vol. B38, no. 1-2, pp. 123-143.
26. Matthews, R. G., Ward, I. M., & Capaccio, G. (1999), "Structural heterogeneity and dynamic mechanical relaxation of ethylene  $\alpha$ -olefin copolymers", *Journal of Polymer Science Part B-Polymer Physics*, vol. 37, pp. 51-60.
27. Boyd, R. H. (1985), "Relaxation processes in crystalline polymers: molecular interpretation - a review", *Polymer*, vol. 26, pp. 1123-1133.
28. Alvarado-Contreras, J. A. (2007), *Micromechanical Modelling of Polyethylene*, PhD Thesis, Department of Civil Engineering, University of Waterloo, Waterloo, Ontario, Canada.
29. Simanke, A. G., Galland, G. B., Freitas, L., da Jornada, J. A. H., Quijada, R., & Mauler, R. S. (1999), "Influence of the comonomer content on the thermal and dynamic mechanical properties of metallocene ethylene/1-octene copolymers", *Polymer*, vol. 40, no. 20, pp. 5489-5495.
30. Simanke, A. G., Galland, G. B., Neto, R. B., Quijada, R., & Mauler, R. S. (1999), "Influence of the type and the comonomer contents on the mechanical behavior of ethylene/ $\alpha$ -olefin copolymers", *Journal of Applied Polymer Science*, vol. 74, no. 5, pp. 1194-1200.
31. Hosoda, S., Nomura, H., Gotoh, Y., & Kihara, H. (1990), "Degree of branch inclusion into the lamellar crystal for various ethylene/ $\alpha$ -olefin copolymers", *Polymer*, vol. 31, pp. 1999-2005.
32. Bodor, G., Dalcolmo, H. J., & Schroeter, O. (2008), "Structural and property correlations of ethylene- $\alpha$ -olefin copolymers", *Colloid and Polymer Science*, vol. 267, no. 6, pp. 480-493.
33. Huang, Y. & Brown, N. (1990), "The dependence of butyl branch density on slow crack growth in polyethylene: kinetics", *Journal of Polymer Science, Part B: Polymer Physics*, vol. 28, pp. 2007-2021.
34. Huang, Y.-L. & Brown, N. (1991), "Dependence of slow crack growth in polyethylene on butyl branch density: morphology and theory", *Journal of Polymer Science, Part B: Polymer Physics*, vol. 29, pp. 129-137.
35. Brown, N., Lu, X., Huang, Y., Harrison, I. P., & Ishikawa, N. (1992), "The Fundamental Material Parameters That Govern Slow Crack-Growth in Linear Polyethylenes", *Plastics Rubber and Composites Processing and Applications*, vol. 17, no. 4, pp. 255-258.

36. Janimak, J. J. & Stevens, G. C. (2001), "Inter-relationships between tie-molecule concentration, molecular characteristics and mechanical properties in metallocene catalysed medium density polyethylenes", *Journal of Materials Science*, vol. 36, no. 8, pp. 1879-1884.
37. Yeh, J. T., Chen, C. Y., & Hong, H. S. (1994), "Static fatigue behaviour of linear low-density polyethylene", *Journal of Materials Science*, vol. 29, pp. 4104-4112.

## **CHAPTER 8 PRACTICAL TIPS AND PRESCRIPTIONS FOR ESCR OF POLYETHYLENE**

### **8.1 Introduction**

The focus of this research was to study the relationships between (micro)molecular properties and mechanical behaviour of polyethylene (PE). In the previous chapters different aspects of the amorphous and crystalline phases of high density polyethylene (HDPE) were investigated and their influence on environmental stress cracking resistance (ESCR) of HDPE discussed. In this chapter we will attempt to offer readers a “bird’s eye view” of the relationship between key material characteristics and ESCR of polyethylene.

### **8.2 ESCR Heuristics**

Polyethylene is chemically a “simple” polymer with (–CH<sub>2</sub>-CH<sub>2</sub>-) repeating units. Comonomers are often incorporated during the polymerization process to produce PE with short chain branching (SCB). Molecular weight (MW) and SCB are two major factors influencing mechanical properties of PE (1). In Table 8.1, a summary of heuristics on molecular property relations to ESCR of polyethylene is presented. The first column of the table contains molecular properties that influence ESCR of polyethylene. The second and third columns indicate changes in molecular properties and the effects of these changes. Finally, the last column of Table 8.1 shows how ESCR of polyethylene is affected with the corresponding change in molecular properties. In addition to MW and SCB, molecular weight distribution (MWD), short chain branching distribution (SCBD) and long chain branching (LCB) influences are also shown. All

these (micro)molecular/ (micro)structural properties affect the formation of inter-lamellar links in polyethylene, which is a key factor eventually affecting ESCR of the polymer. Changes in material properties that contribute to increases of the number of inter-lamellar links improve the ESCR of polyethylene.

**Table 8.1: Molecular properties and ESCR relations of HDPE**

	Property change	Effects	ESCR
MW	↑	<ul style="list-style-type: none"> <li>•Increases chain entanglements</li> <li>•Increases tie-molecule concentration</li> <li>•Increases lamella lateral surface area</li> <li>•Increases crystallinity and strength</li> </ul>	↑
MWD	↑	<ul style="list-style-type: none"> <li>•Improves processability</li> <li>•Increases chain entanglements</li> </ul>	↑
SCB	↑	<ul style="list-style-type: none"> <li>•Increases chain entanglements</li> <li>•Reduces chain slippage</li> </ul>	↑
SCBD	Related to SCB	<ul style="list-style-type: none"> <li>•Higher SCB content in the high MW end of the MWD increases inter-lamellar link formations</li> </ul>	↑
LCB	↑	<ul style="list-style-type: none"> <li>•Increases chain entanglements</li> <li>•HDPE generally does not have sufficiently high levels of LCB to affect its ESCR</li> </ul>	↑

Since there are many different types of polyethylene, the summary of heuristics presented in Table 8.1 is not meant to apply to each and every one. Instead, the information in Table 8.1 is intended to apply more generally to HDPE copolymers because increases in MW and MWD would only effectively increase the number of inter-lamellar linkages if there is short chain branching present (2-6). For the case of HDPE homopolymer, increases in MW would contribute mostly to increasing the crystallinity of the material

and very little change will occur in the number of inter-lamellar linkages (7, 8), hence not improving the ESCR of the material in any significant way.

### **8.3 Prescriptions for ESCR of Polyethylene**

The table of heuristics (Table 8.1) provides some general rules regarding the expected molecular-mechanical property relations on an one to one basis. However, more importantly, for ESCR of polyethylene the combined influence of MW and SCB content is important. The MW-SCB interactions shown in Figures 8.1 and 8.2 can be used as prescriptions (practical “tips”) for producing resins with “better” (higher) ESCR, since MW and SCB are both controlling variables. Polyethylene resins in this study can be divided into high ESCR resins (PE7-10) and low ESCR resins (PE1-4). Figure 8.1 illustrates the behaviour of resins with high ESCR in several hundreds and/or several thousands of hours. On the other hand, Figure 8.2 shows ESCR behaviour of resins with low ESCR values in the order of several hours (but well below one hundred hours).

PE7-10 are pipe resins with rating of PE80 and PE100 (9). These resins have higher short chain branching content in the high molecular weight end of the MWD (see Appendix A), which is key to high ESCR (9). In parts (a) and (b) of Figure 8.1, the  $M_w$  (weight-average molecular weight) and SCB (short chain branches per thousand carbon atoms) ranges that correspond to high ESCR cases are marked by dashed lines; namely,  $M_w$  range of 190000-330000 g/mole and SCB range of 4-12 branches per thousand carbons. Translating these MW and SCB ranges to part (c) of Figure 8.1 shows a relatively linear relationship between MW and SCB, thus demonstrating again that for

high ESCR resins increasing both the MW and SCB concentration are key to increased ESCR of the material.

For low ESCR resins the story is slightly more complex. Figures 8.2 (a) and (b) show that for ESCR values of ten hours or less, the  $M_w$  range is 70000-15000 g/mole and the SCB content range is 0-4 short chain branches per thousand carbon atoms. Translating these values to part (c) of Figure 8.2, the graph shows that a combination of either higher  $M_w$  with lower SCB content, or lower  $M_w$  with higher SCB content can be used to achieve the desired ESCR. In Figure 8.2 (c) there are two points with  $M_w$  less than 70000 g/mole. These resins have SCB content of 4 branches per thousand carbons or higher, yet they do not have any measurable ESCR and thus are not present in parts (a) and (b) of Figure 8.2. These two resins demonstrate the importance of MW in ESCR behaviour of polyethylene. If a resin does not have high enough MW, high SCB content alone would not improve its ESCR.

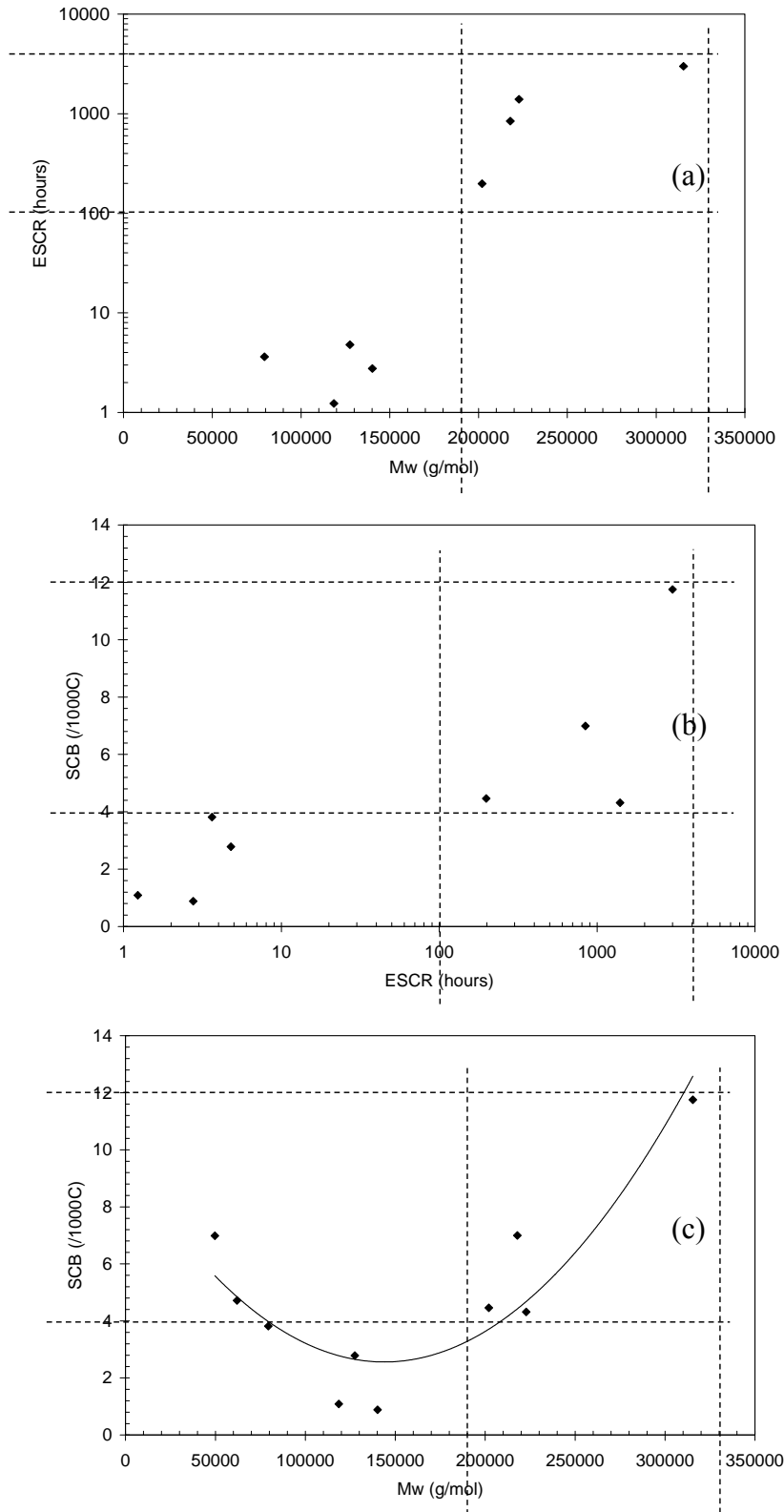
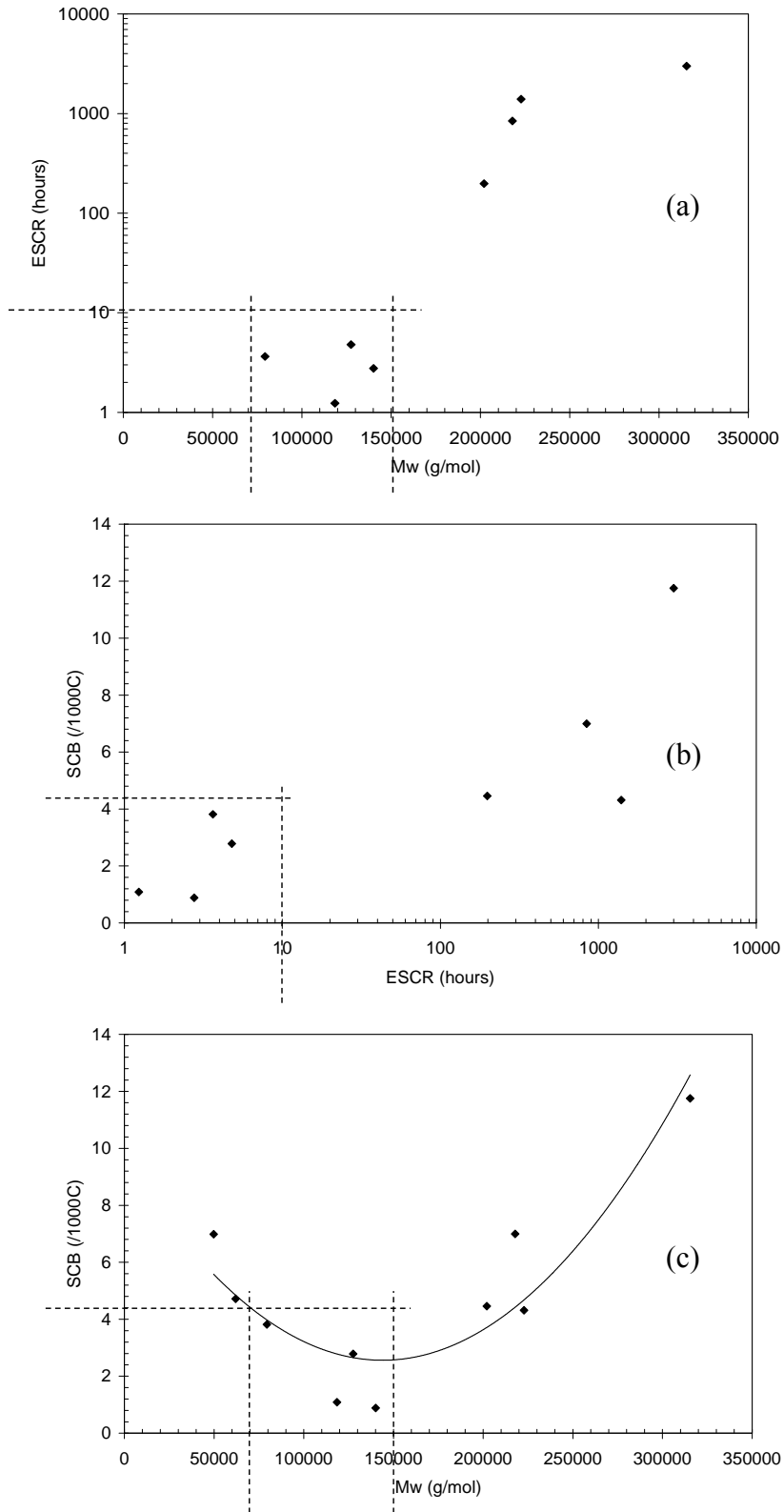


Figure 8.1: MW-SCB combination for high ESCR polyethylene



**Figure 8.2: MW-SCB combination for low ESCR polyethylene**

In addition to the prescriptions for production of better ESCR polyethylene (Figures 8.1 and 8.2), a “prescriptive pathway” for selecting PE with “better” (higher) ESCR is also presented in Figure 8.3. Figure 8.3 is basically a flow chart that contains a series of questions that may help the practitioner in choosing a material with “better” ESCR when resins with similar MW ranges are considered. The questions are formulated in sequence in order to offer simple indirect estimates of the amount of inter-lamellar links in the polymer, which influences the ESCR of the material, without resorting to complex and time-consuming specialized tests (as described in Chapter 4).

$M_w$  in Figure 8.3 refers again to the weight-average molecular weight of polymer, SCBD refers to the short chain branching distribution, SCB is the number of short chain branches per thousand carbon atoms,  $M_z$  is the z-average molecular weight, HS is the hardening stiffness during tensile deformation as discussed in Chapter 4, and crystallinity refers to the percentage crystallinity of polyethylene. The influence these properties have on inter-lamellar links and ESCR of polyethylene has been discussed in detail in Chapters 4-6 of the thesis. In Figure 8.3, the answer of “Yes” or “No” to each question module (diamond-shaped box) leads either to the decision towards a better ESCR resin, or to the next selection criterion that may clarify ESCR differences of resins further. For example, if two resins with similar  $M_w$  values have different SCBD trends (see Appendix A for FTIR-GPC analysis of resin SCBD), then the resin with higher SCB content in the high MW end of the MWD is likely to have better ESCR. If the resins have the same trends in SCBD, then the resin with higher SCB content (determined by  $^{13}\text{C}$  NMR, see Chapters 3 and 4) is likely to have better ESCR.

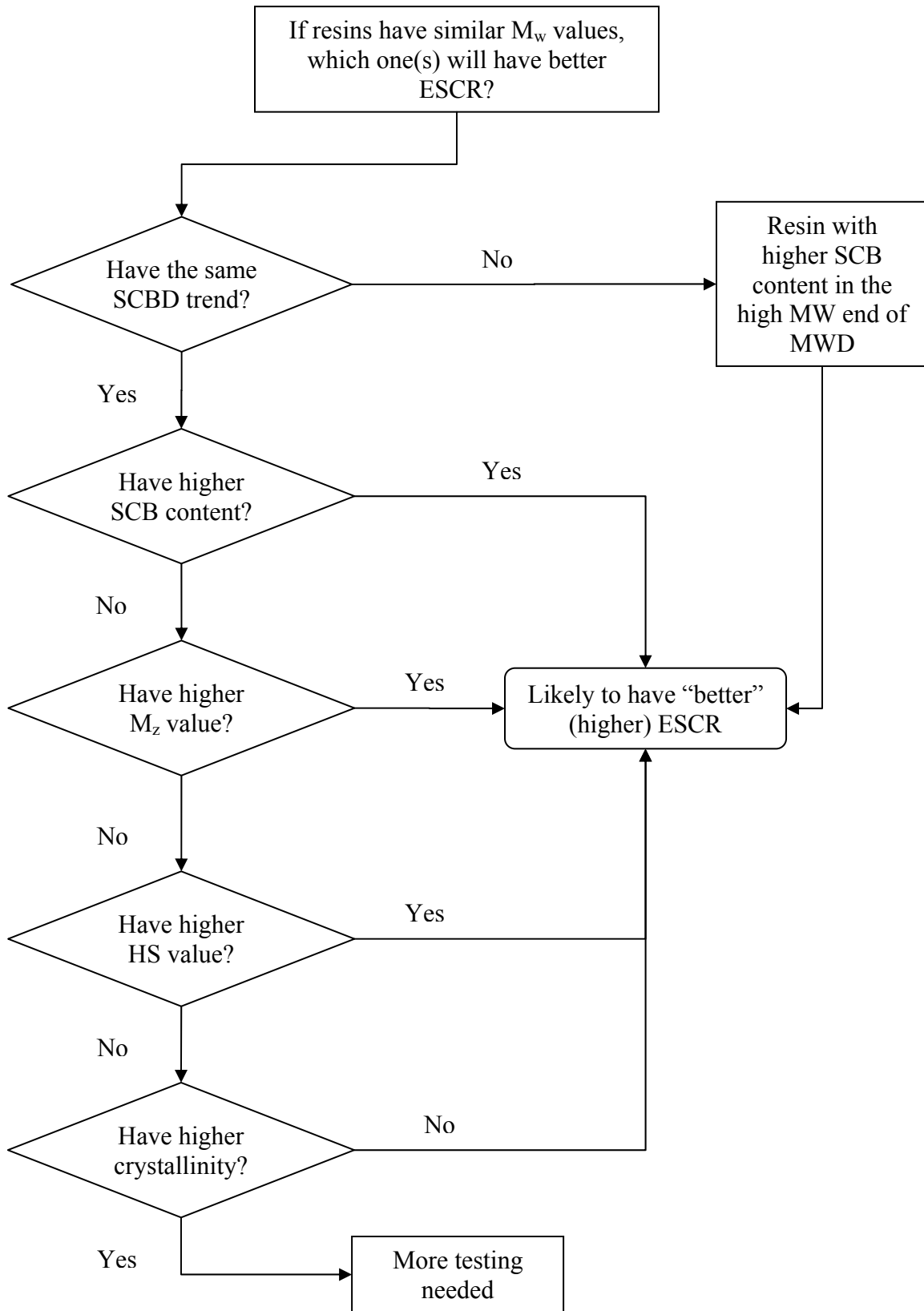


Figure 8.3: Flow chart for selecting resins with better ESCR

## 8.4 Concluding Remarks

In this chapter, we offered an overview of the relationships between molecular properties and environmental stress cracking resistance of polyethylene based on general literature background and our experimental observations. A summary of heuristics relating key molecular properties and ESCR was presented, which discussed one to one influence of molecular characteristics on ESCR of polyethylene. Next, practical prescriptions were given for production of “better” (higher) ESCR resins based on combined influences of molecular weight and short chain branching content of PE. Lastly, as a culmination of our investigation, we presented a decision making pathway, organized in the form of a flow chart with a series of questions, for selection of the resin with optimal ESCR when resins of similar molecular weight are in question. The flow chart is designed to give reasonable (prediction) estimates of the ESCR of resins without necessarily resorting to the use of time consuming tests. The flowchart of Figure 8.3 will be repeated in Chapter 9, in the “Concluding Remarks” section of the thesis, in exactly the same way but with some additional information. In Chapter 9 the diamond-shaped boxes will point to rectangles with the appropriate thesis chapters and/or sections that address the same questions that are posed in the flow chart of Figure 8.3.

## 8.5 References

1. Ward, I. M. (1971), *Mechanical Properties of Solid Polymers*, Wiley-Interscience, Toronto.
2. Janimak, J. J. & Stevens, G. C. (2001), "Inter-relationships between tie-molecule concentration, molecular characteristics and mechanical properties in metallocene catalysed medium density polyethylenes", *Journal of Materials Science*, vol. 36, no. 8, pp. 1879-1884.
3. Huang, Y. & Brown, N. (1988), "The effect of molecular weight on slow crack growth in linear polyethylene homopolymers", *Journal of Materials Science*, vol. 23, pp. 3648-3655.
4. Huang, Y. & Brown, N. (1990), "The dependence of butyl branch density on slow crack growth in polyethylene: kinetics", *Journal of Polymer Science, Part B: Polymer Physics*, vol. 28, pp. 2007-2021.
5. Huang, Y.-L. & Brown, N. (1991), "Dependence of slow crack growth in polyethylene on butyl branch density: morphology and theory", *Journal of Polymer Science, Part B: Polymer Physics*, vol. 29, pp. 129-137.
6. Brown, N., Lu, X., Huang, Y., Harrison, I. P., & Ishikawa, N. (1992), "The Fundamental Material Parameters That Govern Slow Crack-Growth in Linear Polyethylenes", *Plastics Rubber and Composites Processing and Applications*, vol. 17, no. 4, pp. 255-258.
7. Stadler, F. J., Kaschta, J., & Muenstedt, H. (2005), "Dynamic-mechanical behavior of polyethylenes and ethene-/alpha-olefin-co-polymers. Part I. alpha '-relaxation", *Polymer*, vol. 46, no. 23, pp. 10311-10320.
8. Lu, X., Qian, R., & Brown, N. (1995), "The Effect of Crystallinity on Fracture and Yielding of Polyethylenes", *Polymer*, vol. 36, no. 22, pp. 4239-4244.
9. Scheirs, J., Böhm, L. L., Boot, J. C., & Leever, P. S. (1996), "PE100 resins for pipe applications: continuing the development into the 21st century", *Trends in Polymer Science*, vol. 4, no. 12, pp. 408-415.

## **CHAPTER 9 CONCLUDING REMARKS, MAIN CONTRIBUTIONS AND RECOMMENDATIONS**

### **9.1 Concluding Remarks**

In this thesis, relationships between (micro)molecular properties and the mechanical behaviour of polyethylene (PE) were studied. The effects of properties of crystalline and amorphous phases on environmental stress cracking resistance (ESCR) behaviour of polyethylene were investigated. Specific concluding remarks for each topic covered in the chapters of the thesis have been presented at the end of the respective chapters. In this section, the principal conclusions from the research detailed in this thesis are summarized with reference to the relevant chapters.

1. Tensile strain hardening stiffness (HS) is a fast and reliable indicator for evaluating environmental stress cracking resistance of polyethylene (Chapter 4).
2. Physical chain entanglements are a source of inter-lamellar linkages that contribute to ESCR of polyethylene. PE resins with a greater number of chain entanglements have higher environmental stress cracking resistance (Chapters 4 and 5).
3. Polyethylene with a high number of chain entanglements shows greater strain hardening. Physical chain entanglements are the fundamental molecular structure that links tensile strain hardening and environmental stress cracking resistance behaviour of polyethylene (Chapter 5).

4. Investigation of the crystalline phase showed that phase inter-connectivity is an important factor in ESCR of polyethylene. Resins with larger lamella lateral surface area have higher ESCR (Chapter 6).
5. During the course of this project, a duality was observed between environmental stress crack activation energy and the  $\alpha$ -relaxation energy of polyethylene, signifying that environmental stress cracking (ESC) and  $\alpha$ -relaxation may have similar mechanisms (Chapter 7).
6. Polyethylene resins with higher short chain branch (SCB) content have higher ESC crack activation energy (Q), thus pointing to “better” ESCR for these resins (Chapter 7).

## 9.2 Main Contributions of the Thesis

The research in this thesis has made the following original contributions:

1. The tensile strain hardening test method developed in this thesis (Chapter 4) is an extension and improvement on previously presented tensile test methods (1, 2). In the method by Kurelec *et al.* (1) strain hardening tests at room temperature lack sensitivity and are only possible at low strain rates of 0.25 mm/min. Through work in this thesis (Chapter 4), we showed that the strain hardening test at ambient conditions can detect differences in ESCR of resins even at high strain rates of up to at least 7 mm/min, which can ultimately reduce the duration of the test. In the tensile method developed, simpler load-displacement measurements were used rather than true stress and true strain measurements. Thus, the need for specialized, expensive equipment (i.e. optical extensometer) is eliminated. Our

research has provided for a much faster and reliable test that can be readily implemented for practical applications in industry. Discussions are under way with one of our industrial partners regarding using the tensile test developed herein in place of a 25 year old ESCR test standard used in the injection molding industry.

2. Traditionally, most studies on environmental stress cracking resistance of polyethylene had focused solely on the effect of tie-molecules (6). However, there are some deficiencies in the tie-molecule theory when polyethylenes over relatively wide property ranges are considered (7-9). In this thesis, physical chain entanglements are established as another source of inter-lamellar linkages that contribute to environmental stress cracking resistance of polyethylene. Changes in network mobility by changes in molecular weight between chain entanglements ( $M_e$ ) were studied using rheological methods. Reduced network mobility due to an increasing number of chain entanglements was shown to increase ESCR of resins (Chapter 5). A resin with smaller  $M_e$ , and hence a higher number of entanglements, exhibits a higher ESCR.
3. Past work in the field of ESC showed that increasing short chain branch levels increases the ESCR of polyethylene. The reason for this ESCR enhancement was attributed to short chain branches hindering the movement of molecules. Since molecular movements cannot be directly observed, the above reasoning remains a speculation. In our work (Chapter 7), we showed, for the first time, the relationship of increasing ESC crack activation energy ( $Q$ ) with increasing SCB content of resins. Higher ESCR is directly related to higher crack activation

- energy. This observation is a significant contribution towards clarifying the reason why resins with higher SCB content have “better” ESCR.
4. In previous work, molecular weight (MW) and short chain branch (SCB) effects on ESCR of polyethylene were always studied independently of each other (3-5). In this thesis, the combined effects of MW and SCB content were investigated and this revealed complex relationships. For polyethylene with high SCB content in the high molecular weight end of the molecular weight distribution (MWD), increase in ESCR is associated with increases in both the MW and SCB content of the polymer. On the other hand, for polyethylene with high SCB content in the low molecular weight end of the MWD, the same level of ESCR can be achieved by resins that have high MW and low SCB content, or low MW and high SCB content (Chapter 8). It is thus illustrated that the molecular weight and short chain branch effects on environmental stress cracking resistance of polyethylene are multifaceted.
  5. Finally, one of the goals of this research was to contribute to understanding of environmental stress cracking of polyethylene that can lead to the design of resins with “better” (higher) ESCR. In Chapter 8, work from this thesis culminated into a series of heuristics and practical prescriptions that may be used for the production and selection of more environmentally stress cracking resistant polyethylene. Figure 9.1 is a “reproduction” of Figure 8.3 from Chapter 8 but with additional information (all abbreviations used in Figure 9.1 are described later in section 9.3 (as well as in section 8.3)). As explained in section 8.3 of the thesis, by answering the questions in the diamond-shaped boxes selection of

resin(s) with higher ESCR can be achieved. In Figure 9.1, the diamond-shaped boxes point to rectangles with the appropriate thesis chapters and/or sections that address the questions that are posed in the flow chart. This figure serves to illustrate how pieces of work from different chapters of this thesis are inter-related, and eventually contribute to the flow chart for selection of “better” ESCR polyethylene.

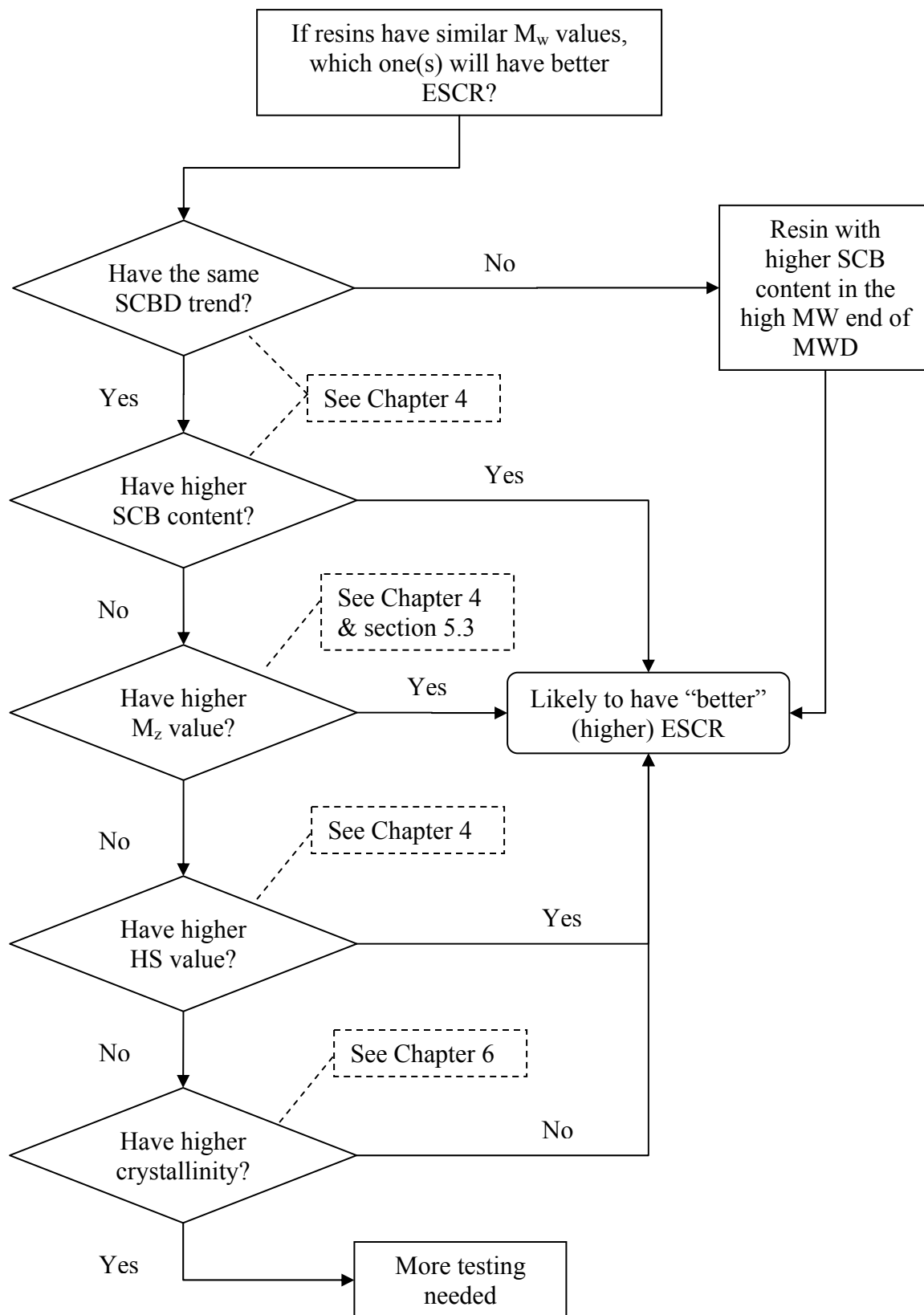


Figure 9.1: Flow chart for selecting resins with better ESCR in relation to thesis chapters

### 9.3 Resin Property Summary

At the beginning of our research, rather limited information was known regarding fundamental properties of our resins, as mentioned in section 3.4. In this section updates to Table 3.1 are presented to demonstrate the progress in understanding of the materials made during the course of this thesis. Table 9.1 contains (micro)molecular properties of resins, and Table 9.2 has mechanical properties of resins determined in the course of the project. In Table 9.1,  $M_n$ ,  $M_w$ , and  $M_z$  stand for number-average, weight-average, and z-average molecular weights. PDI is the polydispersity index, and SCB is short chain branch content per thousand carbon atoms. These properties and the mechanical properties (hardening stiffness (HS), natural draw ratio (NDR), and ESCR) were first presented and discussed in Chapter 4. Discussions regarding rheological indicators,  $\eta_0$  - zero shear viscosity,  $J_e^0$  - steady state compliance,  $G_N^0$  - plateau modulus,  $M_e$  - molecular weight between chain entanglements, and LCBI (long chain branch index (10)) can be found in Chapter 5.  $\Delta H$  is the  $\alpha$ -relaxation energy of resins discussed in Chapter 7 and Appendix E. Lastly, crystalline phase properties (i.e. crystallinity and lamella thickness) were the focus of Chapter 6. Plots for molecular weight distribution (MWD) and short chain branch distribution (SCBD) can be seen in Chapter 4 and Appendix A, respectively. The material property information obtained in this thesis will hopefully aid in the continued advancement of collaborative research (between the disciplines of chemical and civil engineering) on ESCR of polyethylene.

**Table 9.1: Molecular properties of polyethylene resins determined in the course of the thesis**

Resin	M <sub>n</sub> (kg/mol)	M <sub>w</sub> (kg/mol)	M <sub>z</sub> (kg/mol)	PDI M <sub>w</sub> /M <sub>n</sub>	SCB (/1000C)	η <sub>0</sub> (Pa s)	J <sub>e</sub> <sup>0</sup> (1/Pa)	G <sub>N</sub> <sup>0</sup> ( Pa)	M <sub>e</sub> (g/mole)	LCBI	ΔH (kJ/mol)
PE1	16.3	127.5	814.0	7.8	2.8	3.13E+05	2.22E-03	540.2	5403	0.90	109.90
PE2	15.7	118.5	837.1	7.6	1.1	2.00E+05	3.79E-03	317.0	9208	0.86	112.15
PE3	17.9	140.1	889.8	7.8	0.9	5.42E+05	1.43E-03	838.9	3480	0.96	115.14
PE4	19.7	79.4	239.3	4.0	3.8	1.78E+03	3.68E-03	325.9	8958	-0.02	123.86
PE5	11.4	49.7	157.8	4.4	7.0	2.77E+02	7.37E-02	16.3	179194	-0.01	135.27
PE6	14.0	62	195.0	4.4	4.7	6.23E+02	4.14E-02	29	100816	-0.03	128.22
PE7	11.8	222.8	1593.5	18.9	4.3	8.19E+05	6.30E-04	1904.3	1533	0.58	147.05
PE8	14.0	202.1	1398.4	14.4	4.5	2.03E+06	4.07E-04	2950.1	990	0.96	150.48
PE9	10.4	217.9	1244.2	20.9	7.0	1.12E+06	6.51E-04	1843.4	1584	0.69	149.03
PE10	5.9	315.4	2129.3	53.3	11.8	6.07E+06	1.34E-04	8951.7	326	0.86	155.05

**Table 9.1: Molecular properties of polyethylene resins determined in the course of the thesis (Cont'd)**

Resins	Determined from DSC			Determined from X-Ray diffraction		
	%crystallinity	Melting temperature (°C)	Lamella thickness (nm)	%crystallinity	Long period (nm)	Lamella thickness (nm)
PE1	55.4%	130.5	15.3	61.9%	24.27	13.3
PE2	58.8%	135.5	26.8	70.2%	28.68	16.7
PE3	57.9%	134.1	22.3	66.4%	25.53	14.7
PE4	55.1%	130.1	14.7	60.2%	23.31	12.7
PE5	53.9%	129.1	13.6	61.1%	19.94	10.7
PE6	56.6%	129.8	14.4	63.0%	21.6	12.1
PE7	53.3%	130.7	15.5	60.0%	24.75	13.1
PE8	56.2%	128.6	13.1	60.3%	26.61	14.8
PE9	61.5%	129.9	14.6	63.3%	24.27	14.9
PE10	51.1%	127	11.7	59.5%	24.54	12.4

**Table 9.2: Mechanical properties of polyethylene resins determined in the course of the thesis**

Resin	Strain rate - 0.5 mm/min		Strain rate – 7 mm/min		ESCR (hours)
	Hardening stiffness (N/mm)	NDR	Hardening stiffness (N/mm)	NDR	
PE1	0.25	7.2	0.527	8.6	4.8
PE2	-	-	-	-	1.2
PE3	-	-	-	-	2.8
PE4	0.183	9.3	0.287	10.5	3.6
PE5	-	-	-	-	N/A
PE6	-	-	-	-	N/A
PE7	0.657	6.1	0.94	7.1	1395.8
PE8	0.578	7	0.73	6.3	198.3
PE9	0.609	6.4	0.895	7.1	843.4
PE10	0.663	6.6	1.008	6.9	>3000

-, Resin could not be tested using the tensile method, reasons listed in Table 4.12

N/A, Resin ESCR value could not be measured, reasons discussed in section 4.3.1

## 9.4 Recommendations for Future Steps

- Oscillating shear experiments provide insights into the entanglement nature of resins and were used in this thesis. For the next step, rheological experiments in extensional flow should be considered. Strain hardening behaviour of a polymer melt in extensional flow (11) can be more readily linked to influences of chain entanglements in the system. Comparisons between tensile strain hardening behaviour in the melt and the solid state could provide new insights into influences of chain entanglements on mechanical behaviour.
- Although an interactive relationship between molecular weight and short chain branch content of polyethylene is observed, further investigations are needed to clarify the exact nature of the interaction. A full factorial design covering all levels of the key parameters presented in this thesis would give more information about effect interactions. One possible way to cover all levels of a factorial design is to blend resins. For example, PE3 (high MW, low SCB content) could be blended in different proportions with PE4 (low MW and high SCB content) to give rise to materials of different levels of MW and SCB content.
- Tensile strain hardening stiffness (HS) was demonstrated to have a directly proportional relationship with environmental stress cracking resistance of polyethylene. A gap exists between HS data for high ESCR and low ESCR resins. Blending of high ESCR and low ESCR resins could help fill this gap. With more data points, it would be possible to determine the exact nature of the relationship between hardening stiffness and ESCR of polyethylene.

- Efforts should be made to refine the tensile strain hardening test. An investigation should be carried out to determine the best dogbone dimensions for the test. For instance, a shorter dogbone than the one used in the thesis may allow for faster testing because a smaller specimen would reach full extension, and hence strain hardening, faster. In addition, the effects of processing conditions on tensile strain hardening test, such as different cooling rates, should be pursued.
- As part of tensile test measurements, natural draw ratio (NDR) showed promise as a possible indicator of ESCR of polyethylene. Efforts should be spent to resolve the issue of data scattering in NDR measurements, possibly through refinement of the test procedure.
- The attempt at developing a model for estimating the environmental stress cracking lifetime of polyethylene showed large sensitivity to the exponential term in Equation 7.4. To overcome this sensitivity, modifications of the equation or some transformation of the data (e.g., Box-Cox transformation) could be investigated.
- Duality was observed between environmental stress crack activation energy and the  $\alpha$ -relaxation energy for some of the resins tested in this thesis. This topic should be further explored to study the nature of this duality and whether it exists in other polyolefins.
- The approach used in this thesis for relating (micro)molecular properties and mechanical behaviour can be extended to other polymer materials. A collaborative effort with a multi-national company is currently underway to apply

our approaches to the study of creep behaviour of epoxy polymers used in structural concrete anchor applications.

## 9.5 References

1. Kurelec, L., Teeuwen, M., Schoffeleers, H., & Deblieck, R. (2005), "Strain hardening modulus as a measure of environmental stress crack resistance of high density polyethylene", *Polymer*, vol. 46, pp. 6369-6379.
2. Maxwell, A. S. & Pilkington, G. (2008), "Prediction of environmental stress cracking resistance in linear low density polyethylenes", *Polymer Engineering and Science*, vol. 48, no. 2, pp. 360-364.
3. Brown, N., Lu, X., Huang, Y., Harrison, I. P., & Ishikawa, N. (1992), "The Fundamental Material Parameters That Govern Slow Crack-Growth in Linear Polyethylenes", *Plastics Rubber and Composites Processing and Applications*, vol. 17, no. 4, pp. 255-258.
4. Huang, Y. & Brown, N. (1990), "The dependence of butyl branch density on slow crack growth in polyethylene: kinetics", *Journal of Polymer Science, Part B: Polymer Physics*, vol. 28, pp. 2007-2021.
5. Janimak, J. J. & Stevens, G. C. (2001), "Inter-relationships between tie-molecule concentration, molecular characteristics and mechanical properties in metallocene catalysed medium density polyethylenes", *Journal of Materials Science*, vol. 36, no. 8, pp. 1879-1884.
6. Huang, Y. & Brown, N. (1988), "The effect of molecular weight on slow crack growth in linear polyethylene homopolymers", *Journal of Materials Science*, vol. 23, pp. 3648-3655.
7. Yeh, J. T. & Runt, J. (1991), "Fatigue crack propagation in high-density polyethylene", *Journal of Polymer Science, Part B: Polymer Physics*, vol. 29, pp. 371-388.
8. Hubert, L., David, L., Séguéla, R., Vigier, G., Corfias-Zuccalli, C., & Germain, Y. (2001), "Physical and mechanical properties of polyethylene for pipes in relation to molecular architecture. I. microstructure and crystallisation kinetics", *Journal of Applied Polymer Science*, vol. 42, pp. 8425-8434.
9. Brown, N. & Ward, I. M. (1983), "The influence of morphology and molecular weight on ductile-brittle transitions in linear polyethylene", *Journal of Materials Science*, vol. 18, pp. 1405-1420.
10. Shroff, R. N. & Mavridis, H. (1999), "Long-chain-branching index for essentially linear polyethylenes", *Macromolecules*, vol. 32, pp. 8454-8464.

11. Wagner, M. H., Bastian, H., Hachmann, P., Meissner, J., Kurzbeck, S., Munstedt, H., & Langouche, F. (2000), "The strain-hardening behaviour of linear and long-chain-branched polyolefin melts in extensional flows", *Rheologica Acta*, vol. 39, no. 2, pp. 97-109.

## **APPENDICES**

## **APPENDIX A: SHORT CHAIN BRANCH DISTRIBUTION**

Characterization of comonomer (short chain branching (SCB)) distribution of polyethylene is obtained by coupling an online Fourier Transform Infrared Spectroscopy (FTIR) detector to a size exclusion (gel permeation) chromatography (SEC/GPC) set-up (1). In GPC, dissolved polymer molecules move through packed columns with packing of different pore sizes and they are thus fractionated (separated) according to their hydrodynamic volume. In principle, lower molecular weight (MW) molecules have smaller hydrodynamic volume and higher retention time, while higher MW molecules have larger hydrodynamic volume and lower retention time. In FTIR-GPC, each eluting fraction is passed through a FTIR detector where chemical groups are identified based on their absorption spectra. Methyl groups are known to have a peak in the 1200 to 800  $\text{cm}^{-1}$  region of the FTIR spectra (1). In order to quantify the number of methyl groups, a FTIR calibration curve based on polymer of known methyl content is used. The intensity of the methyl group ( $\text{CH}_3$ ) signal in each eluting fraction is compared to the calibration curve and the number of methyl groups per thousand carbon atoms is then estimated. The FTIR determination of methyl groups includes contributions from both short chain branching and polymer chain ends.

In Figures A.1-A.10, the molecular weight distribution (MWD) and short chain branch distribution (SCBD) for PE1-10 (resins used throughout this thesis) are presented. In each graph, the x-axis gives the logarithmic transformation of molecular weight values, the left y-axis gives the weight fraction of polymer chains with a specific molecular weight value, and the right y-axis denotes the number of methyl groups per thousand

carbon atoms for polymer chains of a specific molecular weight. In FTIR, the methyl end unit measurements do not distinguish between different sources of the CH<sub>3</sub> group, therefore, they are not true SCB measurements and should not be directly compared to SCB measured using methods such as <sup>13</sup>C NMR (as discussed in Chapter 4). Despite not being true SCB measurements, on a relative basis the trend of the number of methyl groups per thousand carbon atoms still gives an indication of the SCBD characteristics of a resin. For the purpose of discussion, the number of methyl groups per thousand carbons will be referred to as “SCBD”.

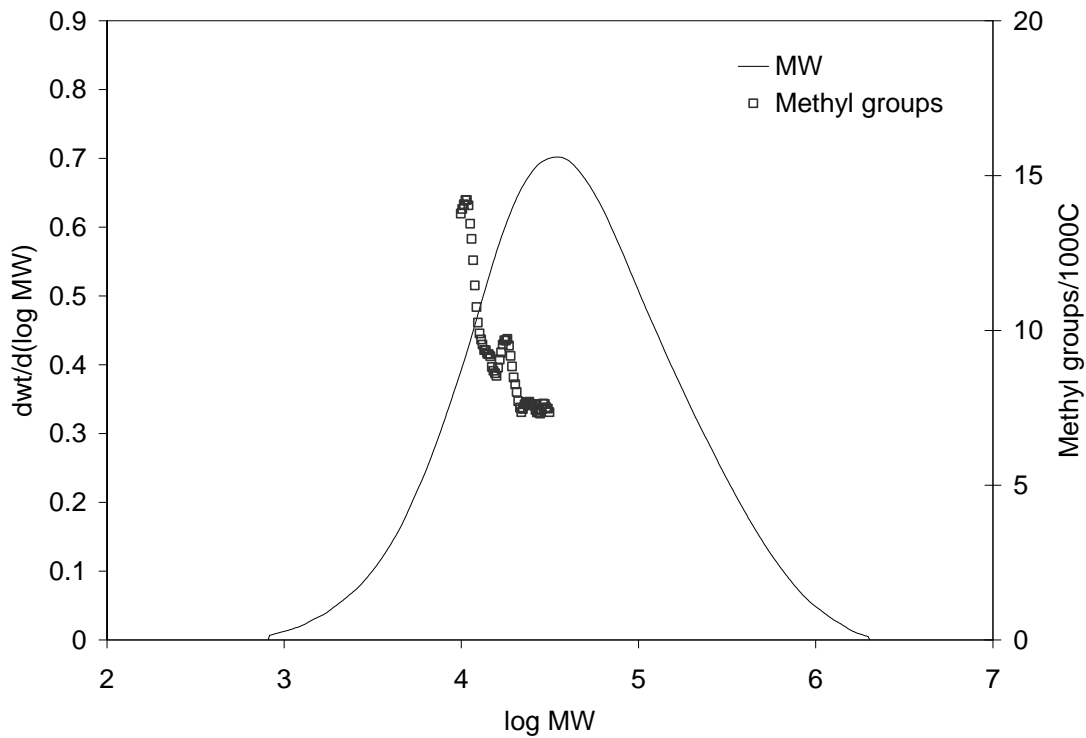
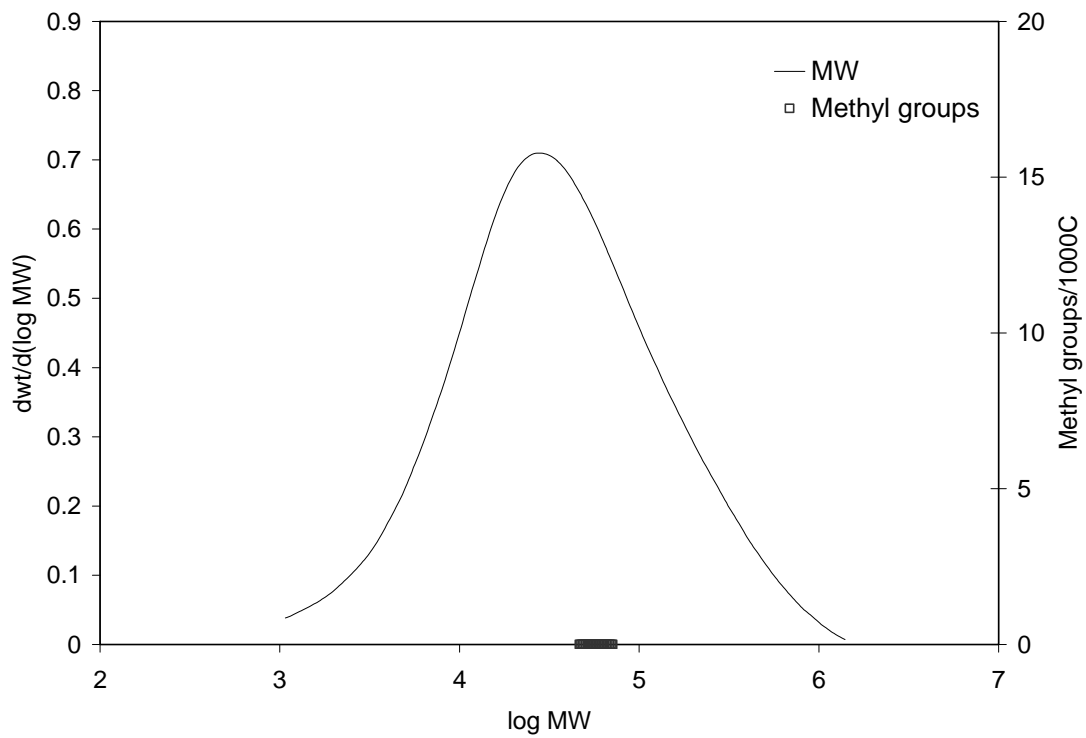
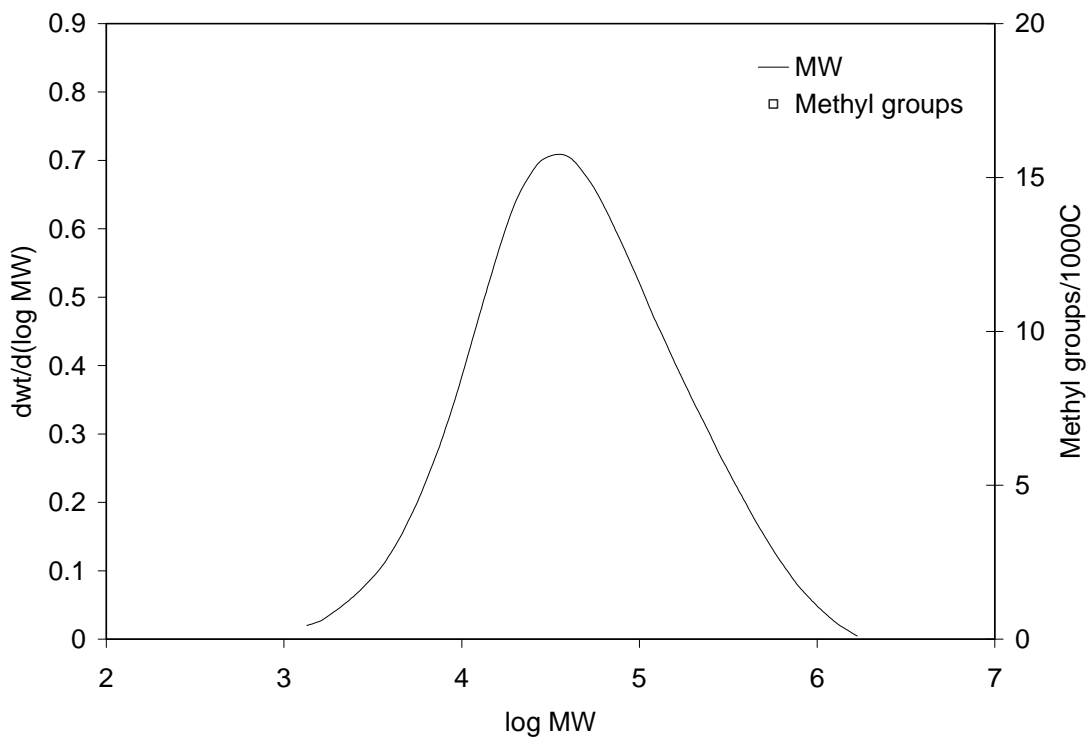


Figure A.1: PE1 MWD and “SCBD”



**Figure A.2: PE2 MWD and "SCBD"**



**Figure A.3: PE3 MWD and "SCBD"**

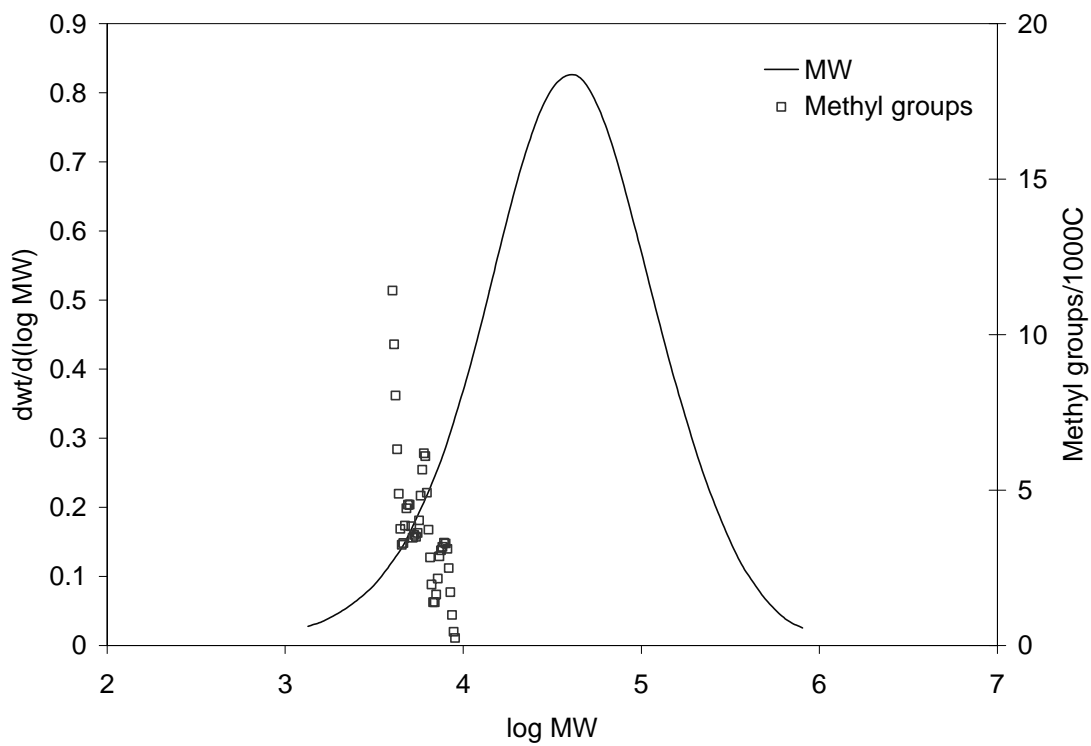


Figure A.4: PE4 MWD and "SCBD"

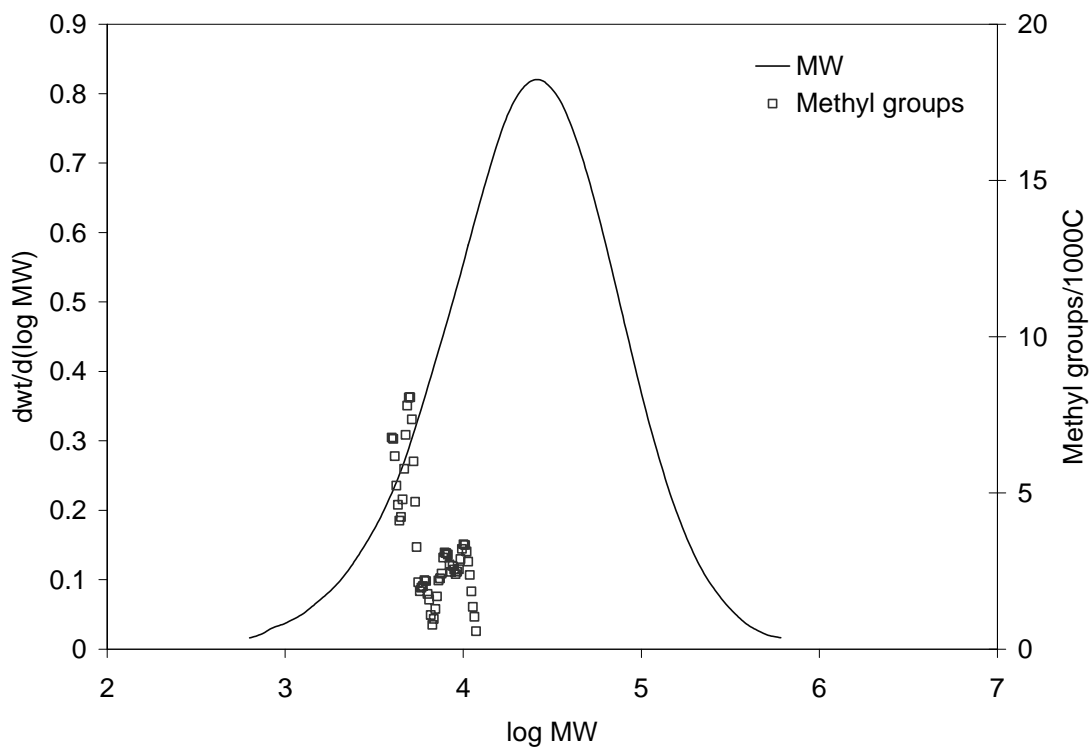


Figure A.5: PE5 MWD and "SCBD"

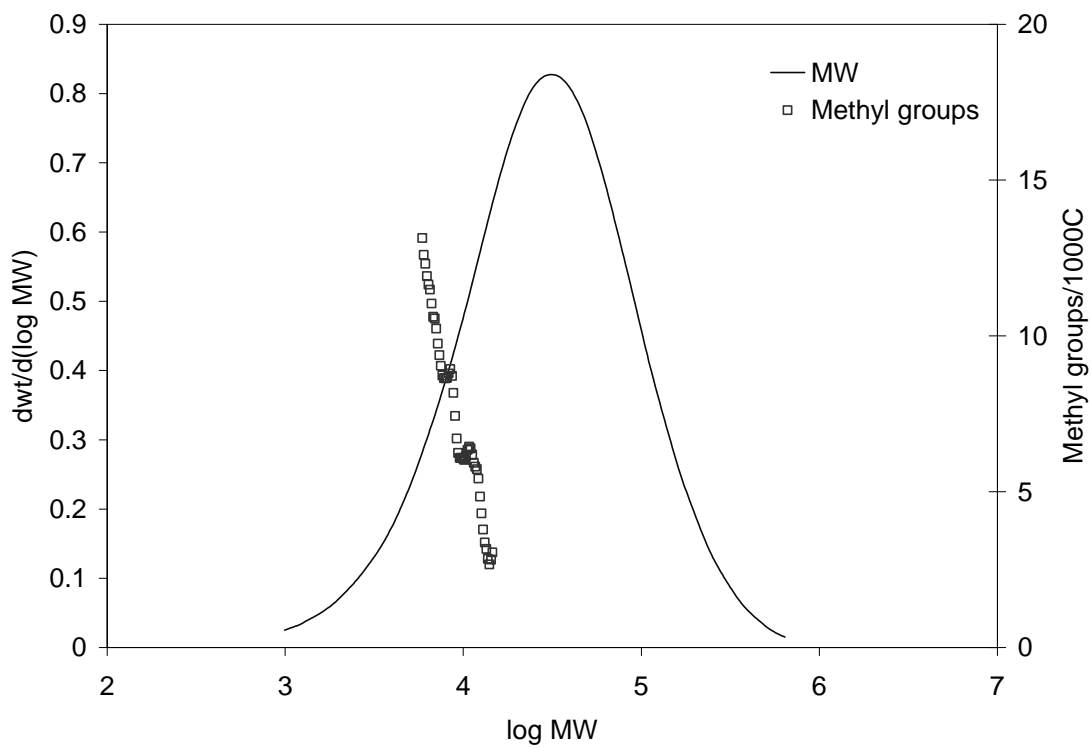


Figure A.6: PE6 MWD and "SCBD"

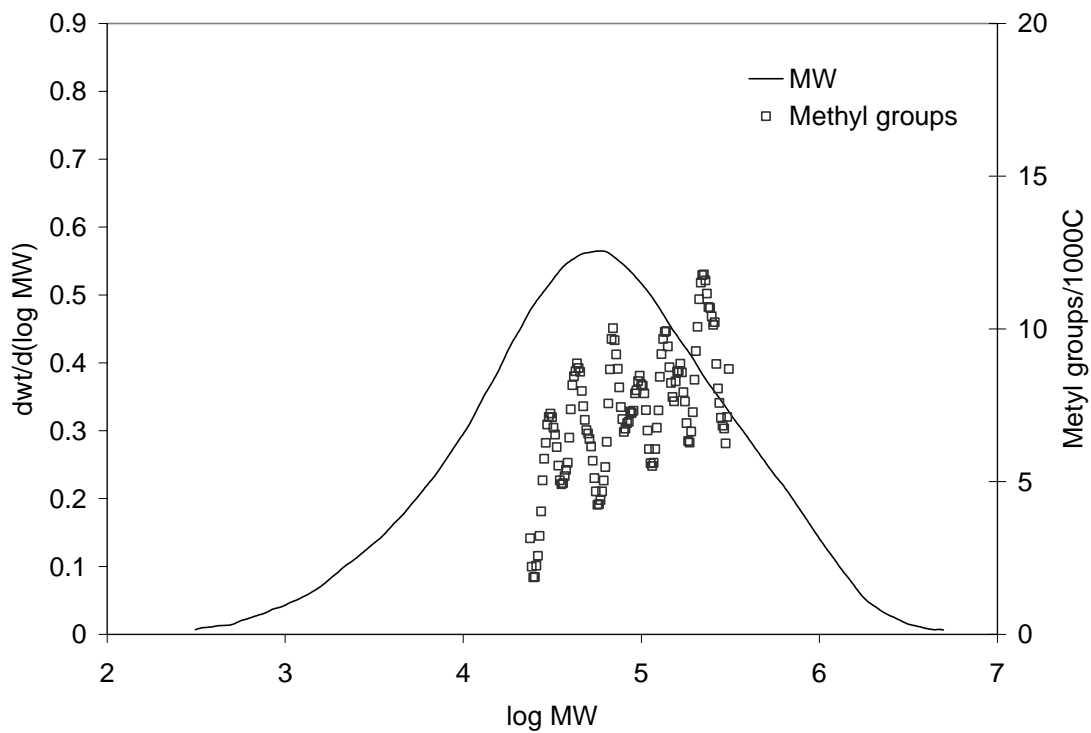


Figure A.7: PE7 MWD and "SCBD"

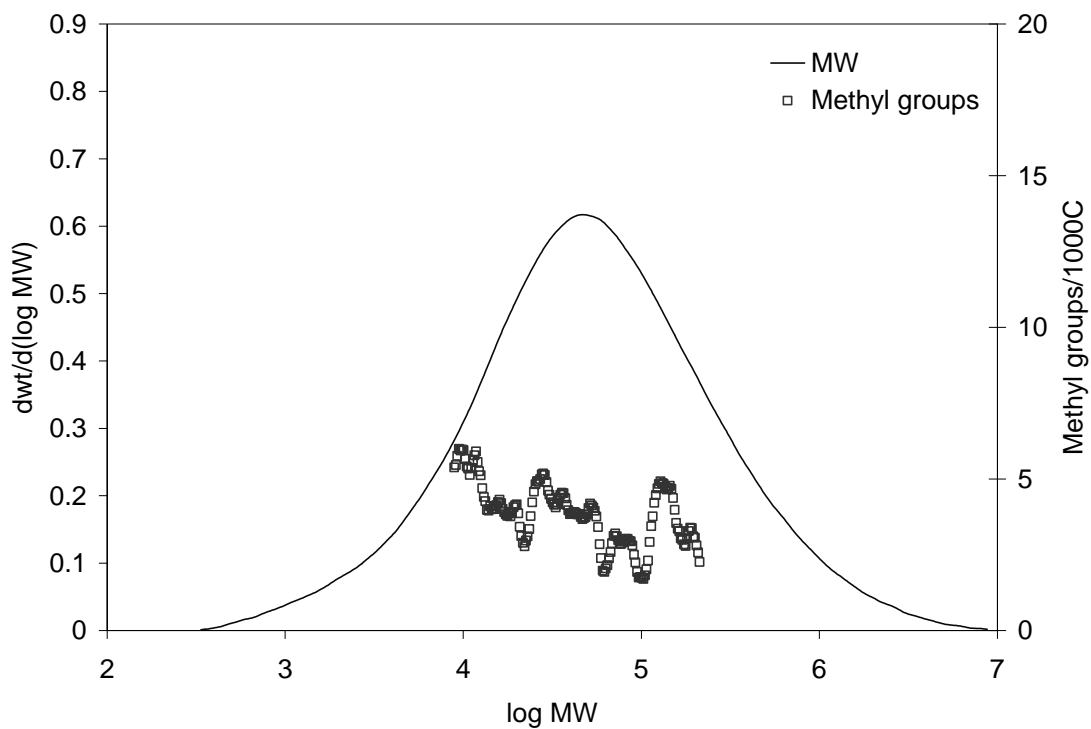


Figure A.8: PE8 MWD and “SCBD”

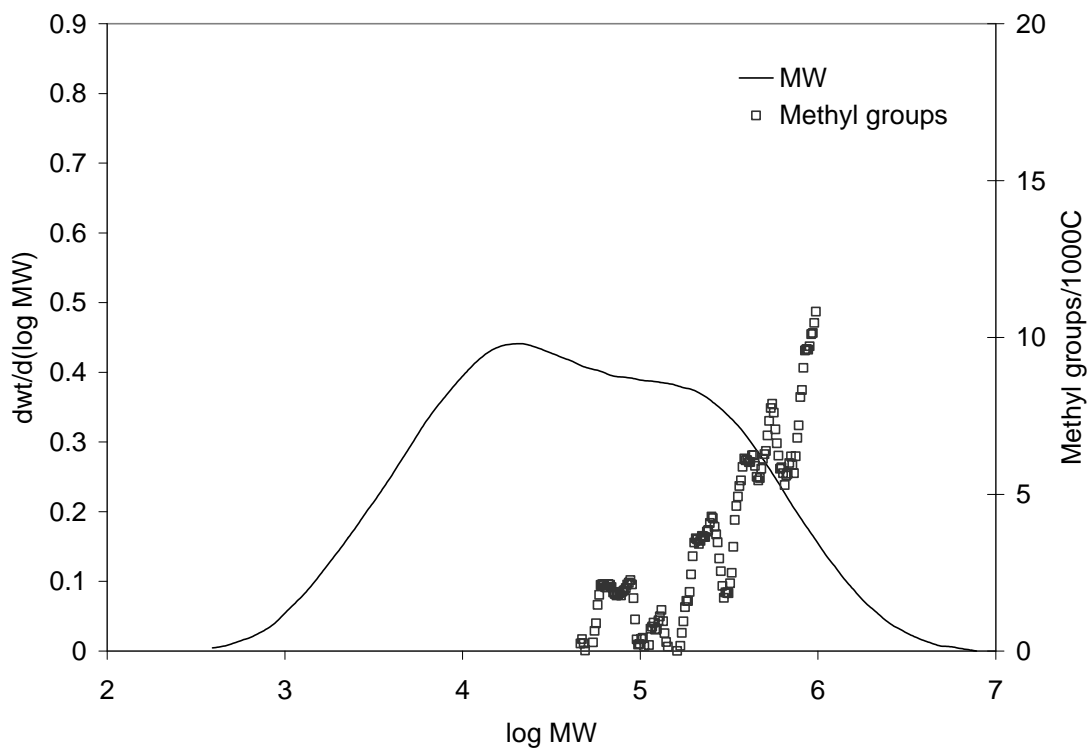
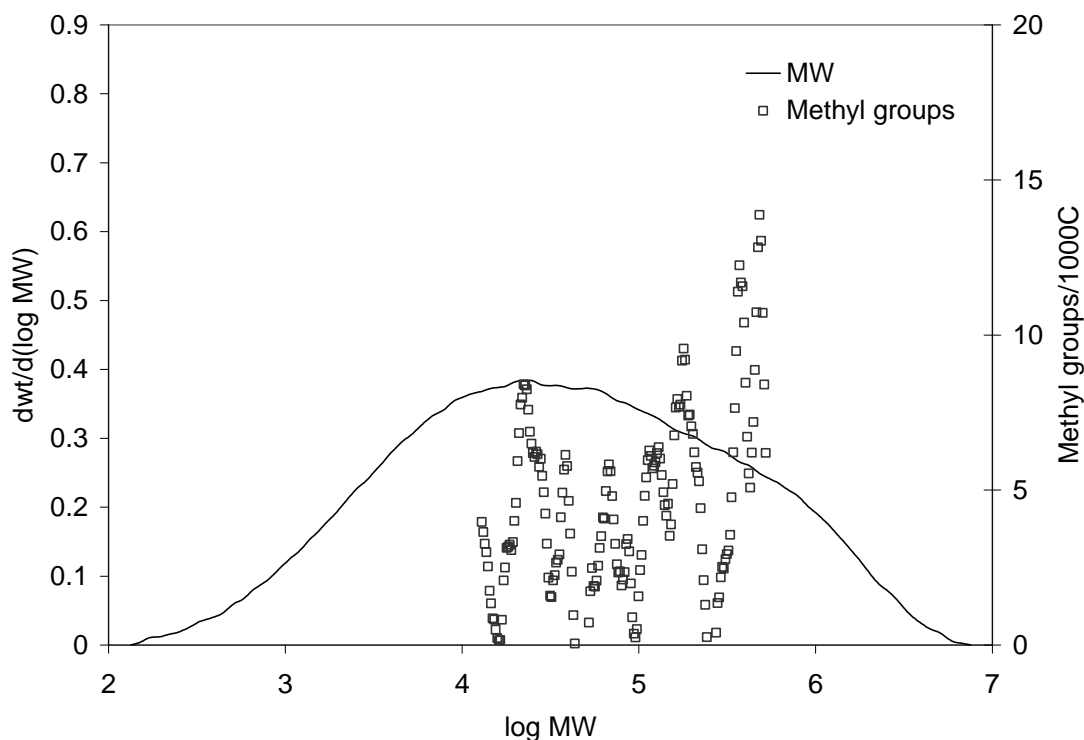


Figure A.9: PE9 MWD and “SCBD”



**Figure A.10: PE10 MWD and “SCBD”**

The graphs for PE1 and PE4-6 (Figure A.1 and Figures A.4-A.6, respectively) show higher methyl content in the lower molecular weight end of the MWD. These resins were produced using Ziegler-Natta catalysts. This type of catalyst is known to produce PE with higher SCB content in the low molecular weight end of the molecular weight distribution (Figure A.11a). For PE2 and PE3, Figures A.2 and A.3, respectively, no “SCBD” was detected because of the low SCB content of these resins.  $^{13}\text{C}$  NMR measurements of PE2 and PE3 showed SCB content of one or fewer SCB per thousand carbon atoms (see Chapter 4). Unlike LLDPEs (linear low density polyethylene) which typically have 50 SCB per 1000 carbon atoms, HDPEs (high density polyethylene) generally have less than 5 SCB per 1000 carbon atoms. The GPC-FTIR technique is

known to have a poor signal to noise ratio when dealing with HDPE because of the low comonomer content of the polymer (1).

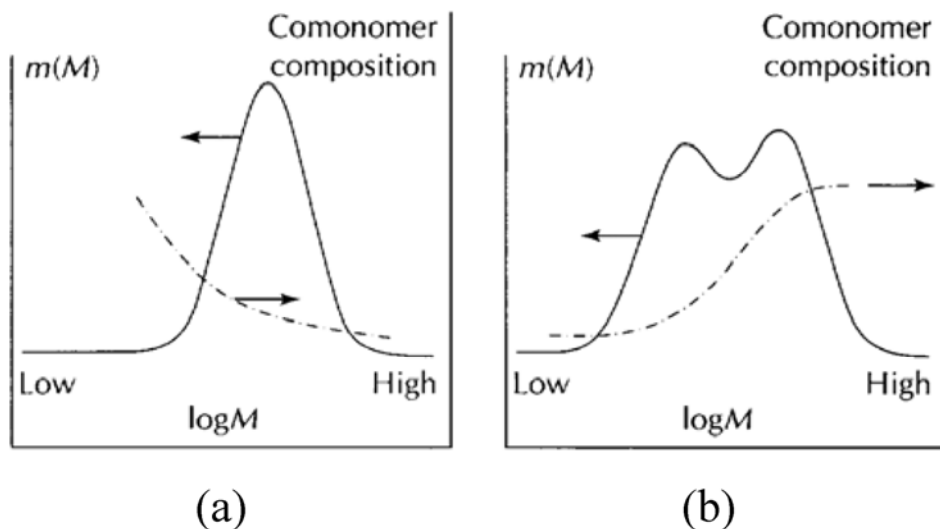


**Figure A.11: Typical comonomer composition/SCB distribution for (a) polyethylene produced using Ziegler-Natta catalyst, (b) polyethylene produced using Ziegler-Natta catalyst in tandem process. From ref. (2)**

On the contrary, for resins PE7, PE9 and PE10 (see Figures A.7 and A.9-A.10) a trend of higher methyl content associated with the higher MW end of the MWD is observed. For polyethylene produced by tandem reactors (2), higher SCB content in the high MW end of the MWD is possible (Figure A.11b). The bimodal MWD of PE9 and PE10 (Figures A.9 and A.10) is a trait typical of the tandem process (2). In Figure A.8, PE8 shows methyl content in the higher MW chains with an overall “flatter” trend, yet the supplier of PE8 stated that it should have a SCB content that is higher in the high MW end of the MWD similar to PE9 and PE10. The detection of a flat “SCBD” trend rather than an increasing “SCBD” trend could be due to the broad MWD of PE8. Indeed, the “SCBD” data for PE7, PE9 and PE10 also shows large fluctuations because of their broad MWD.

In addition to problems related to low comonomer content, the signal to noise ratio of GPC-FTIR is also known to decrease with increasing breadth of the polymer MWD. In Figure A.12, the FTIR signal to noise ratio is plotted as a function of the polydispersity (PDI) of polyethylene. In the plot, as PDI increases from 1 to 70, the signal/noise ratio decreases from 1000/1 to less than 200/1. As the breadth of the MWD increases, the contribution of chain end  $\text{CH}_3$  groups increases as well, thus making the actual detection of “SCBD” increasingly uncertain (1).

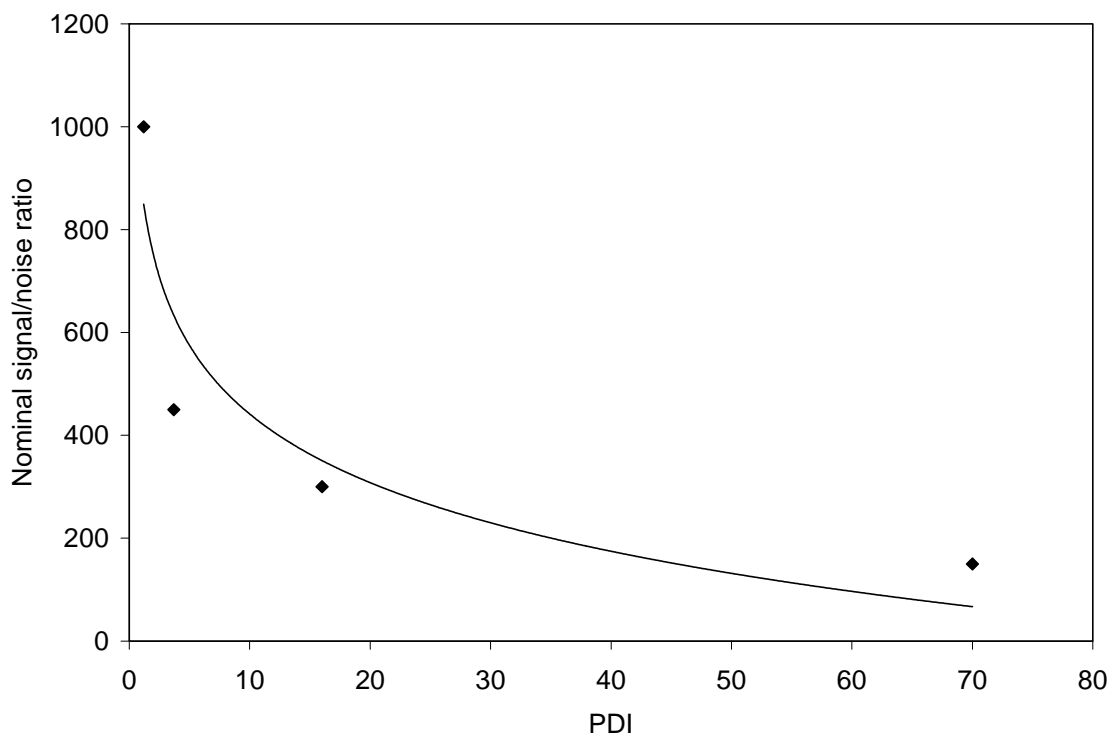


**Figure A.12: FTIR nominal signal to noise ratio vs. polydispersity (PDI). From ref. (1)**

## References

1. DesLauriers, P. J. (2003), "Measuring compositional heterogeneity in polyolefins using size-exclusion chromatography/Fourier transform infrared spectroscopy", *American Chemical Society (ACS) Symposium Series*, vol. 893, pp. 210-229.
2. Scheirs, J., Böhm, L. L., Boot, J. C., & Leever, P. S. (1996), "PE100 resins for pipe applications: continuing the development into the 21st century", *Trends in Polymer Science*, vol. 4, no. 12, pp. 408-415.

## **APPENDIX B: CRYSTALLIZATION ANALYSIS FRACTIONATION (CRYSTAF) AND ESCR**

Environmental stress crack (ESC) is a major concern for the polymer industry (1). It is costly (cost of both materials and labour) to have to replace polyethylene (PE) structures that failed before the end of their expected service life-span. The NCLT test gives some indication of the environmental stress cracking resistance (ESCR) of polyethylene materials relative to one another, but the test is semi-empirical in nature. It is desirable to develop a method for evaluating ESCR of polyethylene based on more fundamental properties of polyethylene. Such a successful effort was described in Chapter 4, whereby tensile strain hardening stiffness (HS) of several polyethylene resins was shown to correlate successfully/reliably to ESCR of the materials. PE with higher ESCR has shown corresponding higher hardening stiffness values. This was the first time a fundamental polyethylene characteristic was related to ESCR. Before our effort in Chapter 4, prior research attempted to derive similar correlations using crystallization analysis fractionation (CRYSTAF), where crystallization behaviour of polyethylene in solution was linked to its ESCR.

Soares *et al.* (2) attempted to relate CRYSTAF results to ESCR of polyethylene. They correlated the weight percentage of chains that crystallize in the 75-85°C temperature range during CRYSTAF analysis to ESCR of PE. An increasing ESCR was associated with an increasing weight percentage of these chains. The crystallization temperature of PE decreases with increasing short chain branch (SCB) content (3, 4) because SCB cannot be incorporated readily into the crystalline lamella of the polymer (5). CRYSTAF

analysis utilizes this behaviour and measures changes in the concentration of dilute polymer solution during cooling to give estimates of weight percentage of polymer material that crystallizes at different temperatures (6).

CRYSTAF analysis was also carried out for resins in this study following procedure stated in section 3.1.2. Figure B.1 is the CRYSTAF plot for PE10. The solid line is the cumulative distribution of polymer solution concentration with respect to temperature. The dotted line shows the first derivative of the cumulative distribution ( $dC/dT$ ). The  $dC/dT$  curve has a peak value around  $85^{\circ}\text{C}$ , typical for polyethylene (6). As the SCB content of the polymer increases, the  $dC/dT$  peak will move towards lower temperatures (6). Similar curves to the ones shown in Figure B.1 were obtained for the other resins (not shown here for all resins for the sake of brevity). In Figure B.2, independent replicates of PE10 are shown, and the close alignment of the  $dC/dT$  curves indicates good reproducibility of the CRYSTAF analysis.

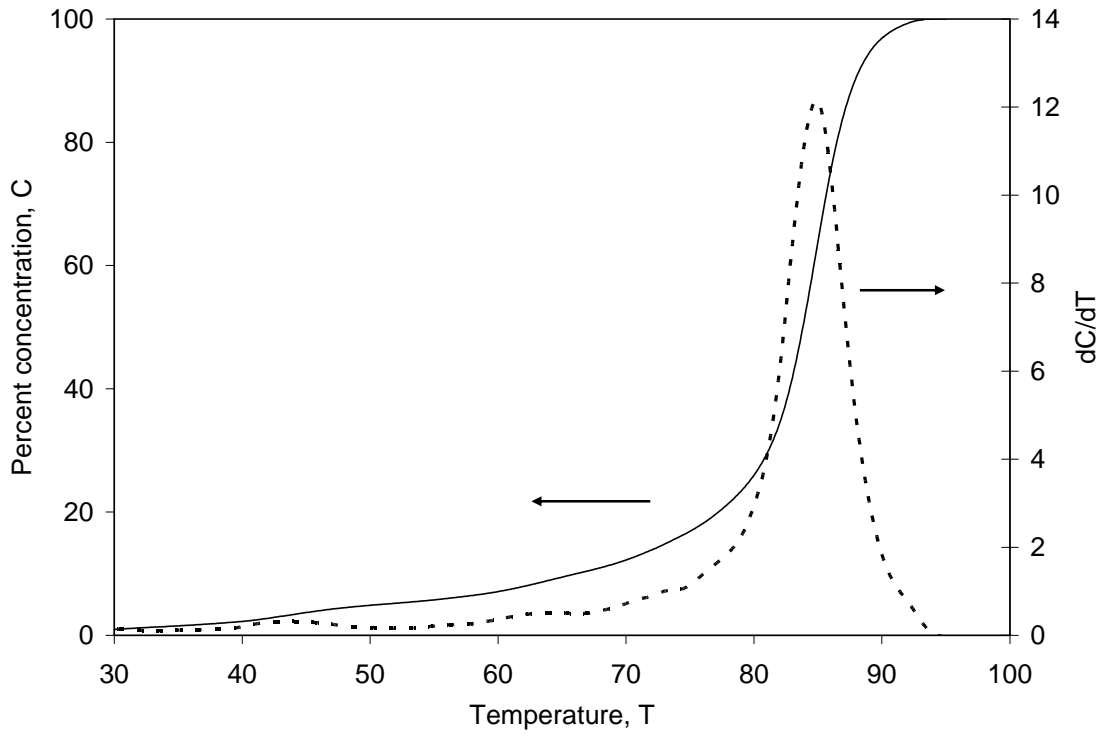


**Figure B.1: CRYSTAF result for PE10**

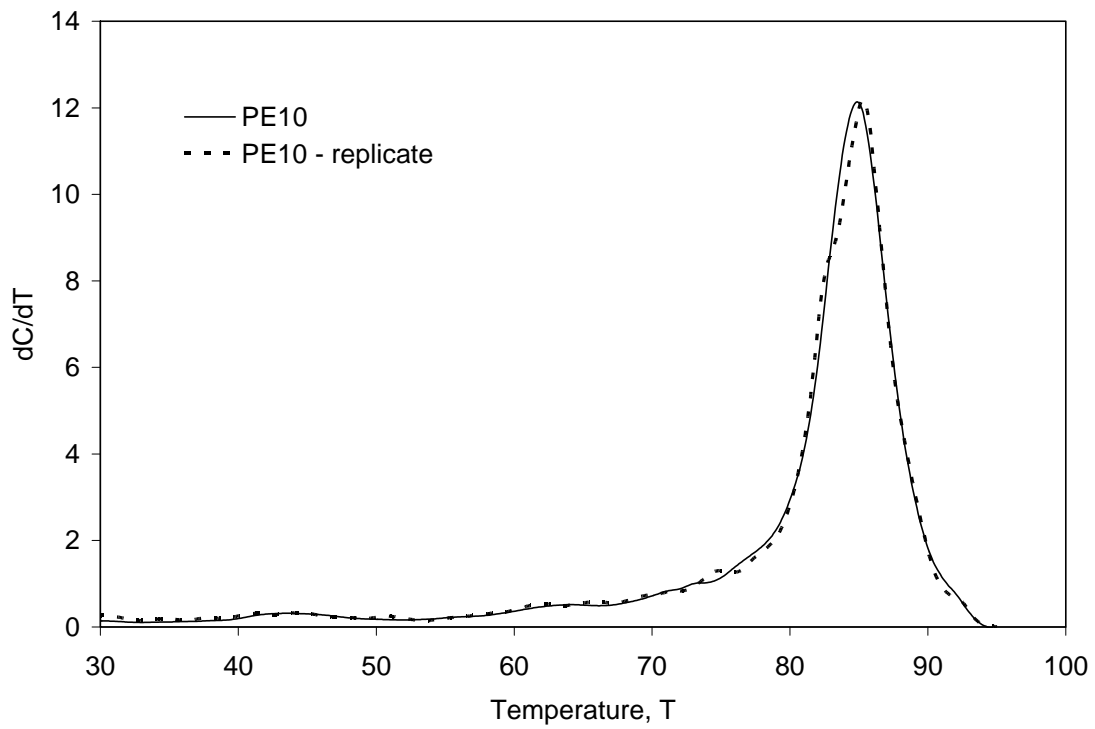


**Figure B.2: CRYSTAF results with independent replication for PE10**

The weight percentage of chains crystallized over a specific temperature interval is calculated by integrating the dC/dT curve. For example, the area under the curve between 80-90°C divided by the whole area under the dC/dT curve gives the weight percentage of chains crystallized in the 80-90°C temperature range. Following this procedure, weight percentages of chains crystallized at different temperature ranges are determined and presented in Table B.1 for the resins in this study. For all resins, over 50% (by weight) of chains crystallize in the 75-90°C range, an indication of low SCB content for the resins, which is characteristic of high density polyethylene.

**Table B.1: Weight percentage of crystallizable chains at different temperature ranges in CRYSTAF and other material properties**

	<75□C	75-85□C	85-90□C	>90□C	M <sub>w</sub> (kg/mol)	SCB (/1000C)	ESCR (hours)
PE1	6.4%	71.0%	22.2%	0.5%	127.5	2.8	4.8
PE2	4.6%	35.1%	59.4%	0.8%	118.5	1.1	1.2
PE3	4.3%	50.7%	44.9%	0.1%	140.1	0.9	2.8
PE4	27.1%	61.0%	11.9%	0.0%	79.4	3.8	3.6
PE5	27.4%	57.1%	15.1%	0.3%	49.7	7	-
PE6	12.7%	58.3%	28.8%	0.3%	62	4.7	-
PE7	24.8%	60.5%	17.5%	0.8%	222.8	4.3	1395
PE8	16.2%	81.4%	2.4%	0.0%	202.1	4.5	198
PE9	16.2%	62.4%	20.4%	0.9%	217.9	7	872
PE10	16.8%	47.9%	32.3%	3.0%	315.4	11.8	>3000

Soares *et al.* (2) proposed a correlation between ESCR and CRYSTAF measurements based on the idea of inter-lamellar links. They theorized that polyethylene chains that crystallize in the 75-85°C temperature range during CRYSTAF contain SCB and have sufficiently high molecular weight (MW) to form into both crystalline lamellae and inter-lamellar linkages, hence their presence enhances the ESCR of the polymer. PE with higher MW is known to have higher ESCR (7). Therefore, polyethylenes which contain a

higher weight percentage of chains that crystallize in the 75-85°C temperature range would have higher environmental stress cracking resistance.

In Figure B.3, ESCR of resins is plotted against weight percentage of chains crystallized in the 75-85°C range. For PE1-4, a relationship of increasing ESCR with increasing weight percentage is observed. This behaviour is similar to that reported by Soares *et al.* (2). In contrast, for PE7-10, decreasing ESCR values are observed with increasing weight percentage of crystallized chains in the 75-85°C temperature range. In addition, PE5 and PE6 have a higher weight percentage of chains crystallized in the 75-85°C temperature range than PE2 and PE3, yet PE5 and PE6 are brittle materials that do not have measureable ESCR. It seems that the proposed chain crystallization temperature range (75-85°C) that is supposed to be an indicator of ESCR of polyethylene cannot be applied to all resins.

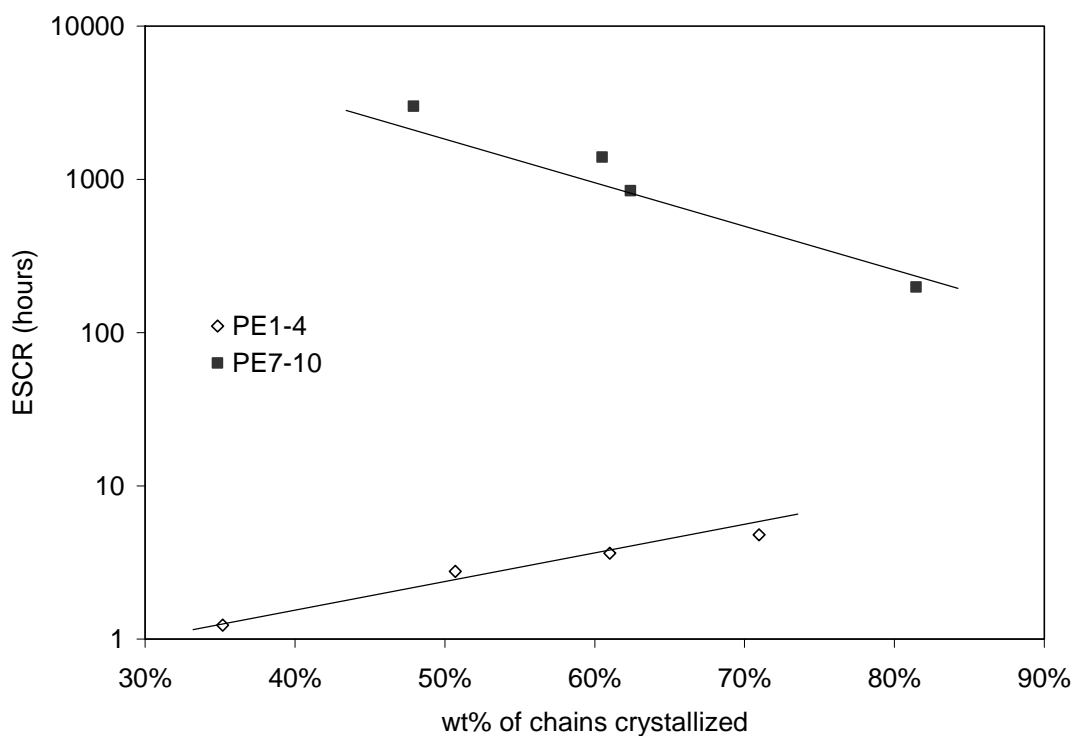


**Figure B.3: Weight percentage of chains crystallized in 75-85°C range and ESCR of resins**

Polymer molecules with sufficiently long chain length for forming inter-lamellar links may not be limited to just chain lengths that crystallize in the 75-85°C temperature range. There may be other chain lengths that allow polymer molecules to form effective inter-lamellar linkages. The specific temperature at which a polymer crystallizes is a function of its chain length (8, 9), therefore, these other chain lengths would crystallize at a temperature different from the 75-85°C temperature range. The identification of crystallization temperature (ranges), hence chain length(s), which would influence the ESCR of resins is subsequently based on the following reasoning. Polyethylene with more inter-lamellar links has higher ESCR; inter-lamellar links are formed by molecules of long chain lengths; the more of these long chain length molecules a resin has, the higher the corresponding weight percentage; this essentially manifests itself as a higher

weight percentage of chains that crystallize at a specific temperature (range) in CRYSTAF. We will call such temperature range(s) “ESCR-TR” for short.

In Figure B.4, ESCR values of resins are plotted against weight percentage values of chains crystallized in CRYSTAF. For PE1-4, data from the 75-85°C temperature range are plotted, similar to those shown in Figure B.3. However, for PE7-10, data on weight percentage of crystallized chains from the 85-90°C range are plotted. This time, an increasing ESCR is observed for both groupings (PE1-4 and PE7-10) with increasing weight percentage of crystallized chains. Figure B.4 clearly illustrates that ESCR-TR is not limited to the 75-85°C temperature range as previously reported (2).

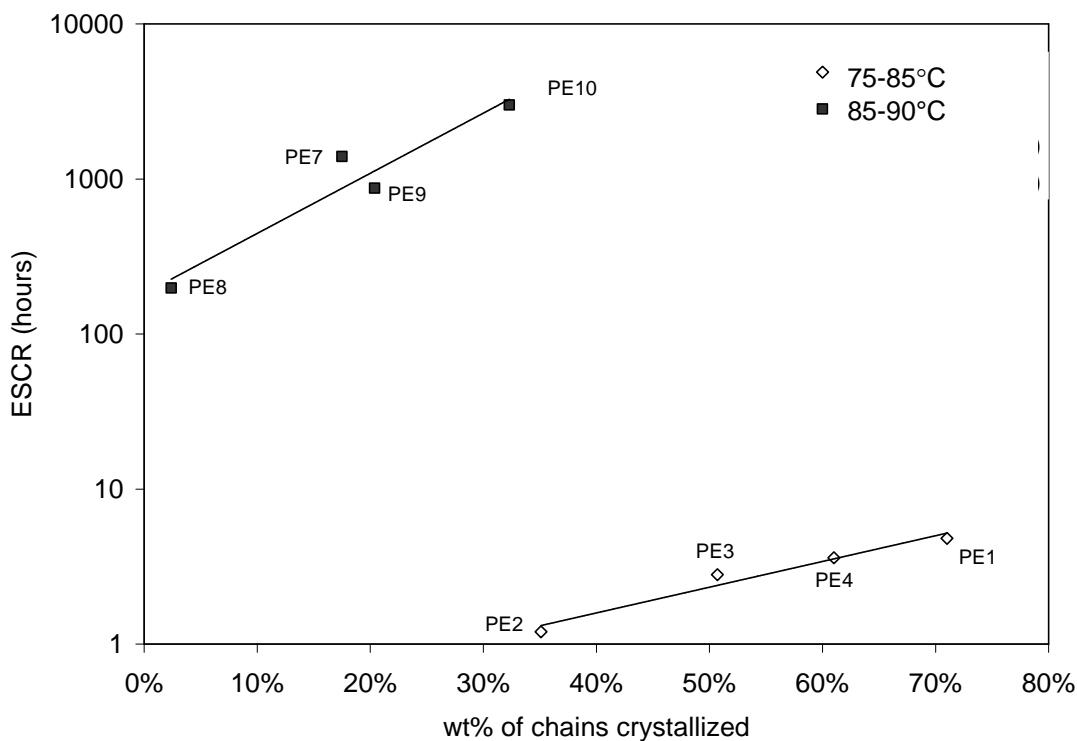


**Figure B.4: ESCR vs. weight percentage of crystallized chains at different temperature ranges, PE1-4 (75-85°C), PE7-10 (85-90°C)**

For polyethylene homopolymer, a higher crystallization temperature means that the polymer chains have higher molecular weight. However, resins in this study are polyethylene copolymers (see SCB/1000C in Table B.1). The crystallization of polyethylene copolymer chains is governed by the length of ethylene sequences between short chain branches (10-12). In the 85-90°C temperature range, the crystallizable ethylene sequence length is large, about 120-1440 repeating units according to Anantawaraskul *et al.* (10). Long ethylene sequence length also means high molecular weight because MW of a polyethylene molecule is equal to its chain length multiplied by the MW of the ethylene repeating unit. PE1-6 resins have higher short chain branch content in the low molecular weight end of the MWD (short chain branch distribution of resins is presented in Appendix A). For PE1-6, polymer chains crystallized in the 85-90°C range are most likely linear chains with few or no short chain branches that do not contribute to the ESCR of the resin. On the other hand, PE7-10 have higher short chain branch content in the high molecular weight end of the molecular weight distribution (MWD). For these resins, long polymer chains crystallized in the 85-90°C temperature range could still contain short chain branches, which is known to improve ESCR. Therefore, for PE7-10, resins with higher content of chains able to crystallize in the 85-90°C temperature range have higher ESCR.

The short chain branch distribution characteristics of resins may explain why the 85-90°C temperature range is an ESCR-TR for PE7-10 and not PE1-6. However, it does not explain why the ESCR-TR of 75-85°C does not work for PE5, PE6 and PE7-10. It may be tempting to quote the molecular weight differences of the resins, but there are two

arguments against it. Firstly, the two groups of resins, PE5-6 and PE7-10, have MW values that are diametrically opposite of each other. PE7-10 have larger  $M_w$  than PE1-4, and PE5-6 have smaller  $M_w$  values than PE-4. Therefore one cannot speculate that the ESCR-TR of 75-85°C does not work because the resin molecular weight is either too high or too low. Any argument in this vein, in favour of PE5-6 or PE7-10, would be negated by the presence of the other group of resins. Secondly, at a specific temperature, the crystallizable chain length for PE copolymer is thermodynamically controlled (8, 9), therefore, it is independent of the overall chain length, and hence the MW of the molecule. Ethylene sequence lengths that are good for formation of inter-lamellar links should not change with respect to resins of different molecular weight. Consequently the ESCR-TR of 75-85°C should have been applicable to all resins.

The correlations between environmental stress cracking resistance and tensile strain hardening stiffness (HS) and the proposed CRYSTAF ESCR-TR(s) are both based on fundamental polyethylene characteristics. CRYSTAF is based on comonomer influences on the crystallization behaviour of PE, while the HS method is based on influence of the number of chain entanglements on the mechanical response of polyethylene. Qualitatively both can offer information regarding ESCR of polyethylene. However, for quantitative relations with polyethylene ESCR, the hardening stiffness method seems superior and thus more meaningful because the correlation between ESCR and HS is very straightforward. Therefore, the use of CRYSTAF measurements to quantitatively evaluate ESCR of polyethylene requires further investigation. CRYSTAF analysis is a relatively new technique, and the exact mechanism of polymer chain crystallization

during analysis is still under debate (10, 13-15). Further light may be shed on the issue of different ESCR-TR(s) with more understanding of the CRYSTAF crystallization mechanism. However, the in-depth study of the CRYSTAF crystallization mechanism is outside the scope of this thesis.

## References

1. Wright, D. (1996), *Environmental Stress Cracking of Plastics*, Rapra Technology Ltd., Shawbury, United Kingdom.
2. Soares, J. B. P., Abbott, R. F., & Kim, J. D. (2000), "Environmental stress cracking resistance of polyethylene: the use of CRYSTAF and SEC to establish structure-property relationships", *Journal of Polymer Science, Part B: Polymer Physics*, vol. 38, pp. 1267-1275.
3. Anantawaraskul, S., Soares, J. B. P., Wood-Adams, P. M., & Monrabal, B. (2003), "Effect of molecular weight and average comonomer content on the crystallization analysis fractionation (Crystaf) of ethylene  $\alpha$ -olefin copolymers", *Polymer*, vol. 44, pp. 2393-2401.
4. Brüll, R., Pasch, H., Raubenheimer, H. G., Sanderson, R., van Reenen, A. J., & Wahner, U. M. (2001), "Investigation of the melt and crystallization behaviour of random propene/ $\alpha$ -olefin copolymers by DSC and CRYSTAF", *Macromolecular Chemistry and Physics*, vol. 202, no. 8, pp. 1281-1288.
5. Hosoda, S., Nomura, H., Gotoh, Y., & Kihara, H. (1990), "Degree of branch inclusion into the lamellar crystal for various ethylene/ $\alpha$ -olefin copolymers", *Polymer*, vol. 31, pp. 1999-2005.
6. Pasch, H., Brüll, R., Wahner, U., & Monrabal, B. (2000), "Analysis of polyolefin blends by crystallization analysis fractionation", *Macromolecular Materials and Engineering*, vol. 279, no. 1, pp. 46-51.
7. Huang, Y. & Brown, N. (1988), "The effect of molecular weight on slow crack growth in linear polyethylene homopolymers", *Journal of Materials Science*, vol. 23, pp. 3648-3655.

8. Jackson, J. F., Mandelkern, L., & Long, O. C. (1968), "Solubility of crystalline polymers. I. Polyethylene fractions crystallized in bulk", *Macromolecules*, vol. 1, no. 3, pp. 218-223.
9. Jackson, J. F. & Mandelkern, L. (1968), "Solubility of crystalline polymers. II. Polyethylene fractions crystallized from dilute solutions", *Macromolecules*, vol. 1, no. 6, pp. 546-554.
10. Anantawaraskul, S., Soares, J. B. P., & Jirachathorn, P. (2007), "A mathematical model for the kinetics of crystallization in CRYSTAF", *Macromolecular Symposia*, vol. 257, pp. 94-102.
11. Borrajo, J., Cordon, C., Carella, J. M., Toso, S., & Goizueta, G. (1995), "Modeling the fractionation process in TREF systems - thermodynamic simple approach", *Journal of Polymer Science Part B-Polymer Physics*, vol. 33, no. 11, pp. 1627-1632.
12. Luo, H. J., Chen, Q., & Yang, G. (2001), "Studies on the minimum crystallizable sequence length of semicrystalline copolymers", *Polymer*, vol. 42, no. 19, pp. 8285-8288.
13. Beigzadeh, D., Soares, J. B. P., & Duever, T. A. (2001), "Modeling of fractionation in CRYSTAF using Monte Carlo simulation of crystallizable sequence lengths: ethylene/1-octene copolymers synthesized with single-site-type catalysts", *Journal of Applied Polymer Science*, vol. 80, no. 12, pp. 2200-2206.
14. Anantawaraskul, S., Soares, J. B. P., & Wood-Adams, P. M. (2003), "Effect of operation parameters on temperature rising elution fractionation and crystallization analysis fractionation", *Journal of Polymer Science Part B-Polymer Physics*, vol. 41, no. 14, pp. 1762-1778.
15. Sarzotti, D. M., Soares, J. B. P., & Penlidis, A. (2002), "Ethylene/1-hexene copolymers synthesized with a single-site catalyst: Crystallization analysis fractionation, modeling, and reactivity ratio estimation", *Journal of Polymer Science Part B-Polymer Physics*, vol. 40, no. 23, pp. 2595-2611.

## **APPENDIX C: MODELING CREEP BEHAVIOUR OF POLYETHYLENE FOR STRUCTURAL APPLICATIONS**

Polyethylene (PE) has material properties that are both liquid-like and solid-like, hence it is a viscoelastic material. In modeling of mechanical behaviour of polyethylene, the liquid-like behaviour is often visualized as a dashpot, while the solid-like behaviour is represented by a spring. The arrangements of dashpot (s) and spring(s) can be in series (as in the Maxwell model) or in parallel (as in the Kelvin/Voigt model) (1). Creep is the tendency of a polymer material to slowly deform (permanently) under the influence of stress over a long exposure time. This mechanical behaviour is often been modeled by a Kelvin element (model). Many mathematical models for the mechanical behaviour of polyethylene have been developed over the years (2-4). However, a statistically proper estimation of the parameters involved in these models was rarely performed. In this appendix, parameter estimation and model analysis for creep of polyethylene is presented as an extension of the work done by Liu *et al.* (5, 6), which was the basis for a proposed practical approach for modeling creep behaviour of polyethylene for structural applications.

In the modeling approach using spring-dashpot element(s), a multi-element model gives more realistic simulation of the mechanical behaviour of the polymer than a single element model (1). Therefore, a multi-element creep model, with Kelvin elements arranged in series (Figure C.1), is used in this work (5, 6). In addition to Kelvin elements,

a spring element is added before the first Kelvin element to account for the instantaneous elastic response of polyethylene at the onset of stress loading.

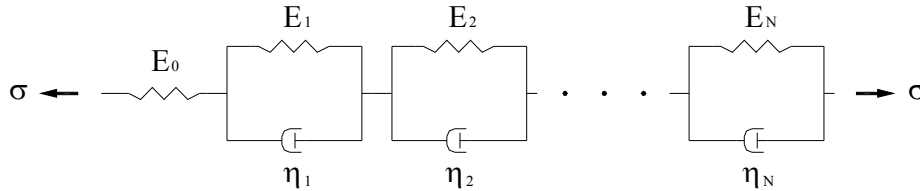


**Figure C.1: Graphic presentation of Kelvin elements in series. From ref. (5)**

For our model, the creep compliance of polyethylene has the form of Equation C.1. The  $1/E_0$  term denotes the spring element in Figure C.1, while the summations of exponential terms represent the series of Kelvin elements. The resistance of spring elements is accounted for by modulus ( $E$ ) terms in Equation C.1, and relaxation time ( $\tau$ ) in the equation accounts for the viscous response of dashpots.

$$\psi(t) = \psi_e + \psi_v(t) = \frac{1}{E_0} + \sum_{i=1}^n \frac{1}{E_i} \left\{ 1 - \exp\left(-\frac{t}{\tau_i}\right) \right\} \quad (C.1)$$

In Equation C.1,  $\psi$  is creep compliance as a function of time ( $t$ ).  $\psi_e$  stands for the instantaneous elastic part of the compliance and  $\psi_v$  is the viscous part of the compliance.  $\tau_i$  is the relaxation time of each Kelvin element.  $E_0$  is the elastic modulus and  $E_i$  is the modulus corresponding to each  $\tau_i$ .  $n$  denotes the number of Kelvin element and equals to 3 for our model. As the first step in modeling, a creep model linear in parameters is

considered, hence  $\tau_i$  is set to be independent of time and assigned a value based on work by Liu *et al.* (5). The values of  $\tau$  for each element are listed in Table C.1.

**Table C.1: Relaxation time of each Kelvin element**

Element #	Relaxation Time (s)
1	500
2	10000
3	200000

In order to estimate  $E_i$  terms in Equation C.1, tensile creep experiments were carried out for PE1, PE2, PE4 and PE8 over a period of 24 hours (5, 6). Each resin was tested at several different stress levels. Figure C.2 is the compliance (y-axis) versus time (x-axis) plot for PE1 at different applied stress levels. The shape of the compliance curves is typical for creep behaviour of polyethylene. At relatively short test times, less than 20000 seconds, a rapid increase in compliance with increase in time is observed. As the experiment continues, the rate of increase in compliance with time diminishes. At higher stress level, higher creep compliance is observed. In Figure C.2, all the compliance curves do not have the same shape, therefore, cannot be superimposed on top of one another, indicating that the creep behaviour is nonlinear (7). Creep compliance curves for the other resins (PE2, PE4 and PE8) have similar shapes and behaviour as those shown in Figure C.2, and will not be shown here for the sake of brevity.

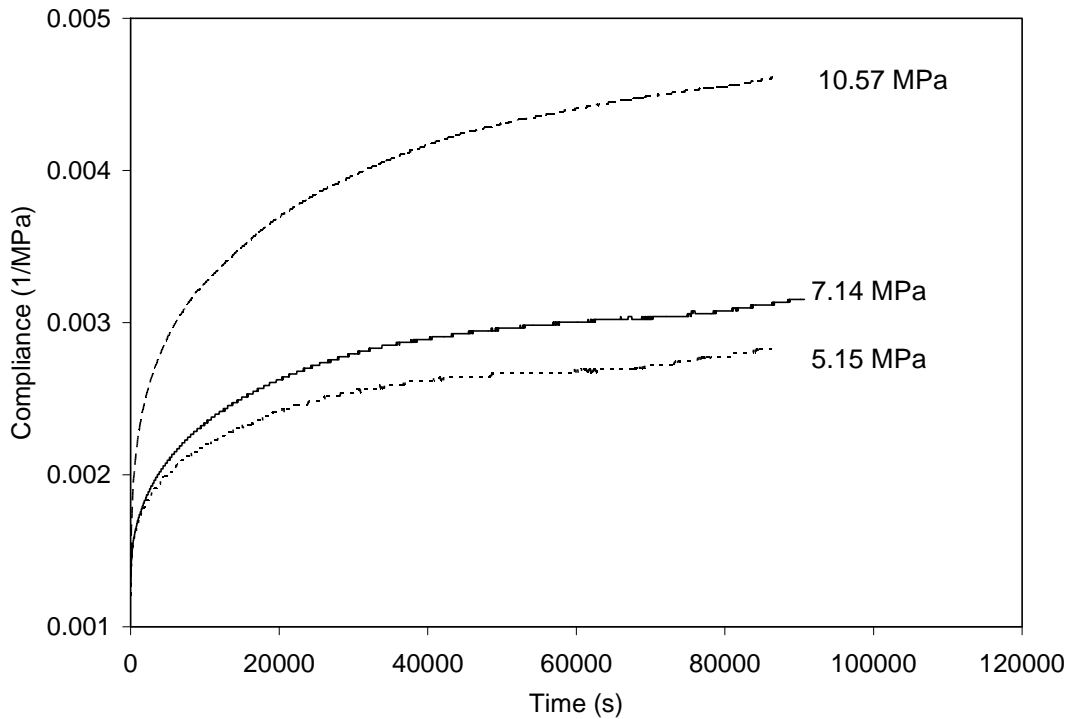


**Figure C.2: Creep compliance curves for PE1. From refs. (5, 6)**

Parameter estimation using the creep compliance model (Equation C.1) was carried out for PE1, PE2, PE4 and PE8. Table C.2 contains modulus values estimated for each resin.  $E_1$ ,  $E_2$  and  $E_3$  are modulus of Kelvin element one, two, and three, respectively. Based on the approach of Liu *et al.* (5, 6), the value of each  $E_0$  is taken as the ratio of applied stress over measured strain within the first sixty seconds of the experiment. Table C.3 contains modulus values for PE1 and PE2 estimated by Liu *et al.* (5, 6). Comparing PE1 and PE2 results in Table C.2 to those in Table C.3, the modulus values estimated showed similar results.

**Table C.2: Modulus estimated for PE1, PE2, PE4 and PE8**

PE1				
Stress (MPa)	E <sub>0</sub>	E <sub>1</sub>	E <sub>2</sub>	E <sub>3</sub>
5.15	830	2016.5	1441.6	840.3
7.14	791	2358.8	1059.3	709.7
10.58	733	1104.5	728.6	347.6
PE2				
Stress (MPa)	E <sub>0</sub>	E <sub>1</sub>	E <sub>2</sub>	E <sub>3</sub>
2.68	2500	2968.4	3420.6	1075.1
7.28	1702	1464.1	1611.3	593.8
13.72	1064	1059.7	788.2	145.8
PE4				
Stress (MPa)	E <sub>0</sub>	E <sub>1</sub>	E <sub>2</sub>	E <sub>3</sub>
2.59	959	1313.9	2362.5	346.2
6.73	656	1142.7	1788.2	455.3
13.01	438	656.3	141.7	448.5
PE8				
Stress (MPa)	E <sub>0</sub>	E <sub>1</sub>	E <sub>2</sub>	E <sub>3</sub>
3.05	666	1347.6	973.7	551.3
8.24	394	539.1	368.5	429.4
10.18	282	246.4	1375.1	265.6

**Table C.3: Modulus estimated for PE1 and PE2. From refs. (5, 6)**

PE1				
Stress (MPa)	E <sub>0</sub>	E <sub>1</sub>	E <sub>2</sub>	E <sub>3</sub>
5.15	830	2153.6	1319.8	949.5
7.14	790	2614.5	993.8	747.8
10.58	730	1153.5	706.9	352.6
PE2				
Stress (MPa)	E <sub>0</sub>	E <sub>1</sub>	E <sub>2</sub>	E <sub>3</sub>
2.68	2500	2848.6	3650.6	1053.9
7.28	1700	1515.6	1811.4	696.3
13.72	1100	1000.0	810.2	145.0

In Tables C.4 and C.5, analysis of variance (ANOVA) on Equation C.1 for PE1 is shown at stress levels of 5.15 MPa and 10.58 MPa. These two stress levels were chosen to represent creep behaviour at (the extremes of) low and high stresses. B1, B2 and B3 denote  $1/E_1$ ,  $1/E_2$ , and  $1/E_3$  terms in Equation C.1, respectively. In Tables C.4 and C.5, the large F values indicate that all terms (Kelvin elements) in Equation C.1 are statistically significant (F-critical value is 4.03 with (1,50) degrees of freedom at 5% significance level, and with (1,78) degrees of freedom at 5% significance level the F-critical value is 3.96). At both the high (10.58 MPa) and low (5.15 MPa) stress levels, the first Kelvin element (B1) has the largest F value, and hence the most influence on the creep model. On the other hand, the third Kelvin element (B3) has the smallest F value, and hence has the least overall influence on the creep model. ANOVA analysis of other resins showed the same ranking of significance for the Kelvin elements.

**Table C.4: ANOVA of creep model for PE1 at 5.15 MPa**

	SS	df	MS	F
B1	2.09E-06	1	2.09E-06	1948.6
B2	7.65E-07	1	7.65E-07	713.3
B3	2.26E-07	1	2.26E-07	211.0
Error	5.36E-08	50	1.07E-09	
Total	3.13E-06	53		

**Table C.5: ANOVA of creep model for PE1 at 10.58 MPa**

	SS	df	MS	F
B1	9.49E-06	1	9.49E-06	6841.1
B2	4.18E-06	1	4.18E-06	3010.3
B3	1.86E-06	1	1.86E-06	1341.3
Error	1.08E-07	78	1.39E-09	
Total	1.56E-05	81		

Figures C.3, C.4 and C.5 are joint confidence plots for parameters of the creep model (Equation C.1), based on PE1 at 7.14 MPa. For scaling purposes, joint confidence regions were estimated based on GPa units. In each graph, the center point (+) denotes the parameter values (B) estimated. It is important to note that none of the joint confidence region contains zero, thus indicating once again that all parameters are significant for the model. In Figure C.3, the elongated elliptical shape of the joint confidence region indicates that B1 and B2 terms in the creep model are highly correlated. In Figure C.4, the joint confidence region for B1 and B3 also has the shape of an ellipse, but less elongated. The result indicates that B1 and B3 are correlated, but the correlation is not as strong as that between B1 and B2. For B2 and B3 (Figure C.5), the elongated elliptical shape of the joint confidence region once again indicates a highly correlated relationship for these two parameters. It is more difficult to determine the effect of individual Kelvin elements when the elements are highly correlated with each other.

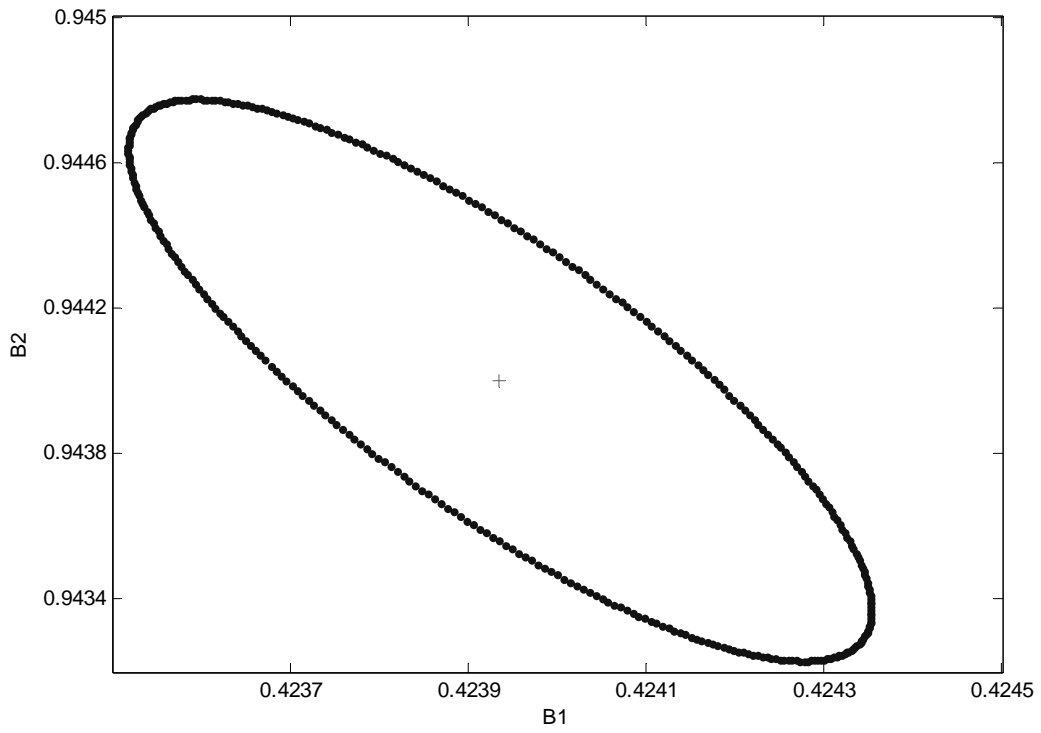


**Figure C.3: Joint confidence plot for B1 and B2, PE1 7.14 MPa**

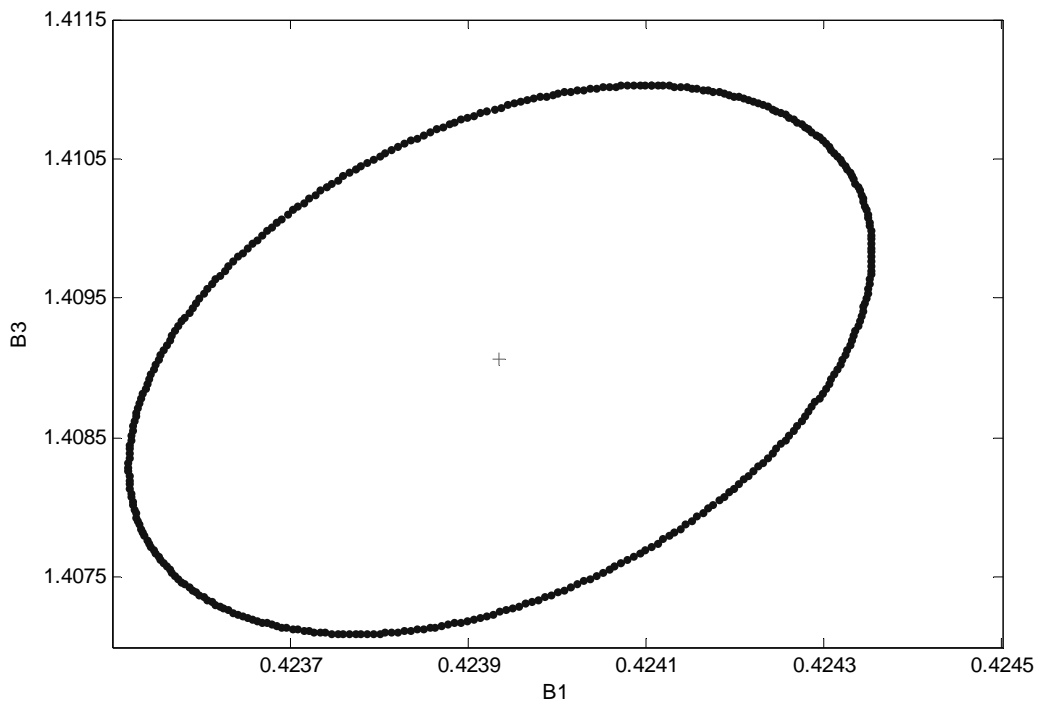


**Figure C.4: Joint confidence plot for B1 and B3, PE1 7.14 MPa**

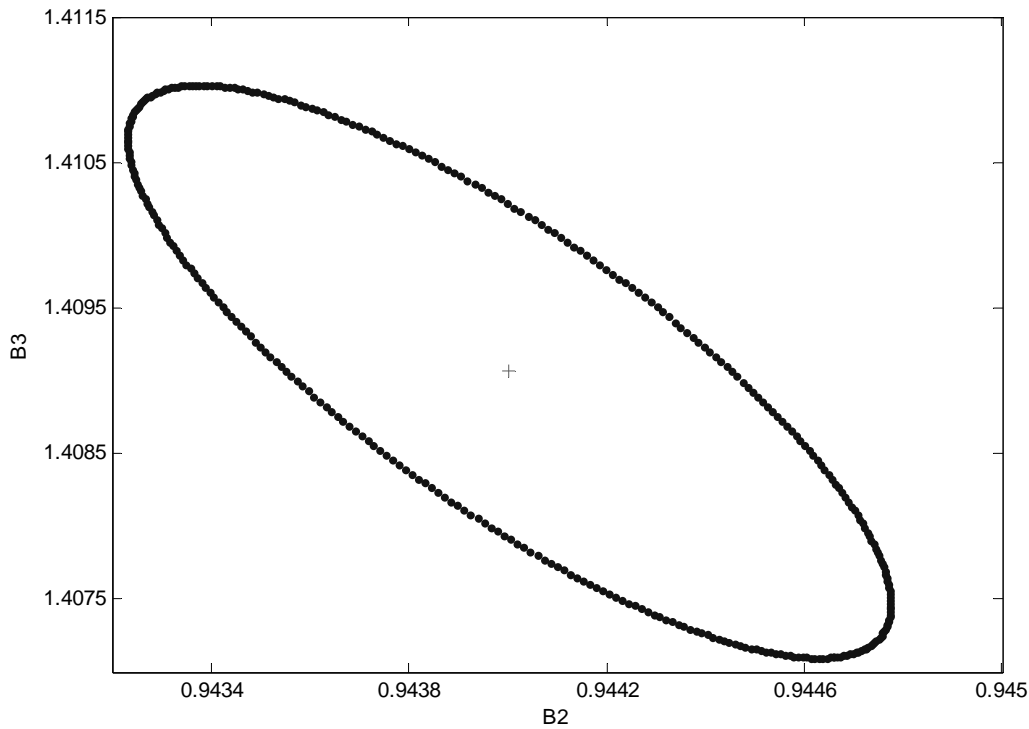


**Figure C.5: Joint confidence plot for B2 and B3, PE1 7.14 MPa**

During parameter estimation based on the approach of Liu *et al.* (5, 6), the value of  $E_0$  is fixed and given as part of the input for the model. As the next step in modeling creep behaviour of polyethylene, model parameter estimation was carried out by estimating the value of  $E_0$  along with the other  $E_i$  terms. Table C.6 contains modulus values of resins with estimated  $E_0$  for PE1, PE2, PE4 and PE8. Comparing Tables C.6 and C.2, estimated  $E_0$  showed similar values to the fixed  $E_0$  value calculated from the stress-strain ratio at the onset of the creep experiment. Parameter estimation based on the two approaches also showed similar values for the  $E_i$  terms. The results of these comparisons indicate that the  $1/E_0$  term in Equation C.1 does not need to be pre-specified as suggested by Liu *et al.* (5, 6).

**Table C.6: Model parameters estimated including  $E_0$** 

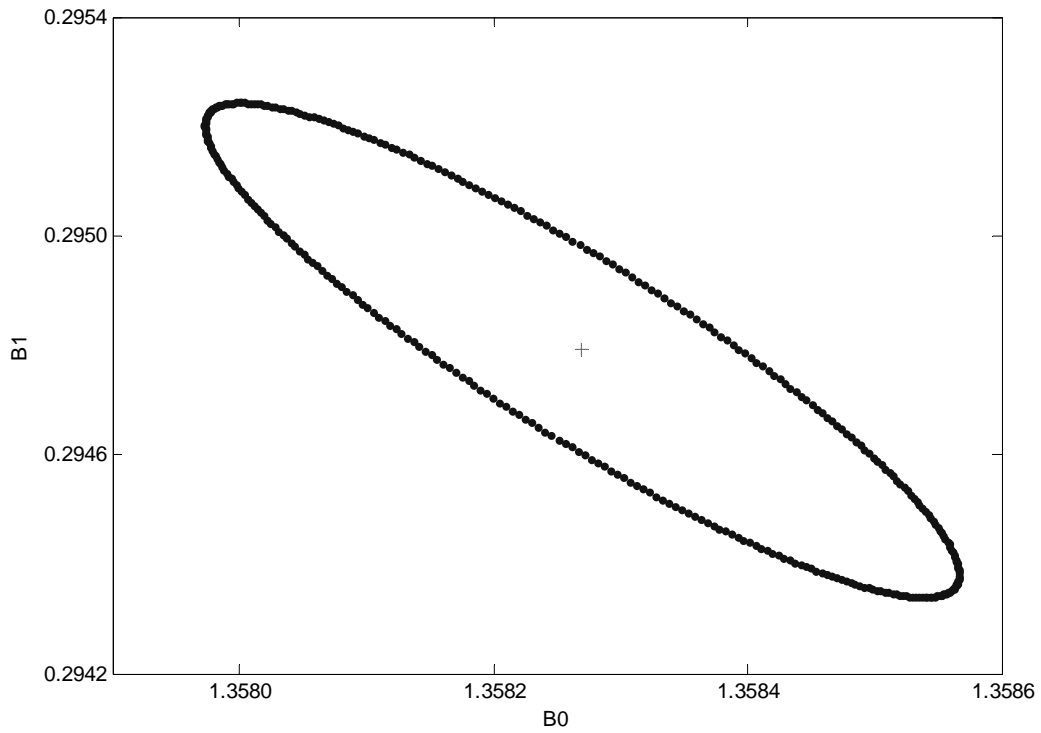
PE1 Stress (MPa)	$E_0$	$E_1$	$E_2$	$E_3$
5.15	767.7	2694.4	1353.4	890.6
7.14	736.2	3392.2	1004.3	739.3
10.58	681.2	1310.0	700.6	355.1
PE2 Stress (MPa)	$E_0$	$E_1$	$E_2$	$E_3$
2.68	2273.7	3568.9	3170.1	1101.8
7.28	1424.0	1941.9	1435.7	624.0
13.72	1040.5	1094.8	780.5	146.1
PE4 Stress (MPa)	$E_0$	$E_1$	$E_2$	$E_3$
2.59	856.7	1734.3	1984.5	355.6
6.73	628.1	1261.2	1740.7	456.4
13.01	412.8	749.1	140.3	466.6
PE8 Stress (MPa)	$E_0$	$E_1$	$E_2$	$E_3$
3.05	611.3	1785.9	910.3	579.9
8.24	338.3	775.0	340.8	486.7
10.18	217.0	382.5	776.2	320.8

Table C.7 contains ANOVA analysis results for the all-inclusive parameter estimation based on Equation C.1. Once again results for PE1 at 5.15 MPa are shown. As expected, the intercept value of  $B_0$  ( $1/E_0$ ) term in the equation has the most significance and the largest F value. All the other terms continue to be significant for the creep model. However, between the three terms ( $B_1$ ,  $B_2$  and  $B_3$ ),  $B_2$  became the most significant compared to  $B_1$  and  $B_3$ .

**Table C.7: ANOVA of creep model with estimated  $E_0$  for PE1 at 5.15 MPa**

	SS	df	MS	F
B0	6.96E-06	1	6.96E-06	26615.7
B1	2.66E-07	1	2.66E-07	1015.4
B2	8.02E-07	1	8.02E-07	3065.0
B3	1.96E-07	1	1.96E-07	749.3
Error	1.28E-08	49	2.62E-10	
Total	8.24E-06	53		

Figures C.6-C.11 are joint confidence plots for the all-inclusive approach (with units of GPa). All the parameters are statistically significant because no joint confidence regions contain zero. In Figure C.6, B0 ( $1/E_0$ ) and B1 ( $1/E_1$ ) are shown to be highly correlated with the very elongated shape of the joint confidence region. For B2 (Figure C.7) and B3 (Figure C.8), the correlation between these terms and B0 is not as strong as these between B0 and B1, as shown by the less elongated ellipses in Figures C.7 and C.8. In Figures C.9-C.11, the joint confidence region between B1 and B2, B1 and B3, and lastly B2 and B3, showed the same behaviour as Figures C.3-C.5. Once again, B1, B2 and B3 are shown to be highly correlated to one another.



**Figure C.6: Joint confidence plot for B0 and B1, PE1 at 7.14 MPa (all-inclusive approach)**

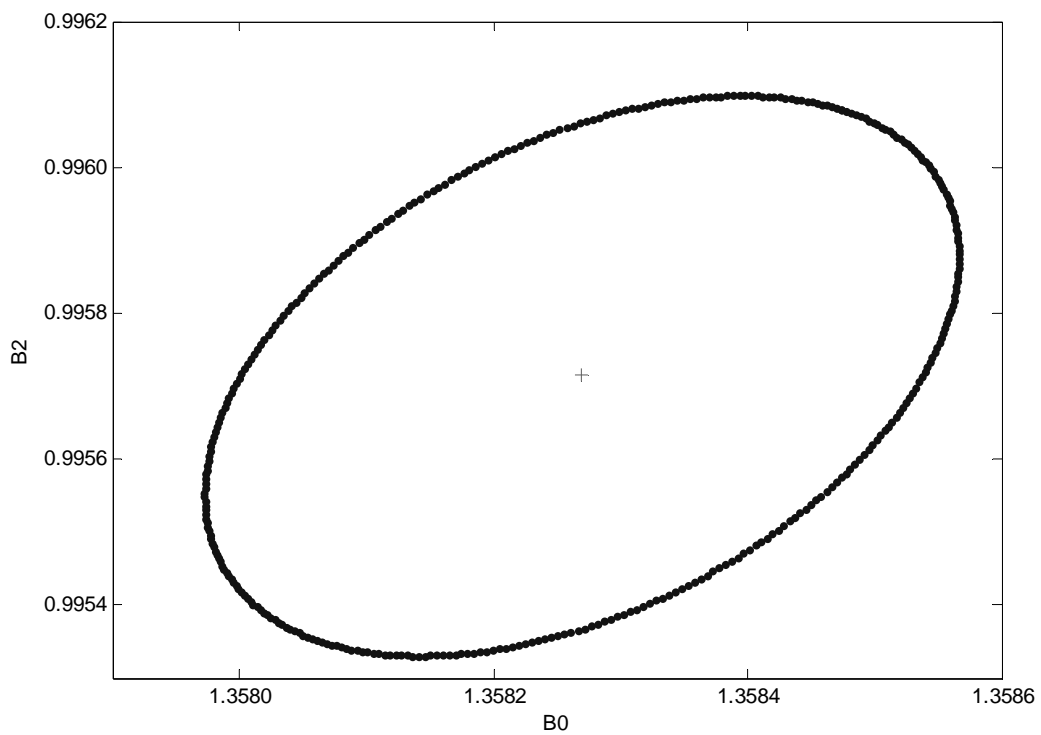


**Figure C.7: Joint confidence plot for B0 and B2, PE1 at 7.14 MPa, (all-inclusive approach)**

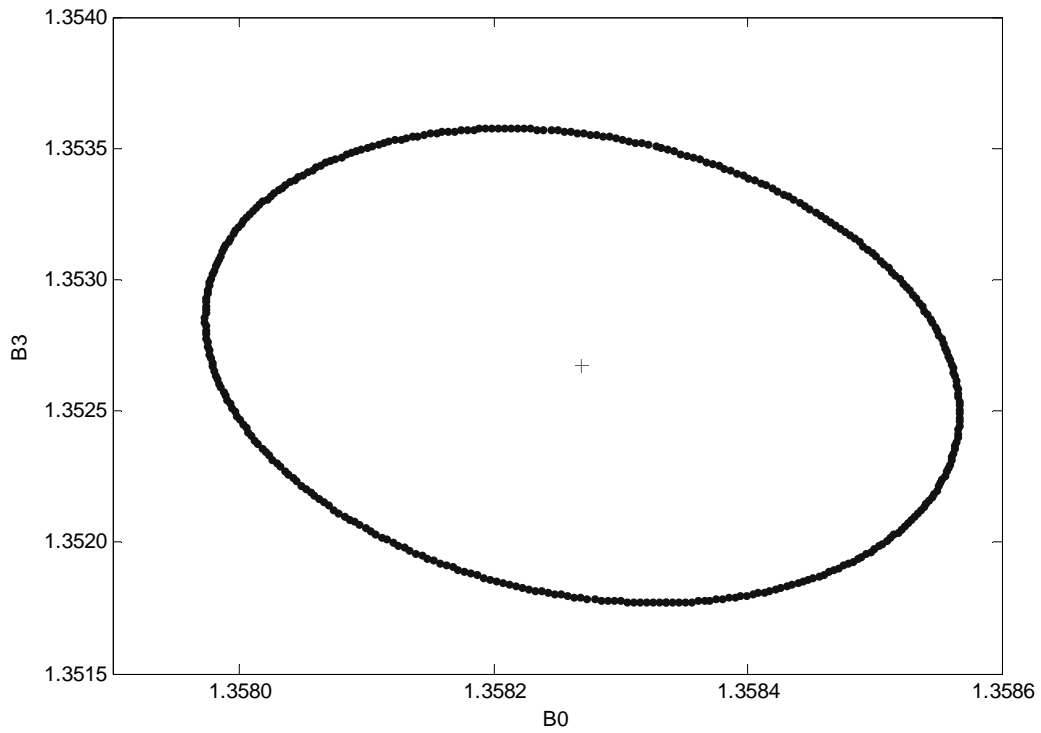


**Figure C.8: Joint confidence plot for B0 and B3, PE1 at 7.14 MPa, (all-inclusive approach)**

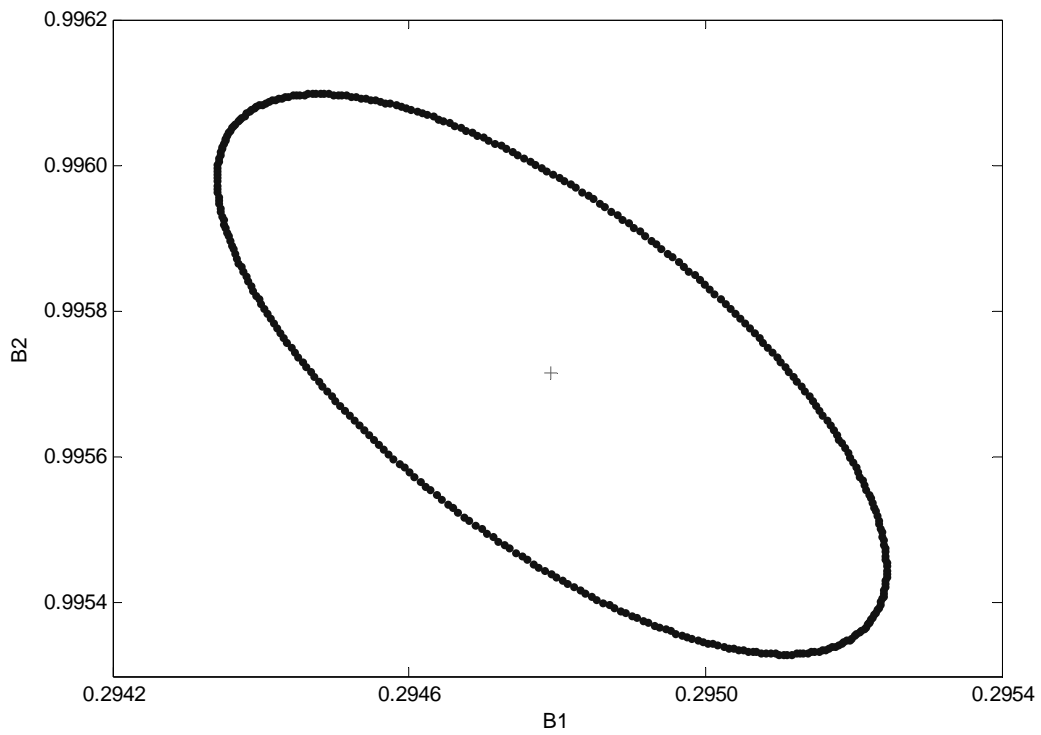


**Figure C.9: Joint confidence plot for B1 and B2, PE1 at 7.14 MPa (all-inclusive approach)**

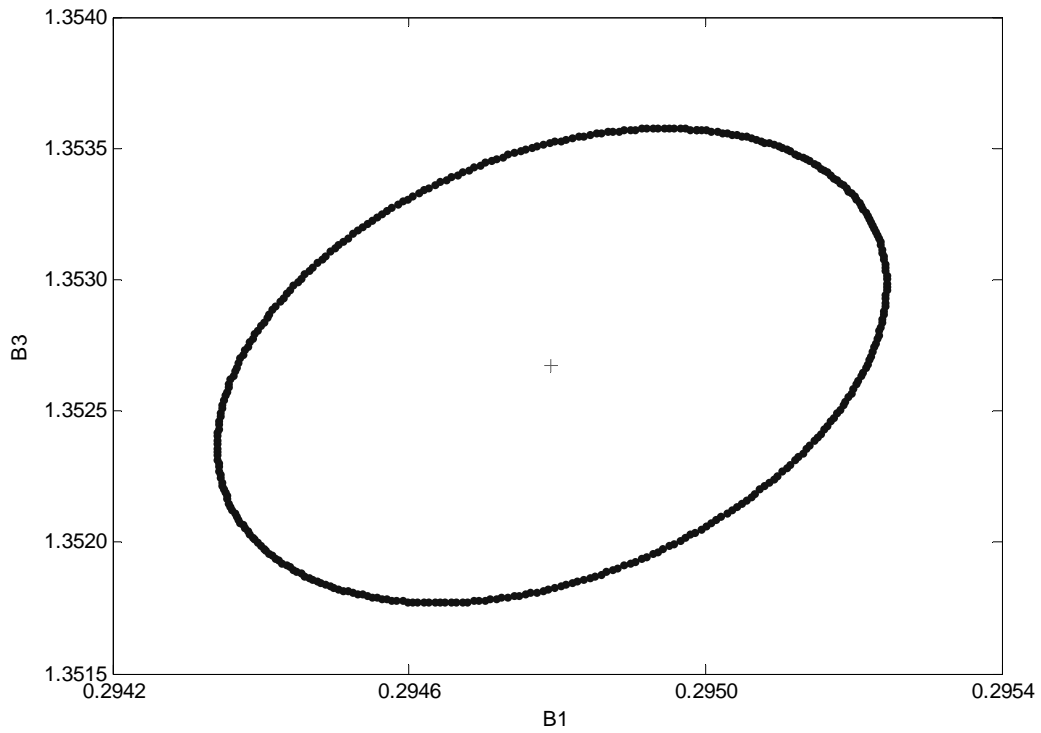


**Figure C.10: Joint confidence plot for B1 and B3, PE1 at 7.14 MPa, (all-inclusive approach)**

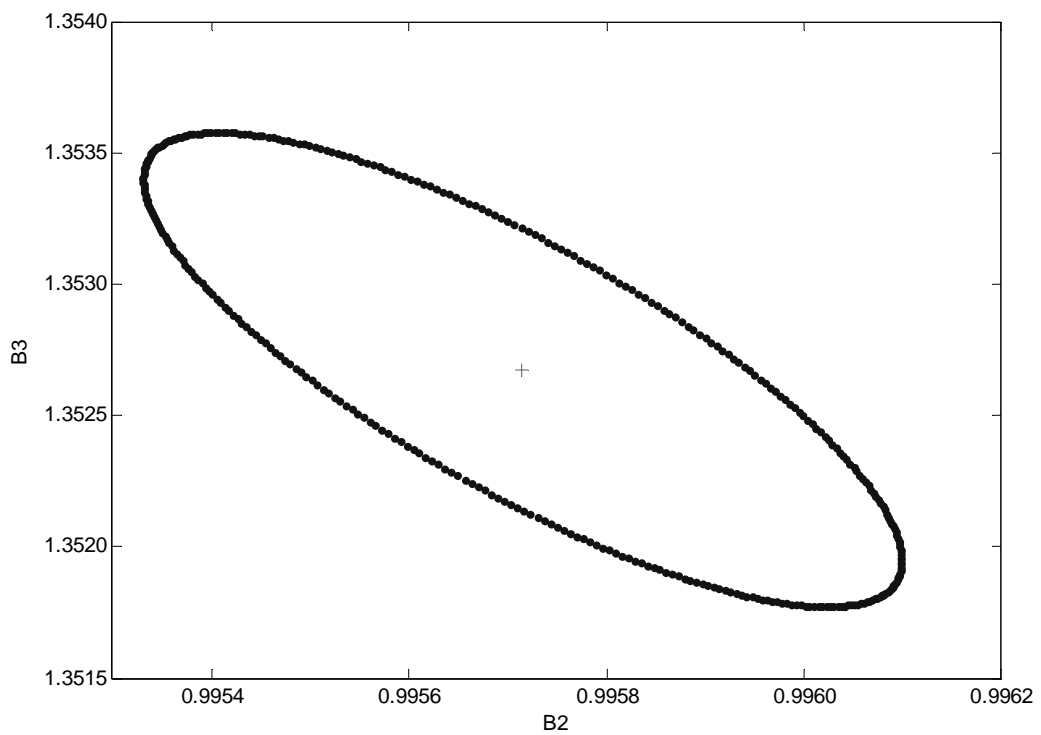


**Figure C.11: Joint confidence plot for B2 and B3, PE1 at 7.14 MPa (all-inclusive approach)**

Parameter estimation for the creep model was carried out using two approaches. In the first, the  $E_0$  value is calculated based on the stress-strain response results at the beginning of the creep experiment and given to the model as part of the input. In the second approach,  $E_0$  was estimated along with the other  $E_i$  terms. The estimated  $E_0$  had similar values to  $E_0$  calculated based on the initial creep response.  $E_i$  values estimated based on the two estimation approaches also had similar values. However, ANOVA analysis indicated that the most important Kelvin element in the creep model is different depending on the parameter estimation approach taken. For the method with fixed  $E_0$  values, the first Kelvin element is the most important. On the other hand, when  $E_0$  is estimated with the other moduli values, the second Kelvin element in the creep model has the most significance. It is not clear as to why this behaviour occurs. It could be due to the highly correlated nature of the model parameters as shown by the joint confidence plots. To clarify the effects of Kelvin elements and of the whole model structure, in general, further investigation is needed.

## References

1. Ward, I. M. (1971), *Mechanical Properties of Solid Polymers*, Wiley-Interscience, Toronto.
2. Krishnaswamy, P., Tuttle, M. E., & Emery, A. F. (1992), "Finite element modeling of the time-dependent behavior of nonlinear ductile polymers", *Polymer Engineering and Science*, vol. 32, no. 16, pp. 1086-1096.
3. Zhang, C. & Moore, I. D. (1997), "Nonlinear mechanical response of high density polyethylene. Part I: experimental investigation and model evaluation", *Polymer Engineering and Science*, vol. 37, no. 2, pp. 404-413.
4. Nikolov, S. & Doghri, I. (2000), "A micro/macro constitutive model for the small-deformation behaviour of polyethylene", *Polymer*, vol. 41, pp. 1883-1891.

5. Liu, H., Polak, M. A., & Penlidis, A. (2007), "A practical approach to modeling time-dependent nonlinear creep behaviour of polyethylene for structural applications", *Polymer Engineering and Science*, vol. 48, no. 1, pp. 159-167.
6. Liu, H. (2007), *Material modelling for structural analysis of polyethylene*, MASC Thesis, Department of Civil engineering, University of Waterloo, Waterloo, Ontario, Canada.
7. Allison, S. W., Pinnock, P. R., & Ward, I. M. (1966), "Cold drawing of poly(ethylene terephthalate)", *Polymer*, vol. 7, no. 1, pp. 66-69.

## APPENDIX D: MICROMECHANICAL MODEL FOR POLYETHYLENE

A micromechanical model incorporating damage laws was used to model uniaxial tensile deformation of polyethylene in section 5.4. Modeling parameters are listed in Table D.1. Key equations used in the model are presented in Table D.2. Model implementing procedures and further discussion can be found in Alvarado-Contreras (1) and Alvarado-Contreras *et al.* (2).

**Table D.1: Material parameters for model simulations under uniaxial tension, ref. (1)**

<b>Crystalline Phase</b>	
Strain rate sensitivity, $n^c$	5.0
Reference strain rate, $\dot{\gamma}_0 [s^{-1}]$	0.001
Damage rate sensitivity, $m$	2.0
Reference damage rate, $\dot{\Omega}_0 [MPa^{-1}]$	0.00025
Spin release, $\zeta$	8.0
Crystallinity, $\chi^c$	70
<b>Amorphous Phase</b>	
Strain rate sensitivity, $n^a$	5.0
Reference strain rate, $\dot{\gamma}_0$ or $\dot{\epsilon}_0 [s^{-1}]$	0.001
Strength $\tau_0$ or $\sigma_0$ , $[MPa]$	6.4
Number of rigid links, $N$	20-200
Rubbery shear modulus, $C_R$	4.0
Critical damage, $\Omega_\infty$	0.8
Damage rate, $\alpha$	0.000005

**Table D.2: Micromechanical model with damage for semicrystalline polyethylene, ref. (1)**

<b>Crystalline Phase</b>		
Stress-strain relationship	$D_{ij} = M_{ijkl} S_{lk}$	$D$ - deformation rate, $M$ - compliance tensor, $S$ - stress
Compliance tensor	$M_{ijkl} = \dot{\gamma}_0 \sum_{\alpha} \frac{1}{(1 - \Omega^{\alpha}) g^{\alpha}} \left  \frac{S_{mn}^* R_{nm}^{\alpha}}{(1 - \Omega^{\alpha}) g^{\alpha}} \right ^{n-1} R_{ij}^{\alpha} R_{kl}^{\alpha}$	$M$ - compliance tensor, $\dot{\gamma}_0$ - reference strain rate, $\alpha$ - slip system index, $\Omega^{\alpha}$ - mechanical damage, $g^{\alpha}$ - reference shear strength, $n$ - strain rate sensitivity, $S^*$ - orthogonal sub-transformation of stress, $R^{\alpha}$ - symmetric component of Schmid tensor
Damage evolution law	$\dot{\Omega}^{\alpha} = \dot{\Omega}_0 \left  \frac{\tau^{\alpha}}{(1 - \Omega^{\alpha}) g^{\alpha}} \right ^m$ $\tau^{\alpha} = S_{ij}^* R_{ji}^{\alpha}$	$\dot{\Omega}^{\alpha}$ - damage rate, $\dot{\Omega}_0$ - reference damage rate, $\tau^{\alpha}$ - nominal shear stress, $\Omega^{\alpha}$ - mechanical damage, $g^{\alpha}$ - reference shear strength, $m$ - damage rate sensitivity, $S^*$ - orthogonal sub-transformation of stress, $R^{\alpha}$ - symmetric component of Schmid tensor
Total spin	$W_{ij} = W_{ij}^m + R W_{lk}^p$ $R = \tanh(\zeta \bar{\Omega})$ $\bar{\Omega} = \frac{1}{8} \sum_{\alpha} \Omega^{\alpha}$	$W$ - spin, $R$ - crystal rotation, $W^m$ - rigid-body spin, $W^p$ - plastic spin, $\zeta$ - spin release, $\bar{\Omega}$ - crystal average damage, $\Omega^{\alpha}$ - mechanical damage
<b>Amorphous Phase</b>		
Stress-strain relationship	$D_{ij} = \frac{3}{2} \dot{\epsilon}_0 \left( \frac{\sigma_{eq}}{\sigma_0} \right)^{n^a - 1} \frac{S_{ij} - H'_{ij}}{\sigma_0}$	$D$ - deformation rate, $\dot{\epsilon}_0$ - reference strain rate, $\sigma_{eq}$ - equivalent stress, $\sigma_0$ - strength, $n^a$ - strain rate sensitivity, $S$ - stress, $\Omega$ - mechanical damage, $H'$ - anisotropic resistance to plastic deformation

Hardening law	$H'_{ij} = \frac{C_R}{3} \sqrt{\frac{3N}{I_1}} L^{-1} \left( \sqrt{\frac{I_1}{3N}} \right) \left( B_{ij} - \frac{1}{3} I_1 I_{ij} \right)$	<p><math>H'</math> - anisotropic resistance to plastic deformation, <math>C_R</math> - rubbery shear modulus, <math>N</math> - number of rigid links, <math>I_1</math> - left Cauchy-Green stretch tensor first invariant, <math>L^{-1}</math> - inverse Langevin function, <math>B_{ij}</math> - back-stress tensor of the network subjected to deformation, <math>I_{ij} = \partial I_1 / \partial B_{ij}</math></p>
Damage evolution law	$\Omega = \Omega_\infty [1 - \exp(-\alpha W^2)]$	<p><math>\Omega</math> - isotropic damage, <math>\Omega_\infty</math> - critical damage, <math>\alpha</math> - damage rate, <math>W</math> - energy of damage</p>

## References

1. Alvarado-Contreras, J. A. (2007), *Micromechanical Modelling of Polyethylene*, PhD Thesis, Department of Civil Engineering, University of Waterloo, Waterloo, Ontario, Canada.
2. Alvarado-Contreras, J. A., Polak, M. A., & Penlidis, A. (2007), "Micromechanical approach to Modeling damage in crystalline polyethylene", *Polymer Engineering and Science*, vol. 47, no. 4, pp. 410-420.

## APPENDIX E: $\alpha$ -RELAXATION ENERGY AND ESC MODEL

The  $\alpha$ -relaxation energy ( $\Delta H$ ) has been speculated to be the same as the crack activation energy in SCG of polyethylene (1, 2). In section 7.4,  $\Delta H$  values for PE1-4 and PE8 were presented. The dynamic mechanical analyses (DMA) used to obtain  $\Delta H$  were not limited to PE1-4 and PE8. Confirmatory experiments were also carried out for the other resins. In Table E.1  $\alpha$ -relaxation energy values for all resins are presented. The  $\Delta H$  values are within the range of reported  $\alpha$ -relaxation energies for polyethylene (97-208 kJ/mole (3-5)).

**Table E.1:  $\alpha$ -relaxation energy of polyethylene**

	$\Delta H$ (kJ/mol)	Coefficient of Variation
PE1	109.90	0.03
PE2	112.15	0.02
PE3	115.14	0.07
PE4	123.86	0.06
PE5	135.27	0.08
PE6	128.22	0.01
PE7	147.05	0.13
PE8	150.48	0.05
PE9	149.03	0.12
PE10	155.05	0.02

In section 7.4  $\alpha$ -relaxation energy ( $\Delta H$ ) has been shown to be related to the ESC crack activation energy ( $Q$ ) for HDPE materials. One possible implication of this relationship is the use of  $\Delta H$  in place of  $Q$  in environmental stress cracking (ESC) and or slow crack growth (SCG) modeling. For PE with high environmental stress cracking resistance, PE7-10 in this study, the standard method for obtaining  $Q$  from the NCLT test at different

temperatures would be time consuming and thus impractical (not to mention the effect of the test noise on the estimated  $Q$ ). The  $\Delta H$  obtained from DMA could be a faster alternative to the standard approach.

An investigation was undertaken to study the possibility of using  $\Delta H$  in place of  $Q$  in the environmental stress cracking model for high ESCR resins. The ESC model attempt was presented in detail in Chapter 7. As per discussions in section 7.4,  $\alpha$ -relaxation energy ( $\Delta H$ ) of polyethylene should only be used in place of  $Q$  in ESC modeling when the short chain branching (SCB) content of the polymer is 2.5 SCB per thousand carbon atoms or higher. PE7-10 in this study are high ESCR resins with four or more SCB per thousand carbon atoms, therefore in the case of these resins  $\Delta H$  can be used in the ESC model in place of the crack activation energy ( $Q$ ).

The material resistance values ( $C$ ) to environmental stress cracking for PE7-10 were calculated the following procedures of in section 7.5, with the average  $n$  value of 3.12 used. Material resistance values presented in Table E.2 are based on individual  $\Delta H$  values of PE7-10, as well as  $Q = 90$  kJ/mol suggested by Brown (2). The  $C$  values calculated based on  $\Delta H$  and  $Q = 90$  kJ/mol are also plotted as a function of the ESCR of resins in Figure E.1. Black symbols in Figure E.1 are material resistance ( $C$ ) values calculated based on  $Q = 90$  kJ/mol, while white symbols are  $C$  values calculated based on the corresponding  $\Delta H$  values. There are several orders of magnitude differences between the material resistance data sets. It is worth noting that the two sets of material resistance ( $C$ ) values show the same trend of increasing material resistance with increasing ESCR.

By showing the same material resistance trend as that calculated based on a constant  $Q = 90\text{kJ/mol}$ , it is thus demonstrated that  $\alpha$ -relaxation energy ( $\Delta H$ ) can be used as an approximation of the crack activation energy ( $Q$ ) in environmental stress cracking model calculations for polyethylene.

**Table E.2: Material resistance (C) to ESC based on  $Q = 90\text{ kJ/mol}$  (2) and  $Q = \Delta H$  for PE7-10**

	Material resistance to ESC with $Q = 90\text{ kJ/mol}$ (hour $\text{MPa}^{3.12}\text{ m}^{1.56}$ )	$\Delta H$ (kJ/mole)	Material resistance to ESC with $\Delta H$ (hour $\text{MPa}^{3.12}\text{ m}^{1.56}$ )
PE7	1.37E-13	147.0	8.23E-23
PE8	4.77E-14	150.5	7.98E-24
PE9	1.97E-13	149.0	5.68E-23
PE10	7.02E-13	155.0	2.14E-23

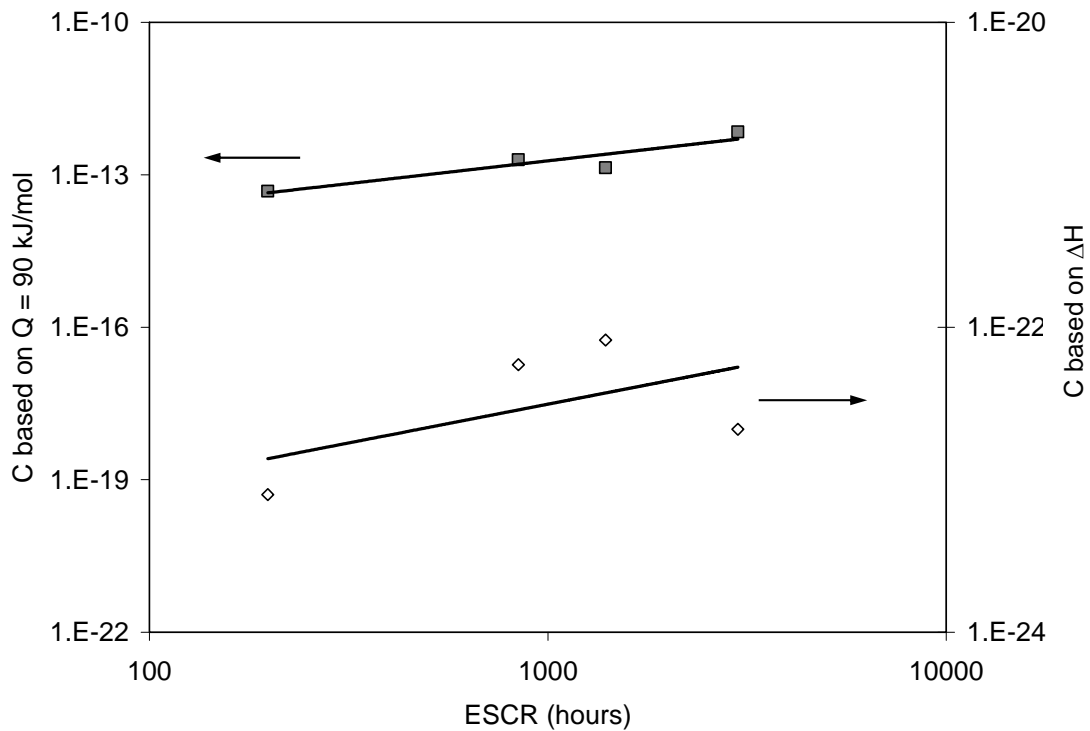


**Figure E.1: Material resistance to ESC based on  $Q = 90\text{ kJ/mol}$  (2) and  $Q = \Delta H$  for PE7-10**

## References

1. Brown, N. & Lu, X. (1995), "A fundamental theory for slow crack growth in polyethylene", *Polymer*, vol. 36, no. 3, pp. 543-548.
2. Brown, N. (2007), "Intrinsic lifetime of polyethylene pipelines", *Polymer Engineering and Science*, vol. 47, pp. 477-480.
3. Matsuo, M., Bin, Y., Xu, C., Ma, L., Nakaoki, T., & Suzuki, T. (2003), "Relaxation mechanism in several kinds of polyethylene estimated by dynamic mechanical measurements, positron annihilation, X-ray and  $^{13}\text{C}$  solid-state NMR", *Polymer* no. 4325, p. 4340.
4. Guan, X. & Phillips, P. J. (2007), "Dynamic mechanical properties of random ethylene/1-octene copolymers prepared by rapid cooling", *European Polymer Journal*, vol. 43, pp. 1219-1233.
5. Stadler, F. J., Kaschta, J., & Muenstedt, H. (2005), "Dynamic-mechanical behavior of polyethylenes and ethene-/alpha-olefin-co-polymers. Part I. alpha '-relaxation", *Polymer*, vol. 46, no. 23, pp. 10311-10320.